The Dissertation Committee for Corinne Wong Certifies that this is the approved version of the following dissertation:

Delineating controls on hydrologic variability and water geochemistry in central Texas

Committee:

Jay L. Banner, Supervisor

MaryLynn Musgrove

M. Bayani Cardenas

Terrence M. Quinn

Suzanne A. Pierce

Delineating controls on hydrologic variability and water geochemistry in central Texas

by

Corinne Wong, B.A.; B.S.; M.S. Geo. Sci.

Dissertation

Presented to the Faculty of the Graduate School of

The University of Texas at Austin

in Partial Fulfillment

of the Requirements

for the Degree of

Doctor of Philosophy

The University of Texas at Austin

August 2013

Acknowledgements

Thanks to all those that have helped during my time at UT. Thanks to Jay for years of guidance and support – my appreciation for your mentorship may approach your combined appreciation for ultimate Frisbee and the Grateful Dead. Thanks to my committee (MaryLynn Musgrove, Bayani Cardenas, Terry Quinn, and Suzanne Pierce) for critical guidance and feedback. Thanks to Banner and Quinn research groups for research support, bouncing ideas around, and social off-gassing. Thanks to the department analytical staff – Larry Mack for clean lab and TIMS training, Nate Miller for all your time and energy chasing Mg/Ca cycles with laser ablation, Staci Lowery for keeping the clean lab and TIMS running, and Dorinda Ostermann and Toti Larsen for stable isotope data. Thanks to Barbara Mahler and MaryLynn Musgrove of the U.S. Geological Survey Texas Water Science Center for engaging me in their research – this provided access to a great data set and a platform from which to define my own research direction. This research also benefitted greatly from collaborations with Chris Herrington and Nico Hauwert with the City of Austin Watershed Protection Department, and Brian Smith and Brian Hunt of the Barton Springs/Edwards Aquifer Conservation District. Thanks to Jack Sharp for the opportunity to co-author a review paper on urban hydrogeology. Thanks to Jill Marshall and Bob Duke for improving my ability to teach science and present my research. Thanks to the Jackson School, EPA, NSF (GK12 and P2C2), PEO, and GSA for funding and logistical support. Thanks to family and friends for loving me despite my tendency for leaving your parties early, skipping weekend outings, and abbreviating holiday visits. Thanks to Liza for being my anchor, having amazing patience and understanding, and for keeping me well-fed and caffeinated.

Delineating controls on hydrologic variability and water geochemistry in central Texas

Corinne Wong, PhD

The University of Texas at Austin, 2013

Supervisor: Jay L. Banner

There is a strong concern about how water resources will be affected by future climate change. Investigation of how a hydrologic system might respond to climate change, however, requires a detailed understanding of the controls on and factors that might affect that system. The research presented in this dissertation focuses on improving the understanding of the Barton Springs segment of the Edwards aquifer in central Texas. The first three chapters of this dissertation present research investigating spatial and temporal controls on groundwater geochemistry. The fourth chapter focuses on characterizing and understanding the controls on long-term hydrologic variability by reconstructing past climate from a speleothem (cave mineral deposit) collected from a central Texas cave. On spatial scales, Edwards aquifer groundwater geochemistry is influenced by water-rock interaction (calcite and dolomite recrystallization, gypsum dissolution, and calcite precipitation) and mixing between fresh groundwater and saline groundwater. On temporal scales, variation in groundwater geochemistry is dictated by the extent to which fresh groundwater mixes with recharging stream water. The degree of mixing is sensitive to changes in climate conditions (i.e., more mixing under wetter conditions) and type of flow path (i.e., conduit or diffuse) that dominantly supplies a given site. The geochemistry of stream water, which provides the majority of recharge to

the aquifer, is degrading over time and indirectly controlled by anthropogenic sources under both wet and dry conditions. Climate reconstructed from a speleothem suggests that central Texas moisture conditions were relatively constant from the mid to late Holocene (0 to 7 ka), except for an extended dry interval from 0.5 to 1.5 ka. Speleothem $\delta^{18}O$ values spike during this dry interval, suggesting that decreases in Pacific-derived moisture or decreased tropical storm activity might have been coincident with the prolonged dry interval. This research has improved understanding of the natural variability of and controls on physical and geochemical components of hydrologic system in central Texas.

Table of Contents

List of Tables

List of Figures

Chapter 1. Introduction

Climate change has important environmental, economic, social, and political impacts. Climate change is defined as any change in the climate over time (IPPC, 2007). The potential impact of future climate change on water resources is a significant concern for sustaining ecosystems and thriving human populations and economies. In the same way, however, that it is necessary to understand climate processes in order to accurately model future climate, it is critical to have a detailed understanding of a given hydrogeologic system in order to be able to assess how that system might respond to future climate conditions. For example, to be able to address the question of how a given system will respond to climate change, it is first necessary to know i) what is and what controls the baseline of that system, ii) how are anthropogenic factors perturbing that baseline, iii) how do natural and anthropogenic controls respond to climate variations? The research presented in this dissertation addresses such questions for the Edwards aquifer in central Texas. Addressing these questions provides an improved understanding with which to inform both current and future management practices.

The Edwards aquifer is a critical groundwater resource that can be affected human activity and climate variability. Central Texas is dependent on Edwards aquifer groundwater for domestic and agricultural water supply. The Edwards aquifer is designated a sole source water supply and relied on by over two million people. Natural points of discharge (i.e., springs) from the Edwards aquifer provide the only habitat for endangered and endemic species, making preservation of spring flow and spring water quality especially critical. The Edwards aquifer is a carbonate aquifer, which is particularly vulnerable to potential surface water contamination. In general, carbonate aquifers are readily susceptible to solutional weathering, which results in features such as

caves, sink holes, and subsurface conduits. These features allow direct infiltration of surface water into the subsurface, rapid movement of water through the system, and the bypass of natural filtration processes. Rapid population growth and urban sprawl around metropolitan areas (e.g., San Antonio and Austin) have lead to increased groundwater withdrawal and degraded water quality. The region lies in the transition zone between the humid east and arid west, and the semi-arid to sub-humid region is subjected to frequent droughts to which the aquifer is hydrologically sensitive. Furthermore, the response of regional rainfall amount, timing, and patterns to future increases in temperature are uncertain.

Current management of groundwater resources seeks to protect groundwater quantity and quality while balancing domestic, municipal, industrial, ecological, and economical needs (EAA, 2009). Threats to the Edwards aquifer include i) water scarcity, defined as a shortage of water supply to demands (Martin-Carrasco et al., 2013), and ii) contamination of groundwater with constituents that degrade groundwater quality for recreational and domestic use and ecosystem health. Groundwater withdrawal from the Edwards aquifer is regulated by the Edwards Aquifer Authority and groundwater conservation districts. Regulation that is deemed to be too limiting, however, may result in the right of landowners to be compensated by the regulating agency. This makes groundwater regulation agencies subject to possible lawsuits and compensation costs, which may affect the degree of regulation the agency chooses to impose (Buchele, 2012). Given challenging regulatory environment and the potential effects of human activities and climate variations on the Edwards aquifer, it is critical to provide a detailed understanding of the hydrogeologic system to inform groundwater management and decision making.

There is great interest in understanding the Edwards aquifer because it is such an important resource. As a result, the hydrogeologic setting is well described, and there is a large and spatially extensive physical and chemical dataset spanning back to the 1970s. There have been multiple recent research efforts to better understand natural and anthropogenic controls on groundwater quantity and quality (e.g., Hauwert, 2009; Musgrove et al., 2010; Wierman et al., 2010; Mahler et al., 2011; Johnson et al., 2012; Musgrove et al., 2012), one of which led to the installation of two multi-port sampling wells that allow precise sampling of distinct stratigraphic units.

The hydrogeologic setting allows for distinct methodological approaches. The contrast of Sr isotope values between soils and bedrock enables the use of Sr isotope variations to track the natural evolution of groundwater via water-rock interactions. The mix of rural, urban, and urbanizing areas provides a dynamic range of urban densities from which anthropogenic affects on water quality can be delineated. Caves formed in the carbonate bedrock hosting the aquifer allow unique access to in-situ sampling of vadose groundwater. Mineral deposits from these caves (i.e., speleothems) have the potential to preserve past climate variations, and there has been over ten years of research dedicated to understanding how speleothems in this region reflect modern climate conditions. The combination of these factors result in an ideal setting for characterizing the variation of and controls on the baseline state of the aquifer and climate system and investigating how the two are linked.

Despite previous research efforts, some key questions about the aquifer remain:

- What is the nature of communication between conduit and diffuse parts of the aquifer?
- To what degree does groundwater from the Edwards aquifer exchange with the adjacent and underlying Trinity aquifer?

- How does the flow of recently recharged surface water through the aquifer vary with changing antecedent moisture conditions?
- What is and what controls the quality of recharging stream water?
- What causes drought in central Texas?

The research presented in this dissertation seeks to address these questions.

OVERVIEW OF THE HYDROGEOLOGIC SETTING

The Edwards Plateau is a regionally extensive carbonate platform deposited in the early Cretaceous as a part of the ancestral Gulf of Mexico (Fig. 1.1). The Edwards Plateau is bound to the south and east by the Balcones Fault Zone (BFZ), which consists of northeast trending normal and en echelon faults resulting from crustal extension related to subsidence of the Gulf of Mexico sedimentary basin and uplift of the Edwards Plateau (Abbot, 1973). The Llano Uplift bounds the plateau to the north, and consists of Paleozoic rocks onto which Lower Cretaceous sediments were deposited (Stricklin et al., 1971). The plateau extends west to the Pecos River where the Edwards Group is no longer exposed at the surface. Post-Miocene karstification (i.e., erosion and dissolution), especially along the BFZ, were critical to the development of the aquifer systems of the Edwards Plateau (Hauwert, 2009).

Three major aquifers are hosted by the rocks of the Edwards Plateau: the Edwards-Trinity aquifer, the Trinity aquifer, and the Edwards aquifer. The Edwards-Trinity aquifer underlies much of the plateau, and consists of several unconfined aquifers within permeable strata of the Edwards and Trinity Groups (Rose, 1972). The Trinity aquifer is hosted by formations of the Trinity Group, and is divided into upper, middle, and lower sections. The middle section has the highest and freshest yields (Wierman et al., 2010). The Edwards aquifer occurs within the Georgetown Formation and Edwards

Group, which lie adjacent to and above the Trinity Group. Water recharges through Edwards group strata along the (BFZ) via discrete recharge points, such as caves and sinkholes, and losing streams flowing south and southeast across the fault zone (Slade, 1985; Hauwert, 2009). The aquifer is confined to the south and southeast of the BFZ beneath younger Cretaceous and Tertiary strata. Regional groundwater flow is to the east. The majority of water draining the area north and northwest of the BFZ (contributing zone) recharges the Edwards aquifer as losing streams cross the BFZ where permeable, faulted, and karstified bedrock of the Edwards aquifer occurs at the surface (recharge zone; Fig. 1.1). Edwards aquifer groundwater mixes with saline groundwater at depth and to the south and southeast of the BFZ, and comprises the southern and eastern boundary of the Edwards aquifer (Fig. 1.1).

The Edwards aquifer is divided into managerial segments, which include the San Antonio, Barton Spring, and Northern segments (Fig. 1.1). Characteristics inherent to carbonate aquifers (conduit and diffuse flow regimes, direct recharge features, responsiveness to changing climate conditions) likely affect groundwater quantity and quality similarly each segment. The segments, however, differ in size, degree of overlying urbanization, amount of groundwater being withdrawn, and, to a small extent, thickness and hydrogeologic properties of the aquifer host units. Such differences likely result in subtle variations in patterns of spatial and temporal variance in groundwater quantity and quality in each segment.

DOCUMENT ORGANIZATION

The research presented here is divided into four additional chapters. The first (Chapter 2) addresses the questions What is the physical and chemical response of the aquifer to variations in climate? Data are presented from 17 months of surface water,

spring water, and groundwater sampling that spanned the intensification of and recovery from a severe drought. Inverse geochemical modeling is used to quantify the timing and magnitude of surface water influence on groundwater compositions. Combined physical and geochemical results are used to modify the existing conceptual model of aquifer recharge dynamics.

Recharging stream water provides the majority of recharge to the aquifer, and, as demonstrated in Chapter 2, has a large influence on groundwater geochemistry. Chapter 3, addresses the question: What is and what controls stream water geochemistry? Results demonstrate that stream water concentrations of some anthropogenic constituents are increasing over time and that these concentrations cannot be accounted for by natural processes. Discrepancies between quantitative estimates of anthropogenic inputs derived using geochemical and physical approaches and the consistency of stream water concentrations relative to increases in stream discharge indicate that anthropogenic sources indirectly control stream water. Anthropogenic sources leach solutes into the shallow soil and epikarst zone, and these solutes are transported to streams during rain events with the magnitude of transport proportional to the size of the rain event.

Chapter 4 focuses on understanding controls on groundwater geochemistry on spatial scales by addressing the sub-question: Is there mixing between groundwater from the Trinity and Edwards aquifers? Physical and chemical data collected from two multiport well placed in the Edwards and Trinity aquifers are used to demonstrate that mixing between the Edwards and Trinity aquifers is likely inhibited by litho-stratigraphic units acting as aquitards. These results are used to refine the existing conceptual model of the relationships between litho- and hydro-stratigraphic units.

The focus of Chapter 5 is the characterization of past climate variability and addressing the question: What controls hydrologic variability on centennial and

millennial scales? Mid- to late-Holocene (0 to 7ka) climate in central Texas is reconstructed from variability in speleothem growth rates and isotopic compositions. Results suggest that moisture conditions in central Texas were relatively constant from the mid to late Holocene, except for a dry interval spanning 0.5 to 1.5 ka. Speleothem $\delta^{18}O$ values spike during the late Holocene dry interval (0.5 to 1.5 ka), suggesting that decreases in Pacific-derived moisture or decreased tropical storm activity might have been coincident with the prolonged dry interval. Collectively, this research improves our understanding of the baseline of the aquifer system. Existing conceptual models of the aquifer have been revised, including how recharge moves through the aquifer, the nature of interaction between conduit and diffuse parts of the aquifer, the link between the urban environment and degraded stream water quality, and the controls on groundwater on spatial and temporal scales. The response of natural and anthropogenic controls to changing climate conditions has been described, and the nature of climate variability on centennial and millennial scales has been characterized and used to gain insight into the regional dynamics governing rainfall.

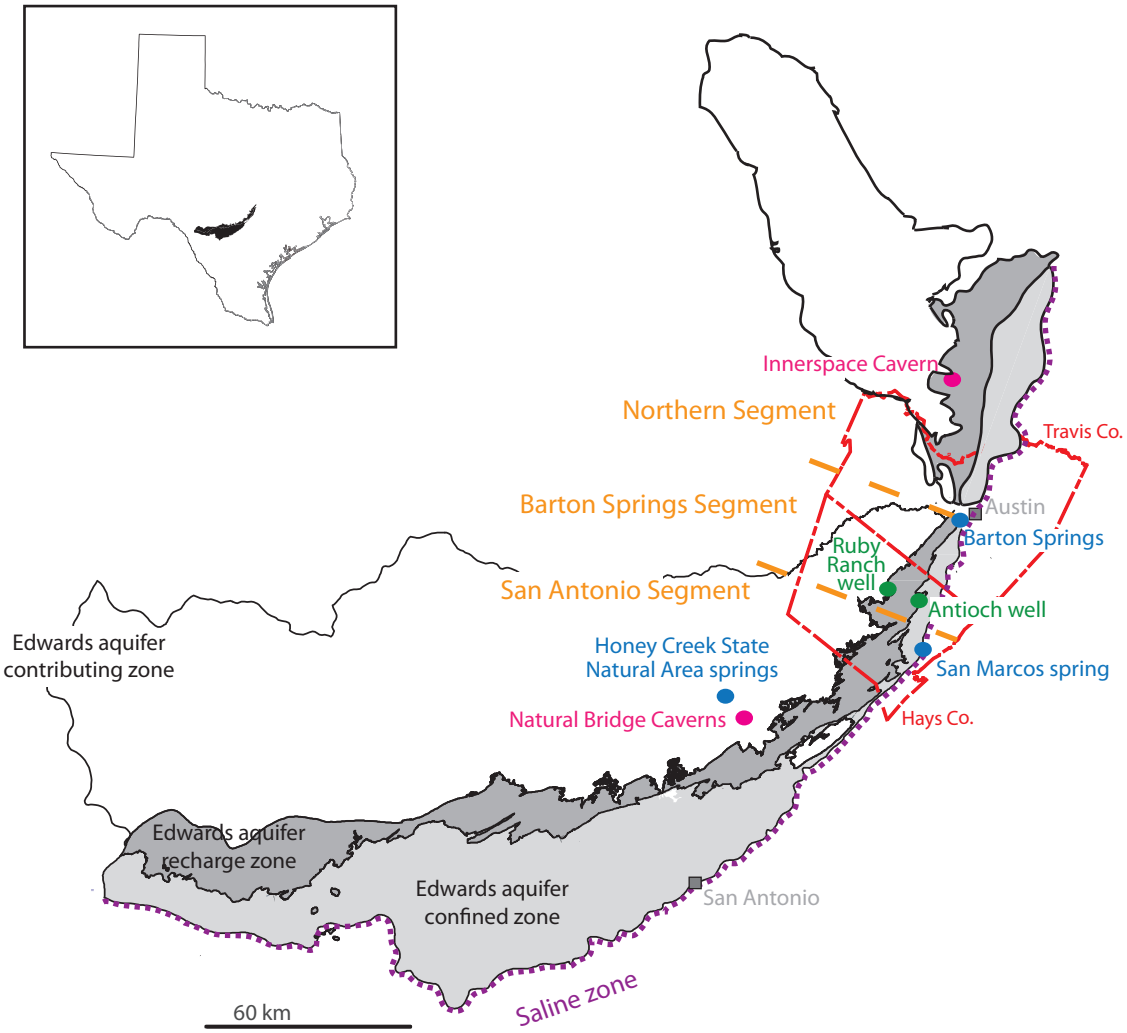

Figure 1.1 Map of the San Antonio, Barton Springs, and Northern segments of the Edwards aquifer along with sampling locations.

Chapter 2. Changes in sources and storage in a karst aquifer during a transition from drought to wet conditions

ABSTRACT

Understanding the sources and processes that control groundwater compositions and the timing and magnitude of groundwater vulnerability to potential surface-water contamination under varying meteorologic conditions is critical to informing groundwater protection policies and practices. This is especially true in karst terrains, where infiltrating surface water can rapidly affect groundwater quality. We analyzed the evolution of groundwater compositions (major ions and Sr isotopes) during the transition from extreme drought to wet conditions, and used inverse geochemical modeling (PHREEQC) to constrain controls on groundwater compositions during this evolution. Spring water and groundwater from two wells dominantly receiving diffuse and conduit flow (termed diffuse site and conduit site, respectively) in the Barton Springs segment of the Edwards aquifer (central Texas, USA) and surface water from losing streams that recharge the aquifer were sampled every 3 to 4 weeks during November 2008–March 2010. During this period, water compositions at the spring and conduit sites changed rapidly but there was no change at the diffuse site, illustrating the dual nature (i.e., diffuse vs. conduit) of flow in this karst system. Geochemical modeling demonstrated that, within a month of the onset of wet conditions, the majority of spring water and groundwater at the conduit site was composed of surface water, providing quantitative information on the timing and magnitude of the vulnerability of groundwater to potential surface-water contamination. The temporal pattern of increasing spring discharge and changing pattern of covariation between spring discharge and surface-water (steam)

recharge indicates that that there were two modes of aquifer response—one with a small amount of storage and a second that accommodates more storage.

INTRODUCTION

Karst groundwater systems are dynamic and can respond rapidly to changes in meteorologic conditions (Hess and White, 1988; Ford and Williams, 1989). Alternation of drought and wet conditions occurs commonly in semi-arid and arid regions and is predicted to intensify with ongoing climate change (Seager et al., 2007; Banner et al., 2010). Understanding the controls on groundwater compositions and vulnerability of groundwater to potential surface-water contamination during dry and wet conditions and transitions between such conditions is critical to informing land management practices and policies concerned with protecting water quality.

Variations in spring discharge and spring water compositions (referred herein as spring responses) have been used to characterize karst systems and investigate the processes that control groundwater quality. Such studies have been used to: i) characterize the general nature of karst systems along the spectrum of diffuse- vs. conduit-dominated groundwater flow (Massei et al., 2007), ii) separate recharging surface water from spring baseflow following storm events (Lakey and Krothe, 1996; Mahler and Garner, 2009; Herman et al., 2009), and iii) investigate exchange between conduit- and matrix-flow routes (Martin and Dean, 2001; Bailly-Comte et al., 2010; Gulley et al., 2011). For clarification, diffuse flow refers to flow in the matrix pore space and micro-joints or fractures of the aquifer bedrock, and conduit flow refers to flow moving through solution-widened joints, fractures, and conduits. An integrated investigation of recharging surface water, spring discharge, and groundwater can yield a more comprehensive understanding of the surface and groundwater sources, processes, and variations in flow

type that control spring and groundwater compositions than can be gained by considering only spring responses (Moore et al., 2009).

Many studies have investigated dynamics of karst systems by interpreting spring response to short-lived events (e.g., storm or flood) to develop a conceptual understanding of how surface water and groundwater move through karst systems (e.g., Smart, 1988; Desmarais and Rojstaczer, 2002; Birk et al., 2004; Florea and Vacher, 2007) and demonstrate the vulnerability of karst groundwater to surface-water contamination (e.g., Andrews, 1984; Ryan and Meiman, 1996; Mahler and Massei, 2007; Pronk et al., 2007; Heinz et al., 2009). To our knowledge, there are no studies that have assessed the geochemical response of karst groundwater to a long-term transition from drought to wet conditions and quantified the timing and magnitude of groundwater vulnerability to potential surface-water contamination during such a transition. This study investigates how the controls on groundwater compositions in a karst system evolve during the transition from a prolonged extreme drought (as defined by the Palmer Drought Severity Index; Palmer 1965) to above-average flow conditions. Groundwater geochemistry (major ions and Sr isotopes) was monitored monthly in the Barton Springs segment of the Edwards aquifer at a well receiving predominantly diffuse flow, at a well receiving predominantly conduit flow, and at Barton Springs, a spring receiving both types of flow during several months of extreme drought and during the recovery from that drought. Surface water from losing streams that provide the majority of recharge to the aquifer (surface-water recharge) also was monitored to determine the potential geochemistry of aquifer recharge. Geochemical variations, statistical analysis, and geochemical modeling were used to identify controls on groundwater compositions and quantify their evolution.

HYDROGEOLOGIC SETTING

The study site is the Barton Springs segment of the Edwards aquifer (BSE). The Edwards aquifer is developed in the extensively karstified, Cretaceous carbonates of the Edwards Group (Rose, 1972). The strata of the Edwards Group have been buried, diagenetically altered during this process, and re-exposed (Rose, 1972), making it a telogenetic karst system (vs. eogenetic) as defined by Vacher and Mylroie (2002). Telogenetic systems are characterized by secondary porosity that generally consists of conduits and fractures, and differ from younger eogenetic (pre-burial) systems, which have secondary porosity consisting of macro-void pathways throughout the matrix (Vacher and Mylroie, 2002). The hydraulic response of telogenetic systems to recharge events typically is restricted to the conduit network, and spring discharge responds immediately to discrete recharge events. In contrast, the void space of the matrix in eogenetic systems, which is enhanced relative to that of telogenetic systems, causes dampening (or even muting) of spring discharge to discrete storm events (Supplementary Data Fig. S2.1; Florea and Vacher, 2006).

The BSE extends southwest from Austin, Tex., and is bounded by the Colorado River to the north and a groundwater divide to the south (Fig. 2.1A). The Trinity aquifer underlies the BSE and extends to the south and west where strata of the Edwards Group have been removed by erosion (Rose, 1972). Barton Springs, in Austin, is the principal discharge point for the BSE, and is a culturally and historically important recreational site that is habitat for endemic and endangered species (Slade et al., 1986). The contributing zone consists of the watersheds to the west of the recharge zone (Fig. 2.1A); the majority of runoff that occurs in this zone drains via five creeks to the recharge zone (from north to south, Barton, Williamson, Slaughter, Bear, and Onion Creeks, Fig. 2.1A) (Slade et al., 1986). A saline zone bounds the aquifer along the eastern part of the BSE (Fig. 2.1A;

Abbott, 1975). The downdip limit of freshwater in the aquifer is the approximate surface defined by the 1,000-mg/L dissolved solids concentration (Perez, 1986).

Sources of recharge

The majority (~70–85%) of recharge to the BSE is surface water from losing streams (Barton, Williamson, Slaughter, Bear, and Onion) that cross the recharge zone (Fig. 2.1A), where the Edwards formation outcrops at the surface and is heavily faulted and fractured (Slade et al., 1986; Barrett and Charbeneau, 1997; Hauwert, 2009). Other sources of recharge include diffuse recharge through the soil zone and direct recharge into karst features (e.g., sinkholes and solution crevices; Fig. 2.1B). These have been estimated to account for ~15–30% of total recharge (Hauwert, 2009). Surface-water recharge along conduit flow routes has been deduced by correlations between groundwater specific conductance values and Barton Spring discharge and between groundwater specific conductance values and estimated stream-loss recharge to the BSE (Garner and Mahler, 2007). Dye traces have delineated major conduit flow routes that allow rapid (up to 12 km/day) transport of surface water to Barton Springs (Hauwert, 2009). Recharge during storms contributes pesticides such as atrazine and simazine to spring discharge (Mahler and Massei, 2007). As much as 55% of Barton Springs discharge following storms could be accounted for by recharging water from losing streams that has been rapidly (2–4 days) transported to the spring (Mahler and Garner, 2009). Previous studies have demonstrated that Edwards aquifer groundwater compositions also can be affected by mixing with water from the adjacent and underlying Trinity aquifer (Senger and Kreitler, 1984) and from the saline zone (Oetting et al., 1996).

Sr isotope tracers of hydrologic processes

Groundwater Sr isotope ($^{87}Sr/^{86}Sr$) values in the BSE generally are lower than those measured in surface water (Oetting et al., 1996; Garner, 2005; Christian et al., 2011), and can potentially be used to quantify mixing between surface and groundwater. Rainfall has low Sr concentrations relative to the Sr acquire from interaction with soils (Garner, 2005). Infiltrating water acquires its initial Sr isotope signature (~ 0.7090) from interaction with silicate minerals in soils overlying the BSE (Musgrove and Banner, 2004; Wong et al., 2011). As water interacts with the underlying carbonate bedrock, $^{87}Sr/^{86}Sr$ progressively decreases, becoming more similar to that of the Cretaceous limestone bedrock ($^{87}Sr/^{86}Sr$ ~ 0.7076) (Musgrove and Banner, 2004; Christian et al., 2011). Longer groundwater residence times and more extensive water-rock interaction with aquifer host rocks result in lower $^{87}Sr/^{86}Sr$ values (Oetting et al., 1996; Garner, 2005). Mixing of municipal water from leaking infrastructure and irrigation runoff with stream water also can result in higher surface water $^{87}Sr/^{86}Sr$ values relative to those in groundwater, because municipal water has a higher Sr isotope signature ($^{87}Sr/^{86}Sr$ ~ 0.7090) than does the Cretaceous limestone; mixing of municipal and natural water has been demonstrated to control $^{87}Sr/^{86}Sr$ values in some Austin-area streams (Christian et al., 2011).

Regional climate

The climate in the area is sub-tropical-sub-humid to semi-arid (Larkin and Bomar, 1983) with average annual rainfall of 860 mm and a range of 390 to 1370 mm (1856–2010; National Weather Service, 2012). Soils are generally thin (<20 cm) and silicate rich (Cooke et al., 2007). Meteorologic conditions in Texas tend to oscillate between extremes of wet and dry (Griffiths and Ainsworth, 1981), and the linkage of the hydrologic system to these oscillations is demonstrated by the covariation between Barton Springs discharge

and the Texas region Palmer Drought Severity Index (National Climate Data Center, 2012) (Fig. 2.2). PDSI is based on the calculation of a regional specific moisture anomaly index using a set of water balance equations, which is used to derive a drought severity value using an empirical relationship (Palmer, 1965; Alley, 1984). PDSI is a widely used drought index in the United States, despite its shortcomings that include an overly simplified water budget model, arbitrary operational procedures and designation of qualitative severity catagories, and normalization methods based on a limited spatial and temporal data set (Alley, 1985).

Transition from dry to wet conditions

The data collection interval spanned 17 months from November 2008 through March 2010, during which the Palmer Drought Severity Index (PDSI) for Texas ranged from -4.4 during a period of prolonged extreme drought to 3.2 during an extended period of well-above average rainfall (National Climate Data Center, 2012; Fig. 2.2). During November 2008–August 2009 (hereinafter the dry interval), which was preceded by 6 months of dry conditions, there was 330 mm of rainfall. Flow was intermittent or absent in the five principal recharging streams, and discharge at Barton Springs decreased from 0.82 m^3/s (29 ft^3/s) to 0.37 m/s (13 ft^3/s), approaching the historic low of 0.28 m^3/s (10 ft^3/s; U.S. Geological Survey, 2012) measured during the 1950s drought of record. During September 2009–March 2010 (hereinafter the wet interval), there was 800 mm of rainfall, and conditions generally became increasingly wetter during September 2009–March 2010. Within a month of the onset of wet conditions, the five streams flowed continuously through the end of the sampling interval and discharge from Barton Springs rebounded to average discharge 1.42 m3/s (50 ft^3/s). Discharge from Barton Springs reached 2.7 m^3/s (95 ft^3/s) prior to the end of the study (Fig. 2.3).

Results are discussed in the context of four time intervals: first (November 2008–May 2009) and second (June–August 2009) parts of the dry interval and first (September–October, 2009) and second (November 2009–March, 2010) parts of the wet interval (Fig. 2.3). Dry and wet intervals were divided on the basis of geochemical modeling results (see Section 4.5) and changes in temporal patterns of spring discharge (see Section 4.1), respectively.

METHODS

Hydrologic measurements

Daily mean rainfall was calculated as a weighted average (Theissen Polygons) of rainfall measured at six rain gages within the contributing zone of the BSE (Lower Colorado River Authority, 2011; sites 4517, 4519, 4593, 4594, 4595, 4596). Stream and spring discharge data (15-min and daily mean) was obtained from the U.S. Geological Survey (USGS) National Water Information System (U.S. Geological Survey, 2012). Following several storms, flooding of surface water over the orifice of Barton Springs precluded determination of spring discharge (Supplementary Material Table S2.1). During these intervals, the USGS estimated daily mean spring discharge by linear interpolation (oral communication, John Snatic, U.S. Geological Survey, 2011).

Daily mean total surface-water recharge to the BSE was estimated from stream flow measured at USGS streamflow-gaging stations immediately upstream from the recharge zone as described by Mahler et al. (2011). Total recharge was computed as the sum of recharge from the five streams, up to a maximum rate for Williamson, Slaughter, Bear, and Onion Creeks and using an algorithm relating stream flow to recharge for Barton Creek (Barrett and Charbeneau, 1997).

Sampling

To investigate the evolution of groundwater compositions during the project interval, groundwater from different parts of the aquifer and water from the five losing streams was sampled. Groundwater samples were collected from two wells: one that was hypothesized to receive predominantly diffuse flow (USGS station number 300453097503301; hereinafter the diffuse site) and one hypothesized to receive predominantly conduit flow (USGS station number 300813097512101; hereinafter the conduit site). The groundwater wells were hypothesized to receive predominantly diffuse and conduit flow on the basis of historical data that showed the absence of a correlation between groundwater specific conductance and estimated surface-water recharge at one well (diffuse site) and presence of a correlation at the other (conduit site) (Garner and Mahler, 2007). Water collected from these two wells was pumped from similar depths in the aquifer and from similar stratigraphic units. Spring water was collected from the main spring orifice of Barton Springs (USGS station 08155500), the principal discharge point of the BSE (Slade et al., 1986) (hereinafter the spring site). The principal discharge point of an aquifer segment integrates all the inputs and processes that occur along the aquifer flow paths (Quinlan, 1989), and Barton Springs, therefore, represents the integrated response of the aquifer system to changing meteorologic conditions. Stream water (surface-water) was collected from the five losing streams at USGS streamflow-gaging stations immediately upstream from the recharge zone (Fig. 2.1).

Samples were collected every 3 to 4 weeks during November 2008–March 2010. Routine collections of discrete samples were collected from the spring site and from stream sites by submerging bottles beneath the water surface at the centroid of flow (Wilde and others, 1999). Samples at wells were collected prior to any filtration, chlorination, or other treatment. Wells were purged prior to sample collection, as

determined by stable readings of water temperature, pH, conductivity, dissolved oxygen, and turbidity measured by a multi-parameter sonde (Wilde and others, 1999). All samples for anions (Br, Cl, F, NO_2+NO_3, SO_4), cations (Ca, Mg, K, Na, Sr), B, Si, alkalinity, and Sr isotope analysis were filtered using a 0.45-μm disc filter. While B, Br, and F are not commonly sampled in karst settings, these constituents can be useful indicators of urban influence and therefore are potentially useful in delineating groundwater mixing with stream water influenced by urbanization (Christian et al., 2011; Barrett et al., 1999). Samples for analysis of cations and Sr isotopes were acidified with HNO_3. Alkalinity was determined by manual titration and the inflection point method (Rounds, 2006).

Analytical methods

Anion and cation analyses were performed by the USGS National Water Quality Lab in Denver, Colo., using ion-exchange chromatography and inductively coupled plasma-mass spectrometry, respectively (Fishman, 1993). The median percent difference of 11 replicate analyses was less than 2.3% for each constituent. The absolute difference between cations and anions was <5% for all samples. Field blank measurements (n = 12) were below method reporting limits for all constituents except Ca, NO_2+NO_3, and Si, which each had a single blank detection of 0.01, 0.04, and 0.04 mg/L, respectively (Mahler et al., 2011). Concentrations of constituents in blank samples were 2 to 3 orders of magnitude less than concentrations measured in environmental samples (Mahler and others, 2011, p. 59-65).

Sr isotope values ($^{87}Sr/^{86}Sr$) were measured following the methods of Banner and Kaufman (1994) using a multi-collector Thermo Scientific Triton Thermal Ionizing Mass Spectrometer in the Department of Geological Sciences at the University of Texas at Austin (2α = 0.000015, where α is the standard error). The mean for all the

measurements of $^{87}Sr/^{86}Sr$ made using isotopic standard National Institute of Standards and Technology Strontium Carbonate Isotopic Standard 987 (National Institute of Standards and Technology, 2012) during the project interval was 0.710256 (2α = 0.000012, n = 59). Replicate analyses of 4 unknown samples were within 0.000009. Samples were analyzed in four sets. Sr mass in blank values associated with the first set (n=36) was 15 pg (n=2). Sr mass in blank values associated with the second (n=12) and third (n=34) sets was 430 and 23–170 pg (n=2), respectively. The highest blank value was ≤5% of the mass of sample Sr used (800 ng to 40 μg) for analysis in spring and groundwater samples. For stream-water analysis, the highest blank value was ≤16% of the mass of sample Sr loaded (~4 mL; 800 ng to 2 μg depending on concentration). The high blank values in stream-water samples were tracked to incompletely cleaned sample vials. A fourth set of analyses was done to measure replicate values (n=5) of samples measured in the second and third sets. Replicate values were within analytical uncertainty, which indicates that high blank values had a negligible impact on the measured values. The blank value associated with this fourth set of samples was 6 pg.

Statistics and Principal Components Analysis

Correlation coefficients (Pearson r) and p-values were used to evaluate the strength of linear correlations between geochemical measurements. Results with p-values less than 0.05 were considered statistically significant.

Interrelations among constituent concentrations were investigated using principal components analysis (PCA). PCA is a statistical technique that creates a new set of variables (the principal components, or factors) that are linear combinations of the original variables. New factors are created on the basis of the common variance among the original variables, with the first factor explaining the most variance and each

subsequent variable explaining less variance (Davis, 2002). The advantage of PCA is that the majority of the variance is encapsulated into one to three variables, which facilitates graphical visualization and interpretation. Input data were the major-ion concentrations in spring and groundwater samples for the project interval and the concentrations of major ions in stream-water composite samples from the wet interval (surface-water recharge was minimal to absent during the dry interval). Major-ion geochemistry of stream-water composite samples was determined on the basis of the proportion that each stream contributed to estimated total recharge. Concentration data were standardized prior to input; specific conductance (also standardized) was input as a supplementary variable.

Geochemical modeling

Inverse modeling was done using the geochemical modeling program PHREEQC (Parkhurst and Appelo, 1999), which simulates a wide variety of end-member mixing and low-temperature aqueous geochemical reactions and processes. In inverse modeling, PHREEQC calculates combinations of end member proportions and amounts (i.e., moles) of mineral and gas mole transfers that account for differences in composition between waters, within specified compositional uncertainty limits. For this study, PHREEQC was used to account for evolving spring and groundwater compositions during the transition from dry to wet conditions. Each inverse model run derived multiple possible scenarios of end-member mixing and geochemical processes that could account for user-specified (sampled) final water compositions. Models with the minimal number of mineral and gas phases (termed minimal models) were identified and reported. Five geochemical interactions were included: i) dissolution and precipitation of calcite ($CaCO_3$); ii)

dissolution of dolomite ($CaMgCO_3$), gypsum ($CaSO_4$), and celestite ($SrSO_4$); iii) consumption or loss of CO_2; iv) loss of O_2; and v) ion exchange of Ca and Na.

Possible end members (initial solutions) considered in the model were fresh Edwards groundwater, Edwards groundwater from the saline zone, recharging stream-water composites, and upland recharge. The composition of fresh Edwards groundwater (herein referred to as Edwards groundwater) was represented by groundwater collected from the conduit site at the peak of the dry interval (August 5, 2009) when no recharge was occurring. Under such conditions, water pressure in the conduit is less than that in the surrounding matrix (White, 1999), and conduits receive groundwater draining from the aquifer matrix. The composition of Edwards groundwater from the saline zone (herein referred to as saline-zone groundwater) was represented by two groundwater samples previously inferred to be predominantly influenced by saline-zone groundwater (well D-1 sampled March 19, 1993, Oetting, et al., 1996; Saint Albans well about 4 kilometers east of the study area, sampled July 13, 2009, Wierman et al., 2010). Recharging stream water was represented by the compositions of stream-water composite samples collected throughout the project interval in the five major streams that recharge the BSE. Upland recharge, surface water that directly recharges the aquifer in the recharge zone by infiltration through karst features, such as caves and sink holes, was represented by the composition of overland runoff entering a sinkhole in the Bear Creek watershed, collected as discrete samples and analyzed by the City of Austin (http://www.ci.austin.tx.us/wrequery/query_form.cfm) during May–September 2007. The area surrounding the sinkhole is undisturbed and is protected as part of a municipal groundwater-quality protection program. Median concentrations of each constituent in all the runoff samples (n=26) were used to define the geochemistry of the upland recharge. The variability in concentrations in upland runoff was small (standard deviation/mean <

0.25 for all major ions, except K) relative to the variation in concentrations between end members and variations within spring-water and groundwater samples. For modeling purposes, Edwards groundwater, saline-zone groundwater compositions, and upland recharge end members were assumed to be constant throughout the period of sample collection (i.e., the same compositions were used for all models). Changes in stream water compositions, however, were incorporated into the modeling (i.e., spring and groundwater compositions were modeled using surface water compositions measured in samples collected on the same day as the spring and groundwater samples).

Upland-recharge samples had the lowest specific conductance of all the end members, and saline-zone samples had the highest (Table 2.1). Upland recharge, Edwards groundwater, and stream water are Ca-HCO_3-type waters with similar Ca and HCO_3 concentrations. Concentrations of K+, Cl, Na, and SO_4 increase from upland recharge to Edwards groundwater to stream water. The saline zone is characterized by Na-Cl-type water, and has higher concentrations of Na, Cl, and SO_4 relative to the other sources (Table 2.1).

For each site, the available geochemical reactions were the same, but the combinations of end members were different. Groundwater at the diffuse site was modeled as a possible mixture of Edwards groundwater, saline zone groundwater, and recharging water from upgradient streams (Bear and Onion). Groundwater at the conduit site was modeled as a possible mixture of Edwards groundwater, recharging water from upgradient streams (Bear and Onion), and upland recharge. Spring water was modeled as a possible mixture of Edwards groundwater, saline-zone groundwater, and stream water from all five streams.

The user-assigned uncertainty for the final water composition (global uncertainty) and each source-water composition was 5% based on typical uncertainty of analytical

methods. In the cases where the model could not produce a result, global uncertainty was increased by integer increments up to 10%. In the rare case that model results could not be produced with a 10% global uncertainty, the uncertainty of all source-water inputs was increased by integer increments until model results could be produced.

RESULTS

Recharge and spring discharge

During the dry interval, surface-water recharge and spring discharge rates were low, although intermittent and short-lived increases following rainfall events occurred; spring discharge and surface-water (stream) recharge increased markedly during the wet interval (Figs. 3 and 4). During the first part (September–November, 2009) of the wet interval, surface-water recharge and spring discharge covaried (Fig. 2.4). Once spring discharge surpassed ~1.42 m^3/s (~50 ft^3/s), spring discharge increased in discrete steps following recharge pulses (Figs. 3 and 4). With the exception of the first month of the wet period (September 2009), specific conductance in spring water decreased by about 16 to 44 μS/cm following recharge pulses (Table S2.2).

Major ion compositions

Stream, spring, and groundwater samples were Ca-HCO_3-type waters with pH values ranging from 6.3 to 8.0 (Supplementary Fig. S2.1 and Table S2.3). Stream-water composite samples generally had high concentrations of Ca, Cl, Na, and SO_4 and low concentrations of Mg and Sr relative to groundwater (Table 2.1). Concentrations of constituents (except Sr) measured in samples collected from the diffuse site were similar to or slightly higher than those collected from the conduit site during the dry interval and similar to or lower than those at the spring site, and varied little throughout the dry and wet intervals (Fig. 2.3). Concentrations of constituents at the conduit site varied little

throughout the dry interval, and gradually evolved towards those of surface water during the wet interval. Concentrations of most constituents in spring-water samples increased slightly over the dry interval, and were similar to those of surface-water samples collected during the wet interval (Fig 3).

Sr isotope compositions

$^{87}Sr/^{86}Sr$ values in spring discharge and groundwater ranged from 0.70778 to 0.70804 (Table 2.1), which are between values measured for the Edwards Group (0.7075 to 0.7080; Koepnick et al., 1985; Christian et al., 2011) and surface water (0.70793 to 0.70818; this study). Values at the diffuse site (0.70788 to 0.70791) varied little throughout the transition from the dry interval to the wet interval (Fig. 2.3), and there was no correlation between Sr concentrations and $^{87}Sr/^{86}Sr$ values (n=5).

At the conduit site, $^{87}Sr/^{86}Sr$ values varied little and were low (0.70778 to 0.70782) relative to the diffuse site during the dry interval, and gradually increased (from 0.70778 to 0.70804) during the wet interval to values similar to those measured in surface water. There was a strong negative correlation ($r = -0.90$, $n=10$, $p<0.001$) between Sr concentrations and $^{87}Sr/^{86}Sr$ values at the conduit site. Spring water $^{87}Sr/^{86}Sr$ values also varied little during the dry interval and values (0.70790 to 0.70792) were similar to those measured at the diffuse site. As at the conduit site, $^{87}Sr/^{86}Sr$ values at the spring increased (from 0.70791 to 0.70801) during the wet interval toward values similar to those measured in surface water. There was a negative correlation ($r = -0.70$, $n=15$, $p<0.01$) between Sr concentrations and $^{87}Sr/^{86}Sr$ values in spring samples, and the correlation was stronger ($r = -0.85$, $n=9$, $p<0.01$) when only samples collected a month or more after the onset of wet conditions (Oct. 2009–Mar. 2010) were considered.

Principal Components Analysis

The first two factors identified by the PCA explain 70% of the variance in major-ion compositions measured in spring water, groundwater, and stream-water-composite samples (Fig. 2.5a). The first factor explains 46% of the variance, and is heavily weighted on B, Br, Cl, HCO_3, K, Na, and SO_4 (all positive except for HCO_3). The second factor explains 24% of the variance, and is heavily weighted on HCO_3, Mg, and Si (all negative). Two constituent groupings are evident: i) B, Br, Cl, K, and Na, and ii) HCO_3, Mg, and Si. SO_4 did not group with any other variables, and Ca, NO_3, and Sr did not strongly influence Factor 1 or 2 (Fig. 2.5a).

Three vertices are apparent when surface water, spring water, and groundwater geochemistry are viewed on the Factor 1-2 plane (Fig. 2.5b). The vertices are defined by i) groundwater sampled at the diffuse site during both the dry and wet interval and at the conduit site during the dry interval only; ii) spring water sampled during the dry interval; and iii) stream-water composites sampled during the wet interval. During the wet interval, the geochemistry of conduit-site groundwater, spring water, and stream-water composites converged towards similar scores on Factors 1 and 2 (Fig. 2.5b).

Geochemical modeling using PHREEQC

Most groundwater compositions at the diffuse site could be modeled with varying amounts of Edwards and saline-zone groundwater or stream water along with specified mineral solution reactions. The amount of saline-zone (<1%) or stream-water (0-19%) contribution to groundwater was temporally inconsistent, and most models could not balance K with global uncertainty less than 9% (Table 2.2).

Groundwater compositions at the conduit site could be modeled with varying amounts of Edwards groundwater, recharging stream water, and upland recharge along with specified mineral solution reactions. During the dry interval, groundwater

compositions could be modeled without any surface water contribution (i.e., upland recharge and stream loss) when recharge was not occurring, but required small contributions (0–6% of total) of recharging surface water, including both upland recharge and losing stream water, when recharge was occurring. The modeled proportional contribution of recharging surface water to groundwater at the conduit site increased rapidly during the first 3 months of the wet interval, and more gradually during the remainder of the wet interval (Fig. 2.6).

Variability in spring-water compositions were accounted for by varying amounts of Edwards groundwater, saline-zone groundwater, and recharging stream water, and mineral-solution reactions. During the first part of the dry interval (Nov 2008–May 2009), with the exception of one sample, the modeled contribution of recharging stream water to spring discharge was similar to the ratio of surface-water recharge to spring discharge (on the basis of measured stream and spring discharge), but was higher than that ratio during the second part of the dry interval (Jun–Aug 2009) (Table 2.2). Models with a mixture of only Edwards groundwater and a small component of saline-zone groundwater (5-6%) were geochemically feasible during this latter interval, but required higher global uncertainties to balance Mg and SO_4 (Table 2.2). During the wet interval, the modeled saline-zone contribution was small (≤1%), and an increasing amount of recharging stream water was required to account for spring-water compositions as the wet interval progressed (Table 2.2 and Fig. 2.6).

In addition to mixing, groundwater and spring water compositions were modeled with varying amounts of calcite dissolution or precipitation and Ca and Na ion exchange (Table 2.2). Models rarely involved the dissolution of dolomite and gypsum. Celestite ($SrSO_4$) dissolution was involved in all of the models of spring water and groundwater at

the diffuse site. There were no temporal patterns in the amount of mineral dissolution (or precipitation) or ion exchange at any of the sites.

DISCUSSION

Controls on spring-water and groundwater compositions under dry and wet conditions

Each site had a unique combination of controls that dictated geochemical compositions under dry and wet conditions. During the dry interval, groundwater compositions at the conduit site were dominated by mineral-solution reactions, whereas the compositions at the diffuse and spring sites were dominated by mixing of Edwards groundwater with other groundwater sources. During the wet interval, mixing of Edwards groundwater with recharging surface water was the dominant control at the conduit and spring sites, while the controls at the diffuse site were the same as during the dry interval.

During the dry interval, the geochemistry of groundwater at the conduit site was consistent with mineral-solution reactions with carbonate minerals. Concentrations of Cl, Na, SO_4, and Sr at the conduit site were low relative to those at the diffuse and spring sites, and concentrations of Ca, Mg, and HCO_3 and values of $^{87}Sr/^{86}Sr$ were static and consistent with extensive and relatively uniform interaction with Edwards aquifer bedrock (Wong et al., 2010). This supports the hypothesis that, during the dry interval, water was draining from the aquifer matrix into conduits.

Elevated concentrations of Cl, Na, SO_4, and Sr and higher values of $^{87}Sr/^{86}Sr$ at the diffuse and spring sites relative to those at the conduit site during the dry interval indicate that groundwater at these sites is a mix of Edwards groundwater and an additional source(s) or chemical reaction(s). A contribution of groundwater from the saline zone, hypothesized to occur when spring discharge is low (Senger and Kreitler, 1984; Mahler et

al., 2006), can account for elevated concentrations of Cl, Na, and SO_4. High Sr concentrations, although sometimes coincident with saline-zone influence, are not characteristic of the saline zone, and indicate an additional source to or geochemical reaction at the diffuse site. This additional source might also have contributed, to a lesser extent, to groundwater at the spring site, which had concentrations of Sr that were much lower than those at the diffuse site but higher than those at the conduit site (Fig. 2.3 and Table S2.3). $^{87}Sr/^{86}Sr$ values at the spring and diffuse sites were similar, indicating that the source of the Sr at the two sites likely was the same. A potential source is "transitional" saline-zone groundwater containing dissolved celestite ($SrSO_4$), or strontianite ($SrCO_3$) associated with fault zones, which previously has been hypothesized to be a source of high Sr concentrations in fresh groundwater (<500 μs/cm) in the Edwards aquifer (Oetting, 1995), or both.

Geochemical modeling supports the hypothesis that additional uncharacterized sources of groundwater contributed to discharge at the diffuse and spring sites during the dry interval. At the diffuse site: i) all geochemical models required the dissolution of celestite, ii) models using a mix of Edwards, saline-zone groundwater, and stream water required large global uncertainties (≥9%), iii) some compositions could not be modeled (Table 2.2), and iv) there was no temporal pattern to the groundwater compositions or to the contributions of the three sources (Table 2.2, Fig. 2.3). Thus, saline-zone groundwater and stream water likely were not sufficient end members to constrain groundwater compositions, indicating either the influence of additional end members or occurrence of more complex mineral-solution interactions than those included in the modeling. At the spring, it was necessary to include celestite dissolution in geochemical models as well as contributions of saline zone groundwater, indicating that an additional end member likely is needed to account for spring water Sr concentrations. Another

uncharacterized source (e.g., municipal recharge) might have been contributing to groundwater at the spring during the second part of the dry interval (June–August 2009). Geochemical models of spring water during the dry interval either required an unrealistically high stream-water contribution (i.e., exceeding the amount of surface-water recharge occurring), or high global uncertainties (7-10%) to balance Mg and SO_4. The saline-zone contribution to the spring varied little during the dry interval and was greater than its contribution to the diffuse site (Table 2.2), even though the spring is farther from the saline zone than is the diffuse site (Fig. 2.1). The relatively large saline-zone contribution to the spring likely is associated with a major conduit flow route that is affected by the saline zone, as demonstrated by dye traces (Hauwert et al., 2004).

During the wet interval, the geochemistry of groundwater at the conduit and spring sites reflected the large contribution from recharging stream water. The major-ion geochemistry and scores for groundwater compositions on PCA Factors 1 and 2 at the diffuse and conduit sites, which were similar during the dry interval, diverged during the wet interval, with concentrations of major ions and PCA scores at the diffuse site remaining static and concentrations and PCA scores at the conduit site becoming more similar to those of stream water (Figs. 3 and 5). The contrasting geochemical dynamics at the diffuse and conduit sites are consistent with the initial hypothesis that one site receives dominantly diffuse flow and the other receives dominantly conduit flow. Concomitantly, the major-ion geochemistry and PCA scores for spring-water samples, initially different from those at the conduit site, converged with those of groundwater at the conduit site and of stream water (Figs. 3 and 5). Concentrations of Sr at the conduit and spring sites, initially higher than that of stream water, decreased during the wet interval, and values of $^{87}Sr/^{86}Sr$ at the conduit and spring sites, initially lower than that of stream water, increased. The strong negative linear correlation between Sr

concentrations and $^{87}Sr/^{86}Sr$ values at the two sites is an additional indication that surface water was mixing with groundwater. The use of Sr concentrations and $^{87}Sr/^{86}Sr$ values in identifying the influence of surface water recharge on spring and groundwater demonstrate a novel use of Sr isotopes in this system.

Timing of vulnerability of groundwater to contamination

The quantification of the contribution of recharging stream water to groundwater is a useful descriptor of the timing and magnitude of the vulnerability of groundwater in the conduit network to contamination from the land surface. Under dry conditions, the ratio of surface-water recharge to spring discharge is a reasonable approximation of the proportional stream water contribution to spring discharge, as indicated by geochemical modeling estimates (Table 2.2). The approximation, however, is not appropriate under wet conditions, as surface-water recharge exceeded spring discharge for the majority of the wet interval but the contribution of surface water to spring discharge was less than 100% (Fig. 2.6).

Within a month of the onset of the wet interval, surface water composed more than 50% of groundwater at the conduit and spring sites (Fig. 2.6). This high contribution—which modeling indicated could be as high as 90% for some samples—continued throughout the wet interval, indicating that stream water was the dominant control on the quality of groundwater and spring discharge, not just during the storm response but also during non-storm flow conditions. By using geochemical modeling to quantify the surface-water influence on groundwater, we also quantify the vulnerability of groundwater in the conduit network to contamination from surface water.

Nature of the matrix and the conduit network

The response of the aquifer system to the transition from drought to wet conditions and the quantification of surface-water contributions to spring and groundwater at each site enable interpretations about how surface water recharges the aquifer and the connection between the matrix and conduit parts of the aquifer. The lack of geochemical response at the diffuse site to the transition from drought to wet conditions indicates either that geochemical changes within the aquifer were limited to the conduit network, or that the amount of recent recharge that entered the matrix was negligible relative to the amount of water in storage. There is evidence that exchange occurs between the aquifer matrix and conduit network in this karst system (e.g., Mahler et al., 2006) and others (e.g., Martin and Dean, 2001; Bailly-Comte et al., 2010). The results presented here indicate that water from the conduits did not flow, to a substantial extent, into the matrix in the area of the diffuse site. Alternatively, flow from the conduit to the matrix, if occurring, had a negligible effect on the matrix water geochemistry on the time scale of this study. This is consistent with previous modeling using matrix porosity, hydraulic conductivity, and specific storage values from this and other karst aquifers that has indicated that the distance to which flow from conduits penetrates the matrix is small (10^{-2} and 10^{-4} m for high and low hydraulic conductivity aquifers, respectively) and that less than 0.1% of solute moves from conduits to the matrix (Peterson and Wicks, 2005). Although this study focuses on recharge originating from stream loss, the static geochemical nature of the diffuse site indicates that the amount, or the geochemical effect, of diffuse recharge to the aquifer also was negligible with respect to the area supplying water to the diffuse site.

Filling of the conduit network with recent recharge was neither spatially uniform nor complete. The proportion of spring discharge and groundwater at the conduit site

composed of surface-water recharge, as determined by geochemical modeling, did not increase at the same rate or follow the same temporal pattern (Fig. 2.6). These differences might result from i) a non-uniform spatial distribution of recharge, ii) a difference in size of recharge area contributing to the sites, iii) differences in groundwater travel times, or iv) a combination of these. Further, at no time was the conduit network filled entirely with recharging stream water. Even though estimated recharge exceeded spring discharge from October 2009 to the end of the study, geochemical modeling indicated that some component of Edwards groundwater was needed to account for spring water and conduit site groundwater compositions throughout the wet interval (Fig. 2.6). The persistence of Edwards groundwater in the conduit network might result from variations in conduit geometry (Raeisi et al., 2007) or the occurrence of eddies in flow through irregular and rough fractures and conduits (Cardenas et al., 2007). Regardless of the mechanism, the persistence of Edwards groundwater indicates that complete piston flow is not occurring, i.e., recharging water does not push all existing water in the conduits ahead and out through the spring orifice.

Two modes of aquifer response

The spring hydrograph transitioned from one characteristic of a telogenetic karst system to that characteristic of an eogenetic system as the wet interval progressed from the first part to the second, indicating a change in mode of aquifer response to increasingly wetter conditions. In the first mode (spring discharge < ~1.5 m^3/s; 50 ft^3/s), spring discharge was correlated with surface-water recharge (Fig. 2.4), indicating that increasing amounts of surface-water recharge resulted in increasing hydrostatic pressure and greater spring discharge. There were discrete responses in spring discharge shortly following recharge events, which is characteristic of telogenetic karst systems

(Supplementary Fig. S2.1; Florea and Vacher, 2006). Because recharge events occurred frequently, however, recharged water did not completely empty from the system before the next event, and there was an overall gradual increase in spring discharge (Fig. 2.6).

The second mode (spring discharge > ~1.5 m^3/s; 50 ft^3/s) of aquifer response was characterized by greater storage of recharging water, which resulted in a hydrograph that was characteristic of a eogenetic karst system (Supplementary Fig. S2.1; Florea and Vacher, 2006). Spring discharge responded to discrete recharge events, but recessions were shortened when spring discharge plateaued in December 2009–January 2010 and in March–April 2010 (Fig. 2.6). Stepped increases and plateaus in spring discharge and a lack of covariation between spring discharge and surface-water recharge during each of these steps (Figs. 4 and 6) indicates that: i) large pulses of recharge resulted in discrete increases in hydrostatic pressure that were maintained at a constant level until another pulse of recharge entered the system, and ii) there was greater storage of recharging water during the second mode relative to the first.

Florea and Vacher (2006) demonstrated how spring response hydrographs vary between aquifer systems on the basis of physical properties (e.g., porosity and permeability) inherent to the formation of the karst system (i.e., eogenetic vs. telogenetic). The transition of the BSE from a mode characteristic of an telogenetic system to one characteristic of a eogenetic system indicates that spring response hydrographs can vary within the same aquifer on the basis of changes in hydrologic conditions. Such a transition within an aquifer has not, to the knowledge of the authors, been previously discussed. This transition could reflect an enhancement of communication between matrix and conduit parts of the aquifer (i.e., a more eogenetic-like porosity and permeability system) at higher aquifer water levels. The chemostatic nature of the matrix demonstrated in this study (Fig. 2.3) and a previous study (Garner

and Mahler, 2007), however, suggests that the contribution of recharging surface water to the matrix part of the aquifer is negligible. Furthermore, recharging surface water would have to enter the matrix in a way that did not substantially affect hydrostatic head pressure as long intervals (up to 4 weeks) of constant spring discharge were observed.

A series of perched, restricted reservoirs could result in intervals of nearly constant spring discharge despite the occurrence of recharge consistently entering the system at rates that exceed spring discharge. Previous numerical modeling of conduit flow in aquifers with reservoirs illustrates that input to a reservoir drained by conduits that are small relative to the reservoir (Fig. 2.7) results in just this phenomenon: a immediate increase in spring discharge followed by a gradual, nearly zero-slope decline (Halihan and Wicks, 1998) and a hydrograph similar to that recorded by this study during the second mode of aquifer response. Alternatively, spring hydrograph plateaus could result from the activation of overflow routes; plateaus in a well hydrograph have previously been deduced to result from the piracy of water from the primary conduit (Ray, 1997). If water was pirated from the spring, then surface-water recharge should grossly exceed spring discharge on long (multiple years) time scales. Slade et al. (1986) reported a long-term balance between recharge from streams and spring discharge for the BSE, which indicates that piracy is likely not occurring.

Although the aquifer likely has two modes of physical response to changing meteorologic conditions, it is less evident that there are different modes of geochemical response. The decrease of spring-water specific conductance following recharge pulses (Table S2.2 and Fig. 2.6) indicates that the spring discharge responses resulted, in part, from the rapid transit of recently recharged surface water, as opposed to resulting solely from a pressure pulse associated with increases in hydrostatic pressure, and that this occurred during both modes of aquifer response. The decrease of specific conductance of

spring water was similar throughout most of the wet interval (Table S2.2 and Fig. 2.6), with the exception of the first month of the wet interval (Sept 2009). A high amount of dilution during this first month, relative to those during the remainder of the wet period, likely reflects the combined effects of a conduit network that initially was relatively empty and low stream-water specific conductance during the first month of the wet interval (September 2009) relative to that during the rest of the wet interval (Table S2.3). The contribution of surface water to spring water increased gradually throughout the entire wet interval, although the rate of increase was constant during the first mode and fluctuated during the second mode (Fig. 2.6). These differences could reflect differences in the modes of aquifer responses, or sampling that did not occur at sufficiently frequency to capture temporal variations in response.

CONCLUSIONS

A 17-month study of groundwater geochemistry in the Barton Springs segment of the Edwards aquifer during the transition from a prolonged and extreme drought (PDSI = -4.4) to an extended period of well-above average rainfall (PDSI = 3.2) provides insight into the geochemical and physical response of this karst system to changes in meteorologic extremes. A striking divergence of geochemical compositions in response to changing meteorologic conditions at groundwater sites receiving conduit and diffuse flow provides a clear illustration of the dual nature of groundwater flow in a karst system. Quantification of the contribution of surface water to spring discharge demonstrates that the majority of spring water and groundwater was composed of surface water within a month of the onset of wet conditions, and provides an improved understanding of the timing and magnitude of vulnerability of groundwater quality to surface-water quality. The documentation of the physical aquifer response to extreme changes in meteorologic

conditions was key in identifying two modes of aquifer response: a first mode (spring discharge <~1.5 m^3/s; 50 ft^3/s) with a spring discharge hydrograph that is characteristic of telogenetic systems, and a second mode with enhanced storage (perhaps in a series of perched, constricted reservoirs) resulting in a spring discharge hydrograph characteristic of eogenetic systems. These conclusions were enabled by the use of a comprehensive set of approaches (real-time monitoring, Sr isotopes, PCA, and geochemical modeling), and integration of the results from multiple sites representing different parts of the aquifer.

Table 2.1 Geochemical compositions (median, range) of spring and groundwater, surface water composites, and model source water inputs

		Specific Conductance (µS/cm)	HCO_3 (mg/L)	Ca (mg/L)	Mg (mg/L)	Sr (mg/L)	Si (mg/L)	K (mg/L)
Observed spring, groundwater, and stream water composite compositions								
Spring								
Dry	n=15 (4)	711 (689-735)	320 (304-348)	84 (78-87)	25 (23-27)	3.1 (2.8-3.5)	12 (11-12)	1.7 (1.6-1.8)
Wet	n=7 (15)	667 (656-689)	312 (296-323)	92 (80-99)	20 (18-22)	1.01 (0.60-2.8)	10 (10-11)	1.5 (1.2-1.8)
Diffuse site (groundwater)								
Dry	n=13 (2)	608 (603-610)	341 (326-349)	82 (76-87)	26 (24-26)	9.6 (8.8-10.4)	11 (10-12)	1.2 (1.2-1.3)
Wet	n=7 (3)	608 (605-618)	344 (340-348)	79 (74-84)	25 (24-26)	9.5 (8.8-10.2)	11 (11-12)	1.2 (1.2-1.3)
Conduit site (groundwater)								
Dry	n=13 (3)	584 (581-587)	342 (320-358)	84 (78-89)	25 (23-26)	0.43 (0.40-0.45)	12 (10-13)	0.9 (0.9-1.0)
Wet	n=7 (7)	590 (587-606)	308 (280-350)	87 (82-99)	18 (15-24)	0.29 (0.20-0.45)	10 (8.7-12)	1.1 (0.9-1.4)
Stream composites								
Dry	n=12 (12)[c]	701 (602-736)	247 (201-272)	75 (67-90)	21 (18-23)	0.32 (0.27-0.33)	10 (7-17)	2.5 (2.0-3.2)
Wet	n=7 (35)[c]	588 (458-634)	247 (148-267)	80 (52-85)	18 (13-19)	0.26 (0.23-0.30)	8 (6-8)	1.6 (1.1-2.5)
Model source water inputs								
Saline zone[d]		2,944	282	175	106	14	15	13
Saline zone[e]		3,280	220	143	87	21	15	15
Upland Recharge[f]		472	240	87	10.5	0.05	--	0.33
Edwards groundwater[g]		581	347	83	25	0.44	12.18	0.90

	Na (mg/L)	SO_4(mg/L)	Cl (mg/L)	NO_3+NO_2 (mg/L)	F (mg/L)	B (mg/L)	Br (mg/L)	$^{87}Sr/^{86}Sr$
Observed spring, groundwater, and stream water composite compositions								
Spring								
Dry	27 (24-32)	40 (37-43)	42 (38-47)	1.5 (1.5-1.6)	0.35[b]	0.087 (0.076-0.10)	0.35 (0.31-0.40)	0.70792 (0.70790-0.70792)
Wet	16 (14-20)	46 (33-53)	30 (25-33)	1.5 (1.4-1.8)	0.24 (0.19-0.33)	0.060 (0.048-0.077)	0.19 (0.16-0.29	0.70796 (0.70791-0.70801)
Diffuse site (groundwater)								
Dry	7.0 (6.7-7.7)	27 (27-28)	12 (12-12)	1.2 (1.2-1.3)	0.40[b]	0.043 (0.036-0.049)	0.07 (0.05-0.10)	0.70791 (0.70791-0.70791)
Wet	6.9 (6.4-7.2)	28 (27-28)	13 (12-13)	1.2 (1.1-1.2)	0.43 (0.41-0.46)	0.044 (0.039-0.047)	0.08 (0.06-0.09)	0.70789 (0.70788-0.70790)
Conduit site (groundwater)								
Dry	6.5 (6.0-7.7)	14 (13-15)	11 (11-11)	1.1 (1.1-1.2)	0.19[b]	0.036 (0.031-0.041)	0.07 (0.05-0.09)	0.70781 (0.70778-0.70782)
Wet	8.0 (6.0-10)	32 (12-48)	17 (10-24)	1.3 (1.2-2.4)	0.16 (0.12-0.18)	0.040 (0.033-0.049)	0.09 (0.07-0.12)	0.70794 (0.70778-0.70804)
Stream composites								
Dry	33 (27-41)	63 (46-77)	56 (50-69)	0.06 (<0.02-0.17)		0.11 (0.089-0.20)	0.21 (0.14-0.40)	0.70806 (0.70796-0.70814)
Wet	16 (13-22)	59 (48-78)	36 (26-42)	0.89 (0.20-0.98)	0.16 (0.14-0.19)	0.058 (0.045-0.095)	0.14 (0.11-0.15)	0.70803 (0.70793-0.70818)
Model source water inputs								
Saline zone[d]	342	491	512	< 0.02	3.7	--	--	--
Saline zone[e]	393	596	533	< 0.02	3.8	--	--	--
Upland Recharge[f]	2.5	5.43	2.8	0.75	0.05	0.03	0.15	--
Edwards groundwater[g]	6.2	13	11	1.15	0.19	0.04	0.09	--

[a] = number of major ion samples, (number of $^{87}Sr/^{86}Sr$ samples); [b]n=1; [c]n for all stream water 87Sr/86Sr analyses
[d]Data from Oetting et al., 1996 (well D-1 sampled Mar 19, 1993)
[e]Data from Saint Albans well sampled July 13, 2009 (Wierman et al., 2010)
[f]Data from City of Austin (http://www.ci.austin.tx.us/wrequery/query_form.cfm)
[g]Groundwater sampled from conduit site (USGS station 300813097512101) on August 5, 2009; F^- value from water sampled on August 26, 2009

Table 2.2 Geochemical modeling results for diffuse, conduit, and spring sites

Diffuse	% of groundwater comprised of			Calcite (mols)	Dolomite (mols)	Gypsum (mols)	Ca^{2+} exchange (mols)	Na^{+} exchange (mols)	Celestite (mols)	Minimal, total models	Global model uncertainty (%)	Constituents requiring uncertainty increase	Stream Recharge Bear & Onion (m^3/s)
	Edwards ground-water	Saline zone	Stream (Bear & Onion)										
Dry interval													
28-Jan-09	99.2	0.8	-	-1.32e-4	9.3e-6	0	4.3e-5	-8.6e-5	1.1e-4	1, 6	10	K^+	0.00
6-Apr-09	*	*	*	*	*	*	*	*	*		10	K^+	0.01
27-Apr-09	*	*	*	*	*	*	*	*	*		10	K^+	0.05
13-May-09	*	*	*	*	*	*	*	*	*		10	K^+	0.01
5-Aug-09	99.4	0.6	-	-3.14e-5	0	0	4.0e-5	-8.1e-5	9.4e-5	1, 8	9	K^+	0.00
Wet interval													
23-Sep-09	86-87	0	12-14	0 to 3.9e-6	0 to 1.1e-4	0 to 2.4e-5	0 to 6.6e-7	-1.3e-6 to 0	9.6e-5	4, 94	5		0.68
14-Oct-09	89-90	0	10-11	-7.1e-5 to 0	0 to 3.2e-5	0	0 to 1.4e-5	-2.8e-5 to 0	9.6e-5	9, 16	9	K^+	0.53
4-Nov-09	*	*	*	*	*	*	*	*	*	*	10	K^+	0.46
2-Dec-09	81-85	0	14-19	-9.1e-5 to 9.6e-5	0 to 8.4e-5	0	0 to 2.5e-5	-5.9e-5	1.1e-4	30, 42	9	K^+	0.98
5-Jan-10	99.3	0.7	0	-3.8e-5 to 0	0 to 1.1e-5	0	4.7e-5	-9.4e-5	1.0e-4	3, 9	10	K^+	1.23
2-Feb-10	99.2	0.08	0	-6.4e-5	0	0	6.7e-5	-1.2e-4	9.8e-5	3, 5	9	K^+	4.16
2-Mar-10	85-99	0.7-0.9	0-14	-4.7e-5 to 2.9e-5	0	0	4.5 to 5.1e-5	-1.0e-4 to -8.9e-5	9.9e-5	7, 14	10	K^+	3.84

Conduit	% of groundwater comprised of			Calcite (mols)	Dolomite (mols)	Gypsum (mols)	Ca^{2+} exchange (mols)	Na^{+} exchange (mols)	Celestite (mols)	Minimal, total models	Global model uncertainty (%)	Constituents requiring uncertainty increase	Stream Recharge Bear & Onion (m^3/s)
	Edwards ground-water	Upland Recharge	Stream (Bear & Onion)										
Dry interval													
28-Jan-09	100	-	-	3.5e-5	0	2.7e-6	-4.5e-6	9.0e-6	-	1, 16	6	SO_4^{2-}, Sr^{2+}	0.00
12-Mar-09	96	3	1	-5.0e-5	0	0	-8.9e-6	-1.8e-5	-	1, 44	5		0.05
22-Apr-09	100	0	0	-3.5e-5	1.8e-5	0	-3.4e-6	-6.7e-6	-	1, 48	5		0.01
13-May-09	94	5	1	1.0e-4	0	0	-2.5e-6	5.0e-6	-	1, 119	5		0.01
15-Jul-09	100	-	-	3.3e-5	0	4.2e-6	1.6e-6	-3.2e-6	-	1, 16	5		0.00
Wet interval													
23-Sep-09	98	2	-	2.29e-5	0	0	2.3e-6	-4.7e-6	-	1, 7	6	all	0.67
14-Oct-09	46	33	21	0 to 9.5e-5	0	0	0 to 2.3 e-5	0 to -4.6e-5	-	4, 4	9	K^+	0.53
4-Nov-09	10	30	60	0 to -1.2e-4	0 to 7.6e-7	0	0 to 1.8e-5	0 to -3.5e-5	-	8, 8	5		0.46
2-Dec-09	27-30	12-14	58-59	-2.0e-4 to 0	-	4.6 to 6.9e-5	2.4 to 3.0e-5	-6.1 to -4.8e-5	-	4, 4	6	K^+	0.98
5-Jan-10	13-26	11-19	63-69	-9.7e-5 to 0	-	-	0 to 1.3e-5	-2.5e-5 to 0	-	14, 20	5		1.23
2-Feb-10	8-13	32-34	56-60	-9.8 to 1.2e-5	0	0	-4.1e-6 to 0	0 to 8.3e-6	-	8, 8	5		1.46
2-Mar-10	7-15	21-25	63-69	0 to 9.1e-5	0 to 4.2e-5	0	-4.7e-6 to 0	0 to 9.4e-6	-	9, 13	5		3.84

Spring	% of groundwater comprised of			Calcite (mols)	Dolomite (mols)	Gypsum (mols)	Ca^{2+} exchange (mols)	Na^{+} exchange (mols)	Celestite (mols)	Minimal, total models	Global model uncertainty (%)	Constituents requiring uncertainty increase	Stream recharge (m^3/s)	Spring discharge (m^3/s)	Recharge/ Discharge (%)
	Edwards ground-water	Saline zone	Stream (Bear & Onion)												
Dry interval															
17-Dec-08	90	5	5	2.6e-6	0	0	-1.0e-4	2.1e-4	2.1e-5	1,4	6	SO_4^{2-}	0.03	0.54	5.8
7-Jan-09	85	4	11	-6.0e-5	0	0	-2.8e-5	5.6e-5	2.3e-5	1, 2	7	SO_4^{2-}	0.05	0.54	9.5
28-Jan-09	88	5	8	-9.5e-5	0	0	-4.0e-5	8.0e-5	2.1e-5	1,2	5		0.05	0.51	10
18-Feb-09	84	4	12	5.9e-5	0	0	-1.3e-4	2.6e-4	2.8e-5	1, 4	7	SO_4^{2-}	0.11	0.48	24
1-Apr-09	74	3	23	-1.5e-5 to 0	0	0	-1.4e-4	2.3e-4	2.6e-6	4, 4	8	SO_4^{2-}	0.10	0.54	19
22-Apr-09	49	0	51	1.1e-4	0	0	1.2e-4	2.4e-4	2.5e-5	1, 29	9	K^+, SO_4^{2-}	0.15	0.54	27
13-May-09	81	4	16	0 to 1.3e-4	0	0	-6.7e-5	1.3e-4	2.2e-5	7, 10	5		0.08	0.45	17
2-Jun-09	57-67	1-2	30-42[1]	0 to 1.0e-4	0	0	-7.0 to -5.0e-5	1.0 to 1.4 e-5	2.7e-5	2, 22	5		0.05	0.45	11

Table 2.2 Geochemical modeling results for diffuse, conduit, and spring sites

	95	5	-	-1.2e-4	0	0	-6.3e-6	1.2e-5	-1.9e-5	1, 16	8	Mg^{2+}, $SO4^{2-}$	0.00		
24-Jun-09	71	3	25[!]	2.2e-4	0	0	-6.4e-5	1.3e-4	2.6e-5	1, 22	5		0.02	0.45	4.8
	95	5	-	3.5e-5	0	0	-2.2e-5	4.5e-5	1.9e-5	1, 32	7	Mg^{2+}, $SO4^{2-}$			
15-Jul-09	69	3	28[!]	-2.3e-5	0	0	-6.3e-5	1.3e-4	2.9e-5	1, 8	5		0.003	0.42	0.7
	94	6	-	-2.1e-4	0	0	1.5e-5	-3.1e-5	2.1e-5	1, 8	10	Mg^{2+}, $SO4^{2-}$			
5-Aug-09	69-84	4-5	11-27[!]	-4.2 to 0	0	0	-5.5e-5 to 0	0 to 1.1e-4	2.5 to 2.8e-5	3, 14	5		0.001	0.40	0.2
	94	6	-	-1.6e-4	0	0	-4.9e-5	9.7e-5	2.2e-5	1,8	7	SO_4^{2-}			
Wet interval															
23-Sep-09	67	1	32	0 to 7.2e-5	0	0	-7.5e-5	1.5e-4	2.6e-5	2,6	8	SO_4^{2-}, Sr^{2+}	0.76	1.22	63
14-Oct-09	49	0	51	-9.9e-5 to 8.0e-5	0	0	0 to 3.2e-5	-6.4e-5 to 0	8.6e-6	12, 12	10	Mg^{2+}	2.63	1.67	160
4-Nov-09	41-48	0	53-60	0 to 7.6e-5	0	0 to 8.8e-5	-7.9e-6 to 1.8e-5	-3.6e-5 to 1.6 e-5	4.1e-6	32, 32	5		2.10	1.47	140
2-Dec-09	24-47	0-1	52-76	0 to 2.0e-4	0 to 4.2e-5	0 to 9.9e-5	-2.2 to 4.3e-5	-8.6e-5 to 4.3e-5	2.0 to 4.2e-6	34, 37	5		6.80	1.78	380
5-Jan-09	26-53	0-1	45-73	0 to 2.7e-4	0 to 7.8e-5	0 to 7.2e-5	-2.5 to 2.5e-5	-4.9e-5 to 5.0e5	2.6 to 5.1e-6	38, 42	5		2.66	2.01	130
2-Feb-10	11-16	0	83-88	0 to 7.2E-5	0	0	-2.1e-5 to 0	0 to 4.2e-5	3.6e-6	8, 8	5		7.22	2.24	320
2-Mar-10	29-37	1	66-71	0 to 1.6e-4	0	0 to 6.2e-7	0 to 2.0e-5	-4.0e-5 to 0	1.6 to 2.3e-6	9, 9	5		6.37	2.58	250

* could not be modeled

"-" not included in model

[!]exceeds percentage of recharge relative to discharge

Supplimentary Table S2.1. Storms resulting in disruption of 15-min spring discharge measurements

Recharge pulse	Onset of flooding	Spring discharge before flooding	End of flooding	Spring discharge after flooding
1st part of wet interval		(m^3/s)		(m^3/s)
1	9/12/09 15:15	1.33	9/14/09 11:15	1.16
2	9/22/09 2:30	0.85	9/23/09 15:45	1.08
3	no flooding			
4	10/9/09 7:45	1.16	10/11/09 15:00	1.39
5	10/21/09 7:00	1.33	10/24/09 0:15	1.30
6	10/26/09 20:45	2.38	10/27/09 8:15	2.46
2nd part of wet interval				
7	11/8/09 15:00	1.42	11/10/09 9:15	1.47
8	11/21/09 2:30	2.04	11/27/09 1:45	1.70
9	no flooding			
10	1/16/10 10:45	2.27	1/17/10 23:45	2.27
11	1/29/10 15:00	2.27	2/1/10 17:45	2.24
12	2/4/10 9:45	2.41	2/9/10 11:30	2.46

Supplementary Table S2.2. Spring specific conductance response to recharge pulses

		Stream water recharge (m^3/s)				Spring response			
		initial	max	pulse	recovery (5 days after max)	initial discharge (m^3/s)	specific conductance (µs/cm@ 25!C) initial	max	response
1st part of wet interval									
1	12-Sep-09	0.00	2.69	2.69	0.01	0.62	722	609	-113
2	22-Sep-09	0.01	2.55	2.54	0.28	0.82	699	640	-59
3	29-Sep-09	0.23	8.50	8.26	0.76	0.99	689	-	-
4	9-Oct-09	0.68	3.37	2.69	1.19	1.16	680	636	-44
5	22-Oct-09	1.56	10.14	8.58	2.80*	1.33	696	660	-36
6	26-Oct-09	1.95	14.19	12.23	4.30	1.27	701	673	-28
2nd part of wet interval									
7	8-Nov-09	1.76	10.19	8.44	2.52	1.42	693	677	-16
8	20-Nov-09	1.76	13.76	12.01	4.50	1.44	686	661	-25
9	1-Dec-09	3.23	12.66	9.43	4.22	1.84	682	662	-20
10	16-Jan-10	3.82	14.19	10.36	7.11	1.98	679	641	-38
11	29-Jan-10	5.27	14.19	8.92	7.22*	2.21	678	645	-33
12	3-Feb-10	7.02	14.19	7.16	13.85	2.27	670	637	-33

*prior to next storm (<5days)

"-" no data

basesd on 15-minute data from U.S. Geological Survey (http://waterdata.usgs.gov/tx/nwis/si)

Supplementary Table S2.3. Geochemical data for surface, spring, and groundwater

Date	Specific conductance (µS/cm)	pH	HCO_3 (mg/L)	Ca (mg/L)	Mg (mg/L)	Sr (mg/L)	Na (mg/L)	K (mg/L)	Cl (mg/L)	SO_4 (mg/L)	F (mg/L)	Br (mg/L)	Si (mg/L)	B (mg/L)	NO_3 + NO_2(mg/L)
Barton Spring Main															
dry															
25-Nov-08	704	7.0	323	85	26	2.87	26	1.64	40	38		0.31	11.1	0.08	1.50
17-Dec-08	711	7.2	330	86	26	2.98	28	1.65	42	39		0.34	12.1	0.08	1.56
7-Jan-09	702	7.1	311	86	26	3.03	25	1.66	40	38		0.32	11.9	0.08	1.51
28-Jan-09	710	7.2	314	83	26	2.97	26	1.64	41	39		0.34	11.4	0.08	1.47
18-Feb-09	711	6.9	321	87	26	3.49	32	1.75	41	40		0.39	11.4	0.09	1.53
1-Apr-09	704	7.0	321	83	23	3.14	28	1.73	41	40		0.33	11.2	0.08	1.55
22-Apr-09	689	6.8	309	84	24	2.85	24	1.81	38	37		0.34	12.2	0.09	1.45
13-May-09	713	6.9	326	85	25	2.96	26	1.59	41	40		0.34	11.5	0.09	1.46
2-Jun-09	717	7.0	326	85	25	3.06	26	1.71	42	39		0.34	11.8	0.09	1.45
24-Jun-09	725	6.8	348	82	26	3.14	27	1.76	44	42		0.38	11.7	0.09	1.50
15-Jul-09	733	6.8	317	78	24	3.39	28	1.66	46	42		0.38	10.5	0.09	1.49
5-Aug-09	735	6.8	317	83	26	3.37	29	1.79	47	43		0.40	11.7	0.10	1.48
26-Aug-09	733	6.7	316	86	27	3.52	30	1.76	47	43	0.35	0.37	11.5	0.10	1.46
wet															
23-Sep-09	656	7.0	306	80	20	2.79	20	1.79	32	33	0.33	0.29	11.0	0.08	1.41
14-Oct-09	657	6.8	313	99	19	1.10	14	1.69	25	44	0.26	0.16	10.8	0.07	1.68
4-Nov-09	687	7.0	313	99	22	0.73	16	1.57	29	53	0.19	0.16	10.4	0.06	1.77
2-Dec-09	663	7.1	296	95	21	0.75	15	1.53	30	53	0.23	0.16	10.3	0.06	1.46
5-Jan-10	689	7.2	318	90	22	0.81	15	1.25	33	53	0.21	0.19	10.0	0.06	1.51
2-Feb-10	668	7.2	315	89	18	0.60	14	1.23	28	45	0.20	0.17	10.1	0.05	1.49
2-Mar-10	667	7.1	323	89	20	0.65	14	1.23	29	42	0.23	0.19	10.5	0.05	1.63
Diffuse site (groundwater)															
dry															
25-Nov-08	603	7.4	344	83	26	9.39	7.1	1.31	12	27		0.07	12.1	0.04	1.19
17-Dec-08	610	7.3	345	84	26	9.07	7.7	1.25	12	27		0.05	12.1	0.04	1.24
7-Jan-09	608	7.2	326	85	26	9.53	7.0	1.28	12	27		0.06	11.4	0.04	1.23
28-Jan-09	610	7.2	333	82	26	10.38	6.9	1.22	12	27		0.08	11.1	0.04	1.20
26-Feb-09	609	7.1	344	76	25	9.71	7.5	1.29	12	28		0.10	10.9	0.04	1.21
6-Apr-09	608	7.2	342	79	25	10.35	7.0	1.26	12	28		0.05	11.3	0.04	1.26
27-Apr-09	607	7.1	349	87	26	9.74	6.8	1.26	12	27		0.06	11.6	0.05	1.16
13-May-09	607	7.0	342	83	26	9.70	7.1	1.27	12	27		0.07	11.4	0.05	1.16
4-Jun-09	608	7.1	343	82	26	9.62	6.9	1.20	12	27		0.06	11.6	0.05	1.19
24-Jun-09	607	6.9	340	80	26	9.43	6.8	1.22	12	27		0.07	11.5	0.05	1.19
15-Jul-09	610	6.9	335	77	24	10.17	6.7	1.21	12	27		0.07	10.2	0.04	1.20
5-Aug-09	607	7.0	342	82	25	8.81	6.9	1.18	12	27		0.08	11.4	0.05	1.23
26-Aug-09	607	7.0	344	82	26	9.31	6.8	1.22	12	28	0.40	0.08	11.3	0.05	1.21
wet															
28-Sep-09	613	6.5	347	79	26	8.79	7.0	1.22	13	28	0.46	0.07	11.2	0.04	1.16
14-Oct-09	607	7.0	346	84	25	9.65	7.0	1.18	12	28	0.41	0.07	10.9	0.05	1.19
4-Nov-09	608	6.8	344	80	26	9.65	7.2	1.25	12	27	0.43	0.06	11.1	0.04	1.12
2-Dec-09	607	7.2	348	81	26	10.25	7.2	1.25	13	28	0.41	0.08	11.8	0.04	1.23
5-Jan-10	612	7.2	344	77	26	9.62	6.6	1.19	13	28	0.44	0.07	11.7	0.05	1.25
2-Feb-10	618	7.2	342	74	24	9.16	6.4	1.16	13	27	0.42	0.08	11.6	0.05	1.22
2-Mar-10	605	7.2	340	75	25	9.22	6.6	1.22	13	27	0.44	0.09	11.8	0.04	1.25
Conduite site (groundwater)															
dry															
19-Dec-08	584	7.0	341	86	23	0.40	6.5	0.90	11	13		0.06	10.3	0.03	1.14
7-Jan-09	584	7.1	330	88	25	0.41	6.3	0.93	11	13		0.06	11.7	0.03	1.12
28-Jan-09	586	7.0	335	86	25	0.40	6.4	0.91	11	14		0.05	12.1	0.03	1.06
18-Feb-09	584	7.0	347	89	25	0.43	7.7	0.96	11	14		0.07	12.2	0.04	1.11
11-Mar-09	586	7.2	326	82	24	0.43	6.7	0.93	11	14		0.06	11.9	0.03	1.13
1-Apr-09	583	7.0	345	82	24	0.45	6.7	0.95	11	14		0.05	11.8	0.04	1.13
22-Apr-09	584	7.0	341	83	26	0.43	6.5	0.96	11	14		0.06	12.6	0.04	1.07
13-May-09	585	6.7	358	83	24	0.42	6.4	0.89	11	14		0.07	11.9	0.04	1.05
2-Jun-09	587	6.6	349	85	25	0.43	6.3	0.91	11	15		0.06	12.3	0.04	1.10
24-Jun-09	584	6.3	320	81	25	0.43	6.0	0.89	11	14		0.08	12.2	0.04	1.11
15-Jul-09	582	6.7	351	78	24	0.41	6.2	0.90	11	14		0.07	10.9	0.03	1.13
5-Aug-09	581	6.7	347	83	25	0.44	6.2	0.90	11	13		0.07	12.2	0.04	1.15
26-Aug-09	582	6.6	358	83	26	0.44	6.1	0.87	11	13	0.19	0.09	12.1	0.04	1.11
wet															
23-Sep-09	587	7.0	350	82	24	0.45	6.0	0.87	10	12	0.18	0.08	12.3	0.04	1.15
14-Oct-09	590	6.7	322	99	16	0.30	6.0	1.13	13	22	0.12	0.07	11.5	0.04	2.44
4-Nov-09	605	6.6	293	93	17	0.26	9.0	1.36	19	43	0.14	0.09	10.1	0.04	1.83
2-Dec-09	593	7.3	280	86	18	0.31	10.0	1.41	22	48	0.16	0.11	9.5	0.05	1.30
5-Jan-10	606	7.2	292	85	19	0.31	9.8	1.12	24	47	0.18	0.12	8.7	0.04	1.22
2-Feb-10	569	7.2	305	82	15	0.20	7.2	0.95	16	25	0.17	0.08	9.6	0.04	1.31
2-Mar-10	577	7.3	312	85	16	0.22	8.1	0.97	18	27	0.17	0.10	9.8	0.03	1.35
Stream Water Composites															
dry															
25-Nov-08	713	7.6	272	85	21	0.30	34	2.55	56	62		0.21	10.2	0.11	0.02
17-Dec-08	736	7.8	268	90	23	0.33	38	2.52	58	71		0.26	10.0	0.10	0.04
7-Jan-09	713	7.6	252	87	23	0.33	32	2.49	55	74		0.17	8.0	0.09	0.15
28-Jan-09	713	7.8	255	89	23	0.31	33	2.35	55	74		0.22	7.3	0.09	0.07
18-Feb-09	691	8.0	242	83	21	0.33	36	2.32	55	77		0.14	6.9	0.09	0.09
12-Mar-09	564	7	186	66	17	0.28	24	2.27	42	64		0.13	7.1	0.07	0.19
1-Apr-09	650	7.2	229	75	19	0.32	32	2.21	53	72		0.16	7.9	0.09	0.17
22-Apr-09	634	7.4	216	71	19	0.28	29	2.11	52	63		0.15	8.9	0.11	0.09
13-May-09	602	6.6	201	67	18	0.27	27	1.97	50	60		0.18	9.5	0.11	0.06
2-Jun-09	692	7.7	234	76	20	0.30	33	2.66	60	61		0.22	11.6	0.15	0.06
24-Jun-09	687	7.6	235	74	20	0.31	34	2.72	58	56		0.23	13.9	0.15	0.03
15-Jul-09	710	7.8	245	72	19	0.32	36	2.81	63	52		0.39	14.2	0.14	0.01
5-Aug-09	725	7.7	251	74	21	0.32	41	3.15	69	46		0.40	17.2	0.19	0.03
wet															
23-Sep-09	458	6.3	148	52	13	0.23	20	2.46	36	52	0.14	0.15	8.4	0.09	0.20
14-Oct-09	634	6.8	221	85	18	0.27	22	2.02	42	78	0.16	0.14	7.9	0.08	0.56
4-Nov-09	614	6.6	247	82	19	0.26	20	1.73	39	62	0.15	0.15	7.5	0.07	0.94
2-Dec-09	588	7.2	251	82	19	0.30	16	1.58	32	59	0.17	0.13	7.9	0.06	0.89
5-Jan-10	610	7.2	229	79	19	0.29	16	1.16	36	63	0.17	0.14	6.3	0.06	0.80
2-Feb-10	581	7.3	267	80	17	0.24	13	1.12	26	48	0.15	0.11	6.9	0.05	0.98
2-Mar-10	569	7.6	264	77	17	0.25	13	1.12	26	49	0.19	0.12	6.4	0.04	0.96

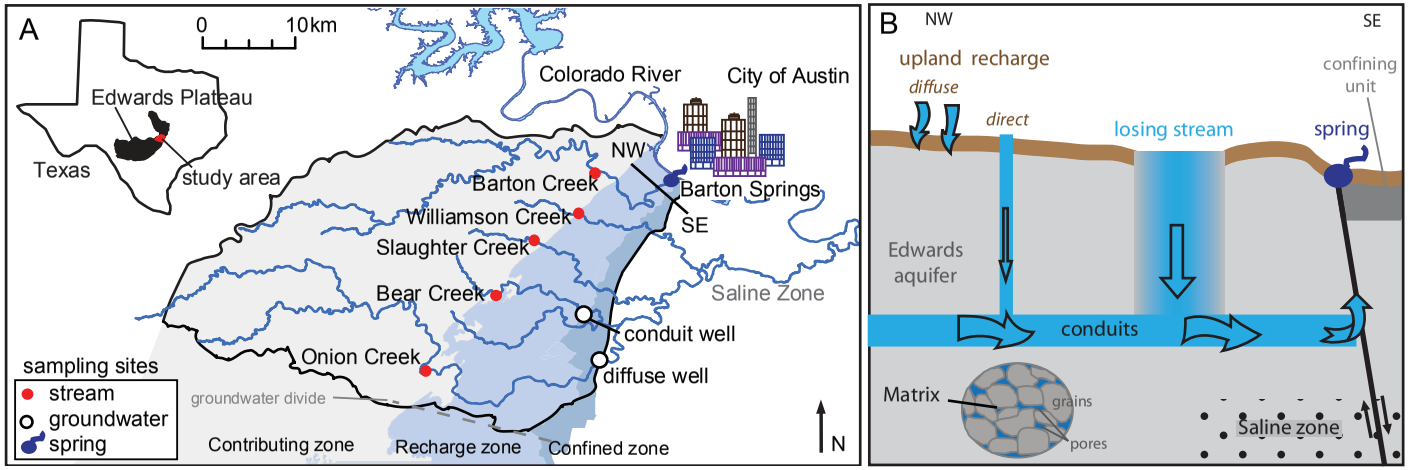

Figure 2.1. A) The Barton Springs segment of the Edwards aquifer and sampling site locations. "NW-SE" indicates line of section shown in B. B) Cross-sectional schematic of the hydrogeologic setting illustrating possible recharge and groundwater flow sources that might affect groundwater compositions.

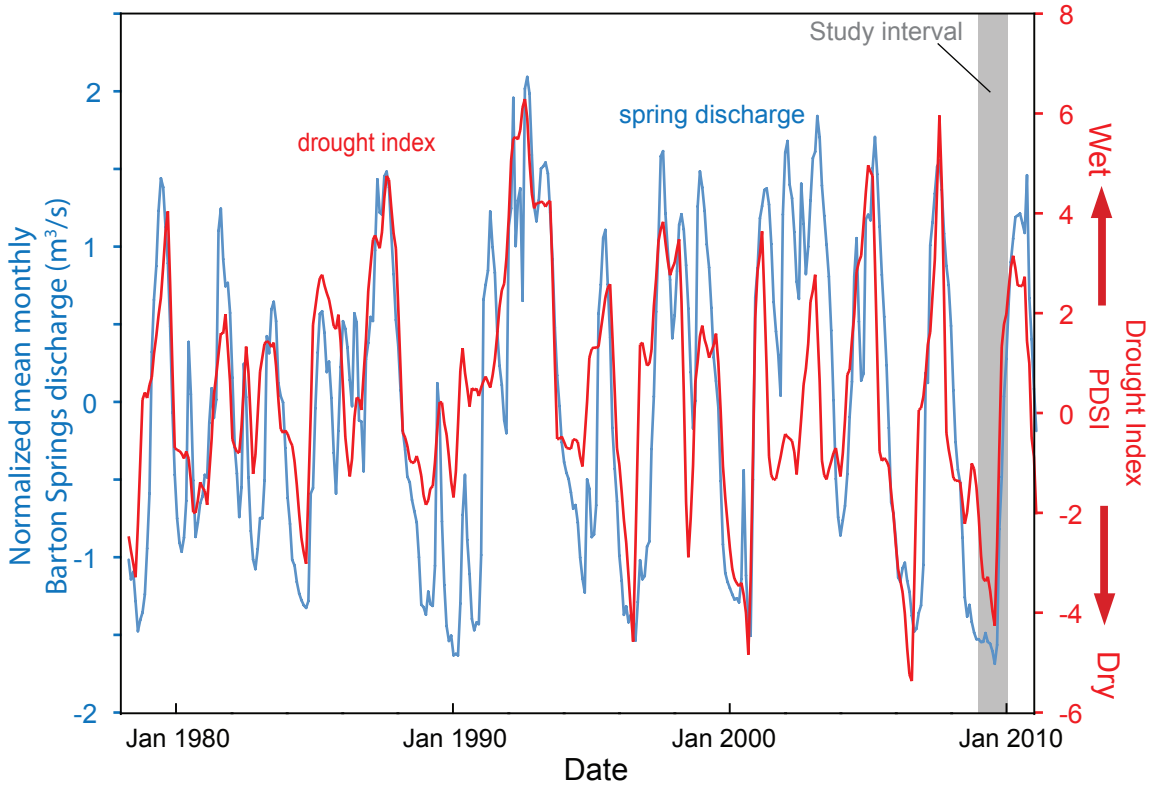

Figure 2.2. Normalized monthly average discharge at Barton Springs (black) and the 3-month regional drought index for Texas (red; PDSI) from 1978 to 2011. The grey bar indicates the interval for which sampling occurred.

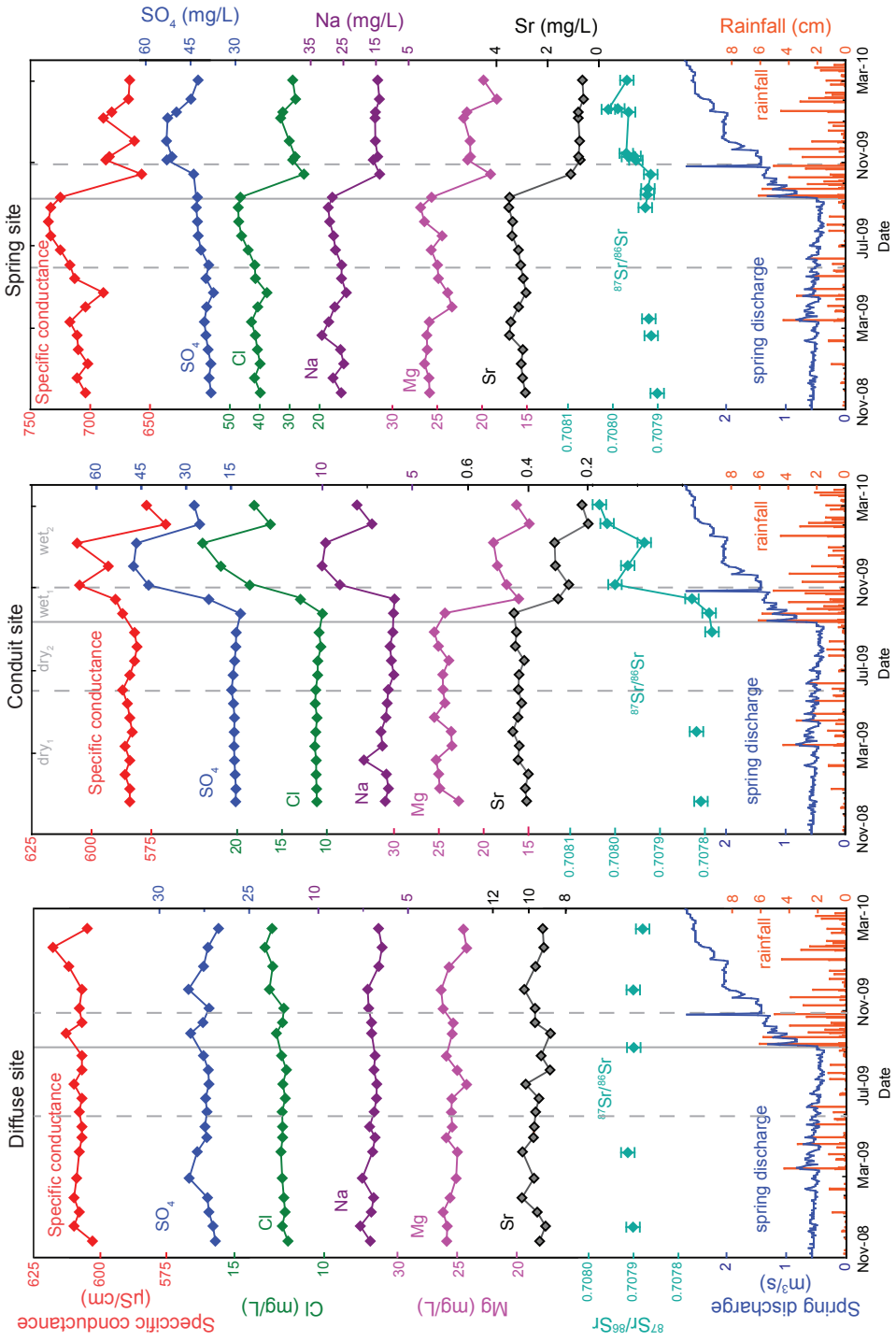

Figure 2.3. Groundwater and spring specific conductance, major ion, and $^{87}Sr/^{86}Sr$ values for the project interval and spring discharge and daily rainfall. Solid (dashed) grey bars indicate the division between the (first and second parts of) dry and wet interval. Note differences of y-axis scales among sites for some constituents.

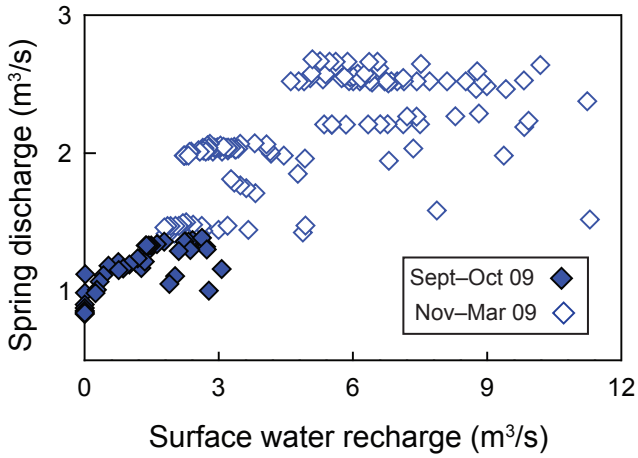

Figure 2.4. The relation between stream recharge and spring discharge for the first (Sept to Oct 2009) and second (Nov 2009 to Mar 2010) parts of the wet interval.

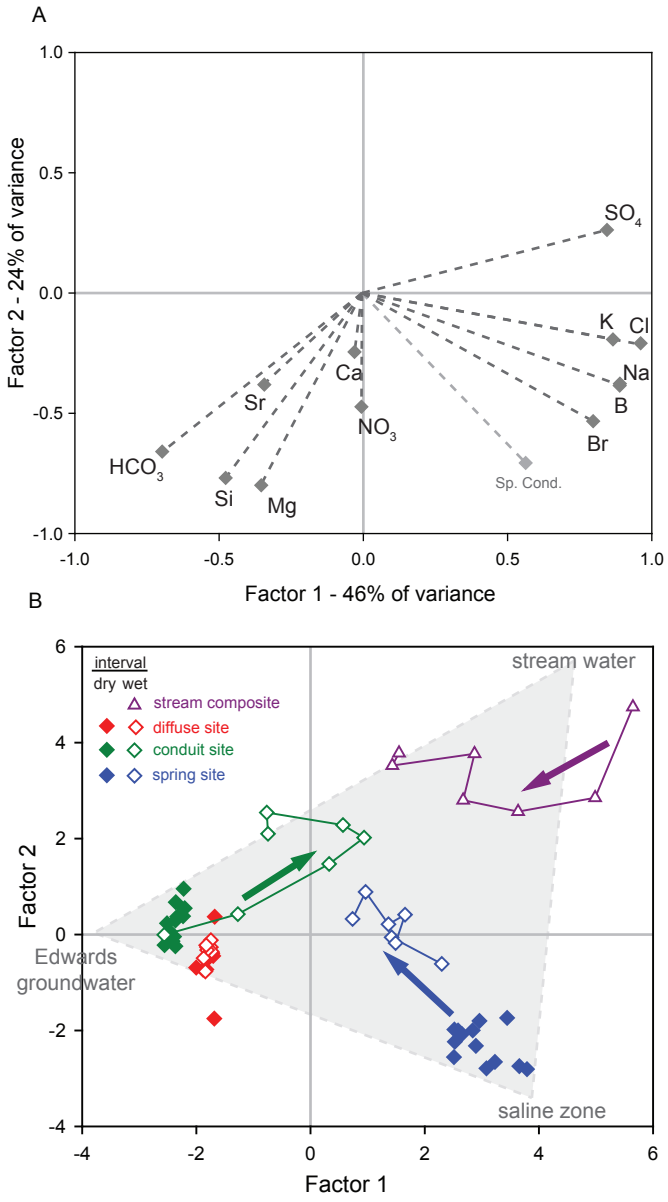

Figure 2.5. A) Principal components (PC) 1 and 2 weightings for each constituent. The percentage of variance explained for by each factor is indicated. B) Evolution through the wet and dry periods of spring and groundwater geochemistry in the PC1-PC2 plane.

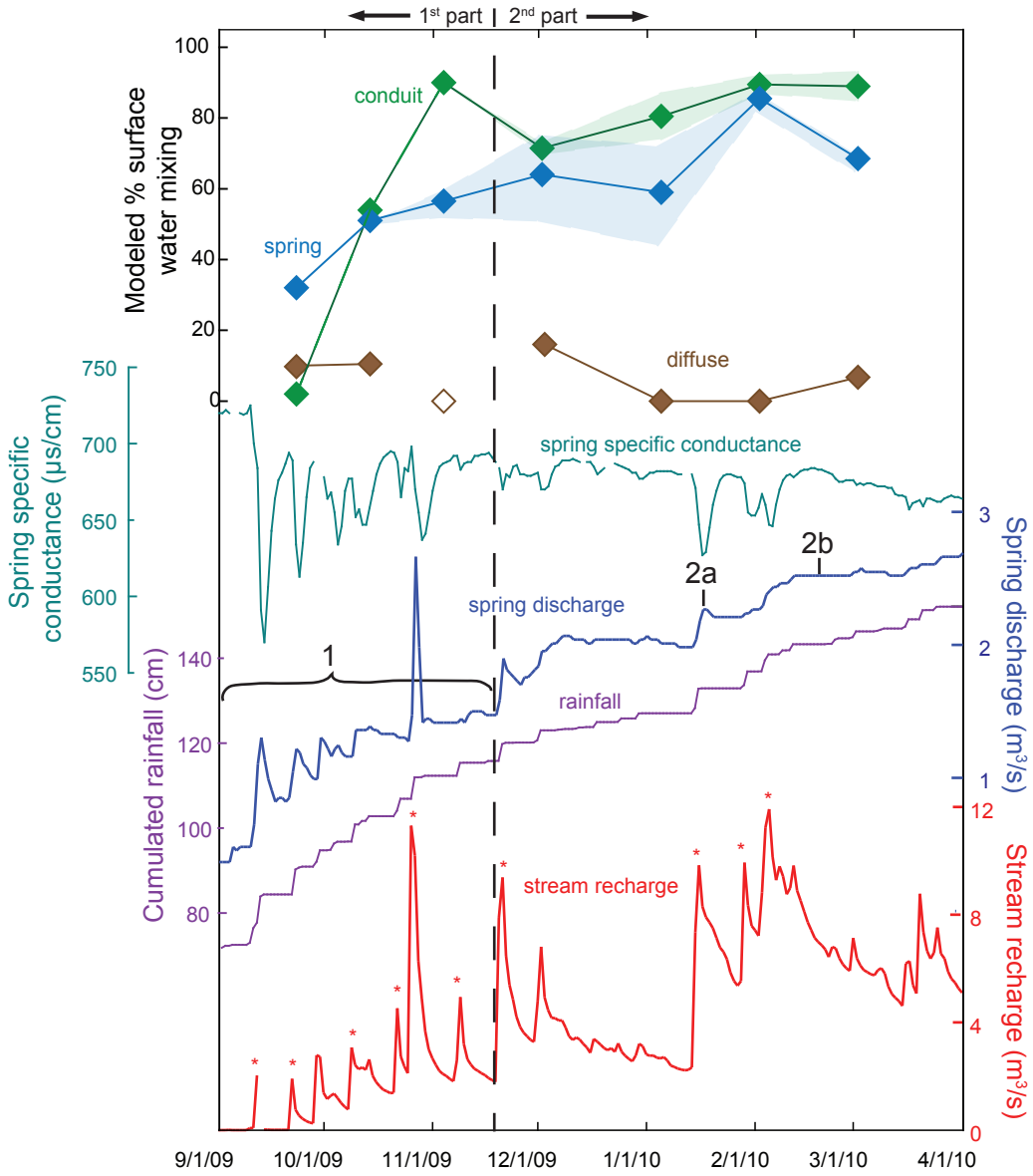

Figure 2.6. Time series for the wet interval. Shown are modeled surface-water contribution (median and range) to spring and groundwater (empty symbol represents a composition that could not be modeled), specific conductance in Barton Springs, Barton Springs discharge, cumulative daily rainfall, and estimated stream recharge. Labeled parts of spring discharge are detailed in Fig. 2.7. Asterisks indicate recharge pulses for which peak discharge was estimated by linear interpolation because flooding precluded discharge measurement.

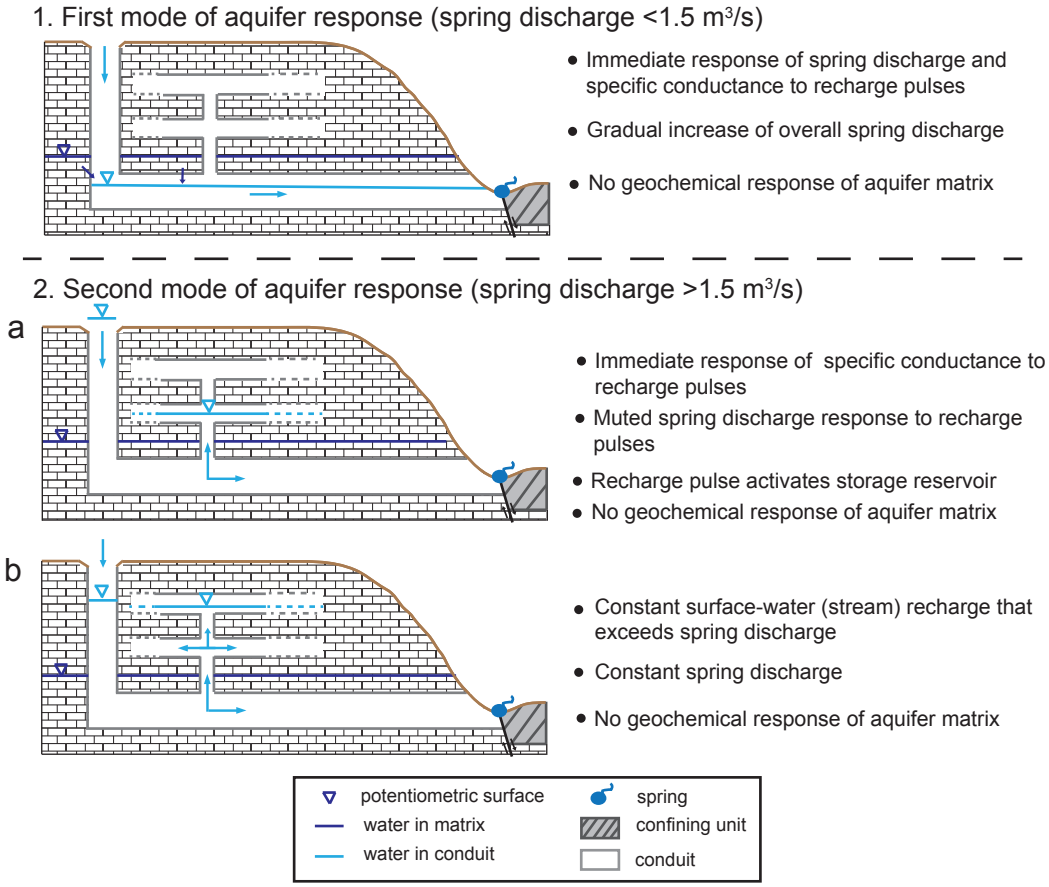

Figure 2.7. Conceptual diagram illustrating the first and second modes of aquifer response. 1, 2a, and 2b refer to parts of spring discharge hydrograph shown in Fig. 2.6.

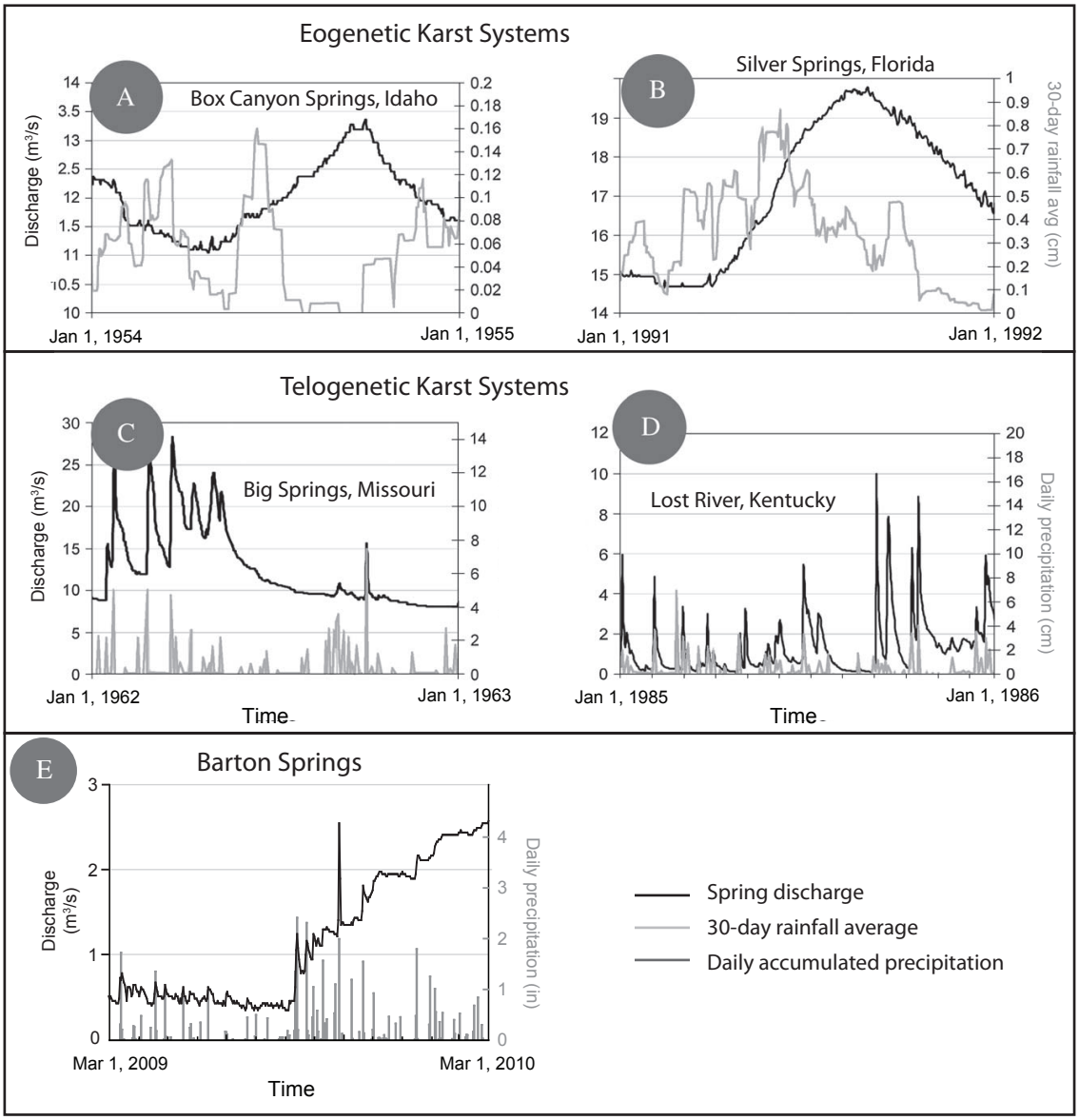

Supplementary Figure S2.1. Comparison of characteristic hydrographs from eogenetic (A & B) and telogenetic (C&D) karst systems to Barton Springs hydrograph (E). Figure modified from Florea and Vacher, 2006.

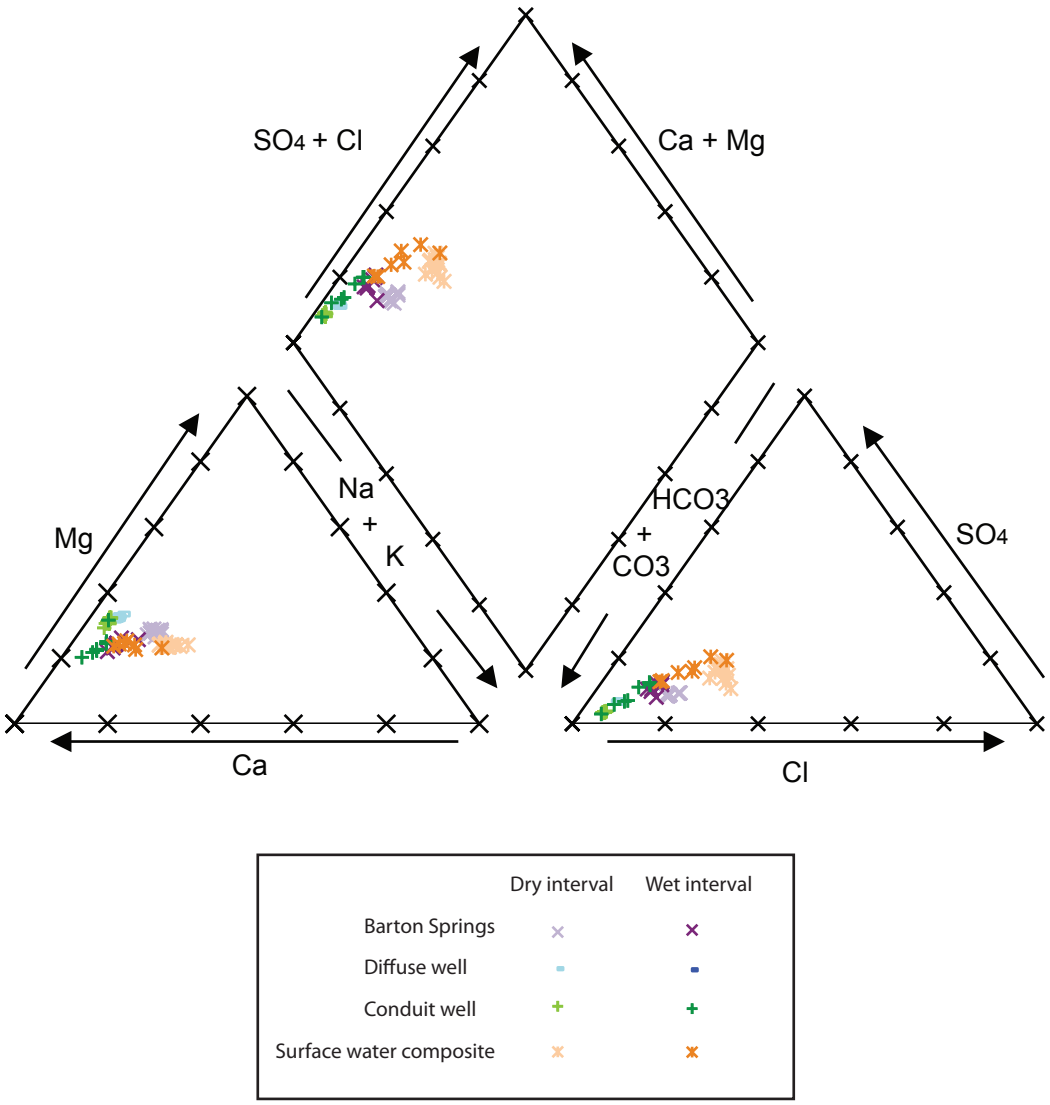

Supplementary Figure S2.2. Piper diagram of geochemical compositions of spring water, groundwater, and surface water composites for dry and wet intervals.

Chapter 3. Investigating influence of wastewater on stream-water compositions using geochemical modeling and mass balance approaches, central Texas

ABSTRACT

The association between high densities of urban land use in watersheds and high concentrations of anthropogenic constituents in corresponding streams is well documented. There are fewer studies, however, that delineate and quantify specific sources and processes responsible for degraded water quality in urban environments. This study investigates the controls on stream-water compositions in five streams that contribute the majority of recharge to an underlying aquifer in central Texas. Comparison of stream-water collected every 3 to 4 weeks during November 2008–March 2010 with 25 years of historical data (1975-2000) documents increases in stream-water specific conductance and concentrations of Cl, Na, and SO_4 over time. Geochemical modeling of fluid mixing and mineral-solution reactions indicate that stream-water compositions cannot be accounted for by natural sources and processes. Instead, models require mixing of natural sources with anthropogenic sources (i.e., municipal drinking water, wastewater, and/or septic leachate). Anthropogenic sources, however, likely contribute substantial amounts of *solutes* to streams indirectly, rather than water *volume* as indicated by i) unrealistic volumes of anthropogenic sources required to account for stream-water compositions at high discharges, and ii) constant stream-water constituent concentrations relative to large changes in discharge. The lack of dilution of stream-water constituent concentrations with higher stream flow indicates that solute fluxes to streams increase with discharge, and reflects the transport of anthropogenic solutes that accumulated in the shallow subsurface by overland and seepage flow. This study has implication for land management practices as it suggests that current practices of disposing of treated

wastewater effluent is impacting stream water quality, especially in areas where streams directly recharge aquifers.

INTRODUCTION

There is a well-documented association between urban environments and degraded stream-water quality, as evidenced by higher specific conductance values and nutrient, bacteria, and pollutant concentrations (e.g., Wang and Yin, 1997; Holland et al., 2004; Schoonover et al., 2005). Many studies have focused on identifying watershed characteristics, such as land use (e.g., Tong and Chen, 2002; Williams et al., 2005), proportion of impervious cover (e.g., Arnold and Gibbons, 1996; May et al., 1997; McMahon and Cuffney, 2000), density of various types of urban infrastructures (e.g., storm water drains, septic system density; Hatt et al., 2004; Mahler et al., 2011a), or socio-economic factors (e.g., Tu et al., 2007; Hong et al., 2009; Pfeifer and Bennett, 2011), that best account for spatial or temporal differences in stream water compositions. While correlations provide predictive information about where or when a stream might be adversely affected by its surrounding urban environment, they do not always identify the mechanistic basis for understanding the cause of degradation (e.g., Booth et al., 2004).

Quantitative approaches that delineate the sources and/or processes responsible for higher specific conductance and constituent concentrations in urban environments relative to those in more pristine areas or time periods are necessary to further understand the sources and processes that cause degradation of water quality. In northern U.S. regions, where winter application of road salt is common, mass-balance approaches have been used to demonstrate accumulation of Cl and Na within watersheds and to discriminate between Cl and Na from road salt and wastewater and from natural sources (e.g., Kelly et al., 2008; Novotny et al., 2009). Geochemical and isotopic fluid-mixing

models also have been used to quantify municipal water contribution to stream-water and groundwater compositions (e.g., Yang et al., 1999; Vazquez-Sune et al., 2010; Christian et al., 2011). Mass-balance approaches provide first-order estimates of solute inputs and exports, and the differences between inputs and exports are commonly attributed to changes in storage without presentation of additional evidence to support such assumptions. With this method, there is no validation that estimated source-water inputs can account for observed water compositions. On the other hand, fluid-mixing models provide scenarios of the *proportions* of source-water mixing that can account for measured geochemical and isotopic compositions, but provide no verification that specified source-water contributions (i.e., volumes) are feasible. These models generally assume that infinite volumes of each source-water type are available. In this study, a mass-balance approach is combined with geochemical modeling of fluid mixing and mineral-solution reactions to investigate the sources and processes influencing stream-water compositions.

We investigate controls on water compositions in streams that provide the majority of recharge to an underlying karst aquifer — the Barton Spring segment of the Edwards (BSE) Aquifer—for several reasons. Karst terrains are generally vulnerable to potential contamination from surface water because karst features (e.g., caves, sink holes, stream swallets) allow water to directly infiltrate and bypass natural mechanisms that can attenuate contaminants. Previous studies in karst landscapes have demonstrated that the diffuse recharge of treated wastewater effluents can affect karst aquifer groundwater compositions (Katz et al., 2009; Katz et al., 2010). In the BSE, increased NO_3 stream-water concentrations in this area have been attributed to increasing septic system density and permitted land application of treated domestic wastewater effluent (TLAP) (Mahler et al., 2011a). Understanding the sources and processes that control stream-water

compositions is especially pertinent for informing wastewater management practices, as direct discharge of treated wastewater effluent to streams was recently (2009) permitted in the contributing zone of the BSE aquifer (Fig. 3.1) (Cottingham, 2009).

Although nutrient concentrations and the presence of pharmaceuticals and personal-care products in water are common focuses of studies characterizing the effect of treated effluent on aquatic systems (e.g., Carey and Migliaccio, 2009; Musolff et al., 2009), here we use major- and trace- (Sr, Br, and B) ion geochemistry to attempt to quantify and understand the mechanisms by which wastewater sources influence water compositions. HCO_3, Ca, Mg, Na, Cl, and SO_4 are common identifying species of wastewater influence, although exact constituent concentrations in and geochemical fingerprints of wastewater can vary among settings because of site-specific urban and hydrogeologic characteristics (Barrett et al., 1999). We focus on Na, Cl, and SO_4 because of the prevalence of HCO_3, Ca, and Mg in carbonate settings,

In this study, stream-water compositions were measured during November 2008–March 2010 in five streams. We found median concentrations of SO_4 and Cl that exceeded water-quality standards (Texas Commission on Environmental Quality, 2012) in some of the streams, and a comparison of 2008–2010 compositions to historical (pre-2008) measurements indicated that stream-water constituent concentrations have increased over time. Geochemical fluid mixing and water-rock interaction modeling was used to quantify possible natural and anthropogenic source-water contributions to stream water, and these results were compared with mass balance estimates of solute inputs and exports. We find that wastewater sources likely can account for increasing concentrations of stream-water solutes, and that the delivery of the wastewater solutes to streams is indirect. Wastewater solutes likely accumulate in the shallow subsurface (soil and epikarst zone) and are transported to streams by seepage and overland flow.

Hydrogeologic Setting

In central Texas, the BSE is a Sole Source Aquifer for about 60,000 people (Barton Springs Edwards Aquifer Conservation District, 2012) and sustains a large spring complex (Barton Springs) that is culturally and historically important and that provides habitat for the endangered Barton Springs Salamander (*Eurycea sosorum)* (City of Austin, 2012a). The majority of recharge (~70-85%) to the aquifer occurs by water loss through the beds of five streams— Barton, Williamson, Slaughter, Bear, and Onion Creeks (Fig. 3.1) (Slade et al., 1986; Hauwert, 2008). Limestone units of the Cretaceous Edwards Group and Georgetown Limestone formation, through which the Edwards Aquifer is recharged, outcrop at the surface in the middle and lower parts of the watersheds of the five streams (hereinafter, the recharge zone) (Fig. 3.1). The Cretaceous-age Glen Rose Limestone, Hensel Sand, and Cow Creek Limestone formations, which are older than the Edwards Group, outcrop in the upper parts of the watersheds of the five streams (hereinafter, the contributing zone) as a result of Miocene-age faulting (Rose, 1972). Watersheds of the five streams range in size and stage of urban development (Fig. 3.1 and Table 3.1), and urban development has increased rapidly in the contributing zone since 2000 as evidenced by a rapid increase in wastewater infrastructure (Mahler et al., 2011a). The project area lies on the boundary between semi-arid and sub-humid climates, and transitions from drought to wet conditions are common (Larkin and Bomar, 1983). Stream flow is intermittent and flashy, and maximum annual peak discharge ranges from 135 m^3/s (4,750 ft^3/s) for Williamson Creek to 753 m^3/s (26,600 ft^3/s) for Barton Creek (1975-2010) (U.S. Geological Survey, 2012).

The sampling period, which was preceded by 6 months of dry conditions, spanned drought and wet conditions during which the Palmer Drought Severity Index (PDSI) ranged from -4.4 to 3.2 (National Climate Data Center, 2012). The PDSI represents the

intensity of dry and wet periods on the basis of monthly temperature, precipitation, and soil-water holding capacity (Palmer, 1965). There was no flow in two streams and intermittent flow in three streams during November 2008–August 2009 (hereinafter, the dry period). Conditions became progressively wetter during September 2009–March 2010 (hereinafter, the wet period), and all streams had sustained flow within a month of the onset of wet conditions (Fig. 3.2).

METHODS

Sample collection and analysis

To characterize stream-water compositions and assess how they change in response to hydrologic conditions, grab samples of stream water were collected every 3 to 4 weeks (hereinafter, routine samples), stream flow permitting, from the five streams during November 2008–March 2010. Water was collected at the U.S. Geological Survey (USGS) gauging station located nearest to the upstream end of the recharge zone (Fig. 3.1). Routine samples, however, do not represent stream base flow because stream flow results from recent rainfall events. Because of intermittent or absent stream flow during the dry interval, there were a smaller number of routine samples collected during the dry period than during the wet period at all the stream sites except Barton Creek. Samples also were collected at stream sites in response to three storm events (hereinafter, storm samples) using auto-samplers, and flow-weighted composites were analyzed for the rising and falling limb of each storm hydrograph. Details of standard sampling methods are presented in Mahler et al. (2011b) and Wong et al. (2012). Water samples were analyzed for major and trace ions to aid in characterizing spatial and temporal variations in stream water compositions, assess evapo-concentration processes, enable the geochemical modeling of stream-water compositions, and inform estimates of solute

exports. Hydrogen (δD) and oxygen ($\delta^{18}O$) isotopic compositions were analyzed to assess the evapo-concentration processes.

Anion and cation analyses were done by the USGS National Water Quality Laboratory using ion-exchange chromatography and inductively coupled plasma-mass spectrometry, respectively (Fishman, 1993). The charge balance was <5% for all samples. The median relative percent difference for 11 replicate analyses was less than 2.3% for each constituent. Constituent concentrations in field blanks (n = 12) were less than method reporting limits for all constituents except Ca, for which concentrations in blank samples were 3 orders of magnitude less than concentrations measured in environmental samples (Mahler et al., 2011b). Stable isotope (δD and $\delta^{18}O$) values were measured in the Department of Geological Sciences at The University of Texas at Austin using a Thermo Scientific Delta V Isotope Ratio Mass Spectrometer equipped with a GasBench sample introduction system. Water isotopic measurements are reported as ‰ relative to Vienna Standard Mean Ocean Water. Analytical precision (2*standard error) was 0.5‰ for δD and 0.1‰ for $\delta^{18}O$ based on measurements of an internal standard (n=9 and 7, respectively).

Historical data (Jan 1974–Oct 2008, of which 80% were pre-2000) for these sites were retrieved from the USGS (U.S. Geological Survey, 2012). Differences between concentrations measured during this study and historical data were assessed using the Mann-Whitney U test, a nonparametric test for comparing two independent groups of data (Helsel and Hirsch, 2002). The Mann-Whitney U test also was used to assess differences between i) data collected during this study and historical data collected under dry (PDSI <-0.5) conditions, and ii) historical data collected under dry and wet (PDSI > 0.5) conditions. Statistical results with p-values less than 0.05 were considered statistically significant. Rainwater compositions measured during the study at the nearest

National Atmospheric Deposition Program station, Beeville, Texas (~225 km from the study area), were retrieved from the National Atmospheric Deposition Program (2012).

Geochemical modeling and source-water definitions

Water compositions were modeled using PHREEQC, a geochemical modeling program that simulates a wide variety of fluid (i.e., source-water) mixing and low-temperature aqueous geochemical reactions and processes (Parkhurst and Appelo, 1999), and following the methods of Wong et al. (2012). Inverse modeling was used to calculate combinations of source-water proportions and amounts (i.e., mols) of mineral and gas dissolution or precipitation that account for, within specified compositional uncertainty limits, measured (user-specified) stream-water and spring-water compositions. The following geochemical interactions are likely to occur in carbonate terrains and were included in each model: i) dissolution and precipitation of calcite; ii) consumption or loss of CO_2; iv) loss of O_2; and v) ion exchange of Ca and Na. Models could not balance K, so ion exchange of K was also included in the models. Evapo-concentration was modeled by allowing the precipitation of H_2O. Only models with the minimal number of mineral and gas phases (termed minimal models) were reported, except where noted.

In general, stream water can include contributions from overland flow, seepage (flow through the soil and epikarst), discrete spring flow, diffuse groundwater base flow, and anthropogenic inputs, such as irrigation runoff and leakage from water distribution and collection networks and septic systems. Local, representative compositions of these sources (i.e., source waters) were compiled from independent data sources (Table 3.2 and Fig. 3.3). Overland flow and seepage were represented by overland flow entering a sinkhole (around which the land is undisturbed and preserved as part of a groundwater protection program) in the Bear Creek watershed as described by Wong et al. (2012).

Similar concentrations measured in overland flow and dripwater collected from an underlying cave (Fig. 3.3) indicate that there are negligible geochemical differences between overland flow and seepage flow, and that both types of flow can be represented by a single composition. Potential groundwater contribution was represented by samples collected from springs discharging from bedrock of the Upper and Middle Trinity aquifer (Upper Glen Rose Limestone and Cow Creek Limestone, respectively) in the Onion Creek watershed that were collected and analyzed by the Barton Springs Segment of the Edwards Aquifer Conservation District (personal communication B. Hunt, 2011).

Three direct anthropogenic inputs were considered in this study: septic leachate, municipal drinking water from leaking distribution systems or irrigation run-off, and wastewater. Septic leachate was represented by the composition of septic leachate collected in the Barton Creek watershed at a single residence by the City of Austin (COA) (City of Austin, 2012b). Municipal drinking water was represented by the median concentration of COA tap water measured at 10 residences by Christian et al. (2011). Municipal wastewater was represented by sewage collected from Austin area manholes by the COA (City of Austin, 2012b). As there was greater variation in wastewater composition relative to drinking-water compositions, a single wastewater sample (from the Barton Creek watershed) with relatively high concentrations of alkalinity, Ca, Cl, and Na was used in the model as the representative wastewater (Fig. 3.3). A wastewater composition with higher constituent concentrations was used so that estimates of municipal wastewater input would be conservative (i.e., a more concentrated wastewater source would require less contribution (i.e., volume) to supply the same amount of solutes as a wastewater source with low concentrations). Because of the general lack of wastewater collection networks throughout most of the contributing zone, wastewater is treated locally and effluent is applied to the land surface. Because no measurements of

treated effluent in the project setting are publicly available, the major and trace ion composition of treated wastewater effluent applied to land is assumed to be similar to that of untreated municipal wastewater. As wastewater treatment processes largely focus on reducing suspended solids, organic matter, and microbes, rather than total dissolved solid concentrations, and add reagents (e.g., chlorine, sulfur dioxide or sodium bisulfite) to sterilize effluent (Dearmont et al., 1998; Carey and Migliaccio, 2009; Austin Water, 2012), it is expected that treated effluent specific conductance values and concentrations of Cl, Na, and SO_4 would be similar to those measured in (untreated) municipal wastewater.

Estimating solute loading

Loads of Cl and Na transported by the streams during the study period were estimated using LOADEST, a regression-based model that uses a time series of stream flow and measured constituent concentrations to estimate constituent loads (Runkel et al., 2004). The model was calibrated using data collected during the study period, and the adjusted maximum likelihood estimation method was used following the discussion presented in Mahler et al. (2011a). Natural loads (i.e., not derived from anthropogenic sources) of Cl and Na transported by the streams during the study period also were estimated using LOADEST. The LOADEST model was calibrated using concentration and discharge data collected at each of the sites during 1975–80, and natural loads were estimated for the study interval (2008-2010) using discharge measurements made during the study interval. This approach assumes that Cl and Na occurring in streams prior to 1980 were naturally sourced because this time period preceded much of the urban development. Because there were no measurements of stream-water compositions made prior to 1980 for the Barton and Slaughter Creeks sites monitored in this study,

measurements made at sites furthest upstream and immediately downstream (which is the only other site with data), respectively, along these streams were used to calibrate the model. Additionally, measurements made during 1978–1983 at Barton Creek and 1979–1985 at Slaughter Creek were used because LOADEST requires at least 12 observations for calibration and there were less than 12 measurements at these sites prior to 1980.

Loads of Cl and Na from municipal drinking water and wastewater were estimated by multiplying constituent concentrations in end-member compositions (Table 3.2) by estimated volumes of leakage in each watershed. Monthly volumes of recharge from the COA water distribution-collection network to the recharge zone were estimated by Passarello et al. (2012). Drinking water and wastewater leakage in the contributing zone of each watershed were estimated by multiplying the leakage in the recharge zone by the ratio of pipe length in the contributing zone of each watershed to total pipe length in the recharge zone. Pipe length in the contributing zone of each watershed includes pipes that are part of the COA distribution-collection network and the Lower Colorado River Authority (LCRA) distribution network. This approach assumes that leakage rates were the same in the contributing zone as they were in the recharge zone and were the same among the COA and LCRA networks. Volumes from December 2009 (the most recent volumes estimated by Passarello et al., 2012) were used to estimate leakage during January–March 2010.

Loads of Cl and Na from septic leachate were estimated by multiplying mean monthly water use by the COA households (32,100 liters per household) (Price, 2009) by the number of septic systems located within each watershed and the concentrations measured in septic leachate (Table 3.1). Loads from the TLAP were estimated by multiplying volumes reported in Mahler et al. (2011a) by the concentration of constituents measured in municipal wastewater. Caution should be taken in using

estimates of solute loading from septic and TLAP because i) a single measurement was used to characterize septic leachate, ii) wastewater from TLAP systems was not measured directly, and, instead, was represented by municipal wastewater (discussed above), and iii) actual volumes of treated wastewater effluent applied are often less than permitted volumes.

RESULTS

Variability of stream-water compositions among streams, over time, and with discharge

During the period of study, stream waters in the watersheds studied were Ca-HCO_3 waters and had greater specific conductance values (median values range from 618 to 812 μS/cm) than groundwater from the matrix of the Edwards aquifer (median value of 580 μS/cm; Table 3.2). Stream-water alkalinity and Ca, Mg, and Sr concentrations were similar to or slightly lower than those measured in groundwater, but Cl, K, Na, SO_4 concentrations were higher (Table 3.2). Median concentrations of SO_4 in all the streams, except Williamson Creek, exceeded the Texas Commission of Environmental Quality (TCEQ) surface water standards of 50 mg/L set for Barton and Onion Creeks (there are no standards set for Williamson, Slaughter, or Bear Creeks since they are unclassified segments) (Texas Commission of Environmental Quality, 2012). The median concentration of Cl in Barton Creek exceeded the standard of 50 mg/L, and median Cl concentrations in Slaughter and Bear Creeks were nearing it (Table 3.2).

Median concentrations of most constituents in stream water collected during this study were significantly higher than those measured historically for all of the streams except Williamson Creek (Fig. 3.4 and Table 3.2). There was no significant difference between constituent concentrations in stream water collected during dry conditions (PDSI

< -0.5) and those collected during wet conditions (PDSI > 0.5) in most of the streams for the historical dataset (Supplementary Table S3.1). Concentrations measured during dry conditions during 2008–2010 also were higher than historical constituent concentrations measured during dry conditions (Supplementary Table S3.2). During the study period, stream-water constituent concentrations (as represented by specific conductance values in Fig. 3.2) varied more at some sites than others. Values measured in storm samples were not consistently lower than those measured in routine samples, nor were values measured during the dry period consistently higher or lower than those measured during the wet period (Fig. 3.2).

Throughout the entire sampling interval, stream-water constituent concentrations did not decrease, or decreased only slightly, with increased discharge at Barton, Slaughter, and Onion Creeks (Fig. 3.5). Godsey et al. (2009) observed a similar trend in concentrations of common mineral weathering solutes (i.e., Ca, Mg, Na, and Si) in pristine headwater catchments of a wide array of climatic, vegetative, and lithologic settings. Such trends were interpreted to indicate that solute fluxes to the streams increased as discharge increased (Godsey et al., 2009). In this study, this trend was documented for carbonate constituents (e.g., Ca, Mg, HCO_3) that would naturally weather from the carbonate terrain, and non-carbonate constituents (Cl, Na, SO_4) that are not abundant in carbonate terrains. In Williamson and Bear Creek, stream-water constituent concentrations tended to decrease at greater rates when the ratio of stream discharge to watershed area (herein referred to as runoff, in units of mm/day) exceeded 1 mm/d (i.e., more negative slope above 1 mm/d than below) (Fig. 3.5), indicating that increases in runoff were not matched by increases in solute fluxes to the stream. Discharge normalized to watershed area so that discharge can be compared between watersheds of

different areas. In this manuscript, runoff will refer to discharge normalized to watershed area and overland flow will refer to water that flows on the surface to streams.

Geochemical and isotopic evidence of evaporative and dilution processes

Stream-water δD and $\delta^{18}O$ isotopic values for all the streams ranged from -87.7‰ to 14.0‰ and -12.1‰ to 0.8‰, respectively, which is similar to the range of rainfall δD and $\delta^{18}O$ isotopic values (-42 to -7‰ and -12.6‰ to -1.1‰, respectively) measured in Austin during 1999–2007 (Pape et al., 2010). Samples collected during the wet interval lie on the meteoric water line (Supplementary Fig S3.1), which indicates that evaporative processes had a negligible effect on stream-water isotopic compositions. Some samples collected during the dry interval plot off the line with heavier $\delta^{18}O$ values (Supplementary Fig S3.1), indicating the influence of evaporative processes on the isotopic composition of stream water during the dry interval (Craig, 1961).

The conservative constituents (i.e., Br and Cl) at each site are correlated, and the covariation between Br and Cl can be described by a constant slope throughout the entire sampling interval. Additionally, Br/Cl ratios are generally constant for all concentrations of Cl (Supplementary Fig. S3.2). This data suggests that evapo-concentration might be a control on stream water compositions.

Geochemical modeling results

Stream-water constituent concentrations were greater than those measured in natural sources (rainwater, overland flow, spring seepage) but less than those in anthropogenic sources (septic leachate, wastewater, drinking water) (Fig. 3.3). Stream-water compositions could not be accounted for by modeled scenarios that i) mix natural sources and allow mineral-solution reactions (Supplementary Table S3.3), or ii) mix natural sources and allow mineral-solution reactions and evaporation. Stream-water

compositions could, however, be accounted for by models with mineral-solution reactions and mixing between natural sources and i) septic leachate, ii) municipal wastewater, or iii) municipal drinking water and wastewater. Proportions of wastewater input estimated using septic leachate were consistently higher by about 10% than wastewater estimates derived using municipal wastewater (Table 3.3). Modeled proportions of septic leachate and municipal drinking and wastewater in stream water did not vary temporally, and substantial contributions (16-78%) to stream water were modeled even when stream discharge was large (greater than 2.83 m^3/s (100 ft^3/s)) (Supplementary Table S3.3). Similar amounts of calcite precipitation, dolomite and gypsum dissolution, and Ca, Na, and K ion exchange were modeled for each site and source-water mixing modeling scenarios (Supplementary Table S3.3).

Estimated Cl and Na solute inputs and outputs

The Cl loads in each stream during the study interval exceeded the estimated combined natural and anthropogenic solute inputs in each watershed, except in Williamson Creek (Table 3.4). The percentage of Cl loads not accounted for by natural and anthropogenic inputs ranged from 25% in Onion Creek to 66% in Barton Creek, and would require 0.6 to 3.3 additional years of anthropogenic inputs, at rates similar to those estimated, to account for excess exports. The combined estimates of natural and anthropogenic Na inputs to each watershed exceeded the exported load in each stream during the study interval in Williamson, Bear, and Onion Creeks (Table 3.4). In Barton and Slaughter Creeks, the loads not accounted for were 53% and 32%, respectively, and would require an additional 1.6 and 1.3 years, respectively, of anthropogenic inputs to account for excesses in the exported loads.

DISCUSSION

Stream-water specific-conductance values and constituent concentrations are higher than those of Edwards aquifer groundwater, and in some streams exceed TCEQ surface-water quality standards for SO_4 and Cl. Comparison of recent and historical concentrations document increased concentrations of Cl, Na, and SO_4 concentrations over time (Fig. 3.3). This increase is consistent with increased densities of septic systems and volumes of land application of treated wastewater effluent documented by Mahler et al. (2011a) (Fig. 3.1). Stream-water compositions cannot be accounted for by natural processes – mixing, interaction, or evapo-concentration of natural sources (i.e., overland runoff and spring seepage). Geochemical modeling results indicate that anthropogenic sources are likely an indirect source of stream-water solutes, but do not directly contribute substantial volumes of stream-water flow. We propose a conceptual model in which anthropogenic solutes are transported from the soil and epikarst zone in overland flow and seepage flow to streams at a rate that co-varies with discharge. This model is consistent with the small variation of the stream-water constituent concentrations, and is assessed using watershed solute mass balances.

Natural sources and processes cannot account for stream-water compositions

In most natural settings, concentrations of dissolved ions are lower in surface water than in groundwater because of mineral-solution interactions in the sub-surface (e.g., Atkinson, 1977). For example, in the carbonate terrain for this project setting, water with increasing amounts of water-rock have increasingly higher concentrations of Mg and Sr, which are common minor and trace ions in carbonate minerals. This is demonstrated by the increase in Mg and Sr concentrations from overland runoff (collected from a protected, natural area) to stream water to Edwards groundwater (Table 3.2). Rapid water equilibration with carbonate minerals likely accounts for similar Ca and

HCO_3 concentrations between overland runoff, stream water, and Edwards groundwater. Specific-conductance values and concentrations of non-carbonate constituents (i.e., Cl, K, Na, and SO_4), however, are higher in stream water than in Edwards aquifer groundwater (Fig. 3.2 and Table 3.2), of which the streams are the largest source of recharge. This indicates that stream-water compositions, particularly non-carbonate constituent concentrations, are controlled by sources or processes in addition to natural interaction with carbonate terrain.

High stream-water SO_4 concentrations relative to those in Edwards groundwater could result from i) interaction with disseminated gypsum/anhydrite or gypsum/anhydrite layers and lenses in the Glen Rose and Cow Creek Limestone Formations, which outcrop in these watersheds (Stricklin, 1971), or ii) mixing with water from springs discharging from these formations. Water interaction with gypsum and anhydrite, however, cannot account for high stream-water Cl and Na concentrations relative to those in Edwards aquifer groundwater, and there is no halite documented in these formations (Stricklin, 1971). In addition, a mechanism by which water interaction with gypsum and anhydrite increased over time would be necessary to account for increasing stream-water constituent concentrations over time. Geochemical modeling results indicate that mixing of stream water with overland and seepage flow and spring water discharging from Glen Rose and Cow Creek formations, water-rock interaction, and evapo-concentration cannot account for measured stream-water compositions (Supplementary Table S3.3). Although spring seepage has SO_4 concentrations that are high enough to account for most stream-water SO_4 concentrations, spring-water Cl and Na concentrations are not high enough to account for stream-water Cl and Na concentrations (Table 3.2 and Fig. 3.3).

Evapo-transpiration is a likely influencing stream water compositions. $\delta^{18}O$ and δD isotopic values of samples collected during the wet interval that lie along the meteoric

water line (Supplementary Fig S3.1) indicate that stream waters did not undergo substantial evaporation during the wet interval. Isotopic values of samples collected during the dry interval, however, do not lie along the meteoric line, which indicates that evapo-concentration could have influenced stream-water compositions. Furthermore, linear correlations between Br and Cl and similar Br/Cl ratios with changing Cl concentration at each site (Supplementary Fig. S3.2) are consistent with dilution and/or evapo-concentration processes.

It is not likely the high stream-water constituent concentrations measured during the project interval relative to historical measurements result from project-interval conditions being drier (i.e., more evapo-concentration) relative to historical sampling conditions (i.e., less evapo-concentration). It is possible that evapo-concentration during the drought could result in i) increased stream-water constituent concentrations during the dry interval, and ii) the precipitation of evaporative minerals in the soil/epikarst zone that were later dissolved and transported to streams during the wet interval. There is, however, a the lack of historical precedence for differences between stream-water constituent concentrations measured during dry and wet conditions (Supplementary Table S3.1). Furthermore, stream-water constituent concentrations measured during and following the 2008-2009 drought conditions are higher than those measured in stream-water during previous, equally severe, droughts (Supplementary Table S3.2). Lastly, geochemical modeling indicates that mixing of natural source waters, water-rock interaction, and evapo-concentration processes cannot account for stream-water compositions.

Indirect influence of anthropogenic sources on stream-water compositions

Geochemical modeling results indicate that large proportions of septic and municipal drinking-water and wastewater end members are necessary to derive stream-water compositions (Table 3.3). These modeling results and the increase in constituent concentrations in stream water over time are consistent with the documented increase in permitted septic system density and volume of land-applied treated wastewater effluent over time (Mahler et al., 2011a). Estimates of source water contributions to stream water compositions, however, represent maximum possible contributions, and actual contributions are likely much less as discussed below.

Although it is likely that anthropogenic sources are large contributors of solutes to stream waters, it is not likely that such sources are responsible for large volumes of stream flow. For example, geochemical modeling indicates that Onion Creek water compositions sampled on February 2nd, 2010, could be accounted for by mixing of natural water and i) 22% septic leachate, ii) 19% wastewater, or iii) 43% municipal drinking water (Supplementary Table S3.3). Discharge on this day was 6.2 m^3/s (220 ft^3/s), and would require contributions of septic leachate, wastewater, or municipal drinking water at rates of 1.4 m^3/s (48 ft^3/s), 1.2 m^3/s (42 ft^3/s), or 2.7 m^3/s (95 ft^3/s), respectively, which are unrealistically high. The septic leachate rate, estimated from mean monthly household water use in the COA (32,100 liters per household; Price, 2009) and the number of septic systems located within Onion watershed, is 0.03 m^3/s (1.1 ft^3/s). Average rates of water mains, leaky wastewater pipes, and irrigation return flow, estimated for the recharge zone using a volumetric water balance approach, were 0.05, 0.02, and 0.02 m^3/s (1.9, 0.76, and 0.76 ft^3/s), respectively (Passarello et al., 2012). Furthermore, volumetric inputs of anthropogenic sources are expected to be constant (see Passarello et al., 2012) relative to variations in stream discharge (as seen in Fig. 3.2) and, therefore, should be diluted when

stream discharge is elevated. Such dilution of stream-water constituent concentrations with increasing stream discharge, however, was not observed at most of the creeks (Fig. 3.5). Decreases in stream-water constituent concentrations did not consistently occur with increased runoff. Instead, the slope of the concentration–discharge relationship on logarithmic axes was closer to zero than to one (Fig. 3.5), which indicates that streams are chemostatic—i.e., concentrations vary little regardless of stream discharge (Godsey et al., 2009).

Conceptual model of source and transport of stream-water solutes

The chemostatic nature of stream-water constituent concentrations in Barton, Slaughter, and Onion Creeks (Figs. 3.2 and 3.5) indicates that solute fluxes to streams increase with increasing discharge. Increased solute fluxes to streams likely result from increased weathering rates, which occur with a greater extent of wetted surface area related to increases in water flux within the watersheds (Godsey et al., 2009). That this occurs during storm conditions in large (Barton and Onion) and small (Slaughter) watersheds is surprising, and indicates that sufficiently large volumes of water are infiltrating and interacting with the soil/epikarst zone to produce such fluxes. Both carbonate and non-carbonate constituent concentrations were relatively invariant as discharge increased, which indicates that constituents with natural sources and those with anthropogenic sources react and are transported similarly. This supports a conceptual model of the evapo-concentration of anthropogenic source waters in the soil and epikarst zone that results in the accumulation of anthropogenic solutes. These solutes are then transported to streams at a rate proportional to runoff within the watershed (Fig. 3.6).

The chemostatic nature of stream water throughout the study interval indicates that accumulated material is not entirely removed by initial wetting events. Instead,

solutes are persistent and, similar to natural solutes, a relatively constant source of solutes to stream water. Accumulation of Cl and Na from frequent application of road salts has previously been deduced to occur in watersheds located in the northern US (e.g., Kelly et al., 2008; Novotny et al., 2009). Although road salt is not used in central Texas, the processes that result in accumulation of anthropogenic solutes might be similar. Mechanisms proposed for the retention of Cl, which commonly is treated as a conservative constituent, include vegetative uptake and incorporation into soil organic matter as organic chlorine compounds (Lovett et al., 2005; Bastviken et al., 2006).

The geochemical behavior in Williamson and Bear Creeks, different from that in the other three streams, indicates that the nature of flow within these watersheds might be different than in the other watersheds. Dilution of stream-water constituent concentrations at elevated runoff (>1 mm/d) was greater than dilution when runoff was lower (i.e., more negative slope above 1 mm/d than below) (Fig. 3.5). This indicates that solute fluxes were reduced during elevated flow, likely resulting from less interaction between the water and solid surfaces in the soil/epikarst zone. Less interaction might result from increased proportions of overland (vs. seepage) flow, flow through storm drains, and/or more rapid flow. It is not apparent what features of the watershed would result in reduction of water-surface interaction at elevated flows in Williamson and Bear Creeks but not in Barton, Slaughter, or Onion Creeks. Williamson is the smallest watershed and has the greatest density of urban development, which suggests watershed size and density of urban structures might play a role (Table 3.1). Such features, however, do not appear to be the controlling factor, as the watershed of Bear Creek is larger than that of Slaughter Creek and has less urban development, yet dilution at elevated flows occurs in Bear Creek and not Slaughter Creek (Fig. 3.5). This indicates that other (or additional) watershed features might contribute to reduced water-surface interaction at

elevated flows. Delineation of such features is beyond the scope of this study, and would likely require a larger sample size and more robust characterization of the watersheds (e.g., channel geometry, hill slope, or riparian zone width and density).

Assessing the conceptual model with solute mass balances

To investigate the feasibility of the conceptual model that anthropogenic solutes accumulate in the soil and epikarst zone and are transported to streams by runoff and seepage flow, first-order estimates of natural and anthropogenic Cl and Na inputs to watersheds were compared to solute loads exported by streams during the study interval (Table 3.4). Solute inputs that exceed exports indicate that inputs are overestimated or that solutes are accumulating within the watershed. Exports that exceed inputs indicate that natural or anthropogenic inputs were unaccounted for or underestimated. In Williamson, Bear, and Onion Creeks, Na inputs exceeded exports, but Cl inputs were less than exports in all the streams except Williamson Creek. The difference between Cl inputs and exports in Bear and Onion Creeks is equivalent to 0.8 and 0.6 additional years of anthropogenic inputs, respectively (Table 3.4), which is similar to the duration of dry conditions, during which there was no flow in Onion or Bear Creek, that preceded study interval. This is not the case in Barton and Slaughter Creeks in which it would require more than a year for anthropogenic Cl and Na inputs to accumulate such that inputs would sufficiently account for exports (Table 3.4). The solute mass balances account for Na and Cl loads carried by Williamson, Bear, and Onion Creeks, and indicate that solutes likely accumulate in all three watersheds. The large amount of accumulation of Na relative to Cl is consistent with the occurrence of Na ion exchange and the more conservative nature of Cl in water relative to Na (e.g., Amrhein et al., 1992; Mason et al., 1999). The large amount of Na and Cl solute accumulation estimated to occur in

Williamson Creek (Table 3.4) indicate either that natural and/or anthropogenic loads are overestimated, or that solutes are accumulating within the watershed. Such accumulation might occur if runoff and/or seepage is unable to access Cl solutes because of impervious cover and/or storm water drainage systems reducing water interaction with soil and epikarst zones. The unaccounted for exports of Cl and Na in Barton and Slaughter Creeks indicate that sources of solutes in these watersheds were underestimated or unaccounted for (e.g., land application of fertilizer on residential and commercial landscapes). The inconsistent mixed solute mass-balance results among the watershed likely indicate that more refined estimates of solute inputs and exports are required to fully quantify the extent to which anthropogenic sources influence stream-water compositions in these watersheds.

CONCLUSIONS

A comparison of stream-water compositions measured as a part of this study (2008–2010) to historical data (pre-2000) indicates that concentrations of Cl, Na, and SO_4 are increasing over time in losing streams that provide the majority of recharge to the Barton Spring Segment of the Edwards aquifer (Fig. 3.4). Natural sources (i.e., overland flow and spring and groundwater input) and processes (i.e., water-surface interactions and evapo-concentration) cannot account for stream-water compositions, which indicates that anthropogenic sources (i.e., municipal drinking water, wastewater, septic leachate) might influence stream-water compositions. Geochemical model results indicate that mixing of natural and anthropogenic sources can account for stream-water compositions. Such mixing, however, would require unrealistically high volumes of direct anthropogenic input (Supplementary Table S3.3), leading to the hypothesis that anthropogenic sources might be the source of solutes to stream-water but not to actual

stream-water flow. We propose a conceptual model in which evapo-transpiration concentrates anthropogenic source waters in the soil/epikarst zone, leading to the accumulation of anthropogenic solutes that are latter transported to streams in overland and seepage flow (Fig. 3.6). The chemostatic nature of streams, even during storm events in the largest watersheds (Fig. 3.5), supports this model and indicates that i) there is a persistent supply of anthropogenic solutes, and ii) the flux of solutes increases at elevated discharges. First-order estimates of solute inputs and exports suggest that the accumulation of solutes occurs in three of the five watersheds (Williamson, Bear, and Onion Creek Watersheds; Table 3.4). The inconsistent solute mass balances among the watersheds indicate that more refined estimates of solute inputs and exports are necessary to precisely quantify the extent to which anthropogenic sources influence stream-water quality. This research has implications for land-use and water-resource management. Preserving stream-water quality is critical to protecting groundwater quality of the Barton Springs Segment of the Edwards Aquifer because these streams provide the majority of groundwater recharge (Slade et al., 1986; Hauwert, 2009). Our results that indicate that wastewater sources are influencing stream water compositions.

Table 3.1. Characteristics for the contributing zone of each watershed

	Area (km^2)	Median annual peak daily flow (m^3/s)	Study interval (2008-2010) peak daily flow (m^3/s)	Impervious cover (km^2)	Drinking-water pipe length (km)	Wastewater pipe length (km)	Number of septic systems
Barton Creek	288	57	20	3.5	320	57	3,138
Williamson Creek	20	29	2	1.7	193	85	245
Slaughter Creek	28	24	4	0.68	126	13	381
Bear Creek	52	38	4	0.70	68	3	1,123
Onion Creek	350	86	15	0.92	57	0	2,608

Table 3.2. Project (2008-2010) and historical (1975-2000) stream water, groundwater, and model end member compositions and number

		Alk (mg/L)	**Ca** (mg/L)	**Mg** (mg/L)	**Sr** (mg/L)	**K** (mg/L)	**Na** (mg/L)	**SO_4** (mg/L)	**Cl** (mg/L)	**Specific conductance** (μS/cm)
Surface water										
Barton Creek	Project (n=26)	204	**82**	**21**	**0.30**	**2.4**	**30**	**66**	**53**	**692**
	Historical (n=25)	207	70	18	0.25	1.6	13	33	21	515
Williamson Creek	Project (n=18)	143	52	12	0.25	**2.2**	8.7	38	16	417
	Historical (n=89)	200	79	23	0.31	1.5	11	26	18	584
Slaughter Creek	Project (n=11)	237	**106**	**26**	**0.29**	**1.7**	25	**109**	48	**812**
	Historical (n=43)	253	92	23	0.24	0.80	24	68	44	699
Bear Creek	Project (n=20)	194	**92**	**20**	**0.27**	**1.9**	**18**	**68**	**43**	**721**
	Historical (n=55)	232	75	16	0.18	1.00	8.8	30	15	510
Onion Creek	Project (n=11)	229	**87**	**19**	0.38	**1.7**	**11**	**62**	**26**	**618**
	Historical (n=110)	204	68	16	0.29	1.2	7.8	28	13	468
Groundwater										
Edwards aquifer matrix[a]	n=13	283	84	25	0.43	0.91	6.4	14	11	584
Model end members										
Upper Glen Rose Spring[b]	n=1	307	114	23	0.2	<0.20	12	30	20	688
Cow Creek Spring[b]	n=1	308	101	37	3.5	2.0	15	83	16	758
Upland runoff[c]	n=26	240	87	10.5	0.05	0.33	2.5	5.4	2.8	473
Municipal Wastewater[c]	n=10	154	15	16	-	18[f]	50	44	63	-
Municipal Drinking water[d]	n=10	67	13	15	0.14	3.3	19	27	35	302
Septic[c]	n=1	388	85.7	22.1	0.52	19	73.3	0.13	64.6	-

Bold font indicates significant difference ($p<0.05$) from historical concentrations based on Mann-Whitney-U test

[a]Data from Wong et al., in press; [b]Data from Barton Springs Edwards Aquifer Conservation District; [c]Data from City of Austin, [d]Data from Christian et al., 2010 [e]Date from City of Austin, [f]Median value of 5 wastewater measurements

Table 3.3. Summary (median values) of stream water geochemical modeling for dry (Nov to Aug 2009) and wet (Sept 2009 to Mar 2010) intervals

		Scenario 2		Scenario 3		Scenario 4		
		Natural Sources (%)	Septic (%)	Natural Sources (%)	Waste-water (%)	Natural Sources (%)	Waste-water (%)	Drinking water (%)
Barton Creek	dry	27	73[b]	37	63	6	49	45
	wet	51	49[b]	62	38	20	22	58
Williamson Creek	dry[a]	86	14	88	12	85	9	6
	wet	62	38	72	28	37	20	44
Slaughter Creek	dry	-	-	-	-	-	-	-
	wet	35	65[b]	48	52	50	28	22
Bear Creek	dry	30	70[b]	44	56	6	34	60
	wet	47	53[b]	59	41	22	34	44
Onion Creek	dry	-	-	-	-	-	-	-
	wet	71	29	78	22	71	0	29

[a]Not all compositions could be modeled

[b]Modelled with high uncertainty due to Sr (see Supplementary Table 3)

Table 3.4. Estimates of Cl and Na inputs to and exports from contributing zones of watersheds

		Exported	Natural inputs	Antropogenic inputs	Excess exports (Exports-Inputs)/Exports	Additional anthropogenic inputs to account for excess exports
		kg	kg (% of export)	kg (% of export)	(%)	(years)
Barton Creek	Cl	3,300,000	660,000 (20)	460,000 (28)	25	3.3
	Na	1,700,000	430,000 (24)	400,000 (23)	53	1.6
Williamson Creek	Cl	56,000	47,000 (84)	37,000 (67)	-	-
	Na	28,000	31,000 (1.1)	25,000 (89)	-	-
Slaughter Creek	Cl	270,000	140,000 (52)	34,000 (12)	35	2.0
	Na	140,000	68,000 (49)	27,000 (19)	-	1.3
Bear Creek	Cl	300,000	110,000 (37)	98,000 (30)	33	0.8
	Na	130,000	53,000 (42)	82,000 (65)	-	-
Onion Creek	Cl	1,000,000	470,000 (47)	280,000 (28)	25	0.6
	Na	440,000	310,000 (69)	260,000 (58)	-	-

Supplementary Table S3.1. Historical (1975-2000) median concentrations (mg/L) and specific conductance (μS/cm) for dry (PDSI<-0.5) and wet intervals (PDSI>0.5) for each stream site

	Barton Creek		Bear Creek		Onion Creek		Slaughter Creek		Williamson Creek	
	dry n=7	wet n=14	dry n=15	wet n=33	dry n= 38	wet n=61	dry n=6	wet n=31	dry n=24	wet n=50
Ca	64	72	68	**80**	63	**71**	83	**93**	57	85
Mg	17	18	17	16	16	**16**	23	24	16	25
Na	17	11	8.3	8.8	8.6	**7.6**	22	25	12	11
Cl	35	20	15	16	13	12	55	43	18	18
SO_4	40	31	30	30	31	**27**	54	**76**	26	27
K	2.0	**1.2**	1.3	0.9	1.3	**1.1**	0.8	0.8	2.0	1.2
Si	8.4	8.4	9.4	7.8	8.9	8.4	7.5	6.8	5.5	5.1
Specific conductance	519	510	489	510	441	**472**	678	712	447	609

Bold font indicates significant differences ($p<0.05$) from historical samples collected under dry conditions

Supplementary Table S3. 2. Median concentrations (mg/L) and specific conductance (µS/cm) for project (2008-2010) and historical (1975-2000) dry conditions for each stream site

	Barton Creek		Bear Creek		Onion Creek		Slaughter Creek		Williamson Creek	
	Hist. Dry n=7	Project n=26	Hist. Dry n=15	Project n=20	Hist. Dry n=38	Project n=11	Hist. Dry n=6	Project n=11	Hist. Dry n=24	Project n=18
Ca	64	82	68	**92**	63	**87**	83	*106*	57	52
Mg	17	21	17	20	16	19	23	26	16	12
Na	17	30	8.3	**18**	8.6	**11**	22	25	12	8.7
Cl	35	53	15	**43**	13	**26**	55	48	18	16
SO_4	40	66	30	**68**	31	**62**	54	**109**	26	38
K	2.0	2.4	1.3	**1.9**	1.3	**1.7**	0.8	1.7	2.0	2.2
Si	8.4	9.1	9.4	**8.1**	8.9	8.9	7.5	8.1	5.5	4.4
Specific conductance	519	692	489	**721**	441	**618**	678	**812**	447	417

Bold font indicate significantly different from historical stream water sampled under dry conditions

Supplementary Table S3.3. Stream water geochemical modeling results

	Modeled percent (median) of stream water composition						Number of minimal models, total	Specifiied global uncertainty	Constituents requiring uncertainty increase[b]	Modeled amount (mols) of mineral dissolution/exchange (+) or precipitation/exchange (-)					
	Overland runoff	Glen Rose spring	Cow Creek spring	Septic leachate	Waste-water	Drinking water[a]				Calcite	Dolomite	Gypsum	Ca ion exchange	Na ion exchange	K ion exchange
Barton Creek															
Dry Interval															
Dec 17, 2008, $ft^3/s = 1.2$															
1	*	*	*	-	-	-	*	0.10	Cl, SO_4, Sr	*	*	*	*	*	*
2	27	0	0	73	-	-	1, 3	0.10	Sr	-1.5e-3	1.6e-4	7.3e-4	5.1e-4	-7.3e-4	-2.9e-4
3	0	32	5	-	63	-	2, 3	0.05		-7.4e-4	2.6e-6	3.2e-4	3.9e-4	-4.8e-4	-3.0e-4
4	0	0	6	-	45	49	2, 10	0.05		4.2e-4	1.1e-4	3.8e-4	1.2e-4	0	-2.3e-4
Feb 18, 2009, $ft^3/s = 4.5$															
1	*	*	*	-	-	-	*	0.10	Cl, SO_4, Sr	*	*	*	*	*	*
2	27	0	0	73	-	-	1, 3	0.08	Sr (0.10)	-1.6e-3	7.8e-4	7.4e-4	5.4e-4	-7.8e-4	-3.0e-4
3	0	37	5	-	58	-	2, 3	0.05		-9.4e-4	0	3.5e-4	3.6e-4	-4.4e-4	-2.8e-4
4	0	0	6	-	36	58	6, 13	0.05		4.3e-4	5.8e-5	3.7e-4	1.0e-4	0	-2.0e-4
May 13, 2009, $ft^3/s = 2.1$															
1	*	*	*	-	-	-			Cl, SO_4, Sr	*					
2	*	*	*	*	-	-			Sr						
3	4	26	5	-	65	-	2, 4	0.05		-1.0e-3	0	2.4e-4	5.3e-4	7.5e-4	-3.1e-4
4	0	0	5	-	53	42	4, 7	0.05		0	2.3e-5	2.3e-4	4.1e-4	-5.5e-4	-2.8e-4
Aug 5 2009, $ft^3/s = 59$															
1	*	*	*	-	-	-	*	0.10	Cl, SO_4, Sr	*	*	*	*	*	*
2	*	*	*	*	-	-	*	0.10	Sr	*	*	*	*	*	*
3	0	14	5	-	81	-	2, 3	0.05		-8.3e-4	0.8e-5	0	6.0e-4	-8.2e-4	-3.9e-4
4	0	0	5	-	70	25	2, 5	0.05		-1.0e-4	1.8e-5	1.0e-5	4.3e-4	-5.2e-4	-3.5e-4
Wet Interval															
Oct 14, 2009, $ft^3/s = 172$															
1	*	*	*	-	-	-			Cl, SO_4, Sr						*
2	35	0	0	65	-	-	1, 3	0.10	Sr	-1.3e-3	1.8e-5	9.0e-4	5.7e-4	-8.8e-4	-2.6e-4
3	3	38	4	-	55	-	2, 3	0.05		-1.0e-3	0	5.3e-4	4.4e-4	-6.3e-4	-2.5e-4
4	0	10	5	-	44	41	4, 9	0.05		0	0	5.2e-4	3.5e-4	-4.8e-4	-2.3e-4
Oct 22, 2009, $ft^3/s = 408$															
1	*	*	*	-	-	-	*	0.10	Cl, SO_4, Sr	*	*	*	*	*	*
2	31	21	0	48	-	-	1, 3	0.05	Sr (0.10)	-1.5e-3	0	6.3e-4	4.4e-4	-7.0e-4	-1.7e-4
3	33	23	4	-	40	-	1, 3	0.05		-1.0e-3	0	3.9e-4	3.1e-4	-4.5e-4	-1.7e-4
4	0	10	3	-	14	73	7, 13	0.05		5.0e-4	1.3e-5	3.7e-4	1.1e-4	-1.4e-4	-7.9e-5
Nov 4, 2009, $ft^3/s = 101$															
1	*	*	*	-	-	-			Cl, SO_4, Sr	*	*	*	*	*	*
2	34	0	0	66	-	-	1, 1	0.05	Sr (0.10)	-1.4e-3	1.8e-4	7.1e-4	6.5e-4	-1.0e-3	-2.7e-4
3	0	49	4	-	47	-	2, 3	0.05		-8.3e-4	1.3e-5	3.6e-4	4.0e-4	-5.8e-4	-2.1e-4
4	0	7	5	-	34	54	2, 11	0.05		3.0e-4	1.7e-4	3.5e-4	3.1e-4	-4.4e-4	-1.9e-4
Nov 20/, 2010, $ft^3/s = 533$															
1	*	*	*	-	-	-			Cl, SO_4, Sr	*	*	*	*	*	*
2	52	0	0	48	-	-	1 ,3	0.05	Sr (0.10)	-1.3e-3	5.7e-5	5.3e-4	4.8e-4	-7.8e-4	-1.8e-4
3	38	25	3	-	34	-	2, 2	0.05		-8.3e-4	4.8e-5	1.4e-4	3.3e-4	-4.5e-4	-1.6e-4

Supplementary Table S3.3. Stream water geochemical modeling results

	Modeled percent (median) of stream water composition						Number of minimal models, total	Specifiied global uncertainty	Constituents requiring uncertainty increase[b]	Modeled amount (mols) of mineral dissolution/exchange (+) or precipitation/exchange (-)					
	Overland runoff	Glen Rose spring	Cow Creek spring	Septic leachate	Waste-water	Drinking water[a]				Calcite	Dolomite	Gypsum	Ca ion exchange	Na ion exchange	K ion exchange
4	0	14	2	-	5	78	8, 23	0.05		7.6e-4	0	2.6e-4	6.4e-5	-8.7e-5	-4.2e-5
Dec 2, 2010, ft^3/s = 276															
1	*	*	*	-	-	-			Cl, SO_4, Sr	*	*	*	*	*	*
2	25	24	0	51	-	-	2, 2	0.05		-1.3e-3	1.0e-4	6.0e-4	4.8e-4	-7.8e-4	-2.0e-4
3	0	61	4	-	35	-	1, 2	0.05		8.8e-4	0	3.3e-4	2.9e-4	-4.3e-4	-1.6e-4
4	0	15	5	-	22	58	7, 13	0.05		3.8e-4	1.5e-4	3.2e-4	2.0e-4	-2.7e-4	1.3e-4
Jan 5, 2010, ft^3/s = 59															
1	*	*	*	-	-	-	*	0.10	Cl, SO_4, Sr	*	*	*	*	*	*
2	35	0	0	65	-	-	1, 1	0.08	Sr (0.10)	-1.7e-4	1.8e-4	7.3e-4	7.1e-4	-1.1e-3	-2.8e-4
3	0	49	4	-	47	-	2, 3	0.05		-1.2e-3	0 to 2.5e-5	3.8e-4	5.0e-4	-7.7 to -7.3e-4	-2.4e-4
4	0	0	5	-	32	64	1, 7	0.05		1.9e-4	1.8e-4	3.7e-4	3.7e-4	-5.4e-4	-2.0e-4
Feb 2, 2010, ft^3/s = 205															
1	*	*	*	-	-	-	*	0.10	Cl, SO_4, Sr	*	*	*	*	*	*
2	15	43	0	42	-	-	2, 4	0.05	Sr (0.10)	-1.2e-3	4.5e-5	5.8e-4	4.4e-4	-7.0e-4	-1.8e-4
3	3	62	3	-	32	-	2, 3	0.05		-7.5e-4	0	3.4e-4	3.0e-4	-4.4e-4	-1.5e-4
4	0	25	4	-	14	57	6, 8	0.05		5.0e-4	1.0e-4	3.5e-5	1.0e-4	-1.4e-4	-1.0e-4
Mar 2, 2010, ft^3/s = 166															
1	*	*	*	-	-	-	*	0.10	Cl, Mg, SO_4, Sr	*	*	*	*	*	*
2	21	35	0	44	-	-	2, 4	0.05		-1.3e-3	0.8e-4	5.8e-4	4.2e-4	-6.5e-4	-1.8e-4
3	6	58	4	-	32	-	2, 3	0.05		-9.0e-4	0	3.5e-4	2.8e-4	-4.1e-4	-1.6e-4
4	0	18	4	-	17	61	8, 16	0.05		4.4e-4	9.2e-5	3.4e-4	1.7e-4	-2.2e-4	-1.2e-4
Williamson Creek															
Dry Interval															
Mar 13, 2009, ft^3/s = 1.0															
1	*	*	*	-	-	-	*	0.10	Cl, Mg, Sr	*	*	*	*	*	*
2	81	0	2	16	-	-	1, 1	0.05		-1.6e-3	0	4.4e-4	1.6e-4	-3.0e-4	-2.3e-5
3	82	0	5	-	13	-	1, 1	0.05		-1.4e-3	0	3.5e-4	1.2e-4	-2.1e-4	-2.1e-5
4	76	0	5	-	9	11	2, 2	0.05		-1.2e-3	0	3.5e-4	7.6e-5	-1.5e-4	-
April 2, 2009, ft^3/s = 0.08															
1	*	*	*	-	-	-	*	0.10	Mg, Sr	*	*	*	*	*	*
2	82	0	5	13	-	-	1, 3	0.05		-1.1e-3	0	2.9e-4	7.4e-5	-1.4e-4	-7.5e-6
3	84	0	6	-	10	-	1, 2	0.05		-1.0e-3	0	2.3e-4	2.4e-5	-4.8e-5	-
4	81	0	6	-	9	4	1, 4	0.05		-9.4e-4	0	2.2e-4	2.3e-5	-4.7e-5	-
May 23, 2009, ft^3/s = 12.1															
1	*	*	*	-	-	-	*	0.10	Mg, Sr	*	*	*	*	*	*
2	*	*	*	*	-	-	*	0.10	Mg, Sr	*	*	*	*	*	*
3	*	*	*	-	*	-	*	0.10	Mg, Sr	*	*	*	*	*	*
4	*	*	*	-	*	*	*	0.10	Mg, Sr	*	*	*	*	*	*
Wet Interval															
Oct 14, 2009, ft^3/s = 0.5															
1	*	*	*	-	-	-	*	0.10	Cl, SO_4, Sr	*	*	*	*	*	*

Supplementary Table S3.3. Stream water geochemical modeling results

	Modeled percent (median) of stream water composition						Number of minimal models, total	Specifiied global uncertainty	Constituents requiring uncertainty increase[b]	Modeled amount (mols) of mineral dissolution/exchange (+) or precipitation/exchange (-)					
	Overland runoff	Glen Rose spring	Cow Creek spring	Septic leachate	Waste-water	Drinking water[a]				Calcite	Dolomite	Gypsum	Ca ion exchange	Na ion exchange	K ion exchange
2	22	31	9	38	-	-	2, 2	0.05		-1.1e-3	2.7e-4	8.4e-4	2.4e-4	-6.5e-4	-1.0e-4
3	25	25	12	-	28	-	2, 2	0.05		-8.0e-4	2.9e-4	6.5e-4	2.4e-4	-3.8e-4	-1.0e-4
4	0	12	13	-	0	76	9, 22	0.05		8.0e-4	3.4e-4	6.4e-4	0	5.2e-6	-1.4e-5
Oct 22, 2009, ft^3/s = 17.4															
1	*	*	*	-	-	-	*	0.10	Cl, Mg, Sr						
2	82	0	1	16	-	-	1, 1	0.08	Sr (0.10)	-1.4e-3	0	2.6e-4	1.6e-4	-2.8e-4	-3.3e-5
3	84	0	3	-	13	-	1, 1	0.06	Sr (0.10)	-1.2e-3	0	1.8e-4	1.0e-4	-1.7e-4	-2.9e-5
4	84	0	3	-	13	0	1, 1	0.06	Sr (0.10)	-1.2e-3	0	1.8e-4	1.0e-4	-1.7e-4	-2.9e-5
Nov 4, 2009, ft^3/s = 0.50															
1	*	*	*	-	-	-	*	0.10	Cl, SO_4, Sr	*	*	*	*	*	*
2	19	26	6	49	-	-	2, 2	0.05		-1.2e-3	4.2e-4	7.6e-4	5.5e-4	-9.0e-4	-2.0e-4
3	21	28	11	-	39	-	2, 2	0.05		-7.1e-4	-4.4e-4	5.2e-4	3.5e-4	-5.1e-4	-1.9e-4
4	0	28	11	-	25	36	5, 11	0.05		0	4.3e-4	5.1e-4	2.5e-4	-3.6e-4	-1.4e-4
Dec 2, 2009, ft^3/s = 11															
1	*	*	*	-	-	-	*	0.10	Cl, Sr	*	*	*	*	*	*
2	0	78	3	19	-	-	2, 3	0.05		-1.2e-3	2.6e-6	3.7e-4	2.2e-4	-3.8e-4	-5.8e-5
3	0	81	5	-	14	-	2, 3	0.05		-9.9e-4	3.1e-6	2.7e-4	1.4e-4	-2.3e-4	-4.6e-5
4	0	50	6	-	0	44	6, 26	0.05		0	9.2e-5	2.8e-4	0	0	0
Jan 5, 2010, ft^3/s = 4															
1	*	*	*	-	-	-	*	0.10	Cl, Sr	*	*	*	*	*	*
2	17	25	3	55	-	-	2, 2	0.05		-1.5e-3	3.5e-4	7.0e-4	6.6e-4	-1.0e-3	-2.4e-4
3	21	28	10	-	41	-	2, 2	0.05		-9.5e-4	4.1e-4	4.3e-4	3.4e-4	-6.7e-4	-2.2e-4
4	0	21	9	-	25	45	4, 8	0.05		0	4.0e-4	4.1e-4	3.0e-4	-4.4e-4	-1.6e-4
Feb 2, 2010, ft^3/s = 7.7															
1	*	*	*	-	-	-	*	0.10	Cl, Mg, Sr	*	*	*	*	*	*
2	20	29	3	48	-	-	2, 2	0.05		-1.2e-3	3.4e-4	6.5e-4	5.5e-4	-8.8e-4	-2.1e-4
3	24	32	8	-	36	-	2, 2	0.05		-7.4e-4	3.1e-4	4.1e-4	3.6e-4	-5.3e-4	-1.9e-4
4	0	29	8	-	20	44	6, 11	0.05		0	4.3e-4	3.9e-4	2.4e-4	-3.6e-4	-1.3e-4
Mar 2, 2010, ft^3/s = 6.1															
1	*	*	*	-	-	-	*	0.10	Cl, Mg, Sr	*	*	*	*	*	*
2	25	35	3	37	-	-	2, 2	0.05		-1.3 e-3	2.0e-4	5.5e-4	4.0e-4	-7.0e-4	-1.5e-4
3	28	37	7	-	28	-	2, 2	0.05		-8.8e-4	2.7e-4	3.7e-4	2.6e-4	-3.9e-4	-1.5e-4
4	0	36	6	-	2	56	9, 27	0.05		0	3.6e-4	3.8e-4	0	3.7e-5	3.7e-5
Slaughter Creek															
Wet Interval															
Oct 14, 2009, ft^3/s = 5.9															
1	*	*	*	-	-	-	*	0.10	Cl, Sr	*	*	*	*	*	*
2	40	0	0	60	-	-	1, 1	0.05*	Sr (0.08)	-1.4e-3	3.2e-4	1.1e-3	6.1e-4	-9.8e-4	-2.4e-4
3	22	28	5	-	45	-	2, 2	0.04		-9.0e-4	2.5e-4	8.1e-4	4.2e-4	-6.2e-4	-2.1e-4
4	0	18	4	-	28	50	4, 9	0.05		0	3.0e-4	8.3e-4	3.1e-4	-4.6e-4	-1.6e-4

Supplementary Table S3.3. Stream water geochemical modeling results

	Modeled percent (median) of stream water composition						Number of minimal models, total	Specifiied global uncertainty	Constituents requiring uncertainty increase[b]	Modeled amount (mols) of mineral dissolution/exchange (+) or precipitation/exchange (-)					
	Overland runoff	Glen Rose spring	Cow Creek spring	Septic leachate	Waste-water	Drinking water[a]				Calcite	Dolomite	Gypsum	Ca ion exchange	Na ion exchange	K ion exchange
Oct 22, 2009, ft^3/s = 21.3															
1	*	*	*	-	-	-	*	0.10	Cl, Sr	*	*	*	*	*	*
2	39	0	0	61	-	-	1, 1	0.05	Sr (0.10)	-1.6e-3	3.1e-4	1.2e-3	6.0e-4	-9.6e-4	-2.4e-4
3	21	28	5	-	46	-	2, 2	0.05		-1.1e-3	2.4e-4	8.5e-4	4.0e-4	-6.0e-4	-2.28e-4
4	0	12	4	-	27	56	4, 5	0.05		1.0e-4	2.7e-4	8.1e-4	2.6e-4	-3.7e-4	-1.5e-4
Nov 4, 2009, ft^3/s = 5.9															
1	*	*	*	-	-	-	*	0.10	Cl, Sr						
2	31	0	0	69	-	-	1, 1	0.05		-1.5e-4	4.4e-4	1.2e-3	6.9e-4	-1.1e-3	-3.0e-4
3	17	22	6	-	55	-	2, 2	0.05		-9.1e-4	4.4e-4	7.9e-4	4.7e-4	-6.8e-4	-2.8e-4
4	0	13	6	-	40	41	4, 8	0.05		0	3.5e-4	7.8e-4	3.4e-4	-4.5e-4	-2.3e-4
Nov 20, 2009, ft^3/s = 35															
1	*	*	*	-	-	-	*	0.10	Cl, Sr	*	*	*	*	*	*
2	35	0	0	65	-	-	1, 1	0.07	Sr (0.10)	-1.7e-3	3.0e-4	1.0e-3	6.4e-4	-1.0e-3	-2.7e-4
3	18	25	5	-	52	-	2, 2	0.05		-1.1e-3	2.4e-4	-6.8e-4	4.8e-4	-6.7e-4	-2.6e-4
4	0	6	4	-	34	56	2, 10	0.05		8.2e-5	2.8e-4	6.7e-4	3.3e-4	-4.6e-4	-2.0e-4
Dec 2, 2009, ft^3/s = 20															
1	*	*	*	-	-	-	*	0.10	Cl, Sr	*	*	*	*	*	*
2	24	2	0	74	-	-	1, 2	0.05*	Sr (0.10)	-1.7e-3	3.7e-4	1.1e-3	7.7e-4	-1.2e-3	-3.3e-4
3	15	20	6	-	59	-	2, 2	0.05		-1.0e-3	3.1e-4	7.1e-4	5.6e-4	-8.0e-4	-3.0e-4
4	0	0	6	-	43	51	4, 4	0.04		4.2e-5	4.0e-4	7.0e-4	4.3e-4	-6.0e-4	-2.6e-4
Jan 5, 2010, ft^3/s = 4.7															
1	*	*	*	-	-	-	*	0.10	Cl, Sr	*	*	*	*	*	*
2	10	13	0	77	-	-	2, 2	0.10	Sr	-1.7e-3	4.1e-4	1.4e-3	7.9e-4	-1.2e-3	-3.6e-4
3	9	11	6	-	74	-	2, 2	0.05		-1.1e-3	4.4e-4	9.0e-4	7.4e-4	-1.1e-3	-4.0e-4
4	0	0	7	-	56	37	2, 4	0.05		0	3.9e-4	9.0e-4	4.3e-4	-5.5e-4	-3.2e-4
Feb 2, 2010, ft^3/s = 14															
1	*	*	*	-	-	-	*	0.10	Cl, Sr	*	*	*	*	*	*
2	32	3	0	65	-	-	2, 3	0.05		-1.6e-3	4.5e-4	1.2e-3	6.3e-4	-9.5e-4	-3.0e-4
3	18	24	6	-	52	-	2, 2	0.05		-1.0e-3	4.0e-4	8.6e-4	4.4e-4	-6.0e-4	-2.8e-4
4	0	14	6	-	37	43	5, 10	0.05		-1.0e-4	4.2e-4	-8.5e-4	3.2e-4	-4.2e-4	-2.2e-4
Mar 2, 2010, ft^3/s = 11.0															
1	*	*	*	-	-	-	*	0.10	Cl, Sr	*	*	*	*	*	*
2	18	24	0	58	-	-	2, 2	0.05		-1.6e-3	3.3e-4	1.2e-3	5.3e-4	-8.0e-4	-2.6e-4
3	19	25	0	-	56	-	2, 2	0.05		-1.1e-3	3.6e-4	8.6e-4	4.0e-4	-5.3e-4	-2.7e-4
4	0	18	6	-	27	49	6, 13	0.05		0	4.0e-4	8.7e-4	8.6e-5	0	-1.7e-4
Bear Creek															
Dry Interval															
Feb 18, 2009, ft^3/s = 0.09															
1	*	*	*	-	-	-	*	0.10	Cl, SO_4, Sr	*	*	*	*	*	*
2	7	11	0	82	-	-	2, 2	0.05	Sr (0.10)	-2.4e-3	3.1e-4	2.1e-3	9.1e-4	-1.4e-3	-3.6e-4

Supplementary Table S3.3. Stream water geochemical modeling results

	Modeled percent (median) of stream water composition						Number of minimal models, total	Specifiied global uncertainty	Constituents requiring uncertainty increase[b]	Modeled amount (mols) of mineral dissolution/exchange (+) or precipitation/exchange (-)					
	Overland runoff	Glen Rose spring	Cow Creek spring	Septic leachate	Waste-water	Drinking water[a]				Calcite	Dolomite	Gypsum	Ca ion exchange	Na ion exchange	K ion exchange
3	10	14	7	-	69	-	2, 2	0.05		-1.6e-3	3.5e-4	1.7e-3	6.5e-4	-9.6e-4	-3.5e-4
4	0	0	7	-	52	41	2, 2	0.05		-5.6e-4	4.1e-4	1.7e-3	3.6e-4	-4.8e-4	-2.4e-4
Mar 13, 2009, ft^3/s = 0.69															
1	*	*	*	-	-	-	*	0.10	Cl, SO_4, Sr	*	*	*	*	*	*
2	6	12	0	65	-	-	2, 2	0.10	Sr	-2.0e-3	1.0e-4	1.3e-3	7.0e-4	-1.2e-3	-2.7e-4
3	0	41	4	-	55	-	2, 3	0.05		-1.5e-3	3.5e-5	9.3e-4	5.8e-4	-9.1e-4	-2.7e-4
4	0	0	5	-	31	64	1, 2	0.05		0	1.6e-4	9.5e-5	3.3e-4	-4.7e-4	-1.9e-4
April 1, 2009, ft^3/s = 0.3															
1	*	*	*	-	-	-	*	0.10	Cl, SO_4, Sr	*	*	*	*	*	*
2	19	9	0	72	-	-	1, 2	0.05	Sr (0.10)	-2.0e-3	1.9e-4	1.3e-3	7.7e-4	-1.2e-3	-3.2e-4
3	16	22	6	-	56	-	2, 2	0.05		-1.3e-3	1.9e-4	9.8e-4	5.3e-4	-7.7e-4	-2.9e-4
4	0	0	6	-	36	58	2, 4	0.05		-7.2e-5	2.6e-4	9.7e-4	3.4e-4	-4.7e-4	-2.2e-4
May 13, 2009, ft^3/s = 0.45															
1	*	*	*	-	-	-	*	0.10	Cl, SO_4, Sr	*	*	*	*	*	*
2	13	19	0	68	-	-	2, 2	0.05		-2.0e-3	-2.5e-6	1.0e-3	8.1e-4	-1.3e-3	-3.0e-4
3	0	41	5	-	54	-	2, 3	0.05		-1.4e-3	1.5e-5	6.8e-4	6.0e-4	-9.1e-4	-2.8e-4
4	0	0	6	-	32	63	2, 5	0.05		0	1.7e-4	6.9e-4	3.6e-4	-5.2e-4	-2.0e-4
Wet Interval															
Oct 14, 2009, ft^3/s = 9.8															
1	*	*	*	-	-	-	*	0.10	Cl, SO_4, Sr	*	*	*	*	*	*
2	39	0	0	61	-	-	1, 3	0.10	Sr	-1.3e-3	1.2e-4	7.2e-4	6.9e-4	-1.4e-3	-2.4e-4
3	5	44	4	-	47	-	2, 3	0.05		-6.5e-4	0	3.8e-4	5.6e-4	-8.9e-4	-2.3e-4
4	0	21	4	-	37	38	6, 9	0.05		2.3e-4	9.6e-6	3.8e-4	4.6e-4	-7.3e-4	-1.9e-4
Oct 22, 2009, ft^3/s = 15.0															
1	*	*	*	-	-	-	*	0.10	Cl, Sr	*	*	*	*	*	*
2	41	0	0	59	-	-	1, 3	0.10	Sr	-1.2e-3	1.0e-4	6.8e-4	6.8e-4	-1.1e-3	-2.4e-4
3	7	43	4	-	46	-	2, 3	0.05		-7.7e-4	0	-3.5e-4	5.3e-4	-8.6e-4	-2.2e-4
4	0	18	4	-	34	44	6, 9	0.05		2.6e-4	1.9e-6	3.4e-4	4.3e-4	-6.9e-4	-1.8e-4
Nov 4, 2009, ft^3/s = 9.8															
1	*	*	*	-	-	-	*	0.10	Cl, SO_4, Sr	*	*	*	*	*	*
2	12	35	0	53	-	-	2, 3	0.05	Sr (0.09)	-1.1e-3	0.7e-4	7.7e-4	6.2e-4	-1.0e-3	-2.2e-4
3	20	26	5	-	49	-	2, 3	0.05		-5.5e-4	0.8e-5	4.7e-4	4.6e-4	-7.4e-4	-2.1e-4
4	0	36	4	-	38	22	5, 8	0.05		0	6.5e-5	4.7e-4	4.4e-4	-6.8e-4	-2.0e-4
Dec 2, 2009, ft^3/s = 16															
1	*	*	*	-	-	-	*	0.10	Cl, Sr	*	*	*	*	*	*
2	48	0	0	52	-	-	1, 1	0.05	Sr (0.08)						
3	6	59	3	-	32	-	2, 3	0.05		-7.8e-4	0	3.4e-4	3.7e-4	-5.9e-4	-1.5e-4
4	0	27	3	-	19	51	7, 8	0.05		6.5e-4	0	3.3e-4	2.5e-4	-3.8e-4	-1.1e-4
Jan 5, 2010, ft^3/s = 7.5															
1	*	*	*	-	-	-	*	0.10	Cl, SO_4, Sr	*	*	*	*	*	*

Supplementary Table S3.3. Stream water geochemical modeling results

	Modeled percent (median) of stream water composition						Number of minimal models, total	Specifiied global uncertainty	Constituents requiring uncertainty increase[b]	Modeled amount (mols) of mineral dissolution/exchange (+) or precipitation/exchange (-)					
	Overland runoff	Glen Rose spring	Cow Creek spring	Septic leachate	Waste-water	Drinking water[a]				Calcite	Dolomite	Gypsum	Ca ion exchange	Na ion exchange	K ion exchange
2	30	13	0	57	-	-	2, 3	0.10	Sr	-9.0e-4	0.8e-4	7.4e-4	6.8e-4	-1.1e-3	-2.5e-4
3	0	55	3	-	42	-	2, 3	0.05		-6.38e-4	1.8e-5	3.9e-4	5.4e-3	-7.9e-4	-2.1e-4
4	0	40	3	-	35	22	6, 8	0.05		0	0	3.9e-4	3.9e-4	-6.0e-4	-1.9e-4
Feb 2, 2010, ft^3/s = 24															
1	*	*	*	-	-	-	*	0.10	Cl,Sr	*	*	*	*	*	*
2	53	0	0	47	-	-	1, 1	0.05		-7.7e-4	1.4e-4	6.2e-4	5.3e-4	-8.5e-4	-2.0e-4
3	39	21	4	-	36	-	2, 2	0.05		-3.9e-4	0.8e-4	3.7e-4	3.9e-4	-5.9e-4	-1.8e-4
4	0	31	3	-	12	54	9, 11	0.05		7.0e-4	1.2e-5	3.5e-4	2.0e-4	-3.12e-4	-8.7e-5
Mar 2, 2010, ft^3/s = 15															
1	*	*	*	-	-	-	*	0.10	Cl,Sr	*	*	*	*	*	*
2	43	16	0	41	-	-	2, 2	0.05		-8.7e-4	0.6e-4	4.0e-4	4.6e-4	-7.6e-4	-1.7e-4
3	43	19	4	-	34	-	2, 2	0.05		-5.0e-4	0.8e-4	3.5e-4	3.6e-4	-5.5e-4	-1.7e-4
4	0	30	3	-	9	58	9, 15	0.05		6.7e-4	2.9e-6	3.2e-4	1.6e-4	-2.5e-4	-7.3e-5
Onion Creek															
Wet Interval															
Oct 14, 2009, ft^3/s = 8.1															
1	4	89	7	-	-	-	2, 3	0.05		-1.0e-3	0	1.1e-3	4.00E-06	-4.8e-5	4.0e-5
2	16	69	7	8	-	-	1,1	0.05		-9.6e-4	0	1.1e-3	1.1e-4	-2.2e-4	-
3	18	67	8	-	7	-	1, 1	0.05		-8.6e-4	0	1.1e-3	8.7e-5	-1.7e-4	-
4	21	43	8	-	0	27	11, 52	0.05		0	0	9.9e-4	0	-1.7e-5	1.7e-5
Oct 26, 2009, ft^3/s = 247															
1	*	*	*	-	-	-	*	0.10	Cl, Mg, Sr	*	*	*	*	*	*
2	76	0	4	20	-	-	1, 1	0.05		-1.1e-3	0	3.9e-4	2.2e-4	-3.9e-4	-4.2e-5
3	78	0	6	-	16	-	1, 1	0.05		-8.6e-4	0	2.9e-4	1.6e-4	-2.7e-4	-3.8e-5
4	59	0	5	-	0	36	3, 6	0.05		-1.2e-4	0	2.9e-4	-1.4e-5	0	2.8e-5
Nov 4, 2009, ft^3/s = 19															
1	*	*	*	-	-	-	*	0.10	Cl, SO_4, Sr	*	*	*	*	*	*
2	47	15	5	33	-	-	2, 2	0.05		-8.1e-4	0.6e-4	5.9e-4	4.1e-4	-7.0e-4	-1.3e-4
3	49	17	9	-	25	-	2, 2	0.05		-5.0e-4	0.7e-4	4.2e-4	2.8e-4	-4.4e-4	-1.1e-4
4	0	42	7	-	0	51	6, 19	0.05		5.2e-4	0	3.9e-4	8.9e-5	-1.7e-4	0
Nov 20, 2010, ft^3/s = 161															
1	*	*	*	-	-	-	*	0.10	Cl, SO_4, Sr	*	*	*	*	*	*
2	47	14	3	36	-	-	2, 2	0.05		-1.2e-3	0.5e-4	6.3e-4	4.3e-4	-7.3e-4	-1.3e-4
3	48	17	7	-	28	-	2, 2	0.05		-8.9e-4	0.6e-4	4.5e-4	2.8e-4	-4.5e-4	-1.1e-5
4	10	36	6	-	0	49	9, 26	0.05		2.5e-5	0	4.8e-4	0	-5.1e-6	5.1e-6
Dec 2, 2010, ft^3/s = 108															
1	*	*	*	-	-	-	*	0.10	Cl, SO_4, Sr	*	*	*	*	*	*
2	47	16	4	33	-	-	2, 2	0.05		-1.0e-3	0.6e-4	5.6e-4	4.0e-4	-7.0e-4	-1.3e-4
3	49	18	8	-	25	-	2, 2	0.05		-7.3e-4	0.7e-4	3.9e-4	2.8e-4	-4.5e-4	-1.0e-4
4	7	29	7	-	0	57	7, 11	0.05		4.2e-4	0	3.7e-4	8.4e-5	-1.6e-4	-1.1e-5

Supplementary Table S3.3. Stream water geochemical modeling results

	Modeled percent (median) of stream water composition						Number of minimal models, total	Specifiied global uncertainty	Constituents requiring uncertainty increase[b]	Modeled amount (mols) of mineral dissolution/exchange (+) or precipitation/exchange (-)					
	Overland runoff	Glen Rose spring	Cow Creek spring	Septic leachate	Waste-water	Drinking water[a]				Calcite	Dolomite	Gypsum	Ca ion exchange	Na ion exchange	K ion exchange
Jan 5, 2010, ft^3/s = 44															
1	*	*	*	-	-	-	*	0.10	Cl, SO_4, Sr	*	*	*	*	*	*
2	44	15	4	37	-	-	2, 2	0.05		-1.0e-3	0.6e-4	5.5e-4	5.0e-4	-8.3e-4	-1.6e-4
3	46	18	8	-	28	-	2, 2	0.05		-6.5e-4	0.7e-4	3.5e-4	3.5e-4	-5.5e-4	-1.4e-4
4	0	30	7	-	0	64	7, 13	0.05		6.1e-4	0	3.3e-4	1.3e-4	-2.3e-4	-2.6e-5
Feb 2, 2010, ft^3/s = 218															
1	*	*	*	-	-	-	*	0.10	Cl, Mg, Sr	*	*	*	*	*	*
2	55	22	2	22	-	-	1, 3	0.05		-6.9e-4	0	3.0e-4	2.9e-4	-5.1e-4	-8.2e-5
3	64	13	4	-	19	-	2, 2	0.05		-4.7e-4	0.5e-5	2.0e-4	2.3e-4	-3.7e-4	-0.9e-4
4	33	20	4	-	0	43	6, 11	0.05		4.0e-4	0	1.8e-4	8..1e-5	-1.5e-4	-1.2e-5
Mar 2, 2010, ft^3/s = 177															
1	*	*	*	-	-	-	*	0.10	Mg, Sr	*	*	*	*	*	*
2	57	17	2	24	-	-	1, 3	0.05		-7.4e-4	0	3.1e-4	3.4e-4	-5.3e-4	-9.6e-5
3	56	21	5	-	18	-	1, 3	0.05		-5.2e-4	0	1.9e-4	2.2e-4	-3.4e-4	-8.1e-5
4	30	37	3	-	0	29	1, 2	0.05		-6.3e-5	0	1.9e-4	5.0e-5	-1.0e-4	0

"-" not included in model; "*" could not be modeled; [a]zero contribution not recorded 3; [b]value in paranthesis specifies the uncertainty assigned to a single constituent

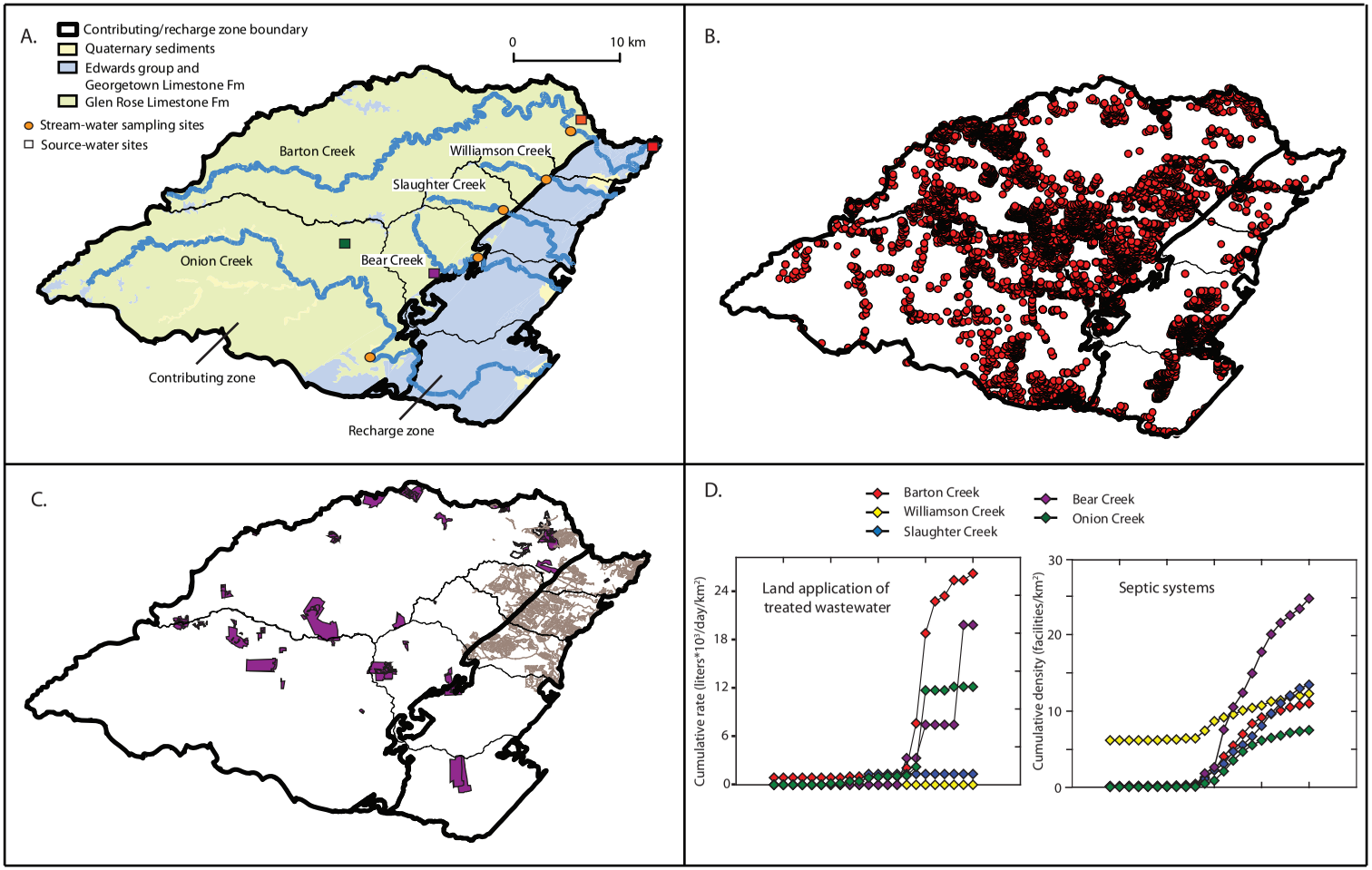

Figure 3.1. A) Geology of contributing and recharge zones for each watershed and steam water and source water end member sampling sites located within the watersheds of the Barton Springs Segment of the Edwards Aquifer. Source water end members include overland runoff (purple), spring (green), wastewater (red), and septic leachate (orange). B) Locations of permitted septic systems for each watershed (2010 data from Mahler et al., 2011a). C) Location of wastewater mains and permitted areas for land application of treated wastewater (data from Herrington et al., 2010 and Mahler et al., 2011a). D) Temporal trends of septic system density and permitted land application of treated wastewater adapted from Mahler et al. (2011a).

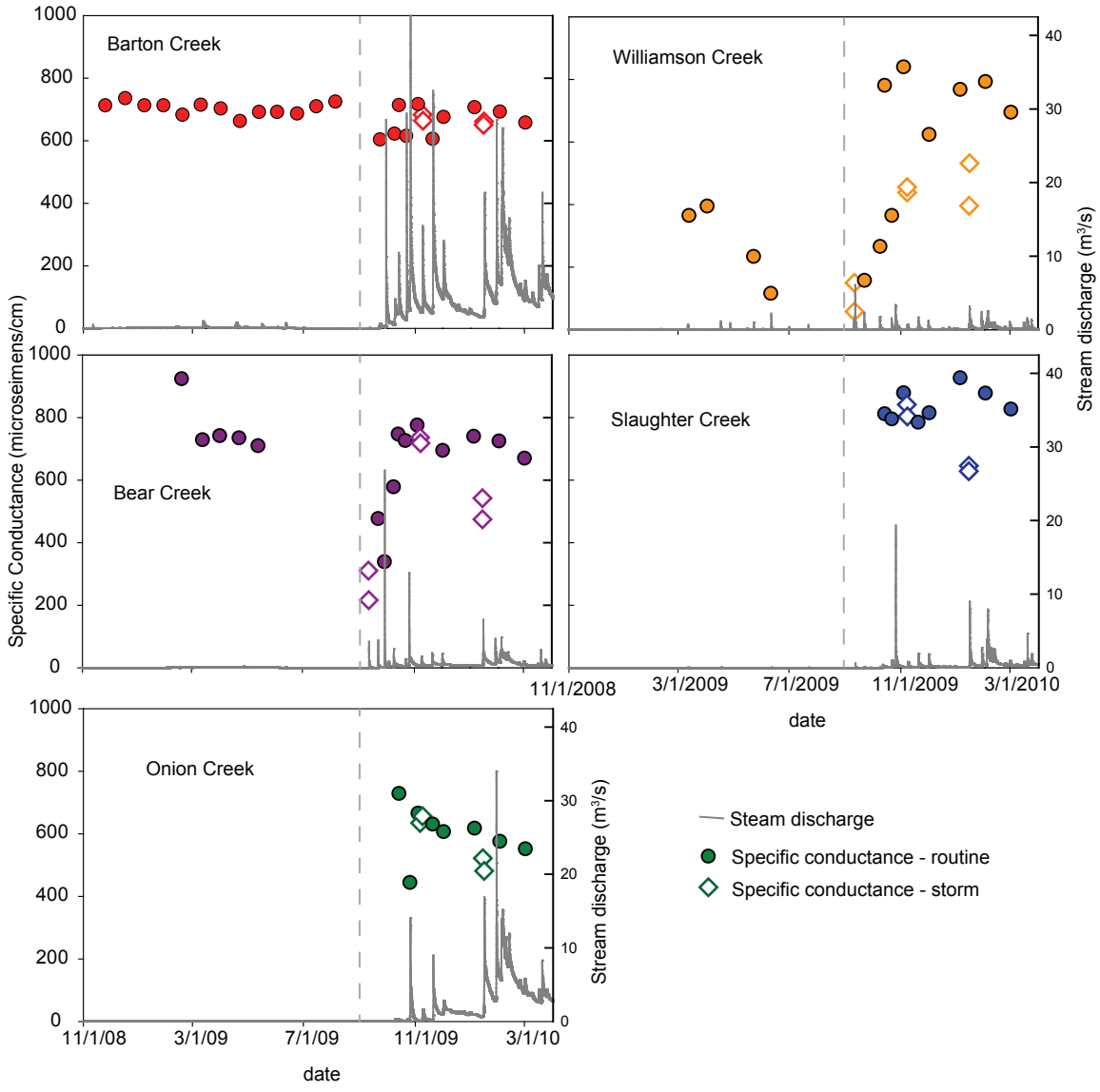

Figure 3.2. Time series of stream water discharge and specific conductance values for each site. Dashed line marks end and start of dry and wet intervals, respectively.

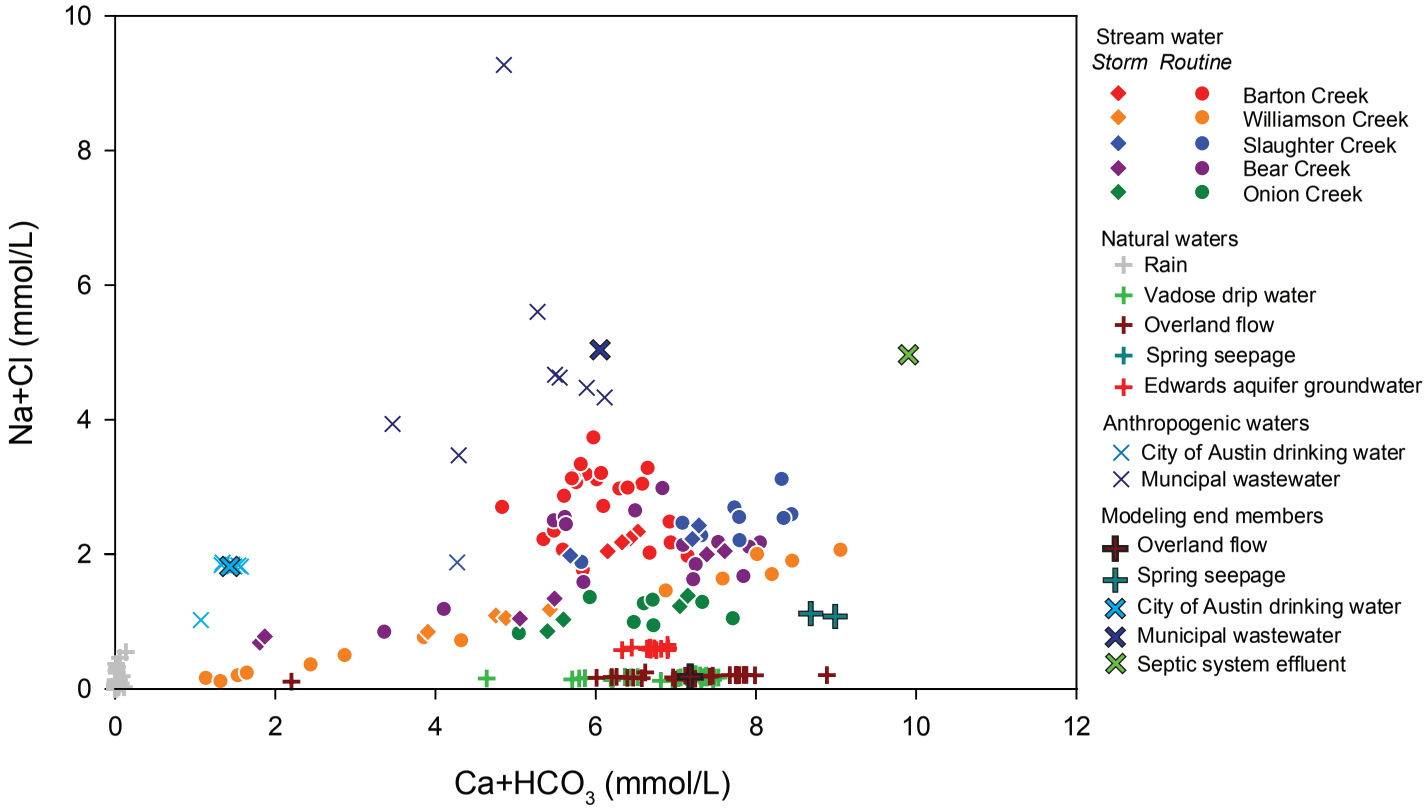

Figure 3.3. $Ca+HCO_3$ and Na+Cl concentrations for rainfall, stream water, and proposed sources of stream water.

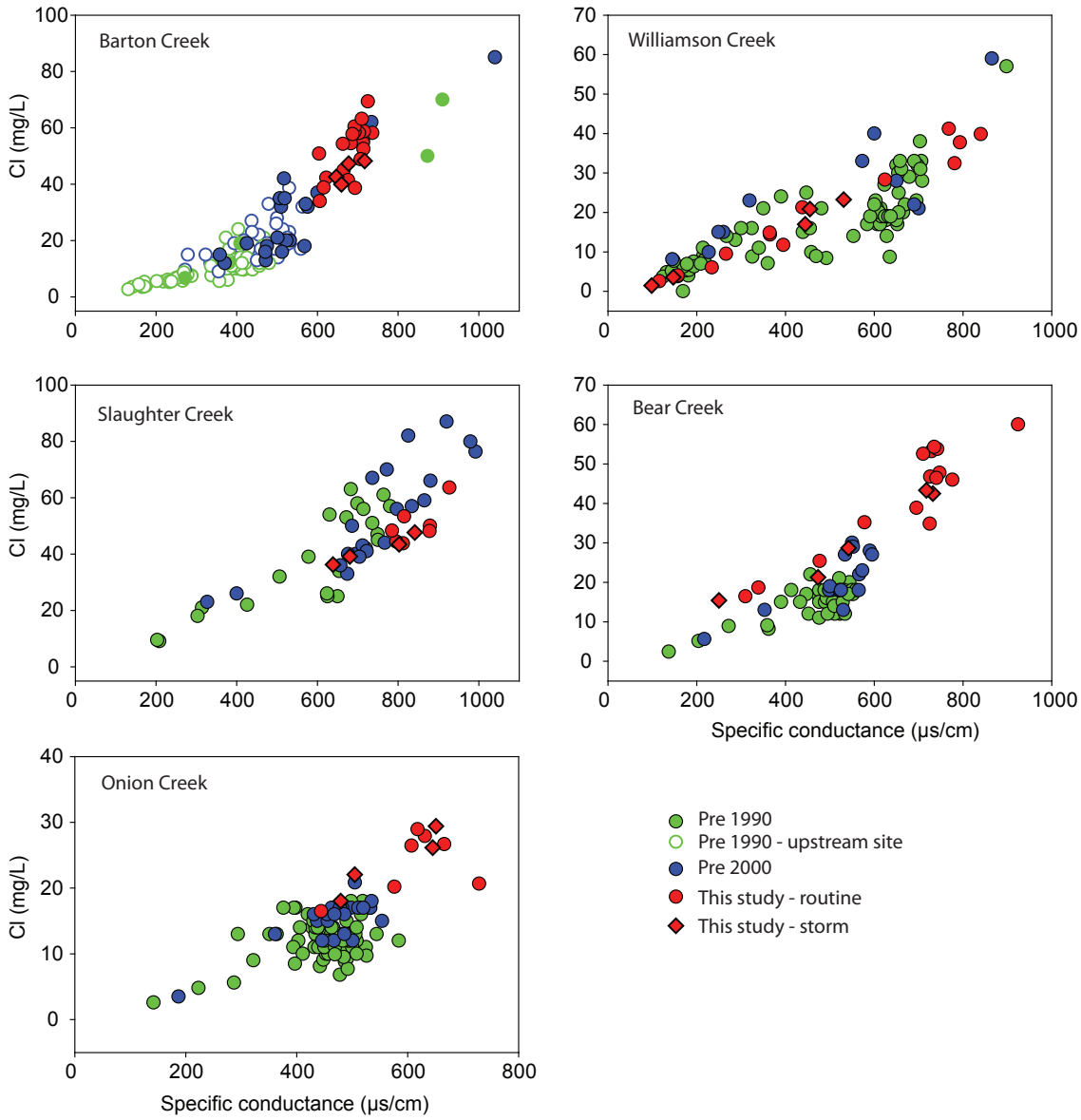

Figure 3.4. Stream water Cl concentrations and specific conductance values for each site grouped by time interval. Historic data from upstream sites (Barton Creek at Hwy 71 and Loop 360) are shown for Barton Creek, respectively, as few historic data are availiable for the Barton at Lost Creek site.

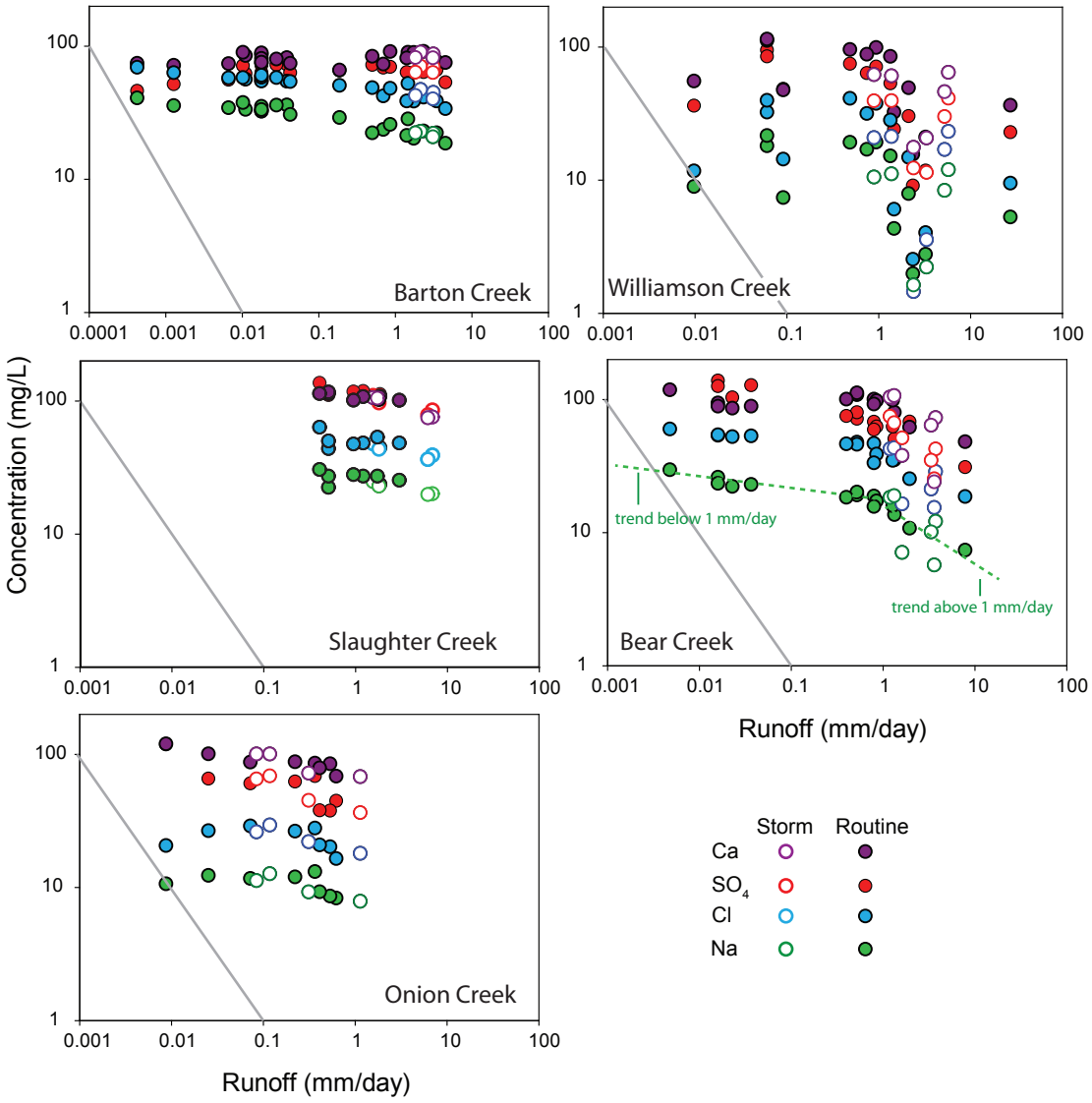

Figure 3.5. Stream water Ca, Cl, Na, and SO_4 concentrations and runoff (i.e., discharge normalized to watershed area) for each site. Stream water concentrations decrease little with increases in runoff (log-log slope close to 0). Concentrations determined by fixed solute flux rates to streams would have the same slope as grey lines that delineate a log-log slope of -1. Note that Barton Creek runoff is plotted on a distinct x-axis. Figure modeled after Godsey et al. (2009).

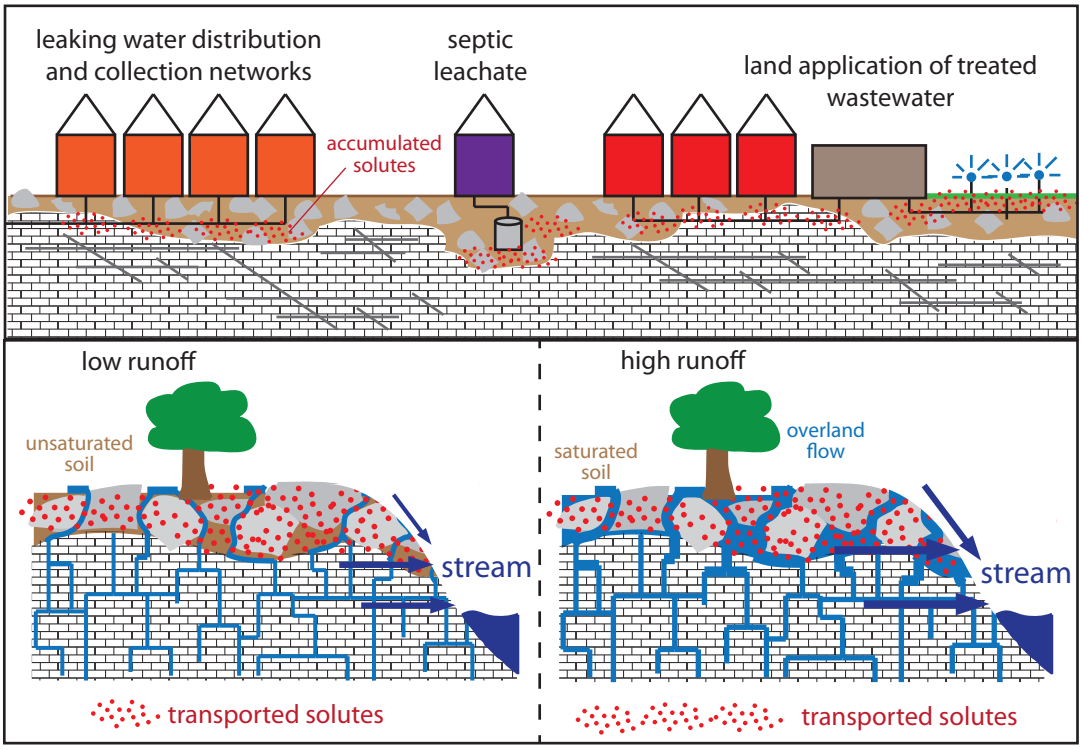

Figure 3.6. Conceptual model of anthropogenic sources and accumulation of solutes in the soil and epikarst zone (top). Solute transport to streams in runoff and seepage flow increases with elevated runoff (i.e., discharge normalized to watershed area) because of faster weathering rates associated with greater extents of wetted surface area (bottom).

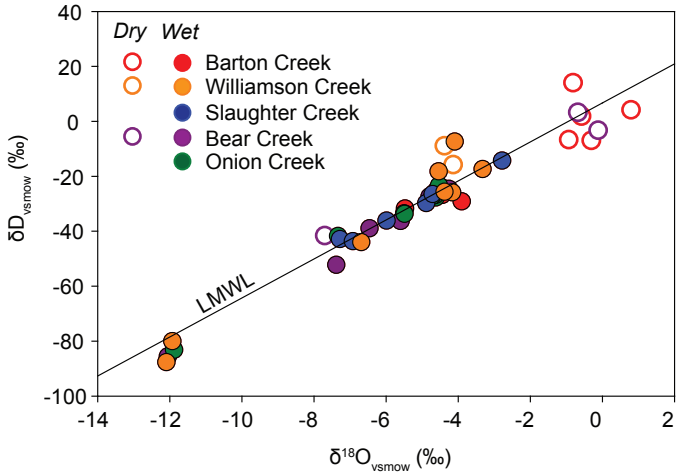

Supplementary Figure S3.1. Stable isotope values measured in stream water during dry and wet intervals along with the local meteroric water line (LMWL) as defined by Pape et al. (2010).

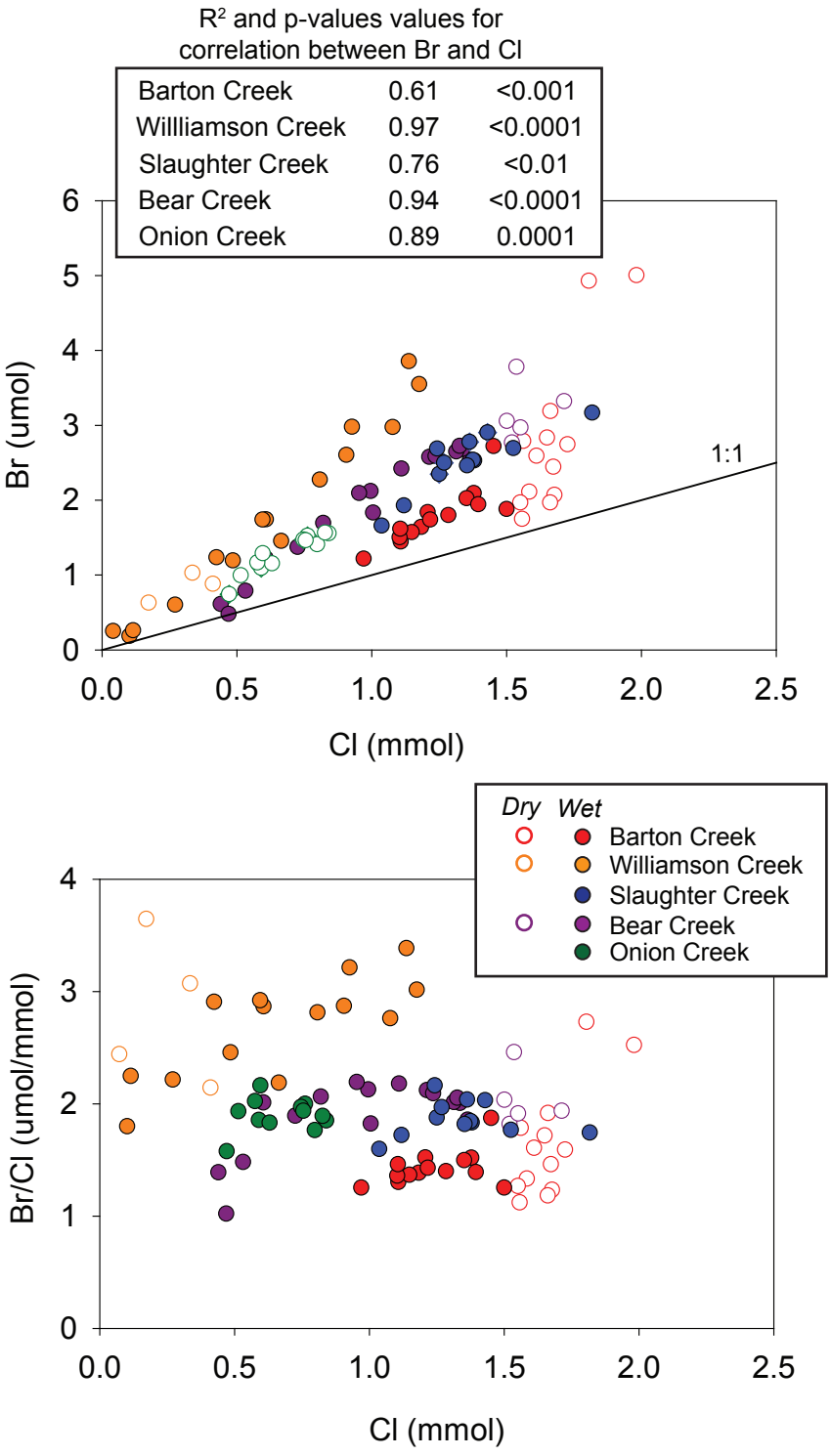

Supplementary Figure S3.2. Br and Cl concentrations and Br/Cl ratios for stream water during dry and wet intervals.

Chapter 4. Investigating groundwater flow between Edwards and Trinity aquifers in central Texas

ABSTRACT

Understanding the nature of communication between aquifers can be challenging when using traditional physical and geochemical groundwater sampling approaches. This study uses two multiport wells completed within the Trinity aquifer and the Barton Springs segment of the Edwards aquifer in central Texas to determine if groundwater is flowing between adjacent aquifers. Potentiometric surfaces, hydraulic conductivities, and groundwater major ion concentrations and Sr isotope values were measured from multiple zones within three hydrostratigraphic units (Edwards and Upper and Middle Trinity aquifers). Physical and geochemical data from the multiport wells were combined with historical measurements of groundwater levels and geochemical compositions from the region to characterize groundwater flow and identify controls on the geochemical compositions of Edwards and Trinity aquifer groundwater. Our results suggest that vertical groundwater flow between the Edwards and Middle Trinity aquifers is likely limited by low permeability, evaporite-rich units within the Upper and Middle Trinity. Potentiometric surface levels in both aquifers vary with changes in wet vs. dry conditions, indicating that recharge to both aquifers occurs through distinct recharge areas. Geochemical compositions of groundwater in the Edwards, Upper, and Middle Trinity aquifers are distinct and likely reflect groundwater interaction with different lithologies (i.e., evaporates and sediments with more/less silicate material) as opposed to mixing of groundwater between the aquifers. These results have implications for the management of these adjacent aquifers as they indicate that, under current conditions, pumping of the Edwards and Middle Trinity aquifers will likely not induce vertical cross-formational flow between the aquifers.

INTRODUCTION

Aquifers are often defined by geologic units (lithostratigraphy) and are managed independently without consideration of the actual hydrostratigraphy of those units (Mazor, 1995; Quinlan et al., 1991). Structural deformation, however, can result in joints and faulting that juxtapose aquifers and/or create vertical flow paths by which flow between distinct aquifers can occur. Determining the occurrence of inter-flow between aquifers is critical to informing decisions about conjunctive versus independent aquifer management as the pumping of one aquifer can impact the other. For example, the Edwards aquifer, in central Texas, is the sole-source water supply for 2 million people. The Barton Springs/Edwards Aquifer Conservation District (BSEACD) has placed limits on groundwater extraction from the Edwards Aquifer within its jurisdiction for sustainable yield considerations (BSEACD, 2008). The result of that policy decision is that the adjacent and underlying Trinity aquifer is one of the targets for alternative to the Edwards aquifer for groundwater supply to the region. Hydrogeologic information is needed to characterize the water quality of the Trinity aquifer and address the potential for inter-flow between these aquifers to guide regulatory (e.g. well construction) and management policies (e.g. pumping permits) of the aquifers.

Multiple organizations concerned with the management of the Edwards aquifer (e.g., Edwards Aquifer Authority, City of Austin, Texas Water Development Board, Hays Trinity Groundwater Conservation District, and BSEACD) have focused recent research efforts on characterizing the potential for inter-aquifer flow to occur between the Edwards and Trinity aquifers. Research approaches have included recharge and geophysical surveys (Gary et al., 2011), stream loss studies (Green et al., 2011), dye tracing experiments (Schindel and Johnson, 2011), groundwater modelling efforts (Jones, 2011), and geochemical analyses (Hauwert, 2011; Kromann et al., 2011). To the

knowledge of the authors, much of this research is largely available in agency reports (e.g., Johnson et al., 2010; Weirmen et al., 2010; Jones et al., 2011), extended abstracts in conference proceedings (e.g., Gary et al., 2011; Hauwert et al., 2011; Smith and Hunt, 2011), or in abstracts associated with national conferences (Kromann et al., 2011; Andrews et al., 2013), but many have not been submitted to peer review. A summary of this research is presented in Supplementary Table S4.1.

The research presented here tests the null hypothesis that flow between aquifers does not occur. This can be perceived as a bold hypothesis because hydrologic systems traditionally thought to occur in isolation (e.g., surface and groundwater) have been reconsidered as a single, inter-connected system in recent decades (e.g., Winter et al, 1998; Barlow and Leake, 2012). The prevailing conceptual understanding of the system, however, considers inter-flow between Trinity and Edwards aquifers to be minimal in the study area (Slade et al., 1986). The results from this study will have critical implications for the co-management of Edwards and Trinity aquifers as the Middle Trinity aquifer is increasingly developed.

The connection between the Trinity and Edwards aquifers is investigated by measuring potentiometric surface levels, hydraulic conductivities, and groundwater geochemistry (major ions and Sr isotopes) using multiport wells at two sites within the Barton Springs segment of the Edwards aquifer in central Texas. These results are combined with a compilation of existing physical and geochemical data to assess controls on spatial and temporal variations in potentiometric surface levels and groundwater geochemistry in each aquifer. The results suggest that, under current conditions, substantial inter-aquifer flow does not occur, and that processes other than inter-aquifer mixing can account for measured physical and geochemical variations.

PROJECT SETTING

Hydrogeologic setting

The Trinity and Edwards aquifers are regionally expansive, Cretaceous carbonate aquifers in central Texas that are juxtaposed by Miocene-age normal faulting in the Balcones Fault Zone (BFZ). The prolific and karstic Edwards aquifer is subdivided into three segments, one of which, the Barton Springs segment, is the focus of this study. The Edwards aquifer is both stratigraphically above and juxtaposed adjacent to the Trinity aquifer due to faulting associated with the BFZ (Fig. 4.1). The Edwards aquifer is composed of the Georgetown Formation and underlying the Edwards Group consisting of the Person and Kainer Formations (Rose, 1972) (Table 4.1).

Recharge to the Edwards aquifer occurs where the bedrock of the Edwards group is heavily faulted, karstified, and exposed at the surface (i.e., recharge zone; Fig. 4.1). Direct recharge to the subsurface can rapidly occur through solution features, such as caves, sinkholes, and swallets in stream channels (e.g., Slade et al., 1986; Hauwert, 2009), making the aquifer system sensitive to changes in local meteorological conditions (Wong et al., 2012). The watersheds to the west of the recharge zone, where the Trinity units are exposed, comprise the contributing zone. The Edwards aquifer is confined to the east of the recharge zone, and is bounded further to the east by saline groundwater. Streams originating in the contributing zone provide the majority of recharge to the aquifer via losing streams that cross the recharge zone (Slade et al., 1986). Groundwater in the Edwards aquifer generally flows to the northeast, and velocities up to 12 km/day have been measured using dye tracing methods (Hauwert, 2009). Groundwater naturally discharges at Barton Springs, which is the fourth largest spring in Texas, a culturally and historically important landmark of Austin, and habitat to endangered and endemic species.

The Trinity aquifer is the sole source of groundwater in much of the Texas Hill Country west of the BFZ. It is divided into three units, of which the Middle and Upper Trinity are pertinent to this study. The Middle Trinity is composed of Cretaceous carbonate and clastic sedimentary units. The Hammett Shale underlies the Middle Trinity and functions as an aquitard. The Middle Trinity aquifer, from oldest to youngest units, consists of the Cow Creek Limestone, Hensel Sand, and Lower Glen Rose Limestone. Overlying the Middle Trinity aquifer is the Upper Trinity aquifer composed of the Upper Glen Rose Limestone (Table 1; Stricklin et al., 1971). The Middle Trinity is the source of most of the groundwater production in the Texas Hill Country west of the BFZ. The Upper Trinity is generally not a target for groundwater production due to low yields, drought vulnerability, and generally poor water quality (high SO_4 and total dissolved solids). The Upper and Middle Trinity aquifers are recharged by infiltration of rainfall or water from losing streams entering the aquifer host rock where it is exposed at the surface (Mace et al, 2000; Ashworth, 1983). The recharge zone of the Trinity aquifers generally corresponds to the contributing zone of the Edwards aquifer.

Groundwater of the Edwards aquifer is typically Ca-HCO_3, reflecting water interaction with carbonate host rock. Trinity aquifer groundwater ranges from Ca-HCO_3 to Ca-SO_4, reflecting water interaction with carbonate host rock and dissolution of evaporite minerals occurring in the aquifer host rock (Senger and Kreitler, 1984). Edwards aquifer groundwater generally has lower concentrations of total dissolved solids (TDS) than groundwater of the Trinity aquifer (median 370 and 670 mg/L for wells in Travis and Hays County identified in the Edwards and Trinity aquifer, respectively) (Texas Water Development Board, 2012).

Application of Sr isotopes in central Texas karst aquifers

Sr isotope ratios ($^{87}Sr/^{86}Sr$) have been demonstrated to be useful in investigations of sources and processes controlling water compositions in central Texas (e.g., Musgrove and Banner, 2004; Wong et al., 2011). In this region, water acquires an initial Sr isotope signature by interacting with siliceous material in soils that overlie Cretaceous carbonate bedrock. As water interacts with the bedrock, its Sr isotope signature evolves from that of the soil (~0.7090) to that of the limestone (~0.7076). Longer groundwater residence times allow for more water-rock interaction with the limestone and, consequently, lower Sr isotope values. Sr isotopes, therefore, can be used as a relative indicator of climate conditions (dry vs. wet) and/or groundwater flow paths (conduit vs. diffuse) as both can influence water residence times (e.g., Banner et al., 1996; Wong et al., 2010; Musgrove et al., 2010). Additionally, water interaction with mineral assemblages that have Sr isotope values that are distinct from those of Cretaceous carbonates, such as terrestrially derived silicate minerals, can influence the Sr isotope values of groundwater (Banner, 2004).

Climate setting

Central Texas is characterized by a sub-humid to semi-arid climate with hot summers and mild winters (Larkin et al., 1983) and has an average annual rainfall of 860 mm and a range of 390 to 1370 mm (1856–2010; National Climate Data Center, 2012). Groundwater in the Barton Springs segment of the Edwards aquifer is sensitive to changes in meteorological conditions, which often cycle between wet and dry intervals (Wong et al., 2012). Drought conditions, as quantified by the Palmer Drought Severity Index, ranged from -6 (extreme drought) to 3 (very moist) during the study interval (February 2008-July 2011; Fig. 2) (National Oceanic and Atmospheric Administration, 2012).

METHODS

Multiport well sampling

Trinity and Edwards aquifers were sampled using two Westbay® multiport wells in Hays County, referred to here as the Antioch and the Ruby Ranch wells (Fig. 4.1). The multiport well approach allows the sampling of multiple known and isolated hydrostratigraphic units at the same location. This approach is advantageous to the traditional approach, which relies on wells that are spatially distributed and can have imprecisely known screened intervals spanning several hydrostratigraphic units (Supplementary Fig. S4.1). The Antioch well is located in the confined zone, and the Ruby Ranch well is located in the recharge zone, west (7 km) and up gradient of Antioch. The closest areas for recharge to the Lower Glen Rose, Hensel Sand, and Cow Creek Limestone formations are about 20 km west southwest of the Ruby Ranch well. Lithostratigraphic units were delineated using geophysical data (Wierman et al., 2010). One to six zones were isolated in each of the several lithostratigraphic units that host each aquifer. A total of 21 and 13 zones were isolated at the Antioch and Ruby Ranch wells, respectively (Table 4.1, and Fig. 4.1).

Potentiometric surface levels were measured monthly to bimonthly in each zone from February 2008 to January 2012 at the Ruby Ranch well and from September 2010 to December 2012 at the Antioch well using Westbay® groundwater pressure probes and controls. At the Ruby Ranch well, groundwater was sampled from each zone in June 2009 and again in June 2010, and from select zones in July 2011. At the Antioch well, groundwater was sampled from each zone in June 2011. Details of well and pressure probe specification and descriptions of sampling methods are included in the Supplementary Material.

Hydraulic conductivity was calculated for each zone in the multiport wells by applying analytical solutions (Bouwer and Rice, 1976; Bouwer, 1989; and Butler 1998) to rising and falling head data. Data was collected from May-June, 2012 under dry conditions (-3.5 PDSI). Details of hydraulic conductivity methods are included in the Supplementary Material.

During installation of the Antioch well, evaporite nodules were observed with a down hole camera at depths corresponding to the Upper and Lower Glen Rose formations. Samples of evaporite nodules (anhydrite and/or gypsum) were recovered from well cuttings collected during the installation of the Antioch well at depths corresponding to the Upper and Lower Glen Rose formations.

Analytical methods

Groundwater samples were analyzed for major ions at the Lower Colorado River Authority Environmental Laboratory Services in Austin, Texas using an inductively coupled plasma optical emission spectrometer and ion chromatograph. Detection limits for the major ions were: 0.2 mg/L for Ca, Mg, K, Na; 20 μg/L Sr; 1 mg/L for Cl and SO_4; 2 mg/L for alkalinity (as $CaCO_3$), 0.02 mg/L for NO_3. The absolute difference between cation and anion charges was <5% for all samples, and there was not a bias to positive or negative charges.

Sr was isolated using ion exchange chemistry, and Sr isotope values were measured using a Finnigan-MAT 261 thermal ionization mass spectrometer at the Department of Geological Sciences at The University of Texas at Austin (UT; n=27) and a multicollection VG Sector 54 mass spectrometer at Massachusetts Institute of Technology (MIT; n=12). Analytical uncertainty, based on the long-term reproducibility of the NIST SRM 987 standard (reported value of 0.712034 +/- 0.00026), was 0.71026

+/- 0.000015 and 0.71024 +/- 0.000018 for samples analyzed at UT and MIT, respectively. Laboratory blanks ranged from 16 to 19 pg (n=2). Replicates of samples analyzed at UT and MIT (n=9) were within analytical uncertainty, except one, which had a difference of 0.000041. One set of evaporite samples was leached using 1 mol/L ammonium acetate (Suarez, 1996), and a replicate set was leached using water. Samples were then partially dissolved in acetic acid, prior to ion exchange chemistry and analysis for Sr isotope values. Additional details regarding analytical methods are included in the Supplemental Material.

Compilation of and comparison to existing data

A map of regional variations in potentiometric surface levels and total dissolved solids (TDS, mg/L) concentrations in the Middle Trinity aquifer was created to assess the potential of lateral groundwater flow in the Middle Trinity aquifer. The maps were created using a compilation of existing groundwater level data. Temporal variations in potentiometric surface levels measured at the Ruby Ranch and Antioch wells were compared to those measured at two wells completed in the Middle Trinity aquifer (Storm Ranch and Downing wells; Fig. 4.1) located up gradient and between the multiport well sites and the recharge area for the Middle Trinity aquifer. Geochemical compositions measured from the Edwards and Trinity aquifers collected from the multiport wells in this study were compared to existing geochemical data collected in the project area. Additional detail regarding data sources and methods is included in the Supplemental Material.

RESULTS

Potentiometric surface levels and hydraulic conductivities

Spatial variations in potentiometric surface levels measured in Hays and adjacent counties indicate that there is a potentiometric ridge that is oriented east-west in the middle of the county (Fig. 4.3). To the north of the ridge, the groundwater gradient is generally to the east and northeast. To the south, the gradient is to the east and southeast. There is an east-west orientated fresh water (TDS<1,000 mg/L) plume to the south of the potentiometric ridge. It originates in the southwestern portion of Hays County where the Blanco River flows across bedrock units of the Middle Trinity aquifer.

Potentiometric surface levels in all of the hydrostratigraphic units at both sites had similar temporal patterns that correspond with changes in the PDSI, except for some zones (e.g., Ruby Ranch well zone 9 and 10 and Antioch well zone 10) in the Upper Glen Rose (UGR) and Lower Glen Rose (LGR) units (Table 4.1 and Fig. 4.2a). Similar temporal variations were measured in Middle Trinity wells (Storm Ranch and Downey) up gradient from the Ruby Ranch and Antioch wells.

At the Ruby Ranch well, potentiometric surface levels in the Edwards and UGR units were higher than those in the LGR and the combined Hensel and Cow Creek (HCC) units for the entire monitoring interval. Potentiometric surface levels measured in zone 1, completed in the Hammett Shale, are similar to those measured in Cow Creek units (zones 2-3). It is likely that zone 1 is representative of the Cow Creek units because i) of this similarity, and ii) the contact between the Cow Creek and Hammett Shale is transitional. At the Antioch well, potentiometric surface levels in the Edwards and uppermost zone of the UGR were higher than surface levels in the LGR, HCC, and some zones of the UGR under wet conditions (PDSI > 0) and lower during dry conditions (PDSI<0). At both sites, potentiometric surface levels within select zones of the UGR

(i.e., zone 10 at both Ruby Ranch and Antioch) varied little with changing climate conditions when compared to the potentiometric surface level differences measured in the zones that were both above and below (Fig. 4.2a and 4.4). Furthermore, depth profiles of potentiometric surface levels illustrate large differences in potentiometric surface levels measured above and below these zones within UGR units (Fig. 4.4).

Hydraulic conductivity results were similar between the two wells, with values in the Edwards and HCC units being 1 to 2 orders of magnitude higher than those measured in most UGR and LGR units (Fig. 4.4). Similar to potentiometric surface levels, uppermost UGR units and lowermost LGR units had hydraulic conductivities that were more consistent with overlying Edwards and underlying HCC units, respectively, than with the majority of UGR and LGR units. For example, hydraulic conductivities in zones 13-14 (the uppermost UGR units) in the Antioch well were more similar to Edwards units than with zones 8-12 (the remaining UGR units) (Fig. 4.4).

Chemical Hydrogeologic Data

Water types range from Ca-HCO_3 in the Edwards to Ca-SO_4 and Ca-HCO_3-SO_4 in the UGR, LGR, and HCC at both sites (Table 4.2 and Supplementary Fig. S4.2). Median concentrations of Ca and HCO_3 are similar between all the Edwards units, but median concentrations of Mg, Sr, K, Na, Cl, and SO_4 in groundwater from the Edwards units are 20% to 100% lower than those measured in UGR, LGR, and HCC units (Supplementary Table S4.2). Concentrations measured in HCC units are lower relative to those measured in UGR and LGR units. Groundwater from the Edwards and select zones of the UGR have a 1:1 correspondence between molar concentrations of Ca+Mg and HCO_3. Groundwater from the remaining zones of UGR and zones of the LGR and HCC have a

1:1 correspondence between molar concentrations of Ca+Mg-SO_4 and HCO_3 (Supplementary Fig. S4.3).

Sr isotope values ($^{87}Sr/^{86}Sr$) range from 0.70753 to 0.70808 and 0.70751 to 0.70834 for Edwards and Trinity aquifer groundwater, respectively (Table 4.2). Values were generally lowest in groundwater from the Edwards aquifer and increased in groundwater from UGR to LGR to HCC units, except for two Edwards aquifer groundwater compositions with high $^{87}Sr/^{86}Sr$ values (Figs. 4.5 and 4.6). $^{87}Sr/^{86}Sr$ values of groundwater measured in this study are i) within the range of values previously measured for groundwater of the Edwards and Trinity aquifers (Fig. 4.5), and ii) higher than the majority of previous measurements of Edwards (22 of 23) and Trinity (11 of 13) aquifer host rock range from 0.7074 to 0.7078 and 0.7074 to 0.7077, respectively (Fig. 4.6) (Koepnick et al., 1985; Musgrove et al., 2004; Christian et al., 2011; Wong et al., 2011). Evaporite nodules recovered from Upper and Lower Glen Rose units ranged from 0.70773 to 0.70795, which is consistent with the range of $^{87}Sr/^{86}Sr$ values measured for most groundwater sampled from UGR and LGR units (Fig. 4.6). The uncertainty in Sr isotope values is 0.000015. This means that the range of Sr isotope values measured in the groundwater is significant, and some groundwater values are distinct from Sr isotope values of Edwards and Trinity aquifer bedrock.

There is a general increase in SO_4 and Sr concentrations in groundwater from Edwards to HCC to UGR and LGR units, although groundwater from some UGR and LGR units have SO_4 and Sr concentrations that are intermediate to Edwards and HCC units (Fig. 4.6). $^{87}Sr/^{86}Sr$ values, however, generally increase from Edwards to UGR and LGR to HCC units (Fig. 4.6). Groundwater samples from the lowermost Edwards and uppermost UGR units at Antioch have anomalously high Sr concentrations (Fig. 4.6). All

groundwater samples from the multiport wells have a trend of increasing SO4/Cl with increasing SO_4 values (Fig. 4.7).

DISCUSSION

The results indicate that, under current conditions, substantial groundwater flow between the Edwards and Middle Trinity aquifers is not likely. Physical and chemical data indicate that low permeability units between the Edwards and Middle Trinity aquifer act as barriers to vertical flow. Furthermore, spatial and temporal variations in potentiometric surface levels and groundwater geochemistry can be accounted for by processes other than inter-aquifer flow. Such processes include rapid recharge and lateral groundwater flow in both aquifers, and water-rock interactions that are unique between aquifers.

Evaluating lateral and vertical groundwater flow

To understand the potential for flow between aquifer systems it is first important to characterize the relative dominance of lateral and vertical flow within each aquifer. Spatial variations in groundwater levels indicate the occurrence of lateral flow within the Middle Trinity aquifer, generally from west to east (Fig. 4.3a). The east-west oriented potentiometric ridge in the middle of Hays County likely reflects an area of lower permeability relative to areas to the south along the Blanco River where there is faulting and significant karst. The Blanco River likely recharges the Middle Trinity through aquifer host units (LGR and HCC) as suggested by the occurrence of low TDS (<500 mg/L) groundwater beneath areas where the Blanco River crosses bedrock units of the Middle Trinity that occur at the surface (Fig. 4.3b). Blanco River water has lower TDS concentrations relative to those in Trinity aquifer groundwater (Musgrove et al., 2012) that would dilute groundwater constituent concentrations upon recharge. The general

west-east orientation of the fresh water plume originating in this recharge area (Fig. 4.3b) suggests an eastward direction of groundwater flow and is consistent with the potentiometric gradient.

The occurrence of lateral eastward groundwater flow through the Middle Trinity aquifer is further supported by temporal and spatial variations in potentiometric surface eleveations (Fig. 4.2b). Water levels in Middle Trinity wells (Storm Ranch and Downey) and units within the Ruby Ranch and Antioch multiport wells have the same pattern of temporal variation, which documents a muted response to changing hydrostatic head pressure in the recharge areas. Most notable is the downgradient change in pressure heads in response to wetter conditions during the 2009-2010 winter months. Potentiometric surface levels measured in all the wells (except Antioch, for which there are no measurements) increase during this time, and increases are progressively lagged in the down-gradient direction (i.e., increase first occurs at Storm Ranch, then Downing, then Ruby Ranch) (Fig. 4.2b). Although faults can be barriers to groundwater flow, it is likely that fault relay-ramps (Fig. 4.1b, inset), which are prevalent in the study area, provide a structural mechanism for lateral continuity of groundwater flow through the Balcones Fault Zone (Collins and Hovorka, 1997).

Co-variation of potentiometric surface levels measured in zones of the Edwards and Trinity aquifer at the Ruby Ranch well is apparent (Fig. 4.2a). This could reflect the recharge from the Edwards aquifer to the Trinity aquifer or concurrent recharge to the Edwards and Trinity aquifer from distinct recharge areas (Fig. 4.10). In regard to the former, the covariation of potentiometric surface levels in the two aquifers could be accounted for by rapid surface water recharge to the Edwards aquifer and subsequent vertical transmission of a head pressure to underlying Trinity aquifer units. This co-variation, however, was not observed at the Antioch well, as temporal variations of

potentiometric surface levels in the Edwards aquifer were decoupled from those in the Trinity aquifer (Fig. 4.2a). Furthermore, spatial and temporal variations in potentiometric surface levels in both wells suggest that units within the UGR and, to a lesser extent, the LGR likely act as aquitards to vertical flow (e.g., Antioch well zone 10, Ruby Ranch well zone 10) as discussed below.

There are several observations that suggest units with UGR and LGR units hinder vertical flow between Edwards and HCC units. Depth profiles of potentiometric surface levels illustrate clear differences in potentiometric surface levels, TDS concentrations, and hydraulic conductivities measured in units above most UGR and below some LGR units (Fig. 4.4). Although potentiometric surface levels measured in units of both the Edwards and Trinity aquifers decline as surface conditions become progressively drier, rates of water level decreases are different. The temporally invariant potentiometric surface levels measured in some UGR units (e.g., zone 10 in both the Ruby Ranch and Antioch well) relative to the rest of the units (Figs. 4.2 and 4.4) likely reflect a muted response to changing hydrostatic head pressure in more permeable units above and below these units. Highest concentrations of TDS and lowest hydraulic conductivities are consistent with units that show limited variation in potentiometric surface levels, which suggests flow within and across these units is minimal. These findings support the hypothesis that parts of the UGR and LGR act as aquitards to vertical flow between the Edwards and Middle Trinity aquifers.

Surface water recharge to Edwards and Trinity aquifers through each aquifer's distinct recharge area likely accounts for the co-variation in potentiometric surface levels in the two aquifers (Figs. 4.2 and 4.8). This suggests that recharge to units of both aquifers occurred with similar timing and at constant relative magnitudes (i.e. similar ratio of Edwards vs. Trinity aquifer recharge through time) at Ruby Ranch. Rapid

recharge in response to changes in meteorological conditions (Mahler and Massei, 2007; Wong et al., 2012) and fast lateral groundwater travel times (Hauwert, 2009) have previously been documented in the Edwards aquifer, but have not been investigated in the Trinity aquifer. This study, however, has provided evidence that surface water is actively recharging the Middle Trinity aquifer (Fig. 4.3b) and head pressure is laterally disseminated within a short time frame (i.e., months) (Fig. 4.2b).

Assessment of processes controlling groundwater geochemical compositions

Understanding the controls on groundwater geochemistry in each hydro-stratigraphic unit is a critical part of assessing the potential of inter-aquifer flow. In the case that significant groundwater flow is occurring, the geochemical compositions of Edwards aquifer groundwater should reflect mixing with Trinity aquifer groundwater at the multiport wells and aquifer wide. In the scenario in which substantial groundwater flow is not occurring, groundwater in each hydro-stratigraphic units should reflect unique controls on groundwater geochemistry.

Groundwater geochemical compositions sampled from the multiport wells do not reflect a continuous mixing gradient between Edwards and Trinity aquifer groundwater. Although there is general increase in SO_4 and Sr concentrations and $^{87}Sr/^{86}Sr$ values in groundwater from Edwards to HCC units, groundwater from most UGR and LGR units do not follow this trend (Fig. 4.6). The distinct geochemical compositions (i.e., high, instead of intermediate, SO_4 and Sr concentrations) of the intermediate UGR and UGR units indicate that continuous vertical mixing of groundwater from the Edwards and Trinity aquifers is not occurring. This suggests that either i) groundwater from Edwards and HCC units is mixing via a vertical flow route that bypasses UGR and LGR units, or ii) water interaction with different lithologic compositions results in Edwards

groundwater having lower SO_4 and Sr concentrations and $^{87}Sr/^{86}Sr$ values relative to groundwater from HCC units. The first hypothesis is not supported by the physical data, which illustrates that the potentiometric surface levels in HCC units are distinct from and do not covary with those in Edwards units (Fig. 4.2a). This finding suggests there are distinct controls on Edwards and Trinity groundwater compositions, which is also consistent with geochemical data from multiport wells and data from the surrounding project area compiled from existing studies as discussed below.

Edwards groundwater compositions reflect interaction with carbonate minerals as i) there is a 1:1 correspondence between Ca+Mg and HCO_3 molar concentrations (Supplementary Fig. S4.3), ii) $^{87}Sr/^{86}Sr$ values are most similar to those measured in Edwards limestone (Fig. 4.6), and iii) models of dolomite recrystallization (i.e., dolomite dissolution and reprecipitation) can account for most Edwards aquifer groundwater compositions (Fig. 4.5). Figure 4.5 illustrates the natural evolution of groundwater compositions within the Edwards aquifer with increasing water residence time. Edwards groundwater evolves from its initial signature acquired from interaction with soils (low Mg/Ca and high $^{87}Sr/^{86}Sr$ values) during recharge to a signature acquired from extensive interaction with carbonate bedrock (high Mg/Ca and low $^{87}Sr/^{86}Sr$ values). This is demonstrated by the progression of increasing Mg/Ca and decreasing $^{87}Sr/^{86}Sr$ values from soil leachates to waters with progressively longer water residence times – i.e., from soil leachates to vadose dripwaters to springs discharging from small watersheds (Honey Creek State Natural Area springs) to large springs that are discharge points of large aquifer segments (Barton Springs and San Marcos Springs), to Edwards aquifer groundwater (Fig. 5; Musgrove and Banner, 2004; Musgrove et al., 2010; Wong et al., 2011). Progressively long water residence times allow increasing amounts of calcite and dolomite recrystallization (i.e., mineral dissolution and re-precipitation) to occur as

demonstrated by the model lines in Figure 4.5. Such a progression is consistent with previous findings of the evolution of natural waters in this area (Musgrove and Banner, 2004; Musgrove et al., 2010; Wong et al., 2011).

A different process likely controls Trinity aquifer groundwater compositions. Trinity aquifer groundwater does not exhibit progression from high to low Sr isotope values and low to high Mg/Ca, and cannot be accounted for by dolomite recrystallization. This indicates that i) Trinity aquifer groundwater is not a more evolved version of Edwards aquifer groundwater, ii) Edwards aquifer groundwater is not a dilute version of Trinity aquifer groundwater, and iii) groundwater does not readily flow between the aquifers. It is more probable that evaporite dissolution influences Trinity aquifer groundwater compositions. The presence of evaporite minerals is consistent with the shallow, restricted depositional environments of the Glen Rose Formation (Table 4.1; Rose, 1972). Furthermore, evaporite nodules were present in well cuttings from and observed using a downhole camera at depths corresponding to UGR and LRG units at the Antioch site. Groundwater compositions from UGR, LGR, and HCC units have a 1:1 molar correspondence between Ca+Mg-HCO_3 and SO_4 (Supplementary Fig. S4.3), which indicates that gypsum dissolution can account for Ca and Mg concentrations that cannot be accounted for by dissolution of carbonate minerals. Sr isotope values in groundwater from UGR and LGR units were similar to those measured in evaporite minerals recovered from these units (Fig. 4.6), which is consistent with the hypothesis that evaporites are the main source of Sr to these groundwaters.

Trinity groundwaters exhibit a clear trend of increasing SO_4/Cl with increasing SO_4 concentrations (Fig. 4.7), which indicates that increases in total dissolved solids likely originate from dissolution of SO_4-rich minerals. Senger and Kreitler (1984) originally suggested that i) trends of increasing SO_4/Cl with increasing SO_4

concentrations in Edwards aquifer groundwater indicated the occurrence of mixing between Edwards and Trinity aquifer groundwater, and ii) trends of static or decreasing SO_4/Cl with increasing SO_4 concentrations in Edwards aquifer groundwater indicated the occurrence of mixing between Edwards and saline zone groundwater. This was based on limited data (n=25) and is consistent with the compilation of historical data (n>3,000) from Edwards and Trinity aquifer wells in Travis and Hays County (Fig. 4.7). However, the original interpretation that trends of increasing SO_4/Cl with increasing SO_4 concentrations reflect Edwards aquifer groundwater mixing with Trinity aquifer groundwater is not supported by the results of this study. The isotopic and geochemical data presented above indicate that Edwards and Trinity aquifer groundwater geochemistry are controlled by different processes. It is more likely that the trend of increasing SO_4/Cl with increasing SO_4 concentrations reflects increasing amounts of gypsum dissolution as opposed to mixing between Edwards and Trinity aquifer groundwater. This is further supported by some zones of UGR and LGR units having SO_4 concentrations that are or are among the highest SO_4 concentrations measured historically. This finding likely reflects the multiport well sampling approach in which individual litho-stratigraphic units with high SO_4 concentrations were isolated. Data from the TWDB database reflects traditional sampling approaches in which groundwater was collected from wells drawing from multiple lithostratigraphic units with varying SO_4 concentrations.

Sr isotope values of groundwater from HCC units that are higher than those of evaporites and groundwater from UGR and LRG units (Fig. 4.6), suggest that evaporites were not the dominant control of Sr isotope values or largest source of Sr to groundwater from HCC units. Higher Sr isotope values might indicate interaction with silicate materials (e.g., terrestrial derived quartz, feldspars, and clays), which are abundant in

HCC units (Table 4.1). Silicate minerals inherently have higher Rb/Sr relative to carbonate materials. Because ^{87}Sr is the daughter product of radiogenic Rb, silicate minerals also inherently have higher $^{87}Sr/^{86}Sr$ values relative to carbonates (Banner, 2004). The hypothesis that high $^{87}Sr/^{86}Sr$ values in groundwater from HCC units reflects interaction with silicate material is tentative. Sr isotope values of HCC bedrock have not been measured and the source of high Sr concentrations to groundwater in this setting is not well characterized (Oetting, 1995; Wong et al., 2012). More specifically, high (>5 mg/L) Sr concentrations (and, therefore, higher Sr/Ca) occur in groundwater from the Edwards (both fresh and saline zones) and Trinity aquifers with a wide range of $^{87}Sr/^{86}Sr$ values (Oetting, 1995; Wong et al., 2012).

Differences in major ion concentrations, Sr isotope values, and the covariation of Mg/Ca and Sr isotope values between groundwaters sampled from the Edwards and Trinity aquifers demonstrate that aquifer host rock lithology is a dominant control on groundwater compositions (Figs. 4.5 and 4.6). Edwards groundwater reflect water interaction with carbonate minerals, whereas groundwater from the Trinity reflect gypsum dissolution and interaction with silicate lithology with higher Sr isotope values. These results suggest that groundwater mixing between the Edwards and Trinity aquifers is not occurring.

Conceptual model of groundwater flow between aquifers

Physical and geochemical evidence indicates that units of the Edwards aquifer are in hydrologic communication with the uppermost units of the UGR, but not the Middle Trinity aquifer (Figs. 4.2, 4.4, and 4.8). The uppermost units of the UGR have potentiometric surface levels (Figs. 4.2 and 4.4), hydraulic conductivities (Fig. 4), and geochemical compositions (Figs. 4.4, 4.6 and 4.7) that are consistent with those in the

Edwards units at both the Ruby Ranch and Antioch wells. The rest of the UGR units, however, are physically and chemically distinct from the uppermost UGR units, which suggest they retard vertical flow. Potentiometric surface levels and hydraulic conductivities measured in some LGR units are similar to those measured in HCC units (Fig. 4.4), which suggests some degree of communication exists between all the lithostratigraphic units of the Middle Trinity. However, geochemical compositions of groundwater from some of the LGR units that are more similar to UGR units than to HCC units (Figs. 4.4, 4.6 and 4.7). This suggests that groundwater flow between HCC and some LGR units is limited, and some LGR layers are associated with aquitard units of the UGR. Changes in potentiometric pressure seen in the HCC units at the Ruby Ranch and Antioch wells are likely due to the transfer of hydrostatic pressure through HCC units that are laterally continuous between recharge areas and the wells, instead of vertical recharge flowing from overlying Edwards units (Fig. 4.8).

The results from the multiport wells indicate a lack of coincidence between lithostratigraphic units with their respective hydrostratigraphic units (Fig. 4.8). We find the Edwards aquifer to be consistent with Edwards units and the uppermost units of the UGR. The remainder of the UGR units likely comprise an aquitard rather of hosting the Upper Trinity aquifer. Some units of the LGR units also serve as aquitards, whereas the remainder of the LGR units and HCC units host the Middle Trinity aquifer. These results illustrate the need for detailed investigations of aquifer boundaries and the hydrologic connections across those boundaries.

Potential of aquifer inter-flow under future pumping conditions

Although substantial inter-flow between Edwards and Trinity aquifer is not substantial under current pumping conditions, it is important to consider the potential of

cross formational flow under scenarios of increased pumping in the Trinity aquifer. Increased pumping of the Trinity in Travis and Hays Counties could result in depleted storage, lowered water tables and associated reduction of spring and stream flow in recharge zones, and/or alteration of the local groundwater flow patterns. Results from groundwater modeling suggest that increases in pumping are offset by changes in storage and capture of spring flow in the Hill Country (Mace et al., 2000; Jones et al., 2011). Evaluation of temporal trends of stream flows in the contributing zone suggest that increases in pumping have resulted in decreases in baseflows to streams (Hunt et al., 2012). Furthermore, pumping tests from large-capacity public supply wells resulted in the capture of flow from a significant Middle Trinity spring (Jacob's Well spring) in the contributing zone (Wierman et al., 2008).

The induction of cross-formational flow due to increasing pumping cannot be ruled out. It is possible that units delineated as aquitards only divide two lateral flow regimes because the vertical gradient is small. Increased pumping of the Trinity aquifer could result in a vertical gradient that would induce vertical flow. The degree of cross-formational flow, however, will be limited by the occurrence of low permeability units between the Edwards and Trinity aquifers. Hydraulic conductivities in UGR and LGR units are two orders of magnitude lower than those in units above and below (Fig. 4.4). Because of these large differences, lateral flow through the aquifers will likely dominant over vertical flow. For example, results of a pump test in a well completed in the Cow Creek (i.e., Middle Trinity aquifer) induced 2 m of draw down in a Cow Creek unit (i.e., zone 3) at the Ruby Ranch multiport well located ~0.8 km up gradient to the northwest (Hunt et al., 2010). There was no measureable drawdown in a nearby (100 m) well completed in the Edwards aquifer. The well was pumped for three days at 0.75-0.95 m3/min (200-250 gallons/min) in February 2010 during wet conditions when

potentiometric surface levels were 20 m higher in Edwards units relative to Middle Trinity units (Fig. 4.2a).

CONCLUSIONS

The extent to which hydrologic communication occurs between the Edwards and Trinity aquifers in central Texas was investigated by using multiport well technology at two locations to monitor potentiometric surfaces, measure hydraulic conductivity, and sample groundwater from multiple hydrostratigraphic zones of Edwards and Upper and Middle Trinity aquifers. Physical and geochemical results indicate that lithostratigraphic units do not correlate to hydrostratigraphic units, and that lateral groundwater flow occurs within the Edwards and Middle Trinity aquifers. Our results suggest that, under current conditions, vertical flow between the Edwards and Middle Trinity aquifer is limited by low permeability units within the Upper and Lower Glen Rose Formations. Groundwater geochemical compositions are likely controlled by water interaction with lithologies unique to each aquifer, and suggest that groundwater mixing between hydrostratigraphic units is not occurring. Edwards aquifer groundwater compositions reflects water interaction with carbonate minerals, whereas compositions of groundwater from the Middle Trinity units reflect dissolution of evaporite minerals and interaction with a more siliceous bedrock unit. These results have implications for the management of the adjacent Edwards and Middle Trinity aquifers as they indicate that, under current conditions, pumping of the Edwards and Middle Trinity aquifers will likely not induce vertical cross-formational flow between the aquifers. Such flow potential, however, should be assessed as vertical gradients evolve with increased pumping.

Table 4.1. Hydrostratigraphy of the Edwards and Trinity aquifers

Aquifer	[a]Lithostratigraphic Formation or Member	[b]Hydrostratigraphic Member	Lithology	Multiport Well Zones	
				Antioch	*Ruby Ranch*
Edwards	Georgetown		marly limestone	21	
	Pearson	Leached and Collapsed	crystalline limestone, mudstone to grainstone, and collapsed breccia	20	
		Regional Dense	dense argillaceous mudstone	19	
	Kainer	Grainstone	mudstone to wackestone	18	
		Kirchberg	evaporites and crystalline limestone, chalky mudstone	17	
		Dolomitic	mudstone to grainstone, crystalline limestone	15-16	13
		Basal Nodular	shaly, nodular limestone, mudstone, and miliolid grainstone	14	12
Upper Trinity	Upper Glen Rose Limestone (UGR)		evaporite beds, thinly bedded limestone and marl	8-13	9-11
Middle Trinity	Lower Glen Rose Limestone (LRG)		fossiliferous limestone, dolomite, marl, and shale	4-7	5-7
	Hensal Sandstone (HCC)		clay, silt, sand, conglomerate, and thin limestone beds	2-3	4
	Cow Creek Limestone (HCC)		fossiliferous argillaceous and dolomitic limestone with some shale and sand	1	2-3
Aquitard	Hammett Shale		fossiliferous dolomitic shale		1

[a]from Stricklin (1971), Rose (1972), and Barker and Ardis (1996)
[b]from Small et al. (1996)

Table 4.2. Number, water type, and median (range) values of groundwater from Antioch and Ruby Ranch wells by geologic unit

Unit	Edwards Group	Upper Glen Rose	Lower Glen Rose	Hensel, Cow Creek, Hammet
Water Type	$Ca\text{-}HCO_3$	$Ca\text{-}HCO_3\text{-}SO_4$	$Ca\text{-}SO_4$& $Ca\text{-}HCO_3\text{-}SO_4$	$Ca\text{-}HCO_3\text{-}SO_4$
Alkalinity (mg/L)	240 (220-290)	220 (190-220)	270 (210-320)	260 (250-270)
Ca (mg/L)	65 (45-76)	530 (54-610)	96 (86-580)	120 (100-140)
Mg (mg/L)	28 (24-41)	180 (31-320)	82 (49-290)	78 (65-97)
Sr (mg/L)	1.3 (0.21-40)	12 (5.7-39)	12 (6.4-16)	12(8.4-22)
K (mg/L)	1.2 (0.80-2.8)	20 (1.9-28)	7.6 (2.9-24)	9.4 (6.6-13)
Na (mg/L)	6.0 (5.7-7.6)	28 (5.9-53)	15 (8.3-33)	15.4 (12-25)
Cl (mg/L)	9.3 (7.9-13)	15 (8.1-25)	12 (9.8-25)	13 (9.2-15)
SO_4 (mg/L)	24 (0.39-160)	2000 (36-2600)	340 (150-2300)	370 (290-500)
$^{87}Sr/^{86}Sr$	0.7077 (0.70753-0.70808)	0.70783 (0.70751-0.77944)	0.70793 (0.70770-0.70813)	0.70818 (0.70808-0.70834)
Sp. Cond. (µS/cm)	560 (470-720)	3100 (540-3700)	1100 (770-3500)	1200 (1000-1400)
n	11	12	13	12

Supplementary Table S4.1. Summary of grey literature addressing potential of flow between Edwards and Trinity aquifers

Agency	Approach	Key Results	References
Barton Springs Edwards Aquifer	Physical and geochemical monitoring in multiport wells	Limited occurrence of vertical inter-aquifer flow	This study; Andrews et al., 2013; Kromann et al., 2011; Smith and Hunt, 2011, 2010, 2009, 2008
City of Austin	Chemical and dye tracing analysis	Trinity aquifer may contribute flow to Barton Springs	Hauwert, 2011
Hays Trinity Groundwater Conservation District	Physical and chemical (Trinity) aquifer characterization using new and existing data	Characterization of occurrence, movement, and availability of Trinity groundwater	Wierman et al., 2010
Edwards Aquifer Authority	Dye trace study, hydrophysical surveys, groundwater modeling	Occurrence of groundwater flow from the Upper Glen Rose formation to Edwards	Johnson, et al., 2010; Schindel and Johnson, 2011
Southwest Research Institute	River gain/loss, water budget assessment	More recharge to Trinity and inter-aquifer flow occurs than previously thought	Green et al., 2011
Texas Water Development Board	Groundwater modeling	Groundwater flow (100,000 acre-ft/year) from Trinity to adjacent Edwards aquifer (Balcones Fault Zone); Minor flow from Edwards to Trinity aquifer	Jones et al., 2011; Jones, 2011
Zara Environmental LLC.	Recharge study, dye tracing, geophysical survey	Groundwater flow between Glen Rose (Trinity) and Edwards	Gary et al., 2011

Supplementary Table S4.2. Groundwater and evaporite geochemical compositions for Ruby Ranch (RR) and Antioch (A)

Geologic Unit	Stratigraphic Unit	Hydrostratigraphic Unit	Well and Zone	Date	Alkalinity (as $CaCO_3$) (mg/L)	Spec Cond (µS/cm)	Ca (mg/L)	Mg (mg/L)	Sr (mg/L)	K (mg/L)	Na (mg/L)	Cl (mg/L)	SO_4 (mg/l)	$^{87}Sr/^{86}Sr$
Edwards Group	Leached and Collapsed	Edwards	A20	Jun-11	220	580	58	27	1.0	1.5	5.8	8.0	29	0.70770
Edwards Group	Regional Dense Member	Edwards	A19	Jun-11	220	520	61	28	1.3	1.5	5.7	7.9	32	0.70771
Edwards Group	Kirschberg Member	Edwards	A17	Jun-11	250	550	65	27	1.0	1.1	6.0	9.6	20	0.70765
Edwards Group	Dolomitic Member	Edwards	A16	Jun-11	260	560	64	28	2.5	1.2	6.0	9.2	26	0.70760
Edwards Group	Dolomitic Member	Edwards	A15	Jun-11	240	550	64	29	3.6	1.2	5.9	9.0	36	0.70759
Edwards Group	Basal Nodular	Edwards	A14	Jun-11	230	720	74	41	40.0	2.8	5.9	9.3	160	0.70793
Edwards Group	Dolomitic Member	Edwards	R13	Jun-09	290	650	76	33	0.2	0.8	6.2	10.0	11	0.70808
Edwards Group	Dolomitic Member	Edwards	R13	Jun-10	250	590	71	24	0.2	1.2	7.6	13.0	24	
Edwards Group	Dolomitic Member	Edwards	R13	Jul-11	290	650	73	31	0.2	1.0	6.5	8.8	10	0.70804
Edwards Group	Basal Nodular	Edwards	R12	Jun-09	230	520	48	31	3.1	1.7	6.9	9.8	14	0.70753
Edwards Group	Basal Nodular	Edwards	R12	Jun-10	230	480	45	28	3.2	1.9	6.9	10.0	15	
Trinity Group	Upper Glen Rose	Upper Trinity	A13	Jun-11	220	720	74	37	39.0	2.6	6.7	8.1	170	0.70758
Trinity Group	Upper Glen Rose	Upper Trinity	A12	Jun-11	190	3500	500	290	12.0	23.0	53.0	21.0	2500	0.70793
Trinity Group	Upper Glen Rose	Upper Trinity	A11	Jun-11	210	3000	560	170	18.0	20.0	28.0	14.0	2000	0.70780
Trinity Group	Upper Glen Rose	Upper Trinity	A10	Jun-11	220	3400	610	190	17.0	21.0	30.0	16.0	2000	0.70783
Trinity Group	Upper Glen Rose	Upper Trinity	A9	Jun-11	220	3200	570	170	16.0	19.0	24.0	14.0	1900	0.70787
Trinity Group	Upper Glen Rose	Upper Trinity	A8	Jun-11	210	3100	600	180	15.0	20.0	26.0	14.0	2000	0.70794
Trinity Group	Upper Glen Rose	Upper Trinity	RR11	Jun-09	220	540	54	31	5.7	1.9	5.9	8.1	36	0.70751
Trinity Group	Upper Glen Rose	Upper Trinity	RR11	Jun-10	220	650	65	37	9.9	3.2	6.9	8.6	110	
Trinity Group	Upper Glen Rose	Upper Trinity	RR10	Jun-09	230	3180	460	300	12.0	24.0	33.0	25.0	2300	0.70780
Trinity Group	Upper Glen Rose	Upper Trinity	RR10	Jun-10	230	2900	380	260	12.0	19.0	28.0	20.0	1900	
Trinity Group	Upper Glen Rose	Upper Trinity	RR9	Jun-09	220	3670	590	320	12.0	28.0	34.0	25.0	2600	0.70786
Trinity Group	Upper Glen Rose	Upper Trinity	RR9	Jun-10	230	3390	550	310	11.0	25.0	34.0	23.0	2600	
Trinity Group	Lower Glen Rose	Middle Trinity	A7	Jun-11	210	3460	590	210	13.0	22.0	33.0	16.0	2300	0.70774
Trinity Group	Lower Glen Rose	Middle Trinity	A6	Jun-11	220	2480	380	150	12.0	15.0	27.0	18.0	1400	0.70770
Trinity Group	Lower Glen Rose	Middle Trinity	A5	Jun-11	280	2500	530	140	13.0	14.0	24.0	15.0	1800	0.70781
Trinity Group	Lower Glen Rose	Middle Trinity	A4	Jun-11	260	810	93	53	7.3	6.4	11.0	12.0	210	0.70793
Trinity Group	Lower Glen Rose	Middle Trinity	R8	Jun-09	220	3270	510	290	12.0	24.0	32.0	25.0	2300	0.70807
Trinity Group	Lower Glen Rose	Middle Trinity	R8	Jun-10	230	3310	510	290	12.0	22.0	31.0	22.0	2200	
Trinity Group	Lower Glen Rose	Middle Trinity	R7	Jun-09	300	770	91	49	6.4	2.9	8.3	9.8	150	0.70784
Trinity Group	Lower Glen Rose	Middle Trinity	R7	Jun-10	250	1020	95	63	7.9	4.8	12.0	12.0	240	
Trinity Group	Lower Glen Rose	Middle Trinity	R7	Jun-11	270	1020	110	78	9.2	6.3	14.0	11.0	350	0.70800
Trinity Group	Lower Glen Rose	Middle Trinity	R6	Jun-09	320	1100	96	82	13.0	7.6	15.0	12.0	340	0.70797
Trinity Group	Lower Glen Rose	Middle Trinity	R6	Jun-10	270	1100	91	82	12.0	7.9	16.0	14.0	290	
Trinity Group	Lower Glen Rose	Middle Trinity	R5	Jun-09	270	1000	92	69	15.0	6.5	13.0	10.0	260	0.70813
Trinity Group	Lower Glen Rose	Middle Trinity	R5	Jun-10	270	980	86	67	16.0	6.8	12.0	12.0	230	
Trinity Group	Hensel	Middle Trinity	A3	Jun-11	270	1100	100	73	15.0	11.0	18.0	14.0	320	0.70818
Trinity Group	Hensel	Middle Trinity	A2	Jun-11	270	1400	130	97	22.0	13.0	25.0	15.0	500	0.70830
Trinity Group	Cow Creek	Middle Trinity	A1	Jun-11	250	1300	140	88	22.0	13.0	23.0	14.0	490	0.70834
Trinity Group	Hensel	Middle Trinity	R4	Jun-09	260	1200	130	82	12.0	8.6	15.0	11.0	430	0.70821

Supplementary Table S4.2. Groundwater and evaporite geochemical compositions for Ruby Ranch (RR) and Antioch (A)

Geologic Unit	Stratigraphic Unit	Hydrostratigraphic Unit	Well and Zone	Date	Alkalinity (as $CaCO_3$) (mg/L)	Spec Cond (µS/cm)	Ca (mg/L)	Mg (mg/L)	Sr (mg/L)	K (mg/L)	Na (mg/L)	Cl (mg/L)	SO_4 (mg/l)	$^{87}Sr/^{86}Sr$
Trinity Group	Hensel	Middle Trinity	R4	Jun-10	26	1300	130	87	13.0	9.6	16.0	13.0	430	
Trinity Group	Cow Creek	Middle Trinity	R3	Jun-09	260	1100	100	65	8.4	6.6	12.0	9.2	300	0.70808
Trinity Group	Cow Creek	Middle Trinity	R3	Jun-10	260	1200	120	77	9.7	8.3	14.0	12.0	350	
Trinity Group	Cow Creek	Middle Trinity	R3	Jun-11	260	1200	120	74	11.0	7.5	14.0	11.0	380	0.70813
Trinity Group	Cow Creek	Middle Trinity	R2	Jun-09	260	1000	100	66	9.2	8.0	12.0	9.2	300	0.70815
Trinity Group	Cow Creek	Middle Trinity	R2	Jun-10	250	1000	100	71	10.0	9.2	13.0	12.0	290	
Trinity Group	Hammett	Middle Trinity	R1	Jun-09	270	1200	130	80	15.0	9.7	19.0	14.0	420	
Trinity Group	Hammett	Middle Trinity	R1	Jun-10	-	1200	110	79	14.0	11.0	16.0	13.0	350	
Evaporite nodules														
Trinity Group	Glen Rose Undifferentiated[1]	Middle Trinity	A4 to 13_1	Jul-11	-	-	-	-	-	-	-	-	-	0.7078750
Trinity Group	Glen Rose Undifferentiated[1]	Middle Trinity	A4 to 13_1	Jul-11	-	-	-	-	-	-	-	-	-	0.7077307
Trinity Group	Glen Rose Undifferentiated[2]	Middle Trinity	A4 to13_2	Jul-11	-	-	-	-	-	-	-	-	-	0.7078407
Trinity Group	Glen Rose Undifferentiated[2]	Middle Trinity	A4 to13_2	Jul-11	-	-	-	-	-	-	-	-	-	0.7079498
Trinity Group	Glen Rose Undifferentiated[2]	Middle Trinity	A4 to13_2 Rep	Jul-11	-	-	-	-	-	-	-	-	-	0.7079485

[1]Acid leached

[2]H_2O leached

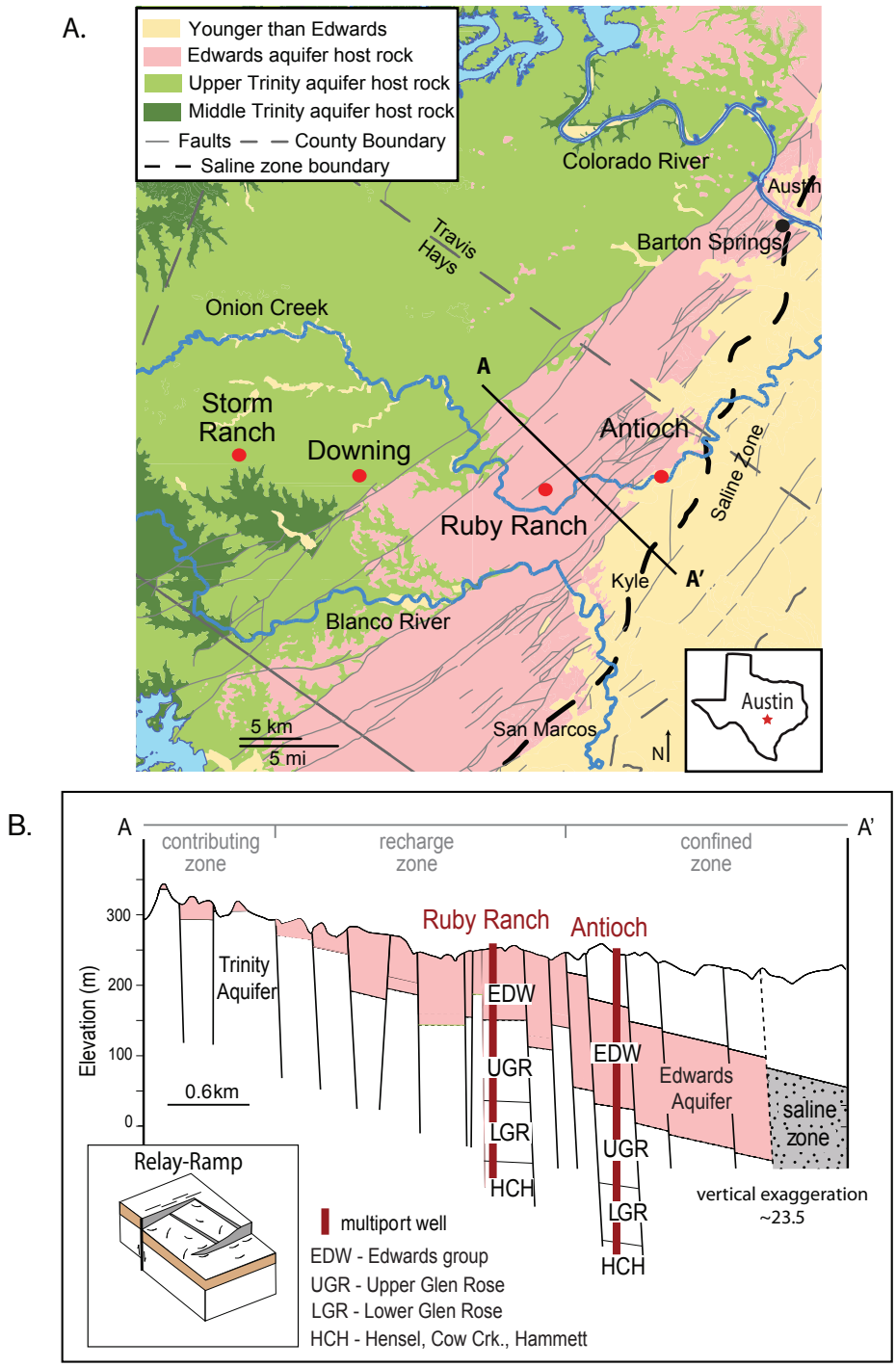

Figure 4.1. A. Geologic map of the Barton Springs segment of the Edwards aquifer (central Texas) with well locations. B. Cross section from A-A' along with diagram of fault structure that could facilitate lateral communication between aquifers. Map and cross section are adapted from Smith and Hunt (2010), and diagram from Collins and Hovorka (1997).

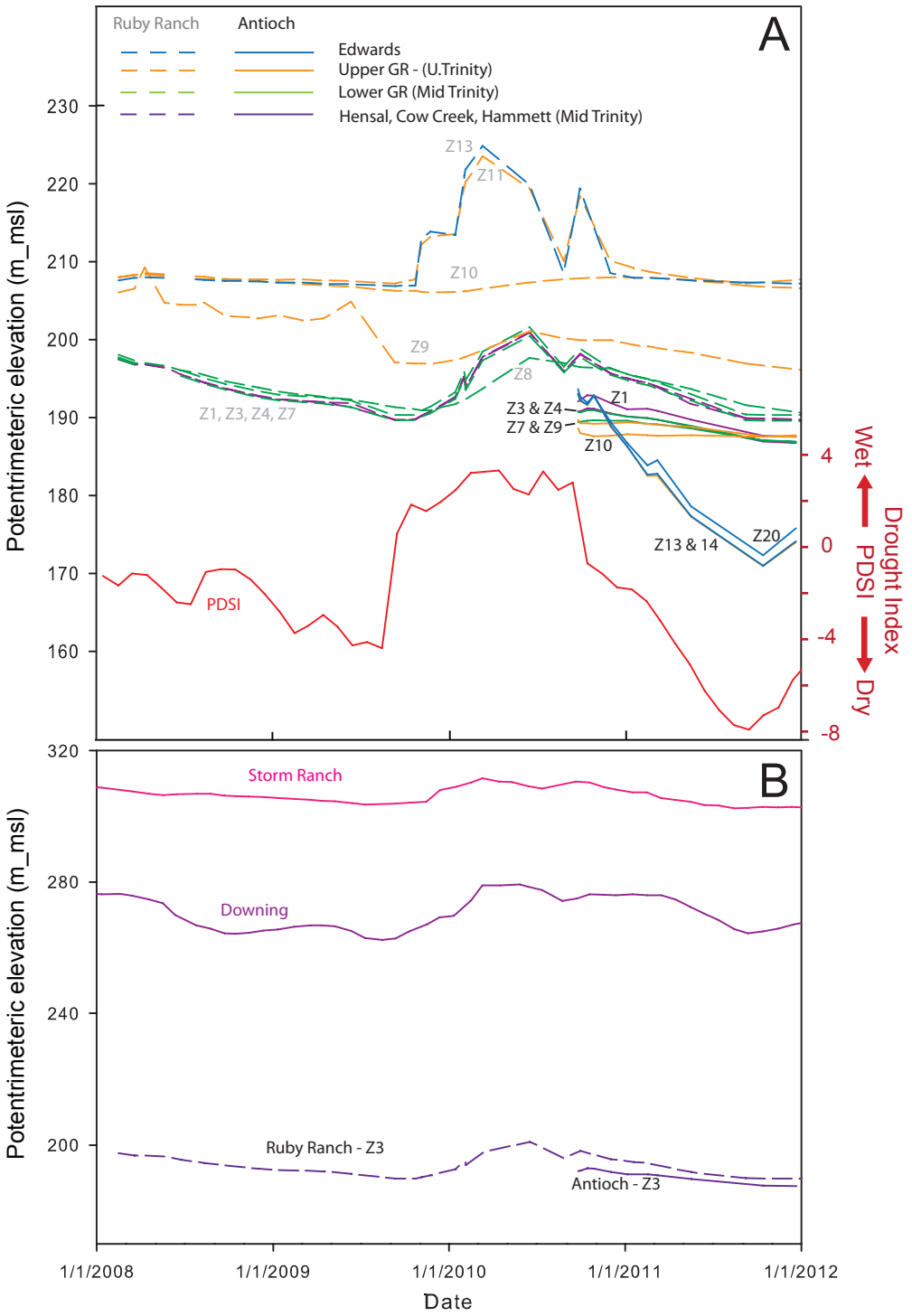

Figure 4.2. A) Time series of PDSI and potentiometric elevations for zones (Z) of the Ruby Ranch and Antioch multiport wells. B) Time series of potentiometric elevations for Middle Trinity wells up gradient of Ruby Ranch and Antioch wells.

A) Middle Trinity potentiometric elevations (m)

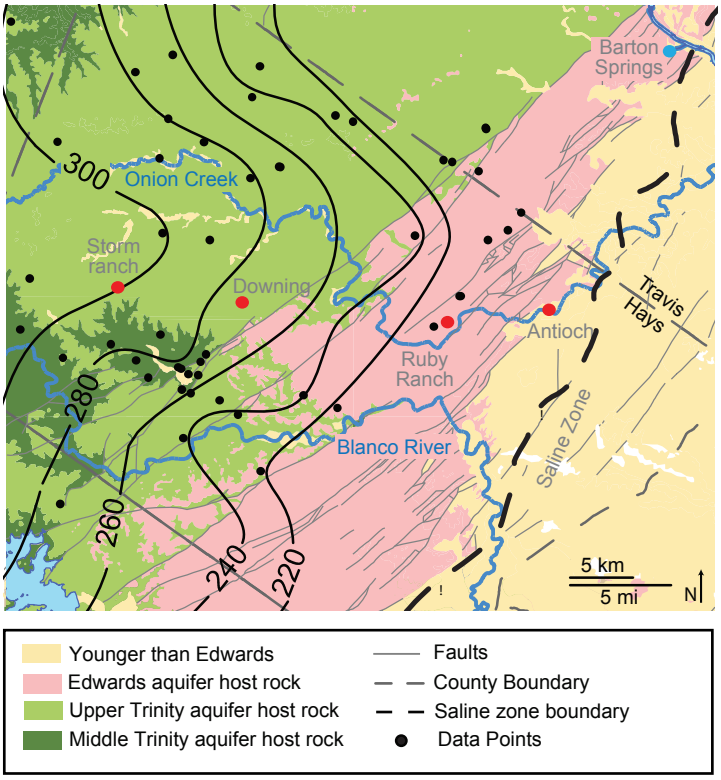

B) Middle Trinity total dissolved solids (mg/L)

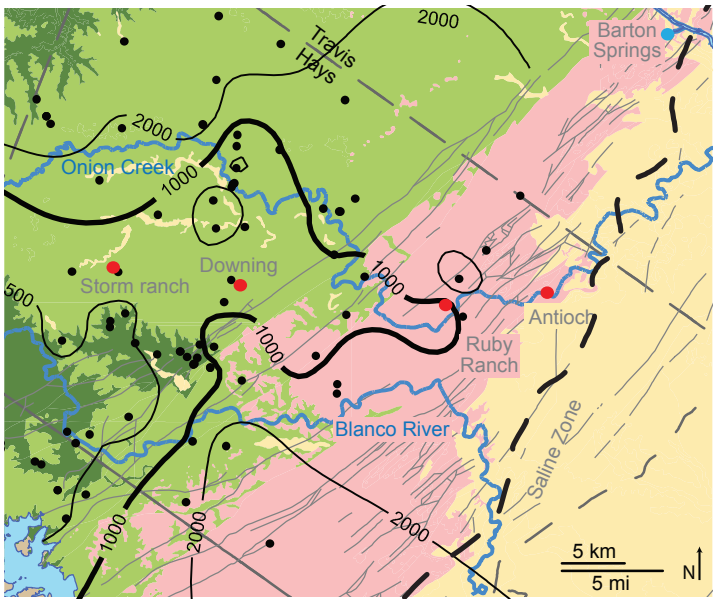

Figure 4.3. Contours of potentiometric elevations (A) and concentrations of total dissolved solids (B) in Middle Trinity aquifer groundwater in Hays and Travis County.

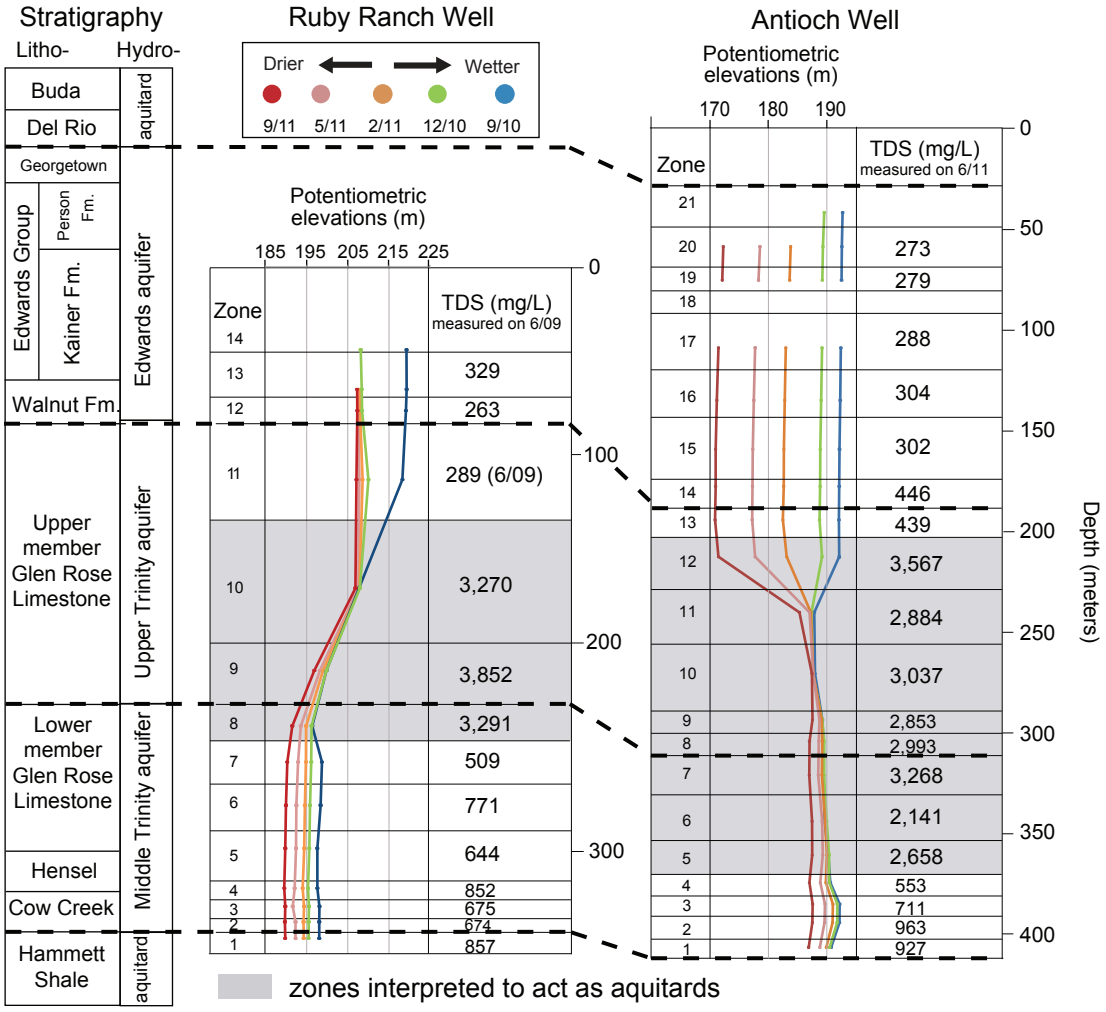

Figure 4.4. Depth profiles of potentiometric elevations measured as surface conditions became drier measured in Ruby Ranch and Antioch multiport wells. Litho- and hydro-stratigraphy and concentrations of total dissolved solids (TDS) are given for each zone. Zones interpreted to act as aquitards are delineated by grey shading. Note that depth scales are different between the wells.

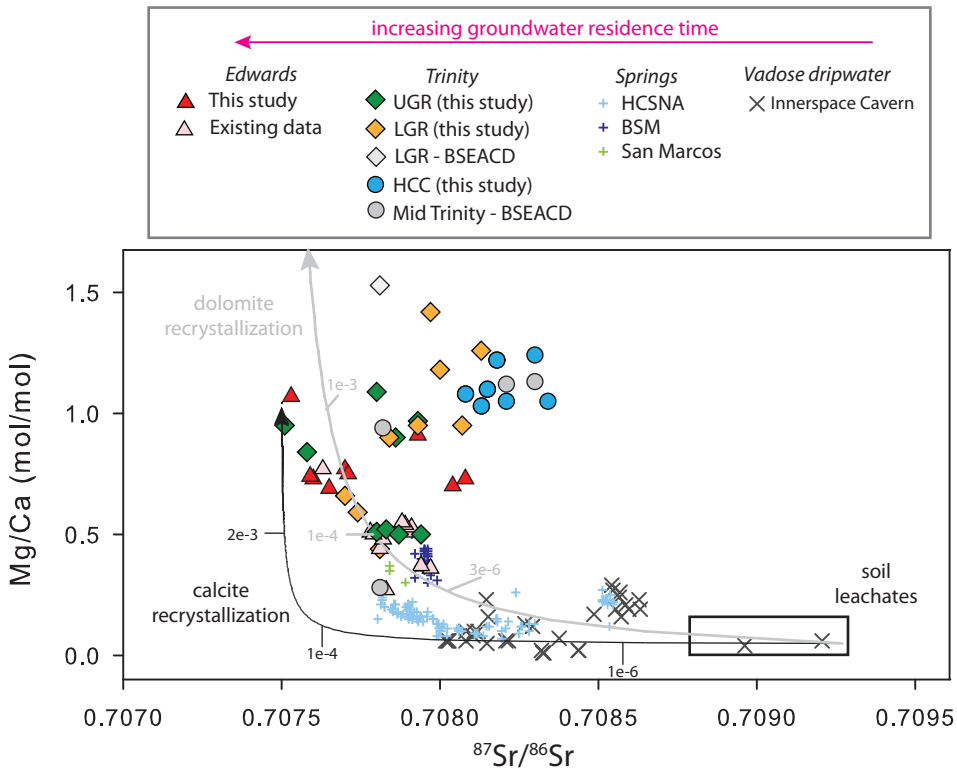

Figure 4.5. Observed and modeled Mg/Ca vs. $^{87}Sr/^{86}Sr$ values in Edwards and Trinity aquifer groundwater. Progressive calcite and/or dolomite recrystallization can account for the evolution of water compositions from vadose dripwater to waters with increasingly longer water residence time - i.e., from vadose dripwaters to springs discharging from small watersheds (HCSNA) to spring discharging from large watersheds (BSM and San Marcos), to Edwards aquifer groundwater. Locations of sites is shown in Supplementary Figure S4.4. Trinity groundwater compositions do not follow such progression and cannot be accounted for by model cures. Data for Edwards groundwater from this study, Wong et al. (2012) and Oetting et al. (1996). Data for Trinity groundwater from this study and the Barton Spring Edwards Aquifer Conservation District (BSEACD). Data for spring water from Musgrove et al. (2010), Wong et al. (2012), and BSEACD. Dripwater data from Musgrove et al. (2004). Shaded boxes represent the ranges of Mg/Ca, Sr/Ca, and $^{87}Sr/^{86}Sr$ values for soil (Mihealsick et al., 2004; Musgrove and Banner, 2004; Musgrove et al., 2010; Wong et al., 2011). Model water–rock interaction curves illustrate the geochemical changes that occur with the progressive recrystallization of calcite and dolomite (Banner and Hanson, 1990). Initial water compositions are represented consist of Mg = 3.5 mg/L, Sr = 0.05 mg/L, Ca = 120 mg/L, Mg/Ca = 0.05 mol/mol, Sr/Ca = 0.19 mmol/mol, and 87Sr/86Sr = 0.70927. Model rock composition is $^{87}Sr/^{86}Sr$ = 0.7075, Mg = 10,000 ppm, Sr = 1,000 ppm, and stoichiometric Ca for calcite recrystallization; and $^{87}Sr/^{86}Sr$ = 0.7075, Sr = 5,000 ppm, and stoichiometric Ca and Mg for dolomite recrystallization. The K_D values for Mg and Sr are 0.04 and 0.1, respectively.

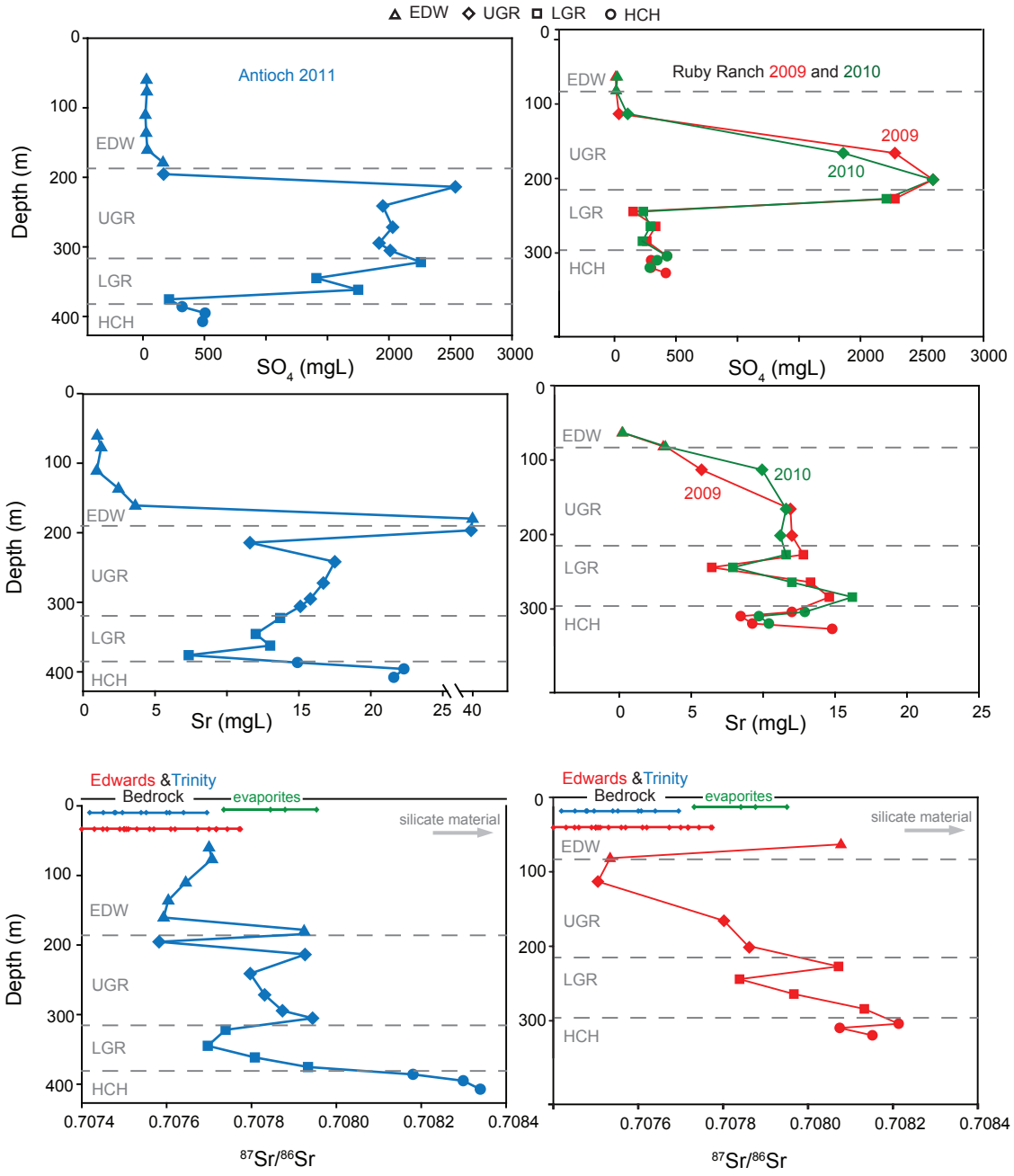

Figure 4.6. Depth profiles of SO_4 and Sr concentrations and $^{87}Sr/^{86}Sr$ values for Ruby Ranch and Antioch wells sampled in 2009 (red), 2010 (green), and 2011 (blue) along with ranges of the majority of $^{87}Sr/^{86}Sr$ values measured for Edwards (red bar) and Trinity (blue bar) aquifer bedrock (compiled from the literature) and evaporites (green bar) recovered from the depth of UGR and LGR zones (this study). Dashed grey bars delineate boundaries between lithostratigraphic units. Note the break in x-axis for Sr conecntrations at the Antioch well.

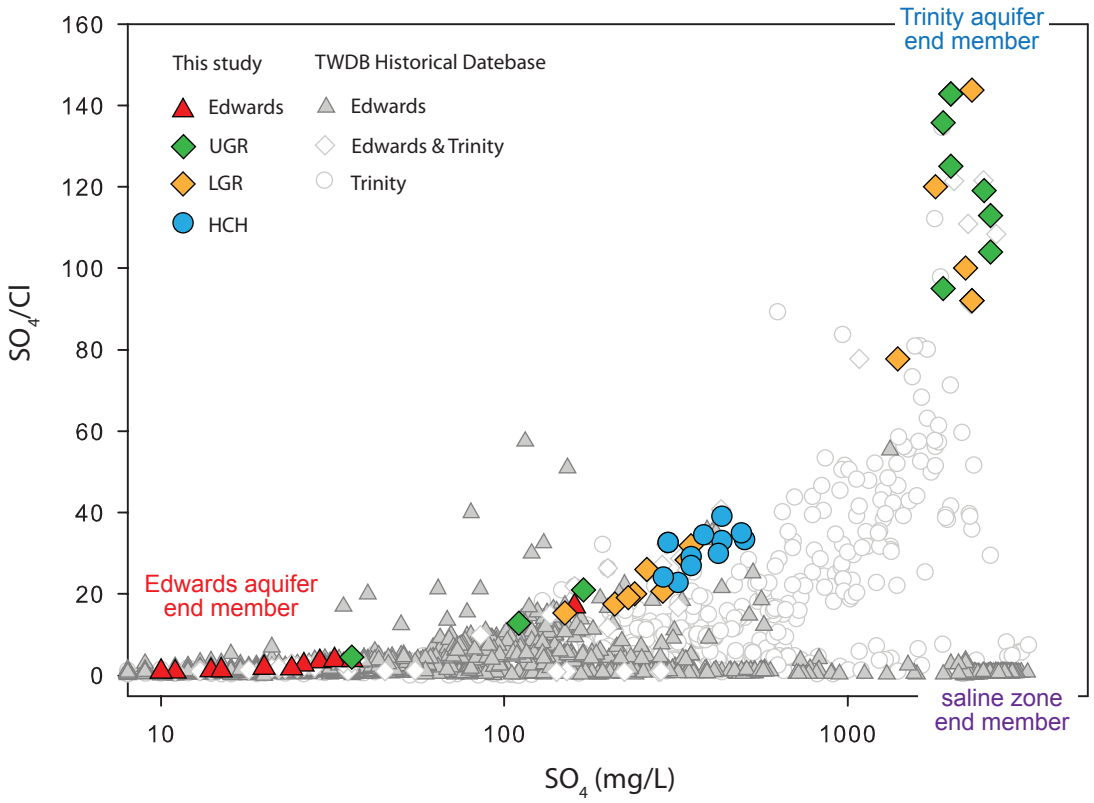

Figure 4.7. SO_4 concentrations and SO_4/Cl are shown for groundwater sampled from Edwards, UGR, LRG, and HCH units from this study as well as historical data for wells located in Edwards (n=2,440), Trinity (n=577), and a combination of Edwards and Trinity aquifer wells (n=27). Historical data from Travis and Hays Counties was retrieved from the TWDB database, and spans the interval of 1937-2009. As sulphate (and TDS) concentrations increase in samples from the Edwards to HCH to UGR and LGR units, SO_4 concentrations increase with respect to Cl indicating that increases in total dissolved solids likely originate from interaction with SO_4 rich minerals.

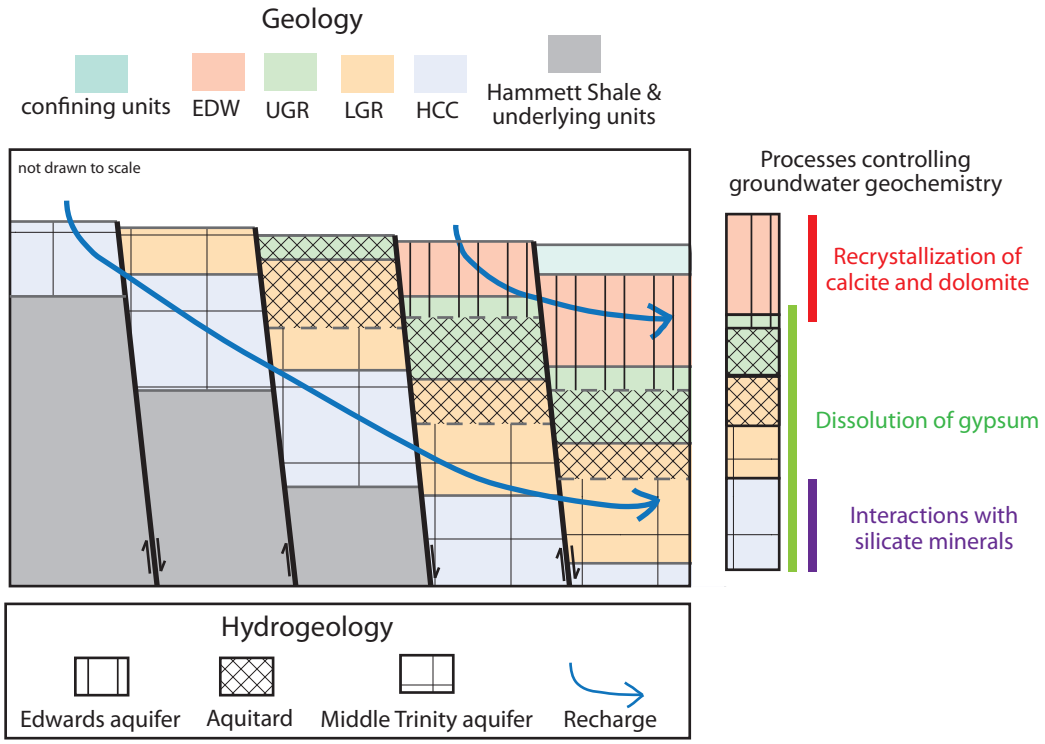

Figure 4.8. Conceptual diagram of the hydrogeologic setting. Although joints and faults might allow vertical recharge from the Edwards aquifer to the Trinity aquifer and/or groundwater mixing between Edwards and Middle Trinity aquifers, lower permeability units within the Upper and Lower Glen Rose Fm likely inhibit vertical communication between Edwards and Middle Trinity aquifers. Recharge to each aquifer occurs through distinct recharge areas.

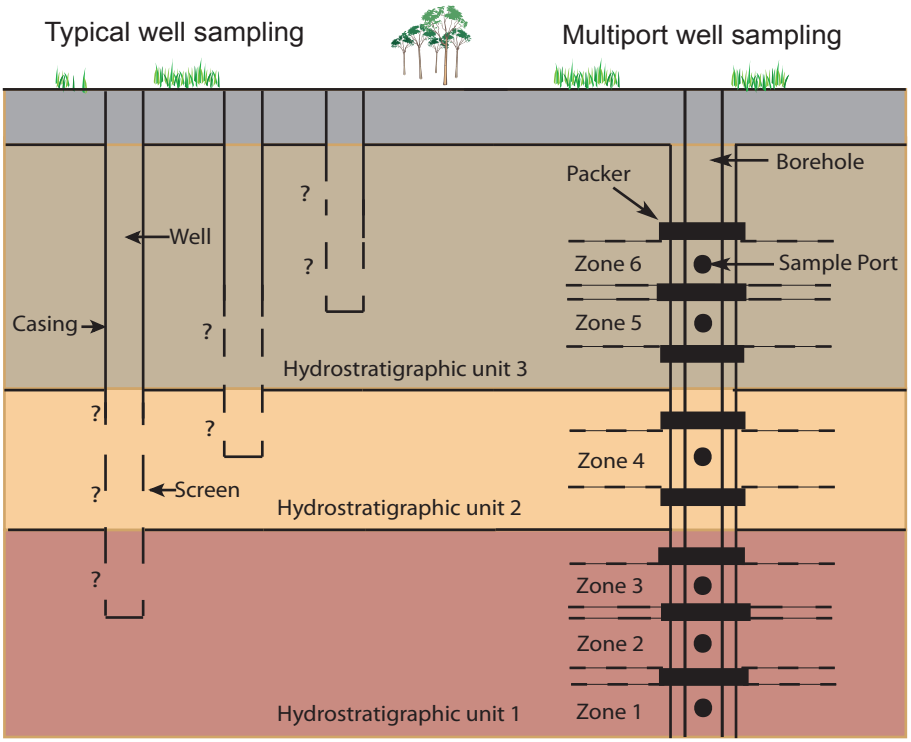

Supplementary Figure S4.1. Schematic illustration of the differences between typical well sampling and multiple well sampling. Traditional wells have unknown screened intervals that can be a mix of multiple hydostratigraphic units and are spatially distributed. Multiport wells have known sampling intervals and ability to sample distinct hydrostratigraphic units at the same location.

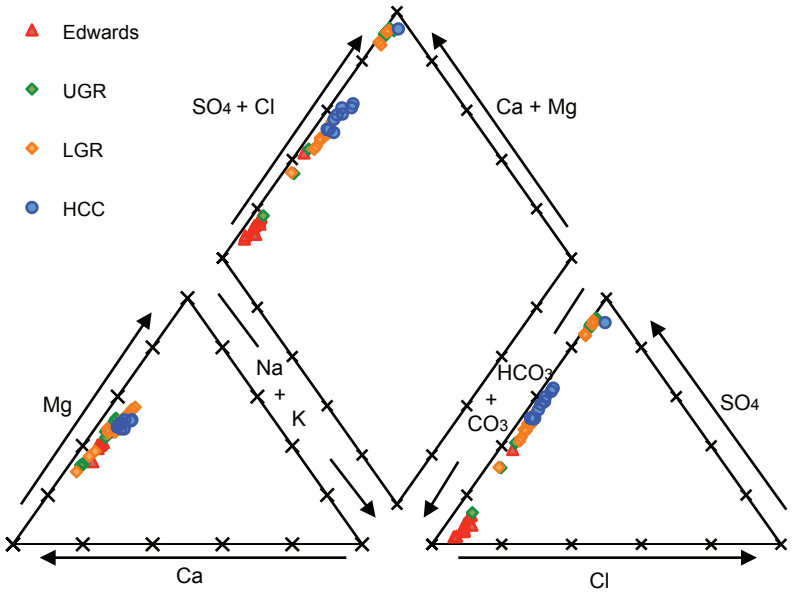

Supplementary Figure S4.2. Piper diagram of geochemical compositions of Edwards and Trinity aquifer groundwater from Antioch and Ruby Ranch wells.

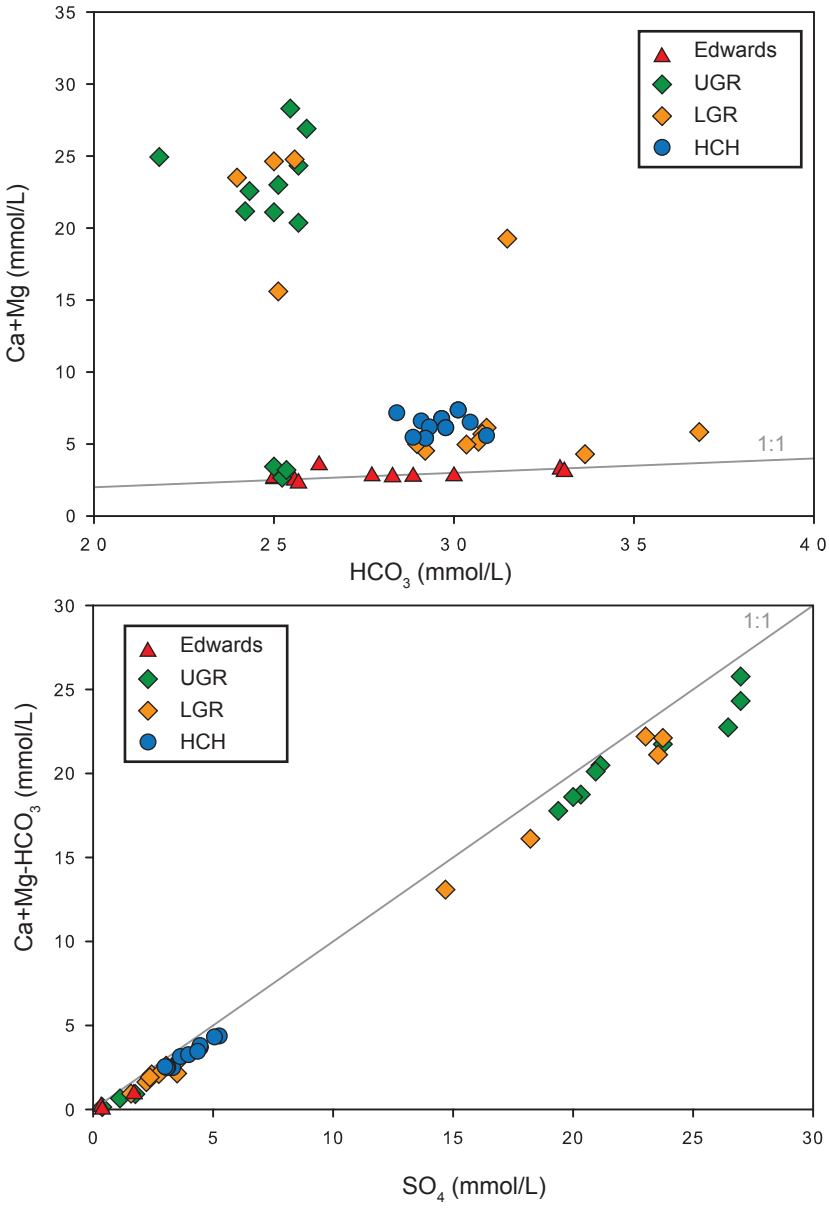

Supplmentary Figure S4.3. Major ion compositions of the Ruby Ranch and Antioch. 1:1 line delineates 1:1 molar ratio of $Ca+Mg:HCO_3$ (upper) and Ca+Mg+HCO3:SO_4 (lower).

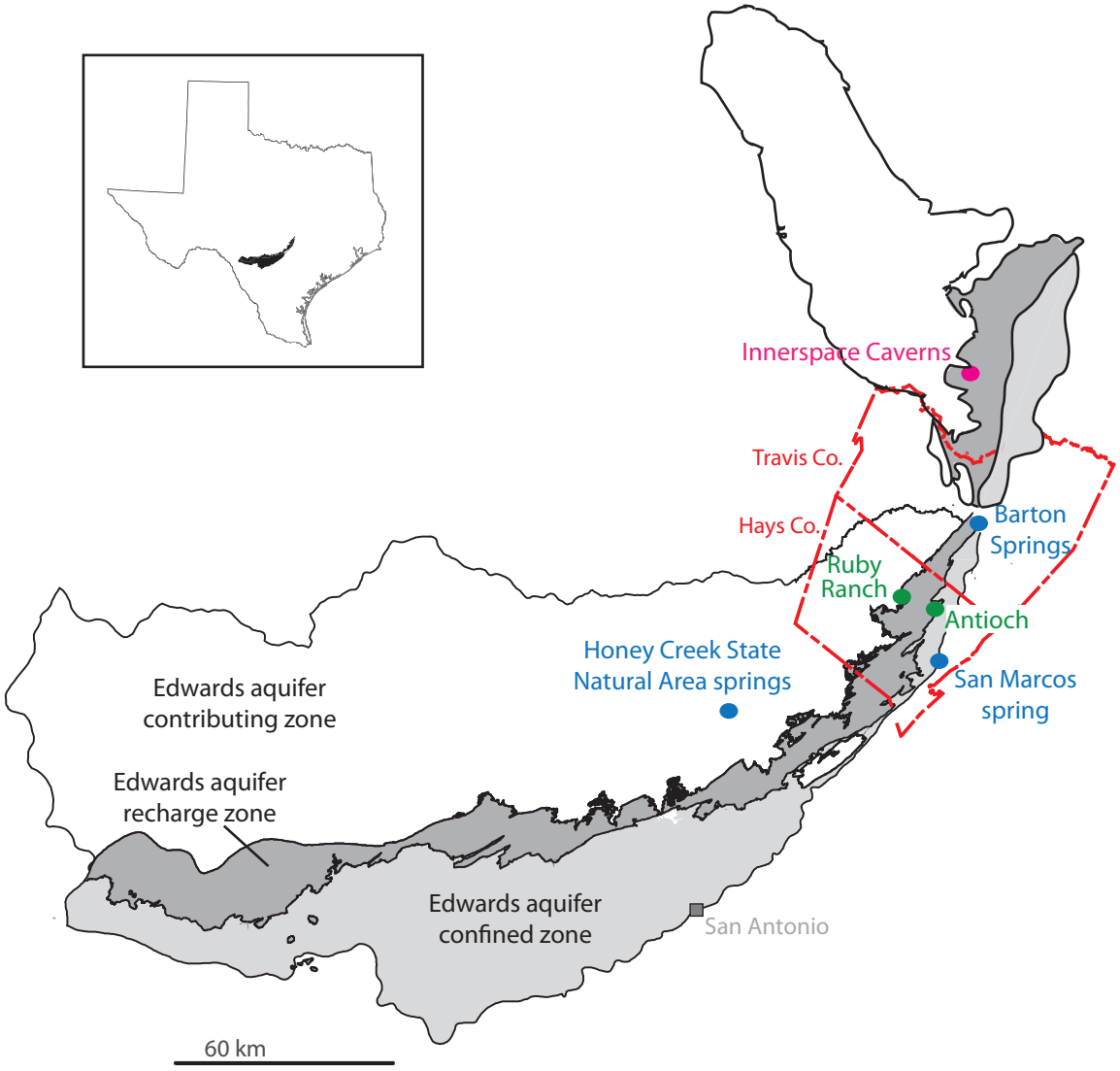

Supplementary Figure S4.4. Site locations (circles) for data presented in Figure 5 along with contributing, recharge, and confined zones of the Edwards aquifer.

SUPPLEMENTARY MATERIAL - EXPANDED METHODS

Multiport well sampling

Groundwater was sampled from two Westbay®[1] multiport wells in Hays County, referred to here as the Antioch and the Ruby Ranch wells (Fig. 2). Antioch is located in the confined zone and is about 3 km southwest of Buda and about 100 m north of Onion Creek. Ruby Ranch is located in the recharge zone, up gradient of Antioch, and is about 7 km (4 miles) west of Antioch. The closest areas for recharge to the Lower Glen Rose, Hensel Sand, and Cow Creek Limestone formations are about 20 km west southwest of the Ruby Ranch well. Groundwater samples were collected from multiple zones within the Edwards and Upper and Middle Trinity aquifers from both sites using multiport wells (specifications detailed below). Lithostratigraphic units were delineated using geophysical data (Wierman et al., 2010). One to six zones were isolated in each of several lithostratigraphic units that host each aquifer, and a total of 21 and 13 zones were sampled at Antioch and Ruby Ranch, respectively (Table 1, and Fig. 2). Prior to sampling, purging of the sampling zones occurred by natural flow of groundwater for periods of 17 and 10 months for the Ruby Ranch and Antioch wells, respectively.

Potentiometric surface levels were measured at least bimonthly in each zone from February 2008 to January 2012 at Ruby Ranch and from September 2010 to December 2012 at Antioch using Westbay® groundwater pressure probes and controls. At Ruby Ranch, groundwater was sampled from each zone in June 2009 and again in June 2010, and from select zones in July 2011. At Antioch, groundwater was sampled from each zone in June 2011. Sampling was conducted using a set of four vacuum-pumped stainless steel sampling bottles attached to a wireline sampling tool. When the sampling tool is

aligned with the sampling port in each zone, the sampling valve was opened and water from the zone filled the depressurized bottles. One liter of sample can be collected for each trip to the sampling zone. Between sampling events for adjacent zones, bottles, hoses, and connectors were cleaned by sequential rinses with Liquinox® soap, deionized water, HCl, and a final rinse with deionized water.

During installation of the Antioch well, evaporite nodules were observed with a down hole camera at depths corresponding to the Upper and Lower Glen Rose formations. Samples of evaporite nodules (anhydrite and/or gypsum) were recovered from well cuttings collected during the installation of the Antioch well at depths corresponding to the Upper and Lower Glen Rose formations.

The Westbay multiport well systems consists of PVC casing with PVC couplings between casing sections, sampling and pumping ports, and packers. Casings are 38-mm inside diameter schedule 40 PVC with an outside diameter of 49 mm; Packers consist of polyurethane tubing over 38-mm inside diameter schedule 40 PVC, and can withstand a maximum pressure differential of 200 psi. The maximum pressure differential across a single packer is 75 psi. Casing couplings consist of PVC. Measurement and pumping ports consist of PVC with 316L stainless steel, Teflon, Viton, and Kevlar components. The MOSDAX® sampling tool consists of 316L stainless steel, Teflon, Viton, and Kevlar. The silicon strain-gauge pressure transducer has a specified accuracy of 0.1% of Full Scale combined non-linearity, repeatability and hysteresis, however, the typically achieved is +/- 0.02% FS with a reproducibility of 0.005 % FS as reported by the manufacturer.

Hydraulic Conductivity Testing

Hydraulic conductivity was calculated for each zone by applying analytical solutions to rising and falling head data. Multiport wells allow for rising or falling head

tests to be performed in specific hydrostratigraphic zones that are hydraulically isolated from overlying and underlying zones by hydraulic packers. The Westbay technology uses a mechanical wireline tool called the Open and Close tool (OC tool) for opening and closing specialized couplings within each zone called pumping ports (PPs). PPs contain a 2 cm screen that can be opened for hydraulic communication between the formation and the inside of the PVC casing. If there is a difference between the head in the formation and the head inside the casing, a pressure transducer (30 psi Insitu LevelTroll 500) records the change in head inside the casing when the PP is opened. Manual eline measurements were taken before and after the tests to confirm results. Once a PP was open and the rising or falling head data was collected, a conventional slug test (using a sealed PVC pipe) was periodically performed on the open zone to verify results.

Data collected from the rising and falling head tests were analyzed using Aqtesolv® Professional for Windows version 4.5. The Bouwer-Rice (1976) slug test solution was chosen to analyze data from zones that exhibited overdamped responses to rising and falling head tests. The solution was originally a method designed for use exclusively on unconfined aquifers, but Bouwer (1989) states the method can also be applied to confined aquifers. The Butler (1998) slug test solution was chosen for zones that exhibited an oscillatory response (underdamped).

Analytical methods

Groundwater samples were analyzed for major ions at the Lower Colorado River Authority Environmental Laboratory Services in Austin, Texas using an Inductively Coupled Plasma Optical Emission Spectrometer and Ion Chromatograph. Detection limits for the major ions were: 0.2 ppm for Ca, Mg, K, Na; 20 μg/L Sr; 1 ppm for Cl and $S0_4$; 2 ppm for alkalinity (as $CaCO_3$), 0.02 ppm for NO_3. The absolute difference between cation and anion charges was <5% for all samples, and there was not a bias to positive or

negative charges. Cation and anion concentrations of equipment and field method blanks were measured using the Agilent 7500ce quadruple inductively coupled plasma–mass spectrometer (ICP-IMS) and Thermo Scientific Dionex ion chromatography, respectively, at the Department of Geological Sciences at the University of Texas at Austin (UT). Constituent concentrations in all blanks were not detectable.

Sr was isolated using ion exchange chemistry, and Sr isotope values were measured using a Finnigan-MAT 261 thermal ionization mass spectrometer at the Department of Geological Sciences at UT following the methods of Banner and Kaufman (1994; n=22) and a multicollection VG Sector 54 mass spectrometer at Massachusetts Institute of Technology (MIT; n=27). Analytical methods used at MIT are similar to those of Banner and Kaufman, except for the use of dynamic collection instead of static collection (personal communication with Francis O. Dudás, MIT Isotope Lab). The target Sr mass for analysis was 200 ng, and volumes of unknown samples necessary to achieve this mass ranged from 0.1 to 1 mL, depending on Sr concentrations in the sample. Analytical uncertainty, based on the long-term reproducibility of the NIST SRM 987 standard (reported value of 0.712034 +/- 0.00026), was 0.71026 +/- 0.000015 and 0.71024 +/- 0.000018 for samples analyzed at UT and MIT, respectively. Laboratory blanks ranged from 16 to 19 pg (n=2). There was 180 pg of Sr in 4 mL of equipment and field blanks. As the volumes in blank samples used in the analyses were at least four times greater than the volumes of unknown samples that were used, the Sr mass in the blanks are negligible relative to the Sr mass of the unknown samples. Measurements of filtered and unfiltered samples were within analytical uncertainty (n=3). Replicates of samples analyzed at UT and MIT (n=9) were within analytical uncertainty, except one, which had a difference of 0.000041. Because results were replicated between labs, results were not normalized.

Mapping spatial variations in potentiometric elevations and total dissolved solids

To assess the lateral groundwater flow in the Middle Trinity aquifer, a regional potentiometric map of the Middle Trinity aquifer was created. The map was created using groundwater levels measured by the Hays Trinity Groundwater Conservation District (HTGCD), Texas Water Development Board (TWDB), Blanco-Pedernales Groundwater District (BPGCD), and the Barton Springs/Edwards Aquifer Conservation District (BSEACD) in wells completed in the Middle Trinity aquifer within Hays Co. (and portions of surrounding counties) from February to April 2009. Water-level measurements were collected using either manual measurements (calibrated electric tape) or with logging pressure transducers. Water elevations were mapped and interpolated using a kriging (linear model) algorithm using Surfer and Geographic Information System (GIS) software. All data were carefully reviewed, and data were omitted from the compilation if suspected of questionable well completion, significant influence from pumping, or other anomalous or non-representative conditions. Potentiometric contours were manually reinterpreted to account for hydrogeologic boundaries, data gaps, and experience of the authors. The accuracy of the surface elevation of a well is estimated to be less than 3 m (10 ft), and sufficient for the 20 m contour interval and regional scale of the map. The resulting map was presented in Wierman et al. (2010), in which detailed information on the wells and data used in creating the potentiometric map can be found.

To assess the spatial distribution of recharge to the Middle Trinity and the relationship between trends in groundwater flow and relative magnitude of groundwater solute concentrations, a map of the total dissolved solids (TDS, mg/L) of the Middle Trinity aquifer was created. Data were compiled from unpublished databases of the TWDB, BPGCD, HTGCD and reports from Muller (1990), Hunt et al. (2010), and Davidson (2008). Data were collected between 1970 and 2012, although most data were

collected within the last 12 years. TDS concentrations were mapped and interpolated following the methods detailed above. An earlier version of this map (using data from 1970-2009) was presented in Wierman et al. (2010), and an update version is presented here.

Compilation of and comparison to existing data

Temporal variations in potentiometric elevations measured at Ruby Ranch and Antioch were compared to those measured at two wells (Storm Ranch and Downing; Fig. 2) located up gradient and between the multiport well sites and the recharge area for the Middle Trinity aquifer. Water level data for these wells were retrieved from the HTGCD online database. Geochemical compositions measured from the Edwards and Trinity aquifers collected from the multiport wells in this study were compared to existing geochemical data retrieved from the TWDB Groundwater Database (Texas Water Development Board, 2012) and compiled from the literature (Musgrove and Banner, 2004; Musgrove et al., 2010; Weirman et al., 2010; Wong et al., 2012). Model curves of calcite and dolomite recrystallization were calculated following the methods of Banner and Hanson (1990) to account for covariation of Mg/Ca and $^{87}Sr/^{86}Sr$ values. Initial water and bedrock geochemical compositions were assigned based on measured soil leachate and Edwards limestone compositions as described in Wong et al. (2011).

Chapter 5. Reconstructing Mid to late Holocene (0-7ka) climate variability from a central Texas speleothem

ABSTRACT

There is strong concern about current and future drought in central Texas necessitating investigations of climate processes controlling rainfall and the potential response of these processes to future climate change. This study addresses these questions by using modern observations to understand how speleothem $\delta^{18}O$ variations might reflect severe droughts, and reconstructs Holocene (0-7ka) climate variability using a speleothem sample collected from a central Texas cave. Speleothem $\delta^{18}O$ values were measured at a 30-year resolution, providing the highest resolution climate reconstruction for the mid to late Holoene in central Texas. Rainfall $\delta^{18}O$ variability reflects intra-annual variations in the proportion of Pacific- vs. Gulf of Mexico-derived moisture and the occurrence of tropical storms. Cave dripwater $\delta^{18}O$ values more directly reflect rainfall $\delta^{18}O$ variations under drought conditions, but it is unlikely that such variability will affect long-term (decadal-scale) speleothem $\delta^{18}O$ values. From the mid to late Holocene, speleothem growth rates were relatively constant (30-40 μm/yr) and speleothem $\delta^{18}O$ values varied cyclically around a mean value with a 1,500 year periodicity. The relative consistency of speleoethem growth rate and $\delta^{18}O$ values suggests that climate dynamics governing rainfall sources and amount water were similar throughout much of the mid to late Holocene. From 0.5-1.5 ka, however, speleothem growth slowed (5 μm/yr), which consistent with a region-wide dry interval. A spike in speleothem $\delta^{18}O$ values was coincident with the start of the slow growth interval, and could reflect a greater proportion of GoM- vs. Pacific- derived moisture or decreased occurrence of tropical storms under prolonged dry conditions.

INTRODUCTION

Central Texas is a region that lies at the transition from the humid east to the arid west, which is subjected to frequent and severe droughts. The region is heavily dependent on groundwater resources, which are currently stressed by population growth and urban expansion, for drinking water and agricultural production. The 2011 drought, which was the most intense drought of record and caused billions of dollars in economic damage (Beach, 2012), has recently raised awareness of water resource issues. This awareness has been accompanied by a renewed interest in delineating the climate processes controlling rainfall in the region and understanding how those processes might respond to future climate change. The research presented here addresses these questions by reconstructing past climate from a central Texas speleothem sample.

Existing Holocene climate reconstructions for central Texas have, to date been, generally coarsely resolved (millennial-scale variability), and often have had limited age constraints (e.g., Boulter et al., 2010; Humphrey et al., 1994; Nordt et al., 1994, 2002; Cooke et al., 2003; Toomey et al., 1993; Blum et al., 2004). Exceptions, however, include tree ring records covering the last 250 years (Cleaveland et al., 2011) and a 19 kyr record of magnetic susceptibility preserved in Halls Cave sediments (Ellwood and Gose, 2006); the latter of which is influenced by both temperature and moisture conditions. Centennial- to decadal-scale climate records spanning the mid to late Holocene that are temporally well constrained have been developed from the Gulf of Mexico (GoM) region, which document centennial-scale climate variability (e.g., Poore et al., 2003, 2004; LoDico et al., 2006; Richey et al., 2007;). The GoM is a significant source of moisture for the mid-North American continent (e.g., Higgins et al., 1997; Vachon et al., 2010), which makes understanding links between GoM and Texas climate variability

potentially an important part of understanding the climate processes controlling drought in Texas.

The first part of this study focuses on characterizing the response of rainfall and cave dripwater $\delta^{18}O$ values to severe droughts in order to assess how such events might be reflected in speleothem $\delta^{18}O$ records. The second part uses variations in speleothem growth rate and $\delta^{18}O$ values to reconstruct mid to late Holocene (0 to 7ka) climate. Results suggest that speleothem $\delta^{18}O$ values will not reflect short-term drought variability, and that long-term speleothem $\delta^{18}O$ values will be dictated by the relative balance of Pacific vs. Gulf of Mexico (GoM)-derived rainfall and relative frequency of tropical storms. Relatively constant speleothem growth and $\delta^{18}O$ values from the mid to late Holocene, suggest that the amount and source of rainfall was stable. In the late Holocene (0.5-1.5 ka), however, reductions in speleothem growth and a spike in $\delta^{18}O$ values were relatively consistent with regionally extensive dry conditions.

PROJECT SETTING

The speleothem sample, NBS1, was collected from Natural Bridge Caverns in central Texas (Fig. 5.1a). The cave is developed in the Edwards Plateau, a regionally extensive, intensely karstified, Cretaceous carbonate platform. Natural Bridge Caverns consists of two adjacent caves (North and South Cave) that, when combined, have a lateral extent of 1160 m and reach a depth of 75 m. NBS1 was collected from the bottom of the Jeremy Room in the south cave.

Central Texas occurs in a transitional region between sub-humid to semi-arid climates, which is prone to frequent droughts (Larkin and Bomar, 1983). There is clear seasonality in temperature, and a tendency of higher rainfall in the spring and fall (Fig.

5.1b; National Weather Service, 2012). Inter-annual variability of rainfall, however, is greater than intra-annual variability, which means that regular rainy seasons do not occur.

Modern cave environments in central Texas have been studied intensively for over a decade (Musgrove and Banner, 2004; Banner et al., 2007; Pape et al., 2010; Wong et al., 2010; Wong et al., 2011; Breecker et al., 2012; Feng et al., 2012; Cowan et al., 2013). From this previous research, there are several, pertinent key results. The type of flow path (i.e., conduit vs. diffuse) that dominantly supplies a drip site strongly influences the transit (i.e., residence) time of water moving from the surface to the cave (Musgrove et al., 2004; Wong et al., 2010; Wong et al., 2011). Seasonal ventilation of the cave atmosphere naturally occurs (Cowan et al., 2013), and drives seasonal variation in calcite growth rates (Banner et al., 2007), dripwater geochemistry (Wong et al., 2011), and speleothem isotopic compositions (Feng et al., 2012) that might bias central Texas speleothem records towards the season of ventilation. Pape et al. (2010) specifically investigated controls on central Texas rainfall and dripwater $\delta^{18}O$ values, and found that rainfall $\delta^{18}O$ values largely reflect moisture derived from the Gulf of Mexico (GoM). Rainfall $\delta^{18}O$ values exhibit a correlation with rainfall amount only under relatively warm (>26.9°C) conditions (Pape et al., 2010). Additionally, Pacific derived tropical storms result in depleted rainfall $\delta^{18}O$ values. Dripwater $\delta^{18}O$ values have limited variability relative to that measured in rainfall $\delta^{18}O$ values, reflecting mixing of infiltrating water in the vadose zone above the cave and water transit times in excess of 1 year. The findings of Pape et al. (2010) are based on data collected from 1998 to 2007. Central Texas has experienced two severe droughts since 2007, 2009 and 2011, the latter of which was the most intense drought of record and resulted in billions of dollars in economic losses according to Texas AgriLife Extension Services (Beach, 2012). This study builds upon the research of Pape et al. (2010) using rainfall and dripwater data that encompasses the

onset of and recovery from both droughts to understand how dripwater $\delta^{18}O$ values, and consequently speleothem $\delta^{18}O$ values, might reflect similar drought events.

METHODS

Cave dripwater was collected every four to six weeks from two sites (NBSB and NBWS) within Natural Bridge Caverns (NB) from 2006-2012. NBSB is located in the North Cave, and drip water samples were collected directly from the drip. NBWS is located in the South Cave, and samples were decanted, on site, from drips collected in a 1 L HPDE collection bottle placed under the drip for 1 to 3 hours. Drip rate responds rapidly to rain events at both sites, and both sites are interpreted to be dominantly supplied by conduit flow (Guilfoyle, 2006; Wong et al., 2011). Samples were collected in 4 mL clear glass vials with no head space. Approximately every other dripwater sample was analyzed for $\delta^{18}O$ values using a Gasbench II interfaced with a Delta V isotope ratio mass spectrometer in the Stable Isotope Lab for Critical Zone Gases in the Department of Geological Sciences (DGS) at The University of Texas at Austin (UT). Analytical uncertainty is ±0.1 based on the standard deviation of 20 replicate analyses of an internal standard. Ten replicate analyses of $\delta^{18}O$ were within analytical uncertainty. Rainfall data from 1998 to 2012 was retrieved from the National Weather Service for the Austin Bergstrom Airport (KAUS; NWS, 2012). Existing Austin-area rainfall monthly to bi-monthly $\delta^{18}O$ values were compiled from Pape et al. (2010) and Feng et al. (2012), and previous NB dripwater $\delta^{18}O$ data were compiled from Pape et al. (2010).

NBS1 was actively growing when it was collected 1986 prior to an expansion of the commercial portion of the cave. The sample is 22 cm long and 7 cm in diameter, and is generally symmetrical along the growth axis (Fig. 5.2). The sample is broadest at the base and mid section, and tapers slightly towards the top. The sample was cut in half, and

each side polished. The mineral structure is consistent throughout the sample, based on visual analysis of slabs and thick sections, except for near the top and bottom (Fig. 5.2). At the top and bottom of the sample, layers of white calcite occur intermittently with clear layers of calcite. Irregularly-spaced, distinct horizons occur in the top 1 cm of the sample, which might represent hiatuses in growth (Fig. 5.2).

Calcite powder (0.5-0.8 g) for U-Th dating was obtained using a handheld dentist drill from select horizons, including above and below two horizons suspected to represent hiatuses in growth. Not all horizons suspected of being hiatuses in growth, however, were sampled due to their close spacing and the sample size necessary for U-Th analysis. Calcite powder (150 μg) for stable isotope analyses ($\delta^{18}O$ and $\delta^{13}C$) was collected from the opposite face using a microdrill capable of stepping at 10 μm increments. Following a coarse scale reconnaissance sampling of 1 mm every 6 mm, samples were drilled from 7 overlapping transects along the speleothem growth axis at increments ranging from 0.1 to 1 mm steps (Fig. 5.2 and Table 5.1).

For U-Th dating, calcite powder was dissolved, and U and Th isolated, following the methods of Edwards (1987, 1993), Cheng (2000), and Musgrove et al. (2001). U and Th separates were loaded onto Re filaments and analyzed using a Thermo Scientific Triton Thermal Ionizing Mass Spectrometer within DGS at UT following the methods of Musgrove et al. (2001). For stable isotope analyses, 30-80 μg aliquots were analyzed using Thermo MAT253 with Kiel IV Carbonate Preparation Device within the Austin Laboratory for Paleoclimate Studies in the DGS at UT. Analytical uncertainty is ±0.06 for $\delta^{18}O$ and ±0.03 for $\delta^{13}C$ based on the standard deviation of 61 replicate analyses of NBS19.

An age model was calculated based on U-series ages using the Stal-Age algorithm developed by Scholtz and Hoffman (2011). The algorithm screens the data for outliers

and then calculates an age model and 95% confidence limits using a Monte Carlo simulation that fits ensembles of positively-sloped straight lines to sub-sets of the age data. Speleothem sampling depths were converted to ages using the resulting age model. Because speleothem growth rate was not constant along the sample and sampling spacing was variable (i.e., steps ranged from 0.1 to 1 mm), the speleothem $\delta^{18}O$ time series was interpolated to represent 30 year intervals.

RESULTS

Rainfall $\delta^{18}O$ values

Monthly to bimonthly composites of Austin rainfall sampled from 2009-2011 ranged from -8.4 to 1‰ (n = 23; Feng et al., 2012), which is similar to values measured from 1999-2007 that ranged from -7.3 to -1.1‰ (n=53; excluding one sample measuring -12.6‰ associated with a tropical storm) (Pape et al., 2010). Two samples collected during the Tropical Storm Hermine (2010) measured -8.6‰ and -10.5‰, which are similar to rainfall $\delta^{18}O$ values associated with Hurricanes Madeline (1998) and Lester (1998) and Tropical Storm Miriam (2006) (-7.4 to -12.6‰) (Pape et al., 2010). Each of these extreme events originated in the Eastern Pacific and crossed Mexico before reaching Texas. Unlike the 1998 and 2006 storms, Tropical Storm Hermine traversed part of the Gulf of Mexico after crossing southern Mexico and before making landfall on the northeast coast of Mexico (National Hurricane Center, 2013).

Composite rainfall $\delta^{18}O$ values from 1999-2011 do not correlate with the average temperature or normalized average monthly rainfall of each collection interval (Fig. 5.3), which is consistent with the findings of Pape et al. (2010). Pape et al. (2010) found a strong correlation (r^2=0.79; $p<0.001$; n=10) between normalized average monthly rainfall and rainfall $\delta^{18}O$ values during warmer (i.e., summer; temperature ranged of 26.9-

30.4°C) conditions. When data collected from 2009-2011 during the summer (temperature range from 26.6-31.1°C) is included, the strength of the correlation declines (r^2=0.31; p=0.02; n=16) (Fig. 5.3). Composite rainfall $\delta^{18}O$ values measured from 1999-2011 are slightly (but not statistically significant) higher in the summer (-4.0‰) relative to fall (-4.8‰) and winter (-4.9‰) values, and significantly (p<0.01) higher in the spring (-3.0‰) relative to fall and winter values (Table 5.2). Differences in average monthly rainfall averages associated with the rainfall composites are not statistically significant between the seasons (Table 5.2).

Dripwater $\delta^{18}O$ values

From 2007-2012 dripwater $\delta^{18}O$ values ranged from -5.2 to -3.5‰ (n=80), which is consistent with ranges measured previously (-5.1 to -0.6‰, n=185) in NB dripwaters during 1998-2007 (Pape et al., 2010). Dripwater $\delta^{18}O$ values are within the range of those measured in monthly to bimonthly composites of Austin rainfall, and are generally consistent with the weighted average of monthly composites of rainfall $\delta^{18}O$ values collected from 1999-2011 (-4.3‰) (Fig. 5.4). Dripwater $\delta^{18}O$ values do not correlate with composite rainfall $\delta^{18}O$ values or with the Palmer Drought Severity Index (PDSI) (Fig. 5.5). Dripwater $\delta^{18}O$ values measured from Nov 2010 to Nov 2011, which was coincident with the most intense historical drought, include the lowest value (-5.2‰) measured for the entire period in which dripwater was monitored (1998-2011). The weighted average rainfall $\delta^{18}O$ values measured during this interval was -3.6‰ (n=3), which included the composite of 2010-11 winter rain that measured -6.0‰ (Table 5.3).

SPELEOTHEM GROWTH RATE AND $\delta^{18}O$ VALUES

Fourteen U-Th dates range from 6985 +/- 122 at the bottom of the stalagmite to 132 +/- 17 near the top (Fig. 5.6). There are four distinct sections of growth that, from the

bottom to top, had an overall growth rate of 40, 30, 5, and 35 μm/year (Fig. 5.6). These growth rates are similar to those measured in central Texas speleothem samples active during the Pleistocene, which ranged from 0.5 to 91 μm/year (Musgrove et al., 2001; Feng et al., in review). In the lowest section of the sample (5.5 to 6.9 ka), there were three instances in which dates for distinct horizons spaced greater than 1 cm apart were within analytical uncertainty (Fig. 5.6). The overall growth rate for this interval, however, was 40 μm/year, suggesting that intervals of slow growth occurred in between intervals of irresolvable fast growth. Speleothem growth from 5.5 to 1.7 ka was the most consistent relative to the rest of the sample (Fig. 5.6). Speleothem growth slowed by nearly an order of magnitude from 1.7 to 0.3 ka, and returned to a growth rate similar to that of the rest of the sample from 0.3 ka to modern. The reduction in growth rate from 0.3 to 1.7 ka might reflect one or more hiatuses in growth. Horizons, however, from above and below suspected hiatuses, had depth-age relationships that were consistent with the growth rate estimates for the time period (Fig. 5.6).

There was correspondence between speleothem $\delta^{18}O$ values in vertically overlapping portions of laterally offset transects, consistent with speleothem growth occurring under equilibrium conditions (Fig. 5.7). This is also supported by the lack of correlation between speleothem $\delta^{18}O$ and $\delta^{13}C$ values in all transects, except for 13 samples collected from track 2 at ~15 mm depth. The strong, positive correlation between $\delta^{18}O$ and $\delta^{13}C$ values over this short interval might reflect speleothem deposition under non-equilibrium conditions. Kinetic fractionation associated with rapid CO_2 degassing and calcite precipitation would cause enrichment of speleothem $\delta^{18}O$ and $\delta^{13}C$ values (Goede et al., 1986; Goede, 1994; Desmarchelier et al., 2000; Mickler et al., 2004). Environmental changes, however, could also result in coincident increases in both $\delta^{18}O$ and $\delta^{13}C$ values (Dorale et al., 1998; Denniston et al., 2001; Genty et al., 2003). In cases

in which it is possible that environmental changes drive co-variation in speleothem $\delta^{18}O$ and $\delta^{13}C$ values, it is difficult to discern between the two possible explanations for positively correlated speleothem $\delta^{18}O$ and $\delta^{13}C$ values, and paleoclimate interpretations should consider both possibilities (Mickler et al., 2004).

Interpolated (as described in the methods section) speleothem $\delta^{18}O$ values ranges from -5.0 to -2.9‰, with an average of -4.2‰. Values do not exhibit an increasing or decreasing temporal trend, and, instead, fluctuate about the mean (Fig. 5.8). Several techniques (i.e., Blackman-Turkey (BT), Multi-Taper Method (MTM), and Monte Carlo Single Spectrum Analysis (MC-SSA)) were performed using K-spectra software to calculate spectra for the entire time series. A brief summary of the differences between these methods, which is discussed in detail by Ghil et al. (2000), is presented here. The BT approach calculates the power spectrum from using a windowed fast Fourier transform (FFT) of the autocorrelation function of a weighted version of a time series. A FFT transforms a time series into a frequency spectrum, essentially, breaking it into a series of sine and cosine components. Data is weighted by tapered shapes (i.e., triangular and cosinusoidal) to reduce artificially high power estimates at frequencies away from the true peak frequencies (i.e., spectral leakage). MTM uses a small set of tapers (i.e., eigentapers), instead of a single taper, to reduce spectral leakage. The BT and MTM approaches both fit data to a fixed sine and cosine model, where SSA does not. In SSA, the variance of the time series is described eigenvalues, where the singular spectrum corresponds with the square roots of the eigenvalues. Monte Carlo analysis is then used to test if the SSA of the time series is distinguishable from a red noise model, where red noise is defined as a linear function in which power declines monotonically with increasing frequency.

The spectra show peaks with respect to red noise background corresponding to cycles with periods near 1,500, 130, 90, and 65 years (Fig. 5.9). Periods at 90 and 65 years are near the lower detection limit of spectral analysis methods (i.e., the Nyquist frequency of 1/60 years), and, therefore, will not be discussed further. The confidence level, for which the 1,500 and 130 year spectra can be considered distinct from red noise, ranged from 95% using the multi-taper method to 90% using Monte Carlo Single Spectrum Analysis techniques. The delineation of these spectral peaks by all three techniques suggest that these cycles are a real part of the variability preserved in the sample, but the low confidence calculated by BT and MC-SSA techniques indicate that caution should be taken with this interpretation.

The uncertainty of the age model was incorporated into the spectral analysis to further test the robustness of the spectral analysis results. A Monte Carlo simulation was used to produce 1,000 realizations of the age model, assuming that the distribution of age model uncertainty was normal. These results were interpolated to create corresponding realizations of the speleothem $\delta^{18}O$ time series, for which the BT approach was used to calculate power spectrums. The convergence of the median, 5^{th} and 95^{th} percentile power spectrums at the frequency corresponding to the 1,500 year cycle, but not the 130 year cycle suggest that the former is likely a robust result (Fig. 5.8a). To further explore the ability of the cyclicity to explain the observed variations in speleothem $\delta^{18}O$ values, a model time series was constructed in Kspectra using the 1,500 periodicity (Fig. 5.8b). This model simply represents the time-series of the spectral component isolated for the frequency 1/1,500 years, and accounts for 14% of the time series variance. The correspondence between the observed and model values for the majority of the time series supports the interpretation that these cycles represent a signal that is distinct from noise. However, the correspondence between observed and modeled values was poor

from ~0.5-1 ka, which included a short lived interval in which $\delta^{18}O$ values spiked (-2.9‰. at 1.2 ka). suggesting that a unique set of climate forcings were active during this interval.

DISCUSSION

Controls on rainwater $\delta^{18}O$ variations

Seasonal differences in rainfall $\delta^{18}O$ values likely reflect small variations in the relative proportions of moisture derived from the GoM vs. the Pacific. Low fall and winter rainfall $\delta^{18}O$ values (-4.8‰ and -4.9‰, respectively) relative to spring and summer values (-3.0‰ and -4.0‰, respectively) could be accounted for by seasonal temperature variations. That is, the temperature dependent fractionation of $\delta^{18}O$, as vapor condenses to water, could easily account for the small differences (0.9 to 1.9‰) measured in rainfall $\delta^{18}O$ values measured in the winter vs. spring/summer. Based on the gradient of 0.38‰/C° (Lachneit, 2009), differences in average winter (10.6°C) vs. summer (28.6°C) and winter vs. spring (21.4°C) temperatures could account for differences in seasonal rainfall $\delta^{18}O$ values of up to 6.8 and 4.1‰, respectively. There was not, however, a significant correlation between rainfall $\delta^{18}O$ values and temperature, and there was a greater difference between winter and spring rainfall $\delta^{18}O$ values relative to the difference in winter and summer. This suggests that temperature is not the dominant control on rainfall $\delta^{18}O$ variations.

Rainfall $\delta^{18}O$ values could reflect variations in the relative contributions of GoM- vs Pacific-derived moisture (Feng et al., in review). Higher rainfall $\delta^{18}O$ values measured during the spring and summer months may reflect a greater dominance of water derived from the GoM (-2 to -4‰), whereas lower values measured during fall and winter months could reflect moisture derived from the Pacific (-6 to -10‰; Vachon et al., 2010). The

weighted average of rainfall $\delta^{18}O$ (-4.3‰) is much closer to the isotopic signature of GoM derived moisture relative to Pacific derived moisture. This suggests that long-term (1999-2011) rainfall $\delta^{18}O$ variation is dominantly influenced by GoM derived moisture. Long-term variations in rainfall $\delta^{18}O$ values could also reflect changes in the frequency of tropical storms, as rainfall associated with tropical storms has $\delta^{18}O$ values (-7.4 to -12.6‰) that are much lower than the average rainfall $\delta^{18}O$ value (-4.3‰).

Controls on dripwater $\delta^{18}O$ variations

Central Texas dripwater $\delta^{18}O$ values largely reflect the homogenization of intra- and inter-annual variations in rainfall $\delta^{18}O$ by mixing in the subsurface above the cave. This is indicated by i) the lack of correlation between dripwater $\delta^{18}O$ values and rainfall $\delta^{18}O$ values (and PDSI), ii) the small range of dripwater $\delta^{18}O$ values relative to rainfall $\delta^{18}O$ values, and iii) the consistency between weighted average rainfall $\delta^{18}O$ values and average dripwater $\delta^{18}O$ values (Pape et al., 2010; this study). This last observation suggests that dripwater reflects annually recharged rainfall in central Texas, which contrasts with other studies demonstrating dripwater $\delta^{18}O$ values reflect rainfall recharging during a certain part of the year in other regions (Jones et al., 2000, 2003; Asmerom et al., 2010). Results during the drought intervals, however, suggest that mixing of infiltrating water in the vadose zone is reduced under drought conditions. This enables the isotopic variability of rainfall to be more directly reflected by dripwater $\delta^{18}O$ values, as discussed below.

The lowest dripwater $\delta^{18}O$ values of the compiled monitoring interval (1998 - 2011) were collected during the 2011 drought, which is the most intense drought of record. Understanding the processes responsible for the low values observed during this interval will inform how such an event might be preserved in a speleothem record.

Evaporation would cause an increase in dripwater $\delta^{18}O$ values, so it is not likely that enhanced evaporation associated with the drought interval resulted in lower dripwater $\delta^{18}O$ values.

It is possible that there was a reduction in vadose zone mixing due to reduced rainfall amounts associated with drought conditions. Such reduction of mixing might have allowed more of the isotopic signature of the 2010-11 winter rain (-6‰), which occurred in the beginning of the drought, to be reflected in dripwater isotopic compositions (-5.2‰ relative to the average value of 4.3‰). In other words, the isotopic signature of the 2010-11 winter rain was homogenized to a lesser degree because there was less "old" water in transit along the flow routes supplying the drip sites. If this were the case, than it would also be expected that recharge from the isotopically heavier rain (-1.2‰) that occurred in March 2011, also during the drought, would be similarly less homoginized. Indeed, dripwater $\delta^{18}O$ values increased despite the small magnitude of the rain event (Fig. 5.4; Table 5.3). Also consistent with these observations is the coincidence between lower rainfall and dripwater $\delta^{18}O$ values during the 2009-10 winter following a 1-year interval of dry conditions (Fig. 5.6). The decrease in *rainfall* $\delta^{18}O$ values was greater in the 2009-2010 winter, although the decrease in *dripwater* $\delta^{18}O$ values was greater in the 2010-11 winter. This suggests that dripwater $\delta^{18}O$ values were not as sensitive to rainfall $\delta^{18}O$ variations in the 2009-10 winter relative to the 2010-11, which is consistent with the drought severity being greater in 2010-11 relative to 2009-10. These observations suggest that the degree to which dripwater $\delta^{18}O$ variations reflect rainwater $\delta^{18}O$ variations is dependent on antecedent moisture conditions. That is, dripwater $\delta^{18}O$ variability will more closely follow rainwater $\delta^{18}O$ variability under dry conditions when there is less water in the vadose zone with which newly recharged water mixes. Under wet conditions, there is more water along the flowpaths with which newly

recharged water mixes and dripwater $\delta^{18}O$ values will reflect the average rainfall $\delta^{18}O$ value. Enhanced dripwater $\delta^{18}O$ variability under drought conditions, however, will likely not significantly alter speleothem $\delta^{18}O$ values on a decadal or multi-decadal scale.

These results are based on data collected from drip sites that are dominantly supplied by conduit (vs. diffuse) flow paths (Guilfolye, 2006; Wong et al., 2010, 2011), and may not be representative of drip sites dominantly supplied by diffuse flow paths. Sites dominantly supplied by diffuse flow paths tend to have less variability in drip rate and extent of water-rock interaction that dictate dripwater geochemistry (e.g., Wong et al., 2010, 2011). This suggests that dripwater $\delta^{18}O$ variability at diffuse sites might reflect the homogenization of intra- and inter-annual rainfall variations and longer residence times. It is unlikely, however, that variation of dripwater $\delta^{18}O$ values would be enhanced to the same degree as was measured at the conduit sites (discussed above) under drought conditions.

It has been demonstrated that calcite growth rates vary seasonally in central Texas caves that experience seasonal ventilation of the cave atmosphere (Banner et al., 2007). This suggests that speleothem compositions from these caves might be biased toward the climate conditions of the season with enhanced calcite growth (Banner et al., 2007). The homogenization, however, of inter- and intra-annual variations in rainfall $\delta^{18}O$ via mixing during the transit of water through the vadose zone indicates that dripwater $\delta^{18}O$ do not reflect seasonal climate variations, and that speleothem $\delta^{18}O$ should not preserve a bias towards winter conditions (this study; Pape et al., 2010).

On time scales of decades to millennia, there are several possible ways to interpret speleothem $\delta^{18}O$ variability. It is possible that speleothem $\delta^{18}O$ variability reflects long term changes in the balance of moisture derived from GoM vs. Pacific Ocean source regions, possibly due to a shift in the annual distribution (i.e., fall/winter vs.

spring/summer) of rainfall. Another possibility is that speleothem variability reflects significant changes in the frequency of tropical storms, as tropical storms produce rainfall with isotopically low values (Lachneit, 2009). A third possibility is that speleothem $\delta^{18}O$ variability reflects changes in the isotopic signature of GoM derived moisture. With regard to the latter, Feng et al. (in review) documented that an isotopic shift in GoM seawater $\delta^{18}O$ values during the transition from the LGM to the Holocene, due to input of isotopically lighter glacial-meltwater pulses, was consistent with shifts in speleothem $\delta^{18}O$ to lighter values. This correspondence suggests that Texas speleothem $\delta^{18}O$ values dominantly reflect variations in the isotopic composition of the GoM. While input of glacial meltwater pulses during the mid to late Holocene likely did not occur, it is possible that changes in the evaporation-precipitation balance in the GoM region could influence the isotopic signature of moisture transported landward from the GoM.

Mid to late Holocene speleothem growth rates and $\delta^{18}O$ values

Speleothem growth rates suggest that moisture availability was relatively constant from the mid to late Holocene, with the exception of a dry interval from 0.5 to 1.5 ka. Reduced speleothem growth rates have been interpreted to reflect changes in moisture availability in this region (Musgrove et al., 2001), and it has been demonstrated that water supply (i.e., drip rate) is the first order control on modern speleothem growth in central Texas (Banner et al., 2007). In central Texas, however, winter ventilation of cave atmospheres result in the majority of speleothem growth occurring in winter, suggesting that central Texas speleothems might be biased towards winter conditions (Banner et al., 2007). Given these controls on speleothem growth rate in central Texas, relatively constant speleothem growth rates from the mid to late Holocene likely reflect constant moisture availability, or, more conservatively, constant *winter* moisture availability from

the mid to late Holocene. The decrease in speleothem growth rate from 30-40 μm/yr to 5 μm/yr (Fig. 10) suggests a substantial decrease in moisture availability.

The slow-growth interval (0.5 to 1.5 ka) of speleothem sample NBS1 is consistent with a drying trend in central Texas from ~1.0 to 0.5 ka reconstructed from cave sediments (Toomey et al., 1993; Ellwood and Gose, 2006) (Fig. 5.10). Although the interval of slow growth in NBS1 is expansive and coarsely resolved (Fig. 5.6), it broadly corresponds with the timing of the Medieval Warm Period (0.8-1.0 ka). It is also coincident with maximum dry conditions (1.1 to 1.3 ka) preserved in a Barbados speleothem (Banner et al., 1996), and a drying trend and extended drought reconstructed from a Belizean speleothem that was hypothesized to contribute to the collapse of the Mayan civilization (0.9-1.3 ka; Kennett et al., 2012) (Fig. 5.10). The similarities in the timing of these dry conditions suggests the slow growth interval of NBS1 reflects a region-wide dry period. Although Ellwood and Gose (2006), Toomey et al. (1993), and Banner et al. (1996) do not speculate on potential causes of dry conditions, Kennett et al. (2012) link dry conditions to ENSO variability. They argue that the Inter-Tropical Convergence Zone shifts northward under El Nino conditions, blocking moisture transport to the Mayan Lowlands. Under modern conditions, El Nino conditions are associated with wetter conditions in Texas (Ropelewski and Halpert, 1986), suggesting that another mechanism is likely responsible for prolonged dry conditions in central Texas.

The strong 1,500 year periodicity of speleothem $\delta^{18}O$ values around a constant value from the mid to late Holocene suggests that the climate dynamics regularly varied around a relatively constant mean state for the latter half of the Holocene. Many studies have documented a 1,500 year periodicity in Holocene climate archives from various locations around the world, including the North Atlantic Ocean (e.g., Bond et al., 2001;

Chapman and Shackleton, 2000; de Menocal et al., 2000) and North and South American (e.g., Viau et al., 2002; Yu et al., 2003; Willard et al., 2005), Eurasian (e.g., Niggemann et al., 2003; Gupta et al., 2005), and African continents (e.g., Russell and Johnson, 2005). Although there are many proposed theories to explain the forcing behind the cyclicity found in individual studies (e.g., variations in solar intensity, teleconnections to North Atlantic cold events, transition between climate regimes), there is not a consistent explanation that can account for the formation of the 1,500 year periodicity (e.g., Debret et al., 2007; Wanner et al., 2008; Wanner et al., 2011). Based on an understanding of controls on rainfall and dripwater $\delta^{18}O$ values in the modern system (discussed above), it is likely that speleothem $\delta^{18}O$ variations reflect variations in the relative proportion of moisture derived from the GoM (higher values) vs. Pacific (lower values) or variations in tropical storm activity. The relative consistency of speleothem growth rates and $\delta^{18}O$ values from the mid to late Holocene (except from 0.5 to 1.5 ka) suggest that, on the millennial-scale, sources and amounts of rainfall were stable.

It is likely that the climate dynamics governing the source of rainfall to central Texas was unique during the late Holocene dry interval (0.5 to 1.5 ka). Anomalously high speleothem $\delta^{18}O$ values in NBS1 were coincident with slow speleothem growth rates. There was poor correspondence between observed and modeled speleothem $\delta^{18}O$ values during this interval, which also suggests that climate dynamics distinct from the rest of the speleothem growth interval were dominant during this time. It is possible, however, that the spike in speleothem $\delta^{18}O$ values could reflect a non-linear response to the onset of dry conditions.

Speleothem $\delta^{18}O$ and $\delta^{13}C$ values varied independently throughout the sample, except when speleothem $\delta^{18}O$ values spiked (Fig. 5.7b). The strong correlation between speleothem $\delta^{18}O$ and $\delta^{13}C$ during this interval would be consistent with kinetic

fractionation. Good correspondence, however, between speleothem $\delta^{18}O$ values of vertically overlapping, yet horizontally offset transects (Fig. 5.9a), indicate that kinetic controls were not dominant during this interval. Although controls on speleothem $\delta^{13}C$ can be complicated, higher $\delta^{13}C$ values generally occur under drier conditions due to enhanced water-rock interaction or prior calcite precipitation, reduced contribution of respired CO_2 from soil zones, and/or greater contribution of C4 vs. C3 vegetation (e.g., Oster et al., 2010; Breecker et al., 2012). Relatively high speleothem $\delta^{13}C$ values are consistent with slowed speleothem growth rates, and their occurrence with high speleothem $\delta^{18}O$ values might indicate a relative increase in the proportion of moisture derived from the GoM relative to the Pacific or reduced tropical storm activity during prolonged dry conditions.

The occurrence of high speleothem $\delta^{18}O$ values under dry conditions might reflect a reduction in moisture sourced from the Pacific. An increase in speleothem $\delta^{18}O$ values could result from i) an increase in moisture sourced from the GoM, ii) a decrease in moisture sourced from the Pacific, or iii) a decrease in tropical storm frequency. The coincidence of high speleothem $\delta^{18}O$ values with a prolonged dry period suggests that a reduction in moisture transport occurred as opposed to an increase in moisture transport from the GoM. Tropical storms resulting in central Texas rainfall during the monitoring period (1998-2011) have all originated from the eastern Pacific (National Hurricane Center, 2013). Therefore, both decreases in moisture sourced from the Pacific and decreases in tropical storm occurrences would involve changes in climate dynamics governing moisture transport from the Pacific to central Texas. It is likely, however, that climate processes leading to tropical storm events are different than climate controls on the delivery of Pacific-sourced rainfall to central Texas.

Controls on centennial-scale variations in speleothem $\delta^{18}O$ values

At the sub-millennial scale, there is an overall direct correspondence between speleothem $\delta^{18}O$ values and GoM sea-surface temperatures (SSTs) reconstructed from sediments collected from Fisk, Pigmy, and Garrison basins (Figs. 5.1 and 5.11) (Richey et al., 2007; Richey et al., 2009). The correspondence between low speleothem $\delta^{18}O$ values and cool GoM SSTs could reflect a decrease in moisture transport from the GoM to central Texas or a shift towards greater amounts of fall/winter rainfall derived from the Pacific under cooler conditions. Oglesby et al. (1989) demonstrated that decreased GoM SSTs resulting from glacial melt water pulses during the late Pleistocene (10-14 ka) likely resulted in a reduction in vapor transport from the GoM to the N. American continent. Furthermore, Feng et al. (in review) suggest that GoM moisture penetrated further inland towards the southwest US region during warm intervals (i.e., Bolling Allerod) relative to cool intervals (i.e., Youger Dryas). These findings, however, are based on simulations and reconstructions of the late Pleistocene when the N. American ice sheet was more extensive, and may not be appropriate to extrapolate to account for the direct correspondence between GoM SSTs and speleothem $\delta^{18}O$ values in the late Holocene. Analysis of the modern relationship between GoM SSTs and Texas rainfall demonstrates that no significant correlation exists between GoM SSTs and spring/summer rainfall and that a weak ($r = 0.1$ to 0.3) positive correlation exists between GoM SSTs and fall/winter rainfall (Fig. 5.12). This suggests that the occurrence of lighter speleothem $\delta^{18}O$ values with lower GoM SSTs is driven neither by a decline in GoM-derived moisture or an increase in Pacific-derived moisture.

Evaporation of GoM water under cooler and drier (lower relative humidity) conditions would be consistent with isotopically lighter GoM vapor (Clark and Fritz, 1997; Lachniet, 2009). For example, the difference between vapor evaporated at 25°C

and 85% humidity would be 0.9‰ heavier than vapor evaporated at 23°C and 80% humidity, which is consistent with the magnitude in offset in the Texas speleothem $\delta^{18}O$ record. This process would shift rainfall off the meteoric water line (deuterium excess effect), and could be assessed in the modern setting. Existing measurements of paired $\delta^{18}O$ and δD values of Austin rainfall (June 2004 to May 2005) lie on the local meteoric water line (n=8; Pape et al., 2010), which suggests that intra-annual variations in the amount of fractionation of $\delta^{18}O$ during evaporation of GoM seawater is negligible. This data set, however, is small, and further analysis would benefit from a larger data set. The precipitation of calcite from dripwater under cooler temperatures would also shift speleothem $\delta^{18}O$ values towards lighter values (-0.2‰/°C). Therefore, the correspondence between GoM SSTs and speleothem $\delta^{18}O$ values at centennial scales in the late Holocene could simply reflect change in the isotopic composition of moisture derived from the GoM and precipitation of calcite from dripwater under cooler temperatures.

CONCLUSIONS

Over a decade's worth of modern rainfall and dripwater $\delta^{18}O$ values are used to delineate potential controls on speleothem $\delta^{18}O$ values, and assess how severe droughts (e.g., 2011 Texas drought) might be reflected in speleothem records. Consistent with findings by Pape et al. (2010), dripwater $\delta^{18}O$ reflects the weighted average rainfall $\delta^{18}O$ value, indicating that intra- and inter-annual rainfall variations are homogenized by mixing in the subsurface above the cave. Under drought conditions, however, dripwater $\delta^{18}O$ values more closely tracks variations in rainfall $\delta^{18}O$ values, likely because less mixing occurs under drying conditions. This is unlikely to be reflected by speleothem sampling on longer time scales (i.e., decades). On this time scale, speleothem $\delta^{18}O$

variability likely represents the balance between Pacific-derived vs. GOM-derived rainfall and/or frequency of tropical storms.

Variations in growth rate and $\delta^{18}O$ values from speleothem sample, NBS1, collected from Natural Bridge Caverns are used to reconstruct mid to late Holocene climate (0-7 ka). Overall speleothem growth rates are constant throughout the sample (30-40 μm/year), except from 0.5-1.5 ka when growth slowed (5 μm/year). Although it is temporally longer and coarsely defined, the slow growth interval is consistent with a drying trend in central Texas and surrounding region. Speleothem $\delta^{18}O$ values consistently vary around a mean, and millennial-scale variations have a 1,500 year periodicity. Speleothem $\delta^{18}O$ values spike during the late Holocene dry interval (0.5 to 1.5 ka), suggesting that decreases in Pacific-derived moisture or decreased tropical storm activity might have been coincident with the prolonged dry interval.

Table 5.1. Drilling specifications for each track

Track	Step (mm)	width (mm)	depth (mm)	sample subset analyzed	sample numbers
1	0.1	2	0.5	1 of 3	900-969
2	0.15	2	0.5	1 of 3	800-859
3	1	0.5	0.2	1 of 1	690-674
4	1	0.5	0.2	1 of 1	645-689
5	1	0.5	0.2	1 of 1	600-644
6	0.16	0.5	0.5	1 of 3	284-553
7	0.16	0.5	0.5	1 of 3	200-284
Reconnaisance sampling	6*			1 of 1	100-137

*1 mm sampled every 6 mm

Table 5.2. Average and standard deviation of $\delta^{18}O$ and rainfall of measurements made during each season 1998-2012

Season	$\delta^{18}O$ average (‰)	$\delta^{18}O$ standard deviation (‰)	Seasonal rainfall average (cm)	Seasonal rainfall standard deviation (cm)
MAM	-3.0	1.2	6.8	4.5
JJA	-3.8	2.9	5.7	4.3
SON	**-4.8**	2.2	8.0	7.2
DJF	**-4.9**	1.7	6.3	4.2

Bold values indicate significant difference from spring season

Table 5.3. Rainfall $\delta^{18}O$ values measured from 1998-2011

Placement date	Retrieval date	Mid-point date	Mean temperature of sampling interval (°C)	Mean normalized monthly rainfall of sampling interval (cm)	Rainfall $\delta^{18}O$
03/03/99	04/02/99	03/18/99	16.6	10.5	-2.4
04/02/99	05/02/99	04/17/99	22.1	1.8	-2.9
05/02/99	06/05/99	05/19/99	25.1	16.7	-3.3
06/05/99	07/08/99	06/21/99	27.1	6.1	-3.3
07/08/99	08/04/99	07/21/99	27.6	13.0	-3.7
08/04/99	09/04/99	08/19/99	29.7	0.0	-3.6
10/01/99	11/05/99	10/18/99	19.0	3.4	-5.0
11/05/99	12/08/99	11/21/99	15.8	0.6	-1.5
12/08/99	01/07/00	12/23/99	10.9	1.6	-4.0
01/07/00	02/02/00	01/20/00	11.6	10.8	-3.8
02/02/00	03/03/00	02/17/00	16.7	0.1	-3.3
03/03/00	04/12/00	03/23/00	18.7	5.4	-4.1
05/01/00	06/12/00	05/22/00	25.7	3.0	-3.5
06/12/00	07/05/00	06/23/00	28.4	2.2	-2.4
07/05/00	08/08/00	07/22/00	29.5	1.3	-1.8
08/08/00	09/03/00	08/21/00	na	na	-6.2
09/03/00	10/01/00	09/17/00	26.2	2.0	-3.4
10/01/00	12/05/00	11/02/00	16.5	11.8	-4.6
12/05/00	02/08/01	01/06/01	7.6	6.6	-4.4
02/08/01	05/02/01	03/21/01	15.5	4.2	-3.8
05/02/01	08/01/01	06/16/01	26.6	6.3	-3.1
08/01/01	09/07/01	08/19/01	27.6	13.7	-7.3
09/07/01	10/12/01	09/24/01	22.7	7.6	-4.3
10/12/01	11/14/01	10/28/01	18.0	5.1	-3.2
11/14/01	12/11/01	11/27/01	14.6	24.6	-4.2
12/11/01	01/10/02	12/26/01	8.1	7.8	-4.0
01/10/02	02/07/02	01/24/02	11.6	3.3	-3.0
04/05/02	07/07/02	05/21/02	25.1	5.7	-1.1
07/07/02	11/04/02	09/05/02	25.1	10.8	-3.2
11/04/02	04/03/03	01/18/03	11.2	7.8	-5.8
04/03/03	05/13/03	04/23/03	22.2	1.0	-1.6
05/13/03	06/17/03	05/30/03	25.8	7.0	-4.9
06/17/03	08/11/03	07/14/03	28.0	4.2	-3.1
08/11/03	10/08/03	09/09/03	25.1	7.5	-6.2
10/08/03	01/09/04	11/23/03	15.4	1.8	-3.4
01/09/04	03/01/04	02/04/04	10.1	10.8	-4.6
04/16/04	06/24/04	05/20/04	24.2	9.8	-3.0
06/24/04	08/16/04	07/20/04	27.2	9.1	-4.3
08/16/04	10/01/04	09/08/04	26.5	3.0	-2.5
10/01/04	11/28/04	10/30/04	19.9	20.0	-4.5
11/28/04	01/25/05	12/27/04	11.3	1.4	-2.0
01/25/05	03/03/05	02/12/05	12.4	11.4	-6.3
03/03/05	03/27/05	03/15/05	15.2	5.0	-3.4
03/27/05	05/02/05	04/14/05	18.9	3.6	-1.7
05/02/05	06/02/05	05/17/05	24.1	9.0	-3.4
07/05/05	08/01/05	07/18/05	28.9	8.5	-2.7
03/20/06	05/10/06	04/14/06	21.8	14.8	-2.8
10/13/06	12/02/06	11/07/06	17.3	6.4	-3.8

Table 5.3. Rainfall $\delta^{18}O$ values measured from 1998-2011

Placement date	Retrieval date	Mid-point date	Mean temperature of sampling interval (°C)	Mean normalized monthly rainfall of sampling interval (cm)	Rainfall $\delta^{18}O$
02/28/07	04/20/07	03/25/07	16.6	13.0	-3.1
04/20/07	05/30/07	05/10/07	22.4	14.8	-2.8
05/30/07	06/20/07	06/09/07	26.9	11.7	-1.7
06/20/07	09/03/07	07/27/07	27.2	14.3	-3.8
09/03/07	10/08/07	09/20/07	26.0	1.8	-5.8
04/02/09	05/12/09	04/22/09	21.9	7.2	-2.5
05/12/09	06/11/09	05/27/09	24.8	4.3	-3.2
06/11/09	07/13/09	06/27/09	30.9	2.5	-2.3
07/13/09	08/02/09	07/23/09	31.1	4.8	1.0
08/02/09	09/11/09	08/22/09	29.8	8.0	-2.2
09/11/09	10/06/09	09/23/09	24.1	19.0	-6.2
10/06/09	11/07/09	10/22/09	18.6	14.3	-5.4
11/07/09	12/03/09	11/20/09	14.1	10.9	-8.4
12/03/09	01/15/10	12/24/09	6.6	4.1	-7.5
01/15/10	02/09/10	01/27/10	10.9	13.5	-8.0
02/09/10	03/05/10	02/21/10	7.9	4.5	-6.2
03/05/10	04/05/10	03/20/10	15.1	5.7	-4.1
04/05/10	05/09/10	04/22/10	20.3	3.2	-2.0
05/09/10	06/06/10	05/23/10	26.3	4.7	-6.5
06/06/10	06/30/10	06/18/10	29.3	11.0	-7.0
07/25/10	09/06/10	08/15/10	30.1	4.0	-2.8
09/17/10	10/12/10	09/29/10	22.3	2.0	-3.5
10/12/10	11/09/10	10/26/10	18.8	1.4	-2.8
11/09/10	02/01/11	12/21/10	11.3	4.4	-6.0
03/04/11	04/21/11	03/28/11	20.0	0.5	-1.2
04/21/11	05/13/11	05/02/11	23.9	6.1	-2.1
Intervals corresponding with tropical storms					
08/09/06	09/19/06	08/29/06	29.0		-12.6
09/06/10	09/07/10	09/06/10	26.1		-8.6
09/07/10	09/10/10	09/08/10	29.4		-10.5

Data from Pape et al., 2010 and Feng et al., 2012

Figure 5.1. A. Location of Edwards Plateau and Natural Bridge Caverns in Texas. B. Central Texas climatology illustrating monthly temperature and rainfall averages and rainfall standard deviations based on data collected from 1998-2012. There is strong seasonality in temperature. Greater rainfall tends to occur in the fall and spring, but inter-annual variability exceeds intra-annual variability. Data from National Weather Service (http://www.srh.noaa.gov/ewx/?n=austinbergstromclidata.htm). C. Location of Natural Bridge Caverns relative to location of other regional paleoclimate reconstructions. Base map from Google Earth.

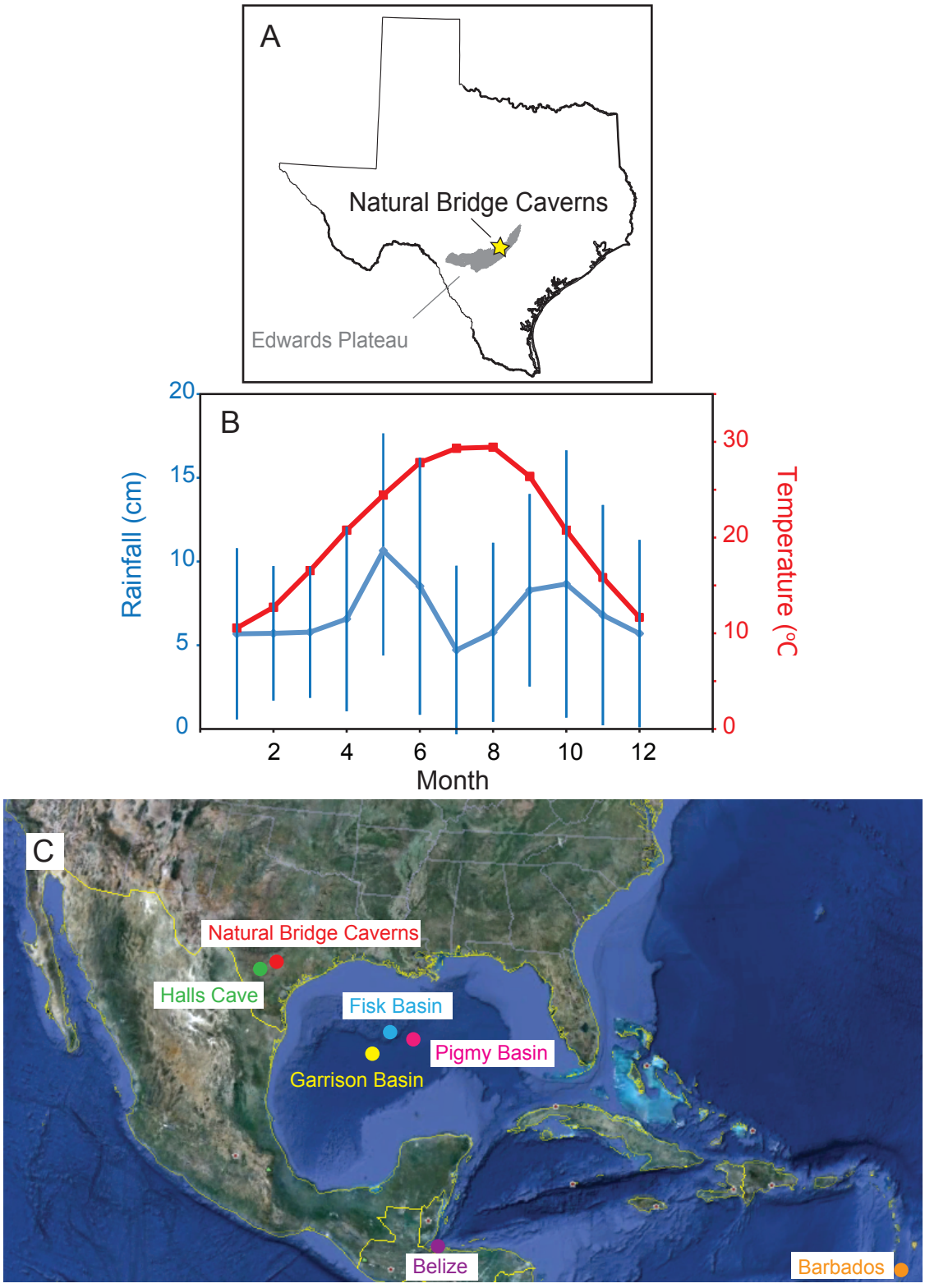
A
Natural Bridge Caverns
Edwards Plateau
B
Rainfall (cm)
Temperature (°C)
Month
0
5
10
15
20
0
10
20
30
2
4
6
8
10
12
C
Natural Bridge Caverns
Halls Cave
Fisk Basin
Pigmy Basin
Garrison Basin
Belize
Barbados

Figure 5.1

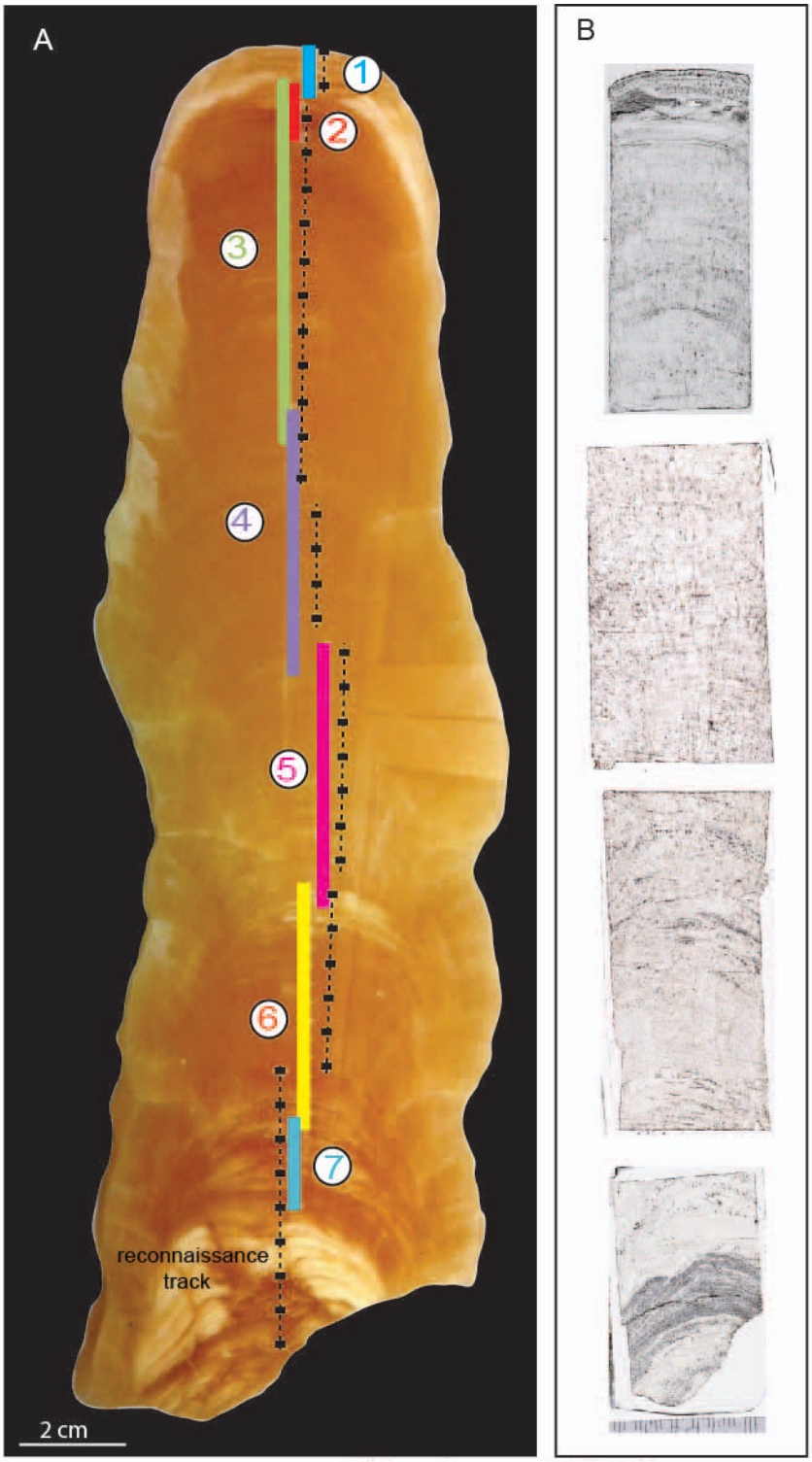

Figure 5.2. A. Samples for speleothem $\delta^{18}O$ analyses was drilled from a reconnassance track and 7 overlapping tracks. See Table 1 for sampling details of each track. B. Thick sections made from the opposing slab.

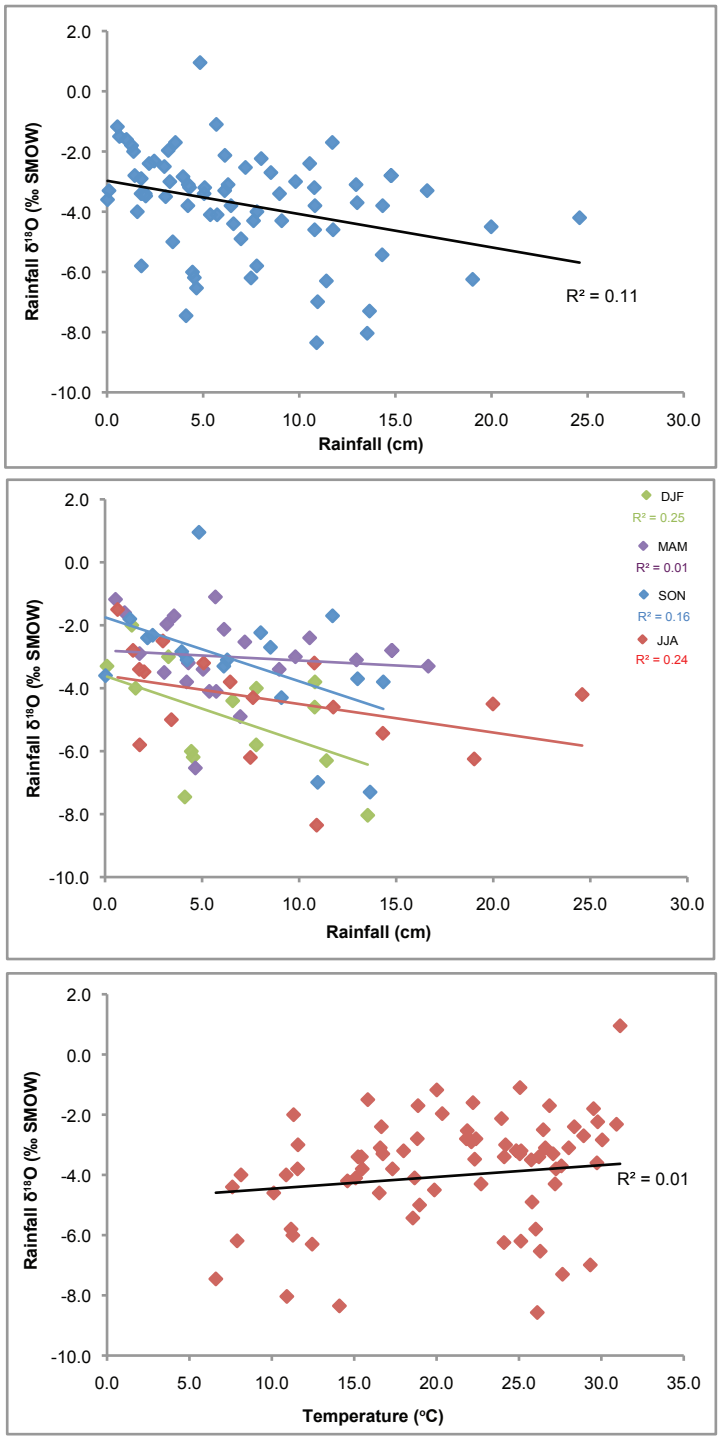

Figure 5.3. Correlations between rainfall $\delta^{18}O$ and rainfall amount for all samples (top) and by season (middle) and rainfall $\delta^{18}O$ and temperature (bottom) for all samples. Data from this study, Feng et al. (2012) and Pape et al. (2010).

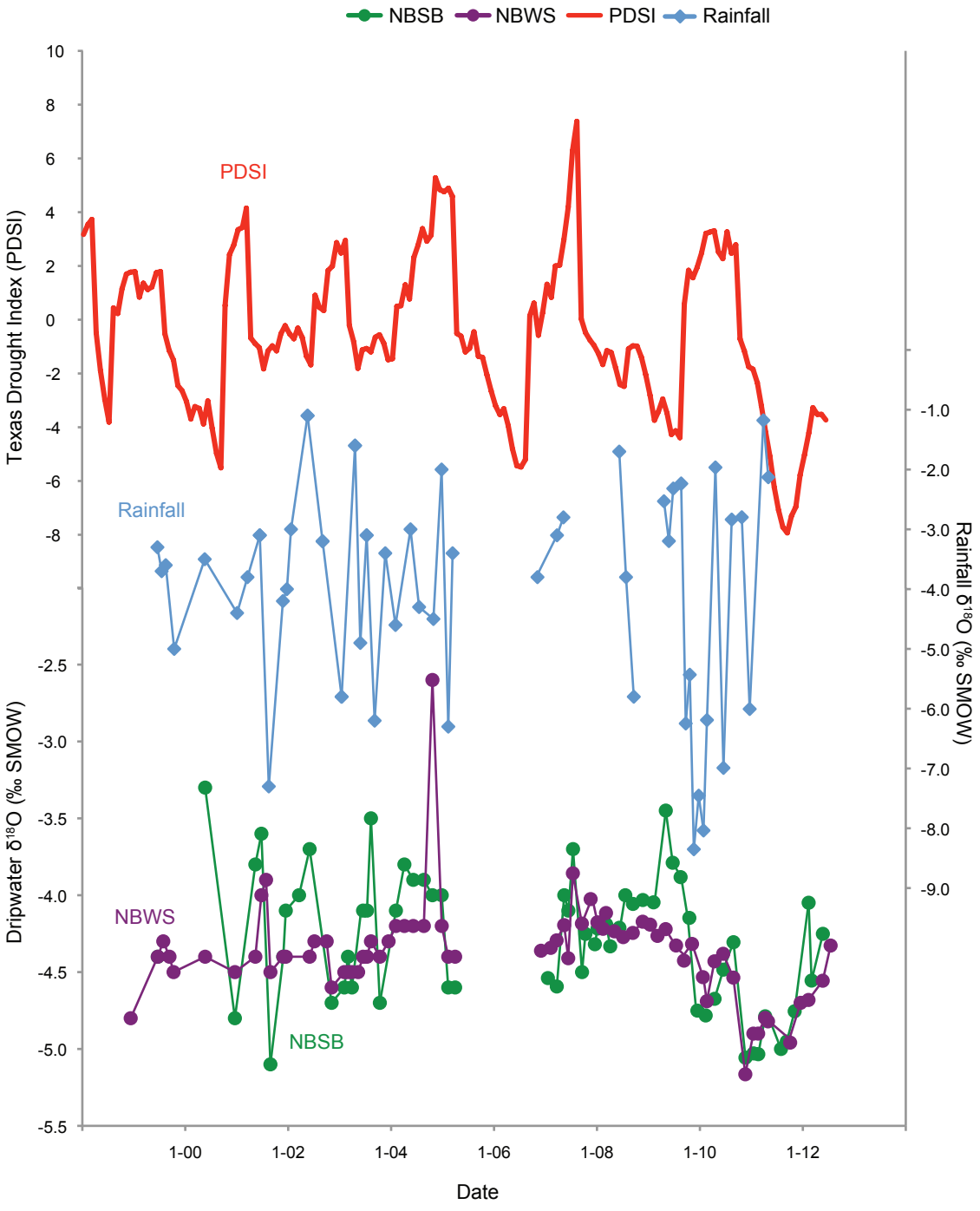

Figure 5.4. Timeseries of PDSI and rainfall and dripwater $\delta^{18}O$

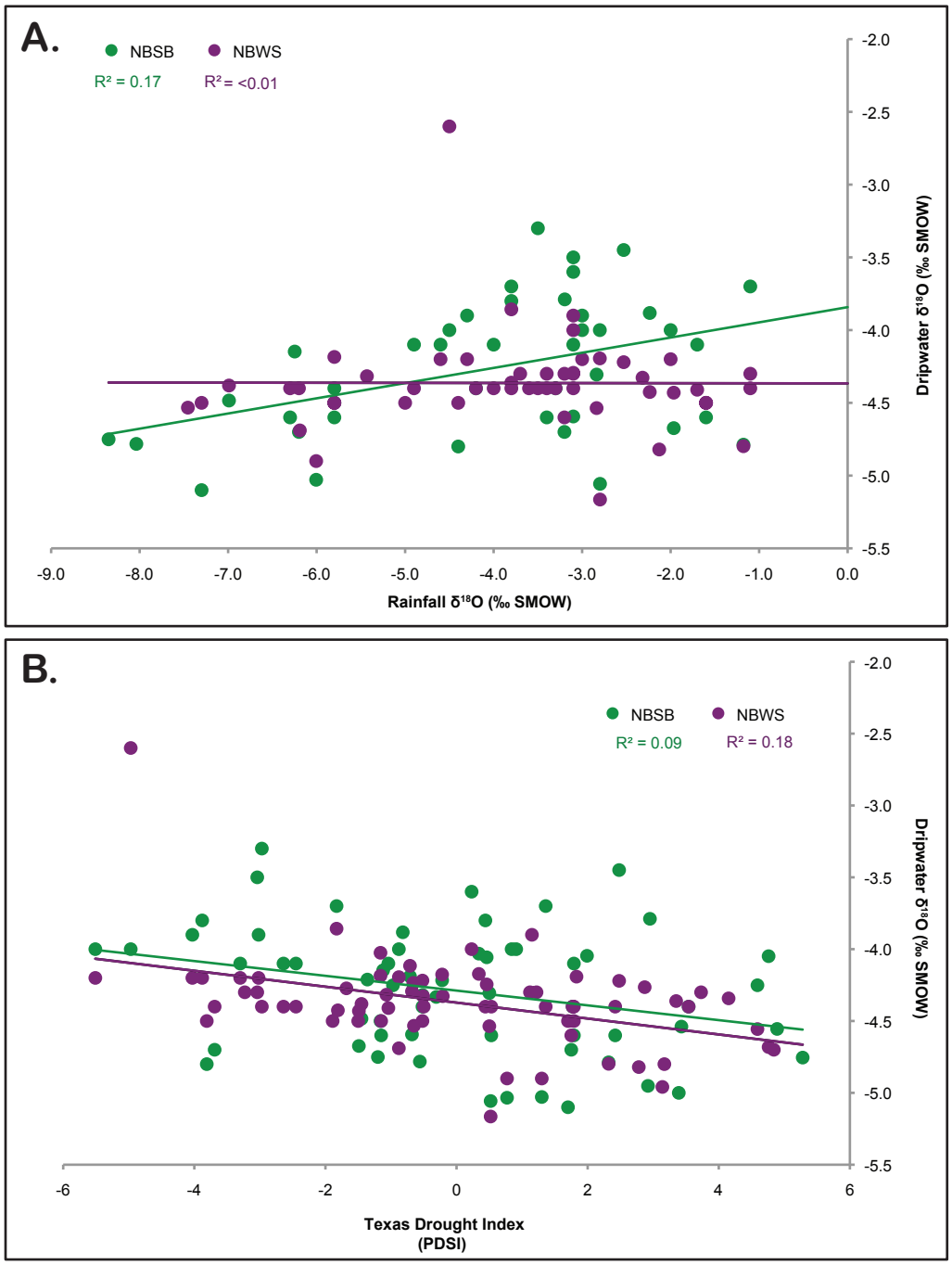

Figure 5.5. A. Bivariate plot of rainfall and dripwater $\delta^{18}O$. Dripwater $\delta^{18}O$ at NBSB has a stronger correlation with rainfall than at NBWS, but correlations at both sites are weak. B. Bivariate plot of PDSI and dripwater $\delta^{18}O$. Neither site has a strong correlation between PDSI and dripwater $\delta^{18}O$.

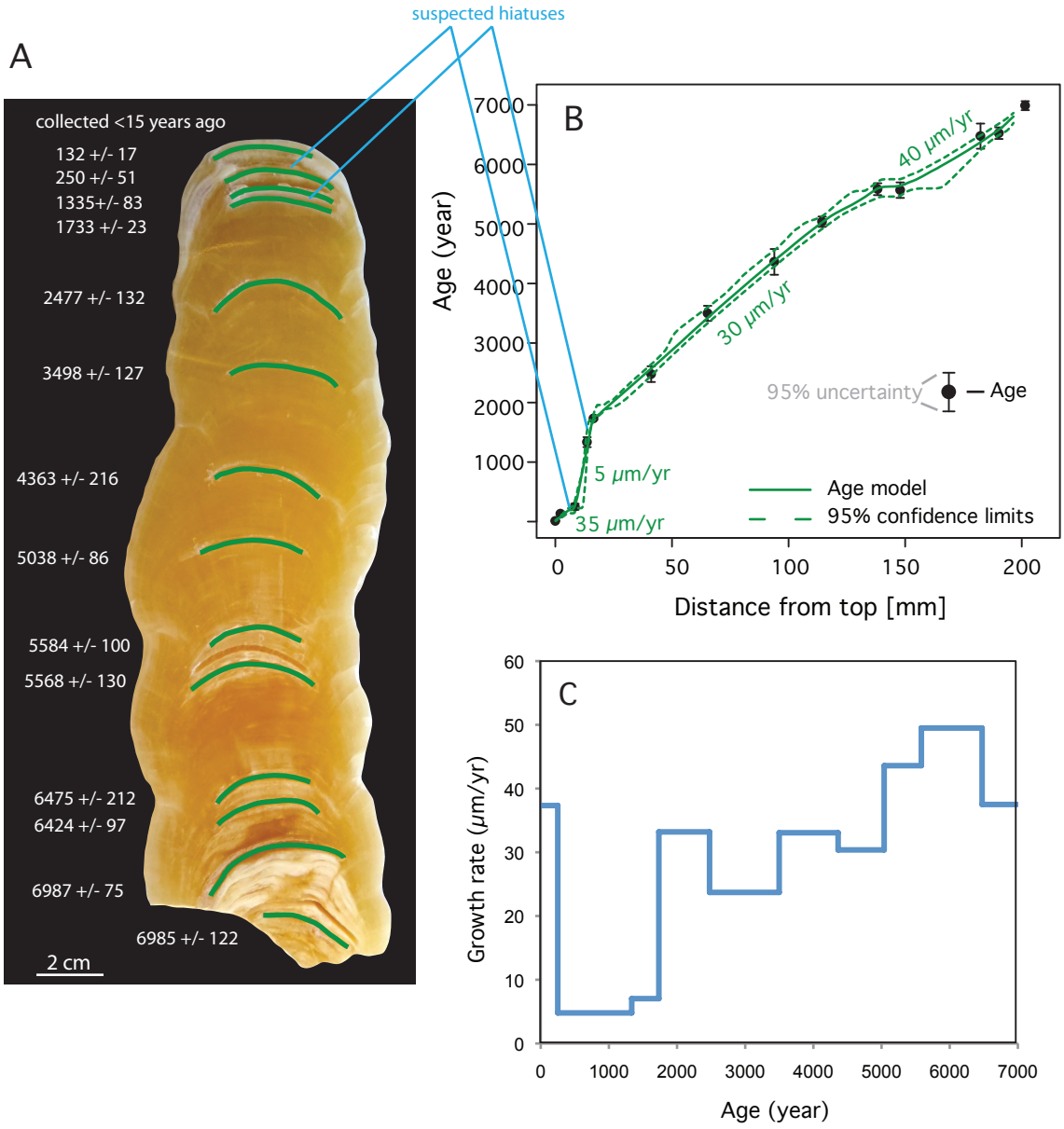

Figure 5.6. A. Location and age of growth horizons on which the age model was calculated. B. Depth-age model and 95% uncertainties based on U series dating calculated using StalAge algorithm by Scholtz and Hoffman (2011) along with approximate growth rates. C. Time series of speleothem growth rate.

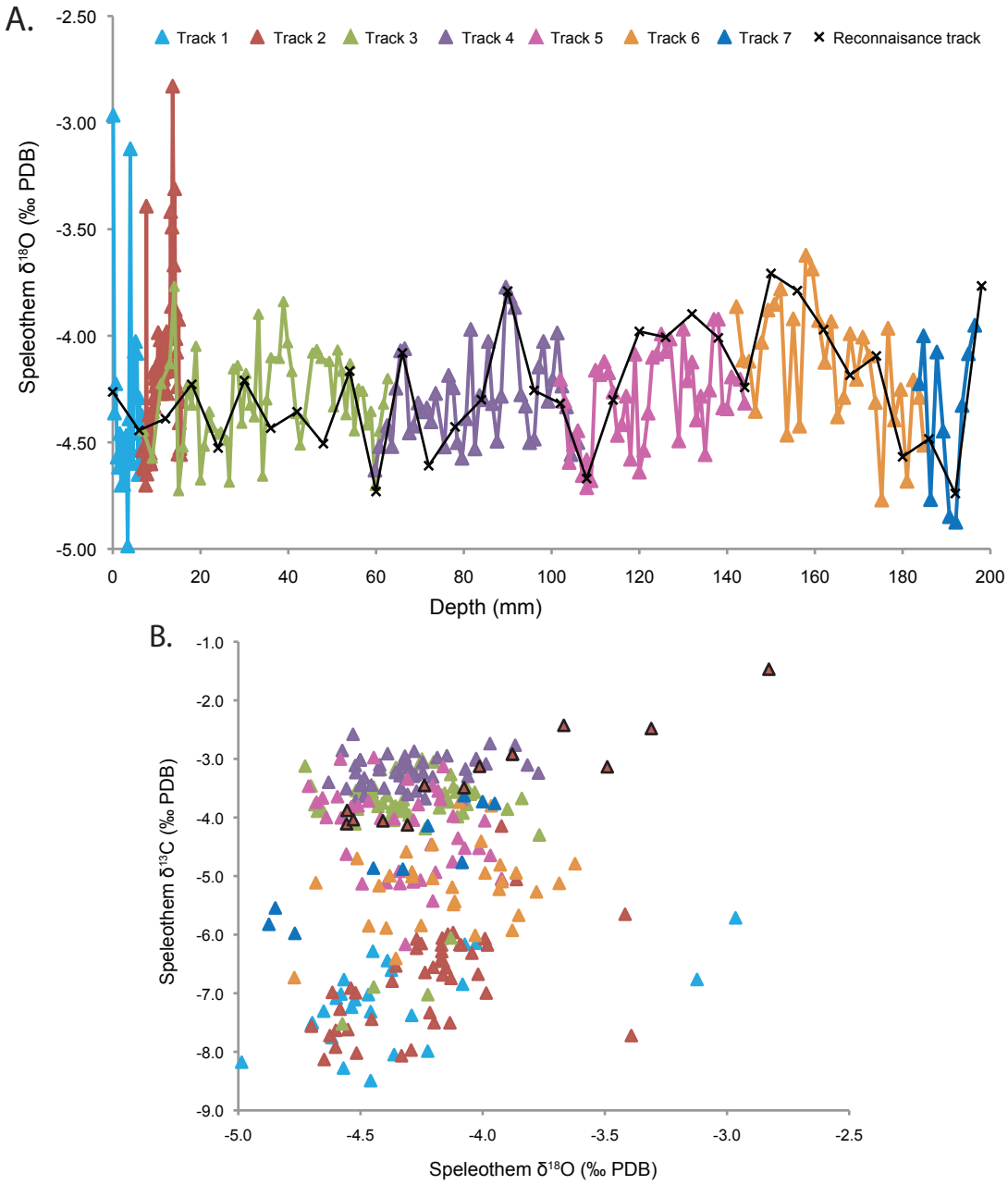

Figure 5.7. A. Overlapping transects of raw speleothem $\delta^{18}O$. See Fig. 5.2 and Table 5.1 for track locations and sampling details, respectively. The lack of offset in $\delta^{18}O$ values between laterally spaced tracks suggests that speleothem growth occurred under equilibrium conditions. B. Bivariate plot of speleothem $\delta^{18}O$ and $\delta^{13}C$ values. Sample from track 2 outlined in black represent the only part of the sample in which $\delta^{18}O$ and $\delta^{13}C$ values are strongly correlated. The overall lack of correspondence between speleothem $\delta^{18}O$ and $\delta^{13}C$ values, as shown in both A and B, also indicates that speleothem growth occurred under equilibrium conditions.

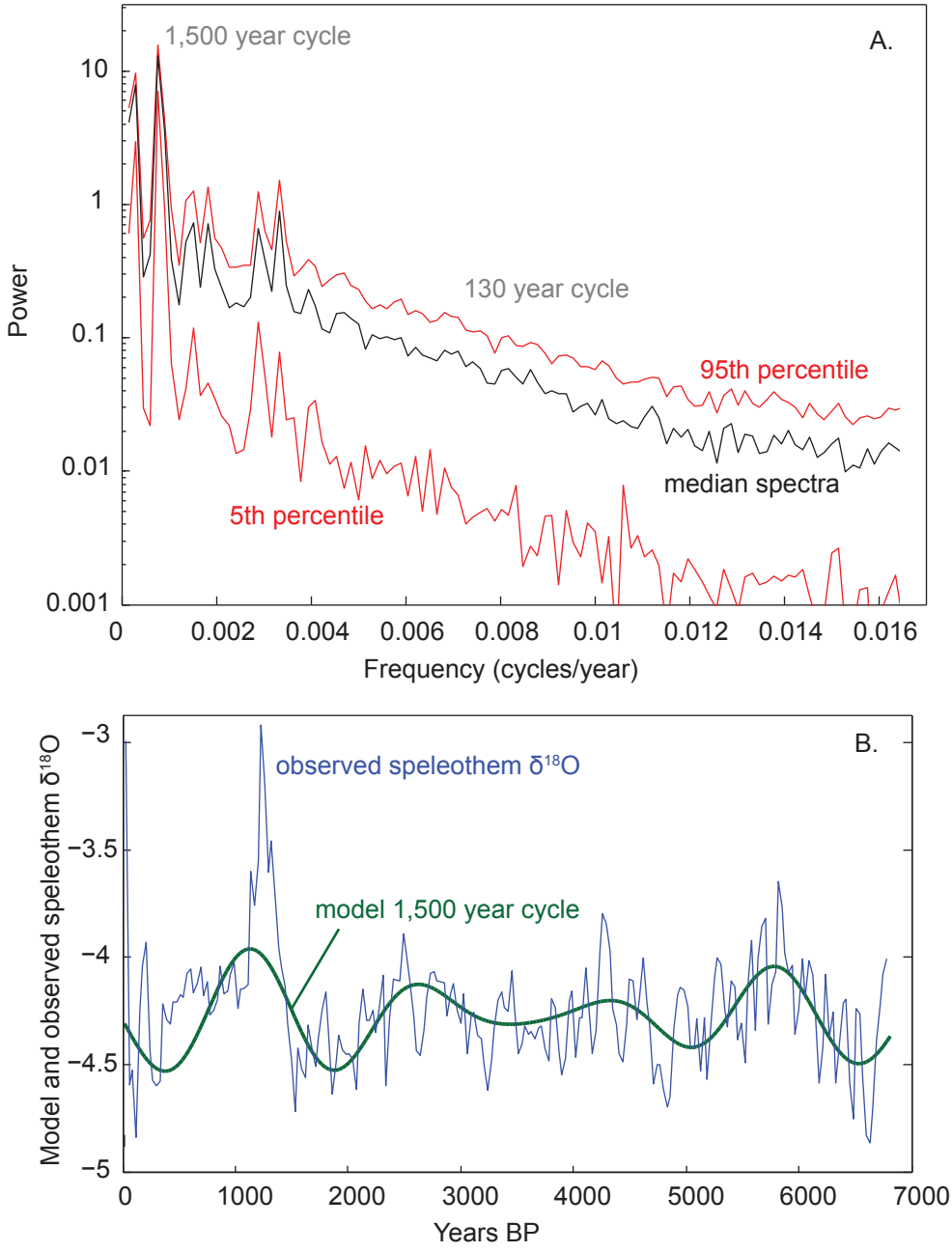

Figure 5.8. A) Spectral analysis results of the median, 5th and 95th percentile values for spectra computed for speleothem $\delta^{18}O$ time series based on 1,000 realizations of the age model. B) Observed and modeled speleothem $\delta^{18}O$ values. Model values represent 1,500 year cycle.

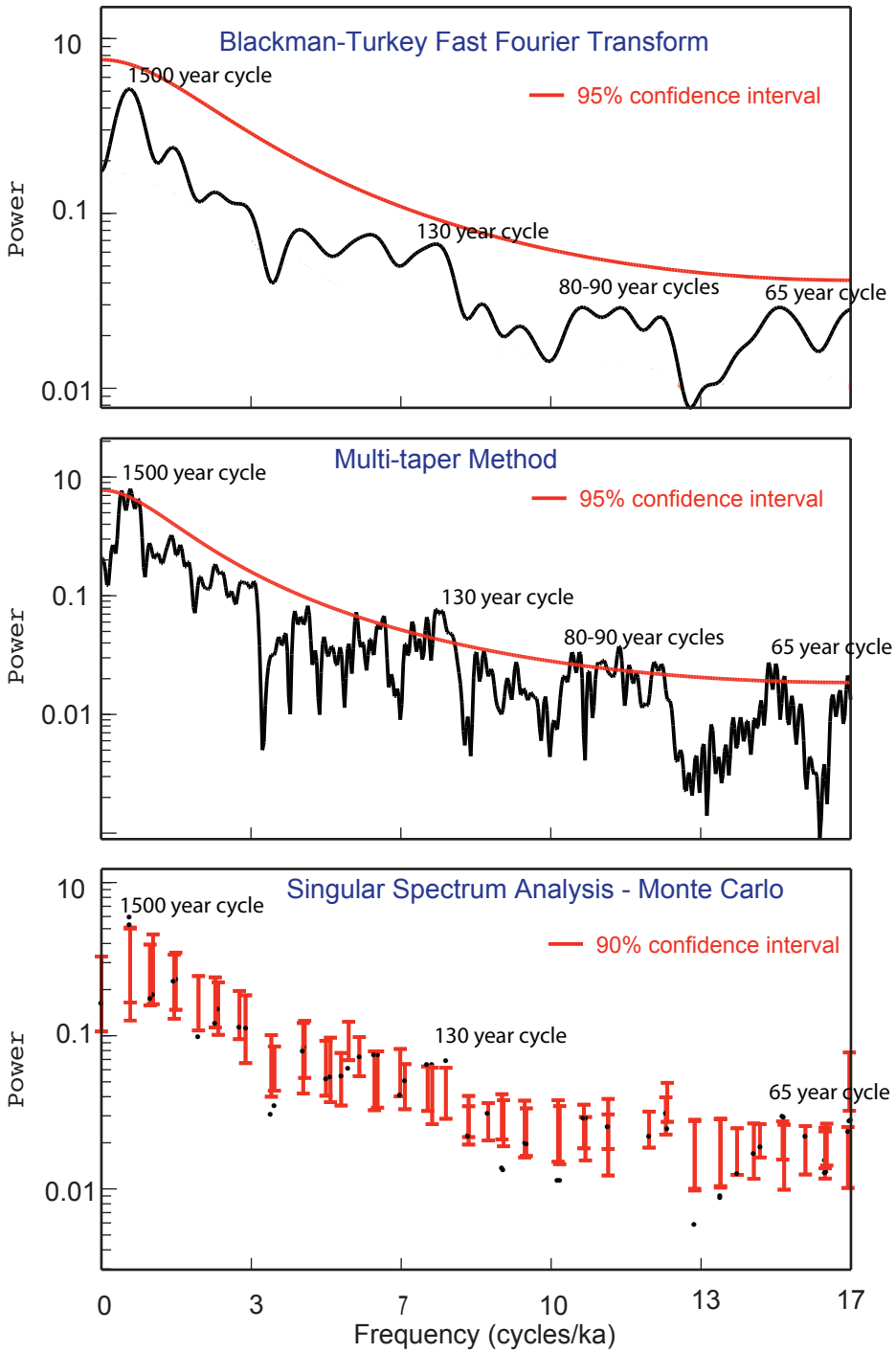

Figure 5.9. Spectral analyses on the entire speleothem $\delta^{18}O$ timeseries (30-year resolution) using multiple techniques. Confidence intervals are relative to red noise background. Peaks identified in each method are labeled in black as years/cycle. Analyses conducted using Kspectra version 3.3.

Figure 5.10. Late Holocene timeseries for NBS1 speleothem growth rate and $\delta^{18}O$ compared to magnetic susceptibility (Ellwood and Gose, 2006) and cave fauna (Toomey et al., 1993) in Halls Cave (central Texas) sediments, and $\delta^{18}O$ and $^{87}Sr/^{86}Sr$ values for speleothems from Belize (Kennett et al., 2012) and Barbados (Banner et al., 1996), respectively. Slow Texas speleothem growth broadly corresponds with dry intervals delineated in other reconstructions from the region during ~0.5-1.5ka.

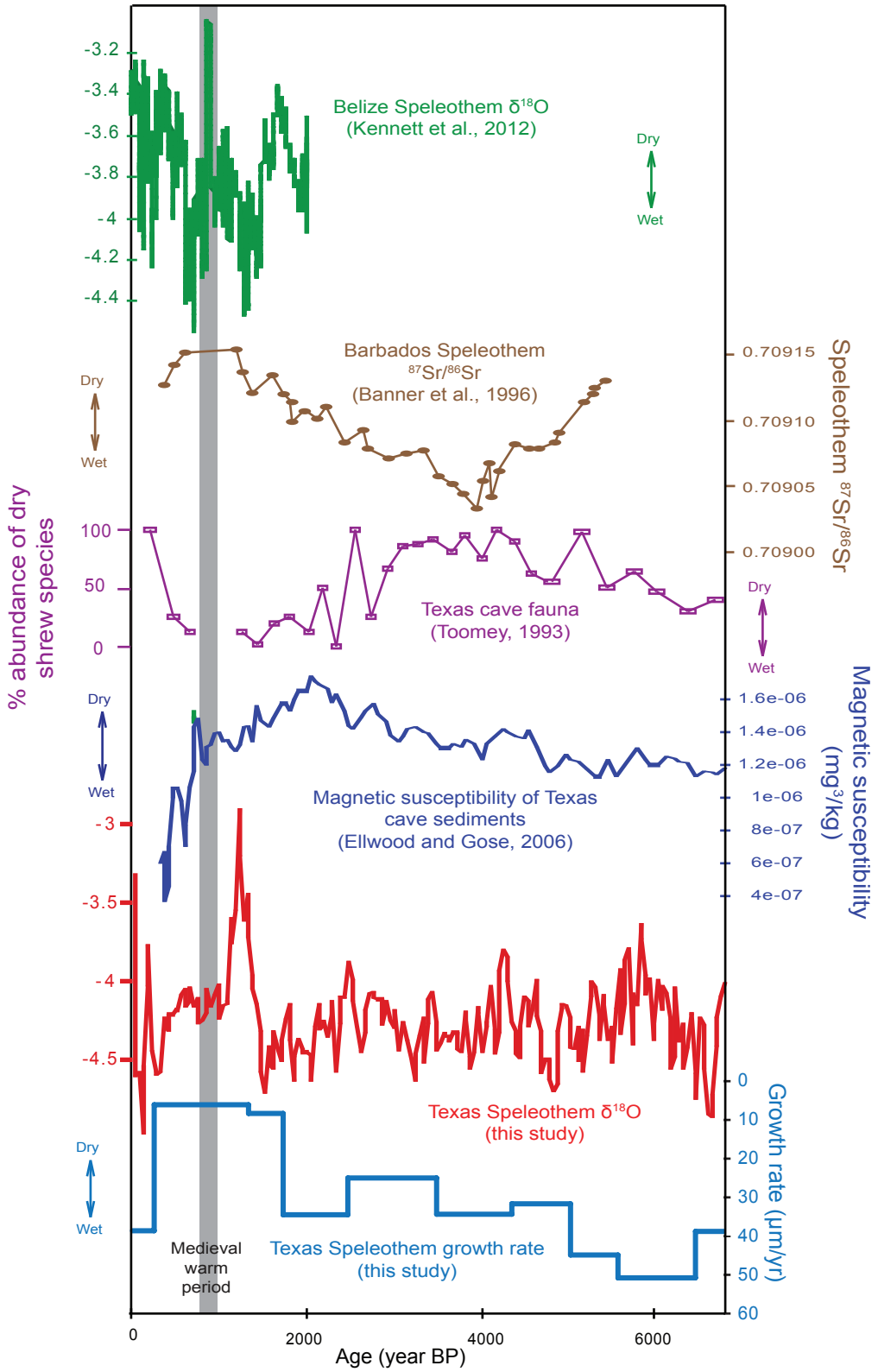
Belize Speleothem δ18O
(Kennett et al., 2012)
Dry
Wet
-3.2
-3.4
-3.6
-3.8
-4
-4.2
-4.4
Barbados Speleothem
87Sr/86Sr
(Banner et al., 1996)
0.70915
0.70910
0.70905
0.70900
Speleothem 87Sr/86Sr
% abundance of dry shrew species
100
50
0
Texas cave fauna
(Toomey, 1993)
Magnetic susceptibility of Texas
cave sediments
(Ellwood and Gose, 2006)
1.6e-06
1.4e-06
1.2e-06
1e-06
8e-07
6e-07
4e-07
Magnetic susceptibility
(mg3/kg)
-3
-3.5
-4
-4.5
Texas Speleothem δ18O
(this study)
0
10
20
30
40
50
60
Growth rate (μm/yr)
Medieval
warm
period
Texas Speleothem growth rate
(this study)
0
2000
4000
6000
Age (year BP)

Figure 5.10

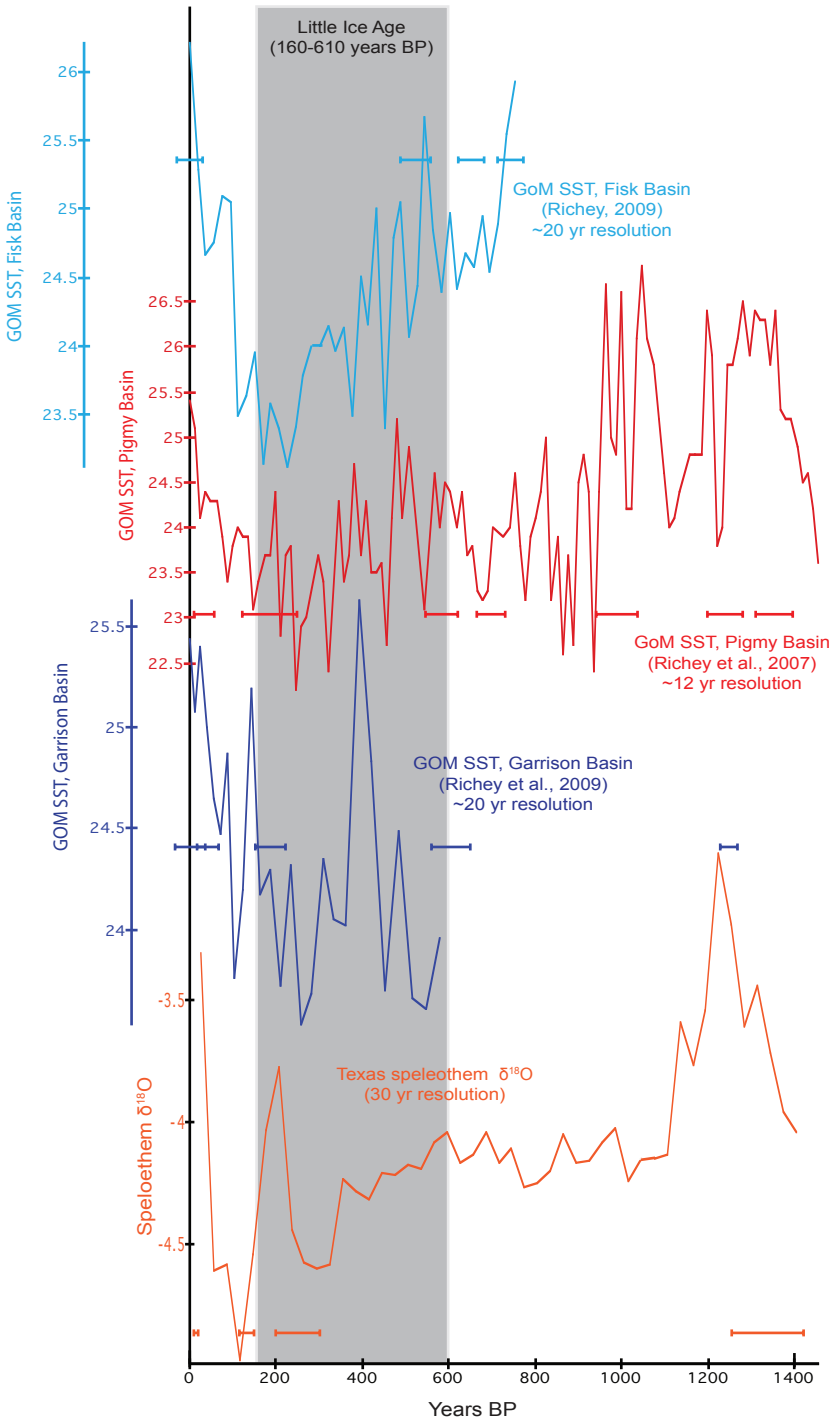

Figure 5.11. Timeseries of GoM SSTs and speleothem $\delta^{18}O$ demonstrating overall correspondence on cennenital timescales. Age control shown as bars.

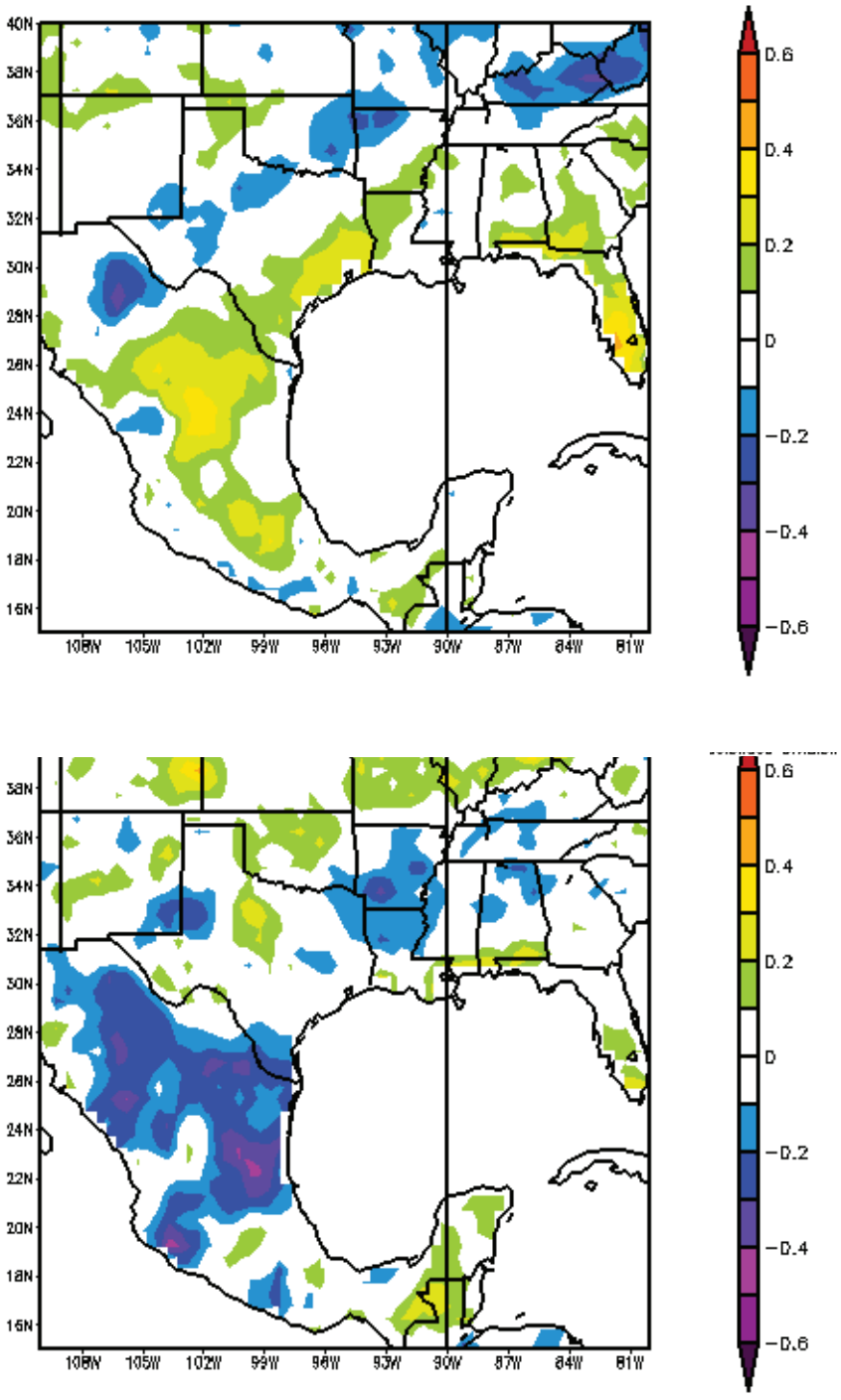

Figure 5.12. Correlation (r) between fall/winter (top) and spring/summer rainfall (U of Delaware Precipitation reanalysis) and Carribean Index SST composites from 1951 to 2008. Data from NCAA/ESRL Physical Science Division (http://www.esrl.noaa.gov/psd/data/correlation/).

Chapter 6. Conclusions

The research presented in this dissertation improves the understanding of the baseline state of the Edwards aquifer, and has implications for managing water resources and addressing how future climate change will affect water resources in this aquifer system. The conceptual understanding of the extent of communication between conduit and diffuse portions of the aquifer and how recharging water flows through the aquifer under varying antecedent moisture conditions has been refined (Chap. 2). These results suggest that communication between conduit and matrix portions of the aquifer is likely spatially limited to areas immediately surrounding conduits. This indicates that the majority of water recharging the aquifer system enters and drains the conduit network on time-scales (years) in response to the fluctuation of climate between wet and dry conditions. Investigation of the long-term (decades) response of the aquifer to climate variability will necessitate the characterization of and delineation of the controls on the variation within the matrix part of the aquifer.

Results from this research suggest that groundwater does not buffer recharging stream water geochemistry (Chap. 2), meaning that groundwater quality directly reflects stream water quality. Stream water quality, however, is degrading over time, likely due to the increase of urbanization in stream watersheds (Chap. 3). The combination of these two results indicate that the future quality of groundwater will be heavily dependent on urbanization rates and watershed management practices. To protect current and future quality of groundwater and the water discharging at Barton Springs, there should be strict regulations on, and monitoring of, the quality of treated septic and wastewater effluent that is discharged directly to or applied in the watersheds of streams that recharge the aquifer. Furthermore, wastewater treatments should involve a reverse osmosis procedure

to reduce concentrations of total dissolved solids entering the contributing and recharge zones of the Edwards aquifer.

This research has refined the conceptual model of the relationship between litho- and hydro-straitigraphic units, and demonstrated that vertical exchange of groundwater between the Edwards and underlying Trinity aquifer is likely inhibited by intermediate units acting as aquitards (Chap. 4). This suggests that groundwater pumping of the Trinity aquifer, under current conditions, will not affect groundwater flow in the Edwards aquifer. The implication of this result is that, under current pumping conditions, the Edwards and Trinity aquifers can be managed independently. The potential for groundwater flow between the Edwards and Trinity aquifer, however, should be monitored and continuously assessed as pumping of the Trinity aquifer increases and climate conditions change.

Reconstruction of mid to late Holocene climate indicate that the amount and source of rainfall varied little from 0 to 7 ka, except for a prolonged dry period from 0.5 to 1.5 ka (Chap 5). The relative consistency of speleothem growth rate and cyclical variations of speleothem $\delta^{18}O$ values around a mean value indicate that climate dynamics governing rainfall in central Texas were stable from the mid to late Holocene. Anomalously high speleothem values during the late Holocene dry period suggests that moisture transport from the Pacific to central Texas was coincident with the dry interval. These results provide the characterization of the variability of moisture conditions on millennial time scales, and indicate that climate processes governing moisture transport from the Pacific to the Texas region might be related to the occurrence of prolonged dryness.

This research integrates the results from several very distinct approaches to enhance understanding of different components of the Edwards aquifer system. In

Chapter 1, geochemical modeling is used to quantify the timing and magnitude of surface and groundwater mixing to delineate how antecedent moisture conditions affect the responsiveness of the Edwards aquifer to changing climate conditions. As Chapter 1 demonstrated that recharging surface water can substantially affect groundwater compositions under dry and wet antecedent moisture conditions, geochemical modeling and mass balance approaches are used in Chapter 2 to identify the source of stream water constituents. Chapter 3 integrates geochemical data from traditional and multiport well sampling approaches to identify the controls on groundwater geochemistry of the Edwards and Trinity aquifer. These results combined with an analysis of temporal and spatial variations in potentiometric surface levels are used to demonstrate that, under current pumping and hydrologic conditions, there is little potential for vertical interflow between the Edwards and Trinity aquifers. As the Edwards aquifer is hydrologically and geochemically responsive to changing climate conditions, Chapter 4 investigates the climate processes that control temporal variations in rainfall by reconstructing Holocene climate in central Texas from a speleothem. Each approach is similar in that physical (e.g., spring and stream discharge, potentiometric surface levels, speleothem growth rates) and geochemical data (e.g., spring water, stream water, groundwater, and drip water major ion concentrations and isotopic compositions, speleothem isotopic compositions) are used to characterize and account for the variability of an aspect of the Edwards aquifer in space and time.

The combined results of the research presented in this dissertation have provided an improved characterization of the controls on hydrologic variability and water quality within the Edwards aquifer. For example, this research has demonstrated that the Edwards aquifer has linear and non-linear modes of recharge (i.e., a mode with limited storage and a mode with enhanced storage) (Chap. 2). Furthermore, this research has

provided a revised conceptual model of groundwater vulnerability to surface water recharge (Chaps 2 and 3) as well as redefined the relationship between litho- and hydrostratigraphic units of the Edwards and Trinity aquifer (Chap 4). With regard to the former, i) groundwater dominantly reflects surface water compositions not only during storm conditions, but under non-storm flow conditions during wet conditions as well (Chap. 2), and ii) surface water compositions are indirectly controlled by anthropogenic sources (Chap. 3). With regard to the latter, the Edwards aquifer is consistent with lithostratigraphic units of the Edwards group and the upper part of the Upper Glen Rose Formation. Lower permeability units within the rest of the Upper Glen Rose Formation and upper parts of the Lower Glen Rose Formation act as a barrier to vertical interflow between the Edwards and Middle Trinity aquifers. Finally, this research has found that central Texas moisture conditions have varied little over the past 7,000 years, except for a dry interval from 500 to 1,500 years ago (Chap. 5). With the exception of this dry interval, it is likely that central Texas hydrological conditions have been generally consistent, on the millennial scale, since the mid-Holocene.

Collectively, this research improves our understanding of the Edwards aquifer system. Existing conceptual models of the aquifer have been revised, including how recharge moves through the aquifer, the nature of interaction between conduit and diffuse parts of the aquifer, the link between the urban environment and degraded stream water quality, and the controls on groundwater on spatial and temporal scales. The response of natural and anthropogenic controls on surface and groundwater quality to changing climate conditions has been described, and the nature of millennial-scale climate variability has been characterized and used to gain insight into the climate processes governing rainfall.

Appendix Table 1. Stream water geochemical concentrations (mg/L)

Date	Discharge (ft^3/s)	Specific conductance (µS/cm)	pH	Alkalinity	Ca	Mg	Sr	Na	K	Cl	SO_4	F	Br	Si	B	NO_2	NO_3+NO_2	NO_3 (calculated)
Barton Creek																		
11/26/12	1.3	713	7.6	223	85	21	0.30	34	2.6	56	62		0.21	10.2	0.11	0.001	0.03	0.02
12/18/12	1.2	736	7.76	221	90	23	0.33	38	2.5	58	71		0.26	10.0	0.10	0.001	0.04	0.04
01/08/13	2.1	713	7.61	207	87	23	0.33	32	2.5	55	74		0.17	8.0	0.09	0.002	0.16	0.15
01/29/13	2.1	713	7.79	209	89	23	0.31	33	2.3	55	74		0.22	7.3	0.09	0.002	0.07	0.07
02/19/13	4.5	683	7.98	199	82	21	0.33	36	2.3	55	73		0.14	6.9	0.09	0.003	0.10	0.10
03/11/13	2.1	715	7.69	193	81	21	0.33	35	2.6	59	72		0.17	9.4	0.11	0.008	0.18	0.17
04/02/13	3.3	703	7.87	204	80	21	0.34	36	2.5	58	73		0.16	8.7	0.10	0.006	0.21	0.20
04/23/13	5	663	7.81	188	74	20	0.30	31	2.3	54	63		0.16	9.4	0.12	0.003	0.10	0.10
05/14/13	2.1	692	7.65	194	76	20	0.30	33	2.4	59	64		0.20	11.4	0.13	0.006	0.09	0.09
06/03/13	2.1	692	7.7	193	76	20	0.30	33	2.7	60	61		0.22	11.6	0.15	0.004	0.07	0.06
06/25/13	0.78	687	7.64	195	74	20	0.31	34	2.7	58	56		0.23	13.9	0.15	0.001	0.03	0.03
07/16/13	0.15	710	7.76	203	72	19	0.32	36	2.8	63	52		0.39	14.2	0.14	0.001	0.01	0.01
08/06/13	0.05	725	7.72	208	74	21	0.32	41	3.2	69	46		0.40	17.2	0.19	0.000	0.03	0.03
09/24/13	22.0	604	7.5	160	66	17	0.30	29	3.0	51	66	0.17	0.22	11.1	0.13	0.004	0.24	0.23
10/10/13	81.9	622	7.69	177	73	19	0.27	24	2.7	42	69	0.17	0.15	9.7	0.12	0.003	0.34	0.34
10/15/13	172	714	7.8	195	90	21	0.29	28	2.5	53	88	0.17	0.15	8.8	0.10	0.002	0.41	0.41
10/23/13	408.0	616	8.04	185	77	18	0.25	22	2.6	39	66	0.15	0.12	9.0	0.09	0.003	0.41	0.41
11/05/13	101	717	7.99	235	91	22	0.30	26	2.3	48	70	0.18	0.17	9.2	0.08	0.005	0.87	0.87
11/10/13	252.5	683	8.14	216	90	21	0.29	23	2.0	47	71	0.16	0.16	8.3	0.08	0.002	0.84	0.84
11/10/13	370.6	665	8.12	214	87	20	0.27	22	2.1	45	70	0.17	0.14	8.5	0.08	0.003	0.69	0.69
11/21/13	533.0	606	8.07	201	75	17	0.23	19	2.2	34	54	0.17	0.10	8.3	0.07	0.003	0.48	0.48
12/03/13	276	676	8.2	236	91	22	0.29	23	2.0	41	64	0.19	0.13	9.1	0.07	0.002	0.71	0.71
01/06/14	59	707	8.18	171	84	22	0.29	22	1.4	49	72	0.18	0.16	6.8	0.07	0.002	0.58	0.58
01/16/14	216	652	7.72	216	82	20	0.29	22	1.7	43	64	0.20	0.14	6.0	0.07	0.003	0.84	0.83
01/17/14	365	659	8.06	208	82	19	0.27	21	1.9	40	63	0.20	0.13	6.9	0.06	0.003	0.67	0.66
02/03/14	205	693	8.21	247	90	21	0.28	20	1.4	39	64	0.17	0.12	7.9	0.07	0.002	0.73	0.72
03/03/14	166	658	8.09	234	82	21	0.28	21	1.5	39	64	0.19	0.13	7.1	0.06	0.003	0.64	0.63
Onion Creek																		
10/15/13	8.1	729	7.67	238	120	21	0.43	11	1.9	21	119	0.19	0.09	10.5	0.07	0.010	1.00	0.99
10/27/13	246.6	444	7.74	168	69	13	0.27	8	2.6	16	45	0.13	0.06	9.3	0.05	0.007	0.89	0.88
11/05/13	19	666	7.59	243	101	19	0.41	12	1.7	27	66	0.19	0.12	9.5	0.06	0.010	2.02	2.01
11/09/13	49.8	637	7.99	229	101	18	0.40	11	1.7	26	65	0.19	0.12	9.0	0.06	0.007	1.31	1.30
11/10/13	65.0	651	8.01	234	101	19	0.44	13	1.7	29	69	0.21	0.12	9.2	0.06	0.007	1.46	1.45
11/21/13	161.0	631	7.98	191	86	19	0.35	13	2.0	28	69	0.20	0.11	7.4	0.06	0.004	0.86	0.85
12/03/13	108	607	8.02	222	88	19	0.38	12	1.7	26	62	0.20	0.12	8.9	0.06	0.003	1.26	1.26
01/06/14	44	618	8.04	229	87	19	0.38	12	1.3	29	60	0.19	0.13	7.3	0.05	0.002	1.13	1.13
01/15/14	141.8	522	7.97	191	72	15	0.30	9	1.3	22	45	0.16	0.09	6.7	0.04	0.003	0.87	0.86
01/17/14	398.7	479	7.83	187	68	13	0.21	8	1.8	18	36	0.15	0.08	7.9	0.04	0.003	0.91	0.91
02/03/14	218	576	8.07	232	85	16	0.24	9	1.2	20	38	0.17	0.09	7.9	0.04	0.002	1.30	1.30
03/03/14	177	552	8.16	227	79	16	0.26	9	1.1	21	38	0.20	0.10	7.0	0.04	0.003	1.24	1.24
Bear Creek																		
02/19/13	0.09	924	7.35	195	118	29	0.38	30	2.2	60	208		0.27	7.7	0.08	0.000	0.01	0.01
03/14/13	0.69	729	7.85	163	89	23	0.30	23	1.7	53	128		0.22	7.4	0.07	0.000	0.03	0.03
04/02/13	0.3	742	7.71	208	94	23	0.34	26	1.5	54	139		0.30	7.3	0.09	0.000	< 0.016	< 0.016
04/23/13	0.3	735	7.47	170	89	24	0.31	23	1.4	54	126		0.24	7.2	0.11	0.000	< 0.016	< 0.016

Appendix Table 1. Stream water geochemical concentrations (mg/L)

Date	Discharge (ft^3/s)	Specific conductance (µS/cm)	pH	Alkalinity	Ca	Mg	Sr	Na	K	Cl	SO_4	F	Br	Si	B	NO_2	NO_3+NO_2	NO_3 (calculated)
05/14/13	0.43	710	7.46	175	86	22	0.33	22	1.4	53	103		0.24	8.4	0.11	0.000	< 0.016	< 0.016
09/13/13	67.9	216	7.66	61	24	5	0.07	6	3.9	15	25	0.09	0.05	6.4	0.04	0.014	1.14	1.13
09/13/13	30.4	310	6.74	47	38	7	0.13	7	4.5	16	51	0.09	0.04	6.5	0.05	0.022	1.73	1.71
09/23/13	36.7	477	7.86	129	62	13	0.26	11	3.1	25	68	0.17	0.11	8.8	0.08	0.011	0.23	0.22
09/30/13	147.3	339	8.27	109	48	9	0.14	7	3.1	19	31	0.14	0.06	7.9	0.05	0.011	0.47	0.46
10/10/13	25.1	578	7.8	194	80	16	0.22	14	2.7	35	51	0.16	0.15	9.9	0.07	0.009	0.67	0.66
10/15/13	9.8	747	7.81	242	109	21	0.28	19	2.1	48	72	0.21	0.20	9.1	0.08	0.009	1.25	1.24
10/23/13	15.0	726	8.02	231	101	20	0.28	19	2.0	47	68	0.19	0.21	8.8	0.08	0.006	0.96	0.96
11/05/13	9.8	776	7.85	266	112	22	0.31	20	1.8	46	80	0.17	0.21	8.8	0.08	0.007	1.72	1.72
11/09/13	22.4	732	7.85	242	104	20	0.27	18	1.7	42	75	0.21	0.21	8.5	0.07	0.007	1.37	1.36
11/09/13	24.9	718	8.03	250	107	20	0.26	19	1.7	43	67	0.17	0.21	8.3	0.07	0.006	1.39	1.39
12/03/13	16	695	8.08	243	98	21	0.26	17	1.6	39	63	0.19	0.19	8.9	0.07	0.004	1.25	1.25
01/06/14	7.5	740	8.06	273	101	22	0.28	18	1.2	46	75	0.18	0.22	7.9	0.07	0.003	1.36	1.36
01/16/14	70.3	542	7.55	185	73	14	0.18	12	2.5	29	43	0.17	0.14	8.9	0.05	0.004	0.84	0.84
01/16/14	63.0	474	7.57	174	64	12	0.16	10	2.4	21	35	0.17	0.10	7.9	0.04	0.005	0.66	0.66
02/03/14	24	725	8.12	271	99	19	0.25	16	1.2	35	63	0.17	0.17	7.7	0.06	0.003	1.47	1.47
03/03/14	15	670	8.07	248	92	19	0.26	16	1.2	33	59	0.22	0.17	6.6	0.05	0.006	1.33	1.32
Slaughter Creek																		
10/15/13	5.9	812	7.85	249	115	25	0.29	22	2.0	44	111	0.22	0.19	9.7	0.10	0.008	1.19	1.18
10/23/13	21.3	796	7.91	233	108	25	0.29	24	2.3	44	113	0.17	0.20	10.0	0.10	0.028	0.80	0.78
11/05/13	5.9	879	7.84	280	117	29	0.34	27	1.5	50	113	0.20	0.23	8.4	0.09	0.005	1.23	1.22
11/09/13	18.0	841	7.87	236	106	26	0.30	25	1.7	48	109	0.20	0.22	8.9	0.09	0.007	1.00	0.99
11/09/13	20.8	803	7.95	237	103	26	0.29	23	1.7	43	97	0.22	0.22	8.5	0.09	0.006	0.86	0.85
11/21/13	35.0	785	8.01	230	101	25	0.29	25	1.7	48	101	0.18	0.20	8.1	0.08	0.004	0.57	0.56
12/03/13	20	815	8.02	258	105	28	0.33	27	1.4	53	107	0.19	0.22	7.9	0.08	0.002	0.61	0.60
01/06/14	4.7	927	8	277	114	31	0.36	30	0.9	64	137	0.21	0.25	7.2	0.09	0.003	0.71	0.70
01/16/14	80.2	628	7.93	191	76	20	0.23	20	1.8	39	85	0.13	0.15	7.6	0.06	0.004	0.34	0.34
01/16/14	71.5	638	7.85	200	75	21	0.25	20	1.8	36	78	0.14	0.13	7.4	0.06	0.003	0.60	0.60
02/03/14	14	878	8.04	285	108	29	0.34	27	1.0	48	118	0.19	0.20	6.8	0.08	0.002	0.85	0.85
03/03/14	11.0	827	8.02	265	101	28	0.34	28	1.0	47	118	0.21	0.20	6.1	0.07	0.003	0.59	0.58
Williamson Creek																		
03/14/13	0.75	365	8.08	112	48	12	0.25	7	2.5	14	49		0.07	4.3	0.03	0.006	0.34	0.33
04/03/13	0.08	395	7.68	147	56	12	0.30	9	2.5	12	36		0.08	3.1	0.05	0.010	0.26	0.25
05/24/13	12.1	234	7.22	82	32	7	0.18	4	2.4	6	24		0.05	2.6	0.04	0.016	0.48	0.46
06/12/13	19.4	116	7.43	37	16	3	0.07	2	2.6	3	9		0.01	1.8	0.03	0.014	0.46	0.45
09/12/13	19.7	57	6.78	44	18	2	0.08	2	2.5	1	12	0.08	0.00	2.1	0.02	0.010	0.23	0.22
09/13/13	27.3	147	6.72	51	21	3	0.07	2	2.9	4	11	0.08	0.01	3.1	0.03	0.069	0.59	0.53
09/23/13	26.6	157	7.5	56	21	4	0.09	3	2.4	4	12	0.07	0.02	3.1	0.03	0.011	0.44	0.42
10/10/13	223.0	266	7.63	98	37	7	0.15	5	2.2	10	23	0.09	0.05	4.4	0.04	0.006	0.33	0.33
10/15/13	0.5	781	8.02	274	112	28	0.58	18	2.5	32	95	0.25	0.24	8.4	0.11	0.005	0.52	0.51
10/23/13	17.4	365	7.81	132	49	11	0.20	8	2.1	15	30	0.11	0.10	4.8	0.05	0.003	0.24	0.24
11/05/13	0.5	840	8.02	314	115	31	0.52	22	1.9	40	85	0.22	0.31	8.4	0.10	0.005	0.94	0.93
11/09/13	11.3	438	7.96	164	61	15	0.25	11	2.2	21	40	0.13	0.14	4.7	0.06	0.009	0.61	0.60
11/09/13	7.3	455	8.02	168	62	16	0.26	11	1.9	21	39	0.14	0.14	5.4	0.06	0.004	0.42	0.42
12/03/13	11	624	8.2	241	85	23	0.36	15	1.6	28	53	0.19	0.18	7.4	0.06	0.002	0.63	0.62
01/06/14	4	768	8.2	284	96	30	0.45	19	1.2	41	75	0.22	0.28	3.4	0.08	0.002	0.51	0.51

Appendix Table 1. Stream water geochemical concentrations (mg/L)

Date	Discharge (ft^3/s)	Specific conductance (µS/cm)	pH	Alkalinity	Ca	Mg	Sr	Na	K	Cl	SO_4	F	Br	Si	B	NO_2	NO_3+NO_2	NO_3 (calculated)
01/16/14	42.8	395	7.47	139	46	12	0.20	8	1.7	17	30	0.12	0.10	3.7	0.04	0.004	0.46	0.46
01/16/14	47.2	531	7.64	192	65	18	0.25	12	2.2	23	41	0.15	0.12	5.8	0.05	0.004	1.04	1.03
02/03/14	7.7	793	8.29	302	99	28	0.41	19	1.2	38	71	0.19	0.24	4.9	0.07	0.003		
03/03/14	6.1	695	8.25	273	88	26	0.38	17	1.0	32	64	0.21	0.21	5.4	0.06	0.004	0.81	0.80

Appendix Table 2. Speleothem U-Th dates

Depth (mm)	**Age (year BP*)**	**+/-**
2.2	132	17
8.4	250	51
13.6	1,335	83
16.4	1,733	23
41.1	2,477	132
65.3	3,498	127
93.9	4,363	216
114.4	5,038	86
138.2	5,584	100
147.9	5,568	130
182.3	6,475	212
190.2	6,524	97
201.5	6,987	75
219.8	6,985	122

*years prior to 2012

Appendix Table 3. Speleothem stable isotope values

Depth (mm)	Track	$\delta^{13}C$ (‰ PBD)	$\delta^{18}O$ (‰PBD)
0.1	1	-5.7	-3.0
0.4	1	-8.0	-4.4
0.7	1	-8.0	-4.2
1.0	1	-8.3	-4.6
1.3	1	-7.8	-4.6
1.6	1	-8.5	-4.5
1.9	1	-7.5	-4.7
2.2	1	-7.1	-4.5
2.5	1	-7.5	-4.7
3.1	1	-7.0	-4.5
3.4	1	-8.2	-5.0
3.7	1	-6.4	-4.4
4.0	1	-6.8	-3.1
4.3	1	-7.2	-4.5
4.6	1	-7.1	-4.6
4.9	1	-6.2	-4.1
5.2	1	-6.1	-4.0
5.5	1	-6.8	-4.1
5.8	1	-7.3	-4.7
6.0	1	-7.4	-4.3
6.3	1	-7.3	-4.5
6.6	1	-6.6	-4.4
6.8	1	-6.3	-4.4
6.9	1	-6.8	-4.6
7.1	1	-7.0	-4.6
6.8	2	-6.9	-4.5
6.9	2	-7.0	-4.6
7.1	2	-7.0	-4.5
7.2	2	-7.7	-4.6
7.4	2	-7.9	-4.6
7.5	2	-7.6	-4.7
7.7	2	-7.7	-3.4
7.8	2	-8.1	-4.6
8.0	2	-8.0	-4.5
8.1	2	-7.4	-4.5
8.3	2	-6.8	-4.4
8.4	2	-7.3	-4.6
8.6	2	-7.6	-4.6
8.7	2	-7.6	-4.6
9.0	2	-6.5	-4.4
9.2	2	-6.4	-4.2
9.3	2	-8.0	-4.3
9.5	2	-8.1	-4.3
9.6	2	-7.5	-4.2
9.8	2	-6.6	-4.2
9.9	2	-6.6	-4.2
10.1	2	-7.3	-4.2
10.2	2	-7.5	-4.1
10.4	2	-7.0	-4.0
10.5	2	-6.3	-4.2
10.7	2	-6.7	-4.2
10.8	2	-6.7	-4.0
11.0	2	-6.7	-4.1
11.1	2	-6.2	-4.1
11.3	2	-6.1	-4.3
11.4	2	-6.2	-4.3
11.6	2	-6.6	-4.2
11.7	2	-6.3	-4.0
11.9	2	-6.2	-4.2
12.0	2	-6.5	-4.2
12.2	2	-6.2	-4.1
12.3	2	-6.2	-4.0
12.5	2	-6.2	-4.3
12.6	2	-6.0	-4.1
12.8	2	-6.1	-4.2
12.9	2	-6.0	-4.1
13.1	2	-6.1	-4.0
13.2	2	-5.7	-3.4
13.4	2	-5.1	-3.9
13.5	2	-3.1	-3.5

Appendix Table 3. Speleothem stable isotope values

Depth (mm)	Track	$\delta^{13}C$ (‰ PBD)	$\delta^{18}O$ (‰PBD)
13.7	2	-1.5	-2.8
14.0	2	-2.4	-3.7
14.1	2	-2.5	-3.3
14.3	2	-2.9	-3.9
14.4	2	-3.1	-4.0
14.6	2	-3.5	-4.1
14.7	2	-3.5	-4.2
14.9	2	-3.9	-4.6
15.0	2	-4.1	-3.9
15.2	2	-4.1	-4.4
15.3	2	-4.0	-4.5
15.5	2	-4.1	-4.6
15.6	2	-4.1	-4.3
7.0	3	-6.9	-4.4
9.0	3	-7.5	-4.6
11.0	3	-7.0	-4.2
13.0	3	-6.1	-4.1
14.0	3	-4.3	-3.8
15.0	3	-3.1	-4.7
16.0	3	-4.1	-4.5
17.0	3	-4.2	-4.2
18.0	3	-3.7	-4.3
19.0	3	-3.6	-4.0
20.0	3	-3.9	-4.7
20.9	3	-3.5	-4.5
22.0	3	-3.8	-4.4
22.8	3	-3.8	-4.4
24.0	3	-3.5	-4.5
24.7	3	-3.6	-4.5
26.0	3	-3.5	-4.5
26.6	3	-3.8	-4.7
27.5	3	-3.6	-4.2
28.5	3	-3.7	-4.1
29.4	3	-3.8	-4.4
30.4	3	-3.8	-4.2
31.3	3	-3.8	-4.3
32.3	3	-4.0	-4.4
33.2	3	-3.9	-3.9
34.2	3	-3.9	-4.7
35.1	3	-4.0	-4.3
36.1	3	-4.0	-4.1
38.0	3	-3.6	-4.1
38.9	3	-3.7	-3.8
39.9	3	-3.6	-4.0
40.8	3	-3.7	-4.2
41.8	3	-4.0	-4.4
42.7	3	-3.9	-4.5
43.7	3	-3.6	-4.4
45.6	3	-3.9	-4.1
46.5	3	-3.8	-4.1
47.5	3	-3.5	-4.1
49.4	3	-3.5	-4.1
50.3	3	-3.9	-4.3
51.3	3	-3.5	-4.1
52.2	3	-3.6	-4.2
53.2	3	-3.8	-4.4
54.1	3	-3.3	-4.1
55.1	3	-3.5	-4.4
56.0	3	-3.0	-4.2
57.0	3	-3.1	-4.3
57.9	3	-3.2	-4.4
58.9	3	-3.1	-4.4
59.8	3	-3.5	-4.7
60.8	3	-3.7	-4.4
61.7	3	-3.2	-4.3
62.7	3	-3.1	-4.2
59.8	4	-3.4	-4.6
60.8	4	-3.7	-4.5
62.5	4	-3.1	-4.4
63.6	4	-3.2	-4.5

Appendix Table 3. Speleothem stable isotope values

Depth (mm)	Track	$\delta^{13}C$ (‰ PBD)	$\delta^{18}O$ (‰PBD)
64.5	4	-3.1	-4.2
65.6	4	-3.2	-4.1
66.5	4	-3.3	-4.1
67.6	4	-3.4	-4.5
68.5	4	-3.2	-4.4
69.6	4	-3.1	-4.3
70.5	4	-3.2	-4.4
71.6	4	-3.3	-4.3
72.5	4	-3.5	-4.4
73.6	4	-3.5	-4.3
75.6	4	-3.1	-4.5
76.5	4	-3.0	-4.2
77.6	4	-3.2	-4.2
78.5	4	-3.4	-4.5
79.6	4	-2.9	-4.6
80.5	4	-2.9	-4.4
81.6	4	-2.7	-4.0
82.5	4	-2.6	-4.5
83.6	4	-2.9	-4.3
84.5	4	-3.1	-4.3
85.6	4	-3.0	-4.0
86.5	4	-3.0	-4.3
87.6	4	-3.4	-4.5
88.5	4	-3.3	-4.3
89.6	4	-3.2	-3.8
90.5	4	-3.1	-3.8
91.6	4	-2.8	-3.9
93.0	4	-3.3	-4.3
94.1	4	-3.1	-4.3
95.0	4	-3.0	-4.5
96.1	4	-3.3	-4.5
97.1	4	-2.9	-4.1
98.2	4	-3.0	-4.0
99.2	4	-3.6	-4.3
100.3	4	-3.3	-4.2
101.3	4	-3.1	-4.0
102.4	4	-3.7	-4.2
103.4	4	-3.5	-4.3
104.5	4	-3.5	-4.6
105.0	4	-3.6	-4.5
106.0	4	-3.0	-4.5
102.0	5	-3.5	-4.2
103.0	5	-3.3	-4.3
104.0	5	-3.6	-4.6
105.0	5	-3.8	-4.5
106.0	5	-3.0	-4.4
107.0	5	-3.7	-4.7
108.0	5	-3.5	-4.7
108.0	5	-3.0	-4.6
109.0	5	-3.7	-4.7
110.0	5	-3.1	-4.2
111.0	5	-3.5	-4.2
112.0	5	-4.0	-4.1
113.0	5	-3.7	-4.2
114.0	5	-3.8	-4.3
115.0	5	-3.7	-4.5
116.0	5	-4.0	-4.4
117.0	5	-4.0	-4.3
118.0	5	-4.0	-4.6
119.0	5	-3.7	-4.1
120.0	5	-4.0	-4.6
121.0	5	-3.8	-4.5
122.0	5	-4.0	-4.4
123.0	5	-4.4	-4.1
124.0	5	-4.8	-4.1
125.0	5	-4.1	-4.0
126.0	5	-4.5	-4.1
127.0	5	-4.5	-4.0
129.0	5	-5.1	-4.5
130.0	5	-4.6	-4.0

Appendix Table 3. Speleothem stable isotope values

Depth (mm)	Track	$\delta^{13}C$ (‰ PBD)	$\delta^{18}O$ (‰PBD)
131.0	5	-4.5	-4.2
132.0	5	-4.8	-4.1
133.0	5	-5.1	-4.4
134.0	5	-5.1	-4.3
135.0	5	-4.6	-4.6
136.0	5	-5.1	-4.3
137.0	5	-5.1	-3.9
138.0	5	-5.0	-3.9
139.0	5	-5.1	-4.3
140.0	5	-4.9	-4.3
141.0	5	-4.9	-4.2
143.0	5	-5.4	-4.2
144.0	5	-6.2	-4.3
142.1	6	-4.9	-3.9
143.6	6	-5.4	-4.1
145.0	6	-5.5	-4.1
146.4	6	-6.4	-4.4
147.9	6	-6.0	-4.0
149.3	6	-5.9	-3.9
150.8	6	-5.7	-3.9
152.2	6	-5.3	-3.8
153.6	6	-5.9	-4.5
155.1	6	-5.1	-3.9
156.5	6	-5.2	-4.4
158.0	6	-4.8	-3.6
159.4	6	-5.1	-3.7
160.8	6	-4.8	-3.9
162.3	6	-5.2	-4.1
163.7	6	-5.2	-3.9
165.2	6	-5.0	-4.4
166.6	6	-5.0	-4.3
168.0	6	-4.9	-4.0
169.5	6	-5.0	-4.2
170.9	6	-4.4	-4.0
172.4	6	-3.7	-4.1
173.8	6	-4.6	-4.3
175.2	6	-6.7	-4.8
176.7	6	-3.8	-4.0
178.1	6	-5.9	-4.4
179.6	6	-5.8	-4.3
181.0	6	-5.1	-4.7
182.4	6	-4.5	-4.2
183.9	6	-4.9	-4.3
184.8	6	-4.7	-4.5
183.8	7	-4.1	-4.2
184.8	7	-3.7	-4.0
186.4	7	-6.0	-4.8
187.8	7	-3.6	-4.1
189.2	7	-4.9	-4.4
190.7	7	-5.5	-4.8
192.1	7	-5.8	-4.9
193.6	7	-4.9	-4.3
195.0	7	-4.8	-4.1
196.4	7	-3.8	-4.0

Appendix Table 4. Interpolated speleothem $\delta^{18}O$ values

Age (years BP*)	**$\delta^{18}O$ (‰ PBD)**
30	-3.0
60	-4.6
90	-4.5
120	-4.8
150	-4.3
180	-4.0
210	-3.9
240	-4.4
270	-4.6
300	-4.6
330	-4.6
360	-4.2
390	-4.3
420	-4.3
450	-4.2
480	-4.2
510	-4.2
540	-4.2
570	-4.1
600	-4.1
630	-4.2
660	-4.1
690	-4.0
720	-4.2
750	-4.1
780	-4.3
810	-4.2
840	-4.2
870	-4.0
900	-4.2
930	-4.2
960	-4.1
990	-4.0
1020	-4.2
1050	-4.2
1080	-4.1
1110	-4.1
1140	-3.6
1170	-3.8
1200	-3.6
1230	-2.9
1260	-3.2
1290	-3.6
1320	-3.5
1350	-3.7
1380	-4.0
1410	-4.0
1440	-4.1
1470	-4.3
1500	-4.5
1530	-4.7
1560	-4.4
1590	-4.5
1620	-4.6
1650	-4.3
1680	-4.4
1710	-4.5
1740	-4.4
1770	-4.2
1800	-4.2
1830	-4.3
1860	-4.6
1890	-4.5
1920	-4.4
1950	-4.4
1980	-4.5
2010	-4.5
2040	-4.5
2070	-4.6
2100	-4.3
2130	-4.1
2160	-4.3
2190	-4.3
2220	-4.2
2250	-4.3
2280	-4.2
2310	-4.1
2340	-4.6

Appendix Table 4. Interpolated speleothem $\delta^{18}O$ values

Age (years BP*)	**$\delta^{18}O$ (‰ PBD)**
2370	-4.3
2400	-4.1
2430	-4.1
2460	-4.1
2490	-3.9
2520	-4.0
2550	-4.1
2580	-4.3
2610	-4.4
2640	-4.5
2670	-4.3
2700	-4.2
2730	-4.1
2760	-4.1
2790	-4.1
2820	-4.1
2850	-4.1
2880	-4.3
2910	-4.2
2940	-4.1
2970	-4.2
3000	-4.3
3030	-4.2
3060	-4.4
3090	-4.3
3120	-4.3
3150	-4.4
3180	-4.4
3210	-4.5
3240	-4.6
3270	-4.5
3300	-4.3
3330	-4.2
3360	-4.2
3390	-4.2
3420	-4.3
3450	-4.1
3480	-4.2
3510	-4.4
3540	-4.4
3570	-4.3
3600	-4.4
3630	-4.3
3660	-4.4
3690	-4.3
3720	-4.3
3750	-4.4
3780	-4.5
3810	-4.2
3840	-4.2
3870	-4.4
3900	-4.5
3930	-4.5
3960	-4.2
3990	-4.2
4020	-4.5
4050	-4.3
4080	-4.3
4110	-4.0
4140	-4.3
4170	-4.5
4200	-4.3
4230	-4.0
4260	-3.8
4290	-3.8
4320	-4.0
4350	-4.2
4380	-4.3
4410	-4.5
4440	-4.5
4470	-4.3
4500	-4.1
4530	-4.1
4560	-4.3
4590	-4.2
4620	-4.0
4650	-4.2
4680	-4.3

Appendix Table 4. Interpolated speleothem $\delta^{18}O$ values

Age (years BP*)	$\delta^{18}O$ (‰ PBD)
4710	-4.6
4740	-4.5
4770	-4.5
4800	-4.6
4830	-4.7
4860	-4.7
4890	-4.3
4920	-4.2
4950	-4.1
4980	-4.2
5010	-4.2
5040	-4.4
5070	-4.4
5100	-4.3
5130	-4.5
5160	-4.3
5190	-4.6
5220	-4.3
5250	-4.1
5280	-4.0
5310	-4.0
5340	-4.2
5370	-4.3
5400	-4.1
5430	-4.1
5460	-4.4
5490	-4.3
5520	-4.5
5550	-4.1
5580	-3.9
5610	-4.3
5640	-4.0
5670	-3.9
5700	-3.8
5730	-4.3
5760	-4.1
5790	-4.1
5820	-3.6
5850	-3.8
5880	-4.0
5910	-4.1
5940	-4.0
5970	-4.4
6000	-4.2
6030	-4.0
6060	-4.2
6090	-4.0
6120	-4.1
6150	-4.3
6180	-4.6
6210	-4.4
6240	-4.1
6270	-4.4
6300	-4.3
6330	-4.6
6360	-4.4
6390	-4.2
6420	-4.2
6450	-4.6
6480	-4.8
6510	-4.2
6540	-4.3
6570	-4.5
6600	-4.8
6630	-4.9
6660	-4.7
6690	-4.4
6720	-4.2
6750	-4.1
6780	-4.0

*years prior to 2012

QUANTIFICATION OF EQUATIONS

PHREEQC

PHREEQC models mixing and chemical reactions using mole-balance equations for individual elements (or redox states), alkalinity, electrons, and solvent water (Pankhurst, 1997). The model also includes a charge balances, and incorporates uncertainty for each element. Equations are solved for all unique combinations of mixing and reactions while minimizing uncertainty terms and identifying the simplest solutions.

Mole-balance is defined as:

$$\sum_{q}^{Q} c_q \alpha_q (T_{m,q} + \delta_{m,q}) + \sum_{q} c_{m,p} \alpha_p + \sum_{q} c_{m,r} \alpha_r = 0,$$

where $T_{m,q}$ is the total number of moles, m, of an element or element valance state in aqueous solution, q, $\delta_{m,q}$ is a term for the uncertainty in the number of moles $T_{m,q}$, $c_{m,p}$ is the stoichiometric coefficient of element, m, in the dissolution reaction for phase p, and $c_{m,r}$ is the coefficient of the element valence state, m, in redox reaction r (Parkhusrt, 1997). Additional balance equations are defined in Pankhurst (1997).

LOADEST

LOADEST is a program that estimates loads (Runkel et al., 2004). A regression equation is defined for the relationship between stream discharge and stream water constituent concentrations using data collected during the project interval. In this study, the regression was calculated by using which relates instantaneous load, $\hat{L}$, to one or more explanatory variable, X (e.g., discharge), via a linear regression with coefficients a_0 and a_j:

$$\ln(\hat{L}) = a_0 + \sum_{j=1}^{NV} a_j X_j ,$$

where NV is the number of explanatory variables (Cohen, 1995). Coefficients a_0 and a_j are developed using the maximum likelihood estimation:

$$\hat{L} = \exp(a_0 + \sum_{j=1}^{M} a_j X_j) g_m(m, s^2, V),$$

where m is the number of degrees of freedom, s^2 is the residual variance, and V is the function of the explanatory variables (Cohen et al., 1989). $g_m(m,s^2,V)$ is a bias correction factor described by Finney (1941). Total load is estimated from instantaneous estimates calculated from a time series of explanatory variables (e.g., 15-min discharge).

Principle components analysis

A principal components analysis compresses a data set by transforming (linear and orthogonal) the a large multivariate data set into a smaller number variables that best describe the variance of the dataset (Davis, 2002). For a normalized data set, the covariance of the matrix is calculated. The covariance, for example, of a matrix X x Y is calculated:

$$\mathrm{cov}(X,Y) = \frac{\sum_{i=1}^{n} (Xi - \overline{X})(Yi - \overline{Y})}{(n-1)}$$

The eigenvectors of the covariance matrix are then solved for and ordered by the significance to which each is related to the normalized data. The desired number of eigenvectors are then selected, and then multiplied by the normalized dataset.

V = E x D, where V is the matrix of new variables calculated by the PCA analysis, E is the matrix of selected eigenvectors, and D is the normalized dataset. V will have the same number of vectors of E, despite the number of vectors in D (Davis, 2002).

Regression and p-values

Pearson's r is the measure of linear dependence between two variables.

$$r = \frac{\sum_{i=1}^{n}(Xi - \overline{X})(Yi - \overline{Y})}{\sqrt{\sum_{i=1}^{n}(Xi - X)^2}\sqrt{\sum_{i=1}^{n}(Yi - Y)^2}}$$

The coefficient of determination, r^2, is the square of the correlation coefficient.

Significance of a correlation is determined by calculating the probability that r would occur given that the null hypothesis is true (i.e., r=0, meaning there is no correlation).

$$t = \frac{r}{\sqrt{(1 - r^2)/(N - 2)}}$$

The probability is based on the t-value and the degrees of freedom (Davis, 2002).

Palmer drought severity index

PDSI is based on the calculation of a regional specific moisture anomaly index using a set of water balance equations. Potential values for evapotranspriation (PE), recharge (PR), soil moisture (PL), and runoff (PRO) are used to derive climate-dependent coefficients that are used to compute differences, d, between actual and expected (based on the historical climatology) precipitation for each month. A moisture anomaly index, Z, is calculated from this difference and a region- and time-specific weighting factor, Kj. The moisture anomaly index, X, is converted to a drought severity index using an empirical relationship between (Palmer, 1965; Alley, 1984).

$$X(i) = Z(i)/3 + cX(i-1), \text{ where c was determined to be 0.897;}$$

$$Z = Kjd;$$

Refer to Alley (1984) for the definitions of Kj and d and the full derivation of X.

PDSI is a widely used drought index in the United States, despite its shortcomings that include an overly simplified water budget model, arbitrary operational procedures and designation of qualitative severity categories, and normalization methods based on a limited spatial and temporal data set (Alley, 1984).

StalAge

StalAges calculates an age model using an iterative procedure to increase data error to account for major and minor data outliers and then calculates an age-depth model based on the median value and 95%-confidence of a Monte-Carlo simulation that fits straight lines to subsets of age-depth data (Scholz and Hoffmann, 2011).

Fitting a line requires the minimization of r^2,

$$r^2 = \sum [y_i - f(x_i, a_1, a_2, ..., a_n)]^2 .$$

For a linear fit, $f(a,b) = a + bx$, the condition, $\frac{\partial (r^2)}{\partial a_i} = 0$, must be minimized. This can be reduced to:

$$a\sum_{i=1}^{n} x_i + b\sum_{i=1}^{n} x_i^{\,2} = \sum_{i=1}^{n} x_i + y_i$$ (Weisstein, 2013a).

Spectral analysis

Spectral analyses estimate the power spectrum using a Fourier transform, $P_x(f)$. There are several approaches to calculating $P_x(f)$. The MultiTaper Method estimates $P_x(f)$ by averaging the individual spectra given by each window ($w_k(t)$) of the data set:

$$Px(f) = \frac{\sum_{k=1}^{K} \mu_k \, | X_k(f) |^2}{\sum_{k=1}^{K} \mu_k},$$

where X_k is the discrete Fourier transform of $[X_k(t)w_k(t):t=1,\ldots,N]$ and the spectrum is weighted by μ_k (Ghil et al., 2001).

A Fourier transform converts a function from its original domain (e.g., time) to the frequency domain. A continues Fourier transform is defined by, $f(v) = \int_{-\infty}^{\infty} f(t) e^{-2\pi i v t} dt$.

For a discrete function, $f(t) \rightarrow f(t_k)$ with k=0,1,….,N-1, and $F_n = \sum_{k=0}^{N-1} f_k e^{-2\pi i n k / N}$ (Weisstein, 2013b).

Appendix References

Alley, W.M., 1984, The Palmer Drought Severity Index: Limitations and assumptions, Journal of Climate and Applied Meteorology, 23, 1100-1109.

Cohen, T.A., Delong, L.L., Gilroy, E.J., Hirsch, R.M., and Wells, D.K., 1989, Estimating constituent loads: Water Resources Research, v. 25, no. 5, p. 937-942.

Cohen, T.A., 1995, Recent advances in statistical methods for the estimation of sediment and nutrient transport in rivers: Reviews in Geophysics, v. 33 (Supplement), p. 1117–1124.

Davis, J.C., 2002, Statistics and data analysis in geology: New York, Wiley, 638 p.

Finney, D.J., 1941, On the distribution of a variate whose logarithm is normally distributed: Supplement to the Journal of the Royal Statistical Society, v. 7, p. 155–161.

Ghil M., R. M. Allen, M. D. Dettinger, K. Ide, D. Kondrashov, M. E. Mann,A. Robertson, A. Saunders, Y. Tian, F. Varadi, and P. Yiou, 2000, Advanced spectral methods for climatic time series, Reviews of Geophysics,40, 3.1-3.41.

Parkhurst, D.L., Appelo, C.A.J., 1999. User's guide to PHREEQC (ver. 2)—A computer program for speciation, reaction-path, one-dimensional transport, and inverse geochemical calculations. U.S. Geological Survey Water-Resources Investigations 99–4259, 312 p.

Palmer WC. 1965. Meteorological Drought. Research Paper No. 45. Washington (DC): U.S. Weather Bureau. 58 p.

Runkel, R.L., C.G. Crawford, and T.A Cohn (2004) Load Estimator (LOADEST)—A FORTRAN program for estimating constituent loads in streams and rivers: U.S. Geological Survey Techniques and Methods Book 4, Chapter A5, 69 p.

Scholtz, D., Hoffman, D.L., 2011. StalAge – An algorithm designed for construction of speleothem age models. Quaternary Geochronology, 6, 369-382.

Weisstein, E.W, 2013a, Least Squares Fitting. From MathWorld--A Wolfram Web Resource. http://mathworld.wolfram.com/LeastSquaresFitting.html

Weisstein, E.W., 2013b, Fourier Transform. From MathWorld--A Wolfram Web Resource. http://mathworld.wolfram.com/FourierTransform.html

References

Chapter 1 references

Abbott, P.L., 1975, On the hydrology of the Edwards Limestone, south-central Texas: Journal of Hydrology, v. 24, p. 251–269.

Buchele, M., 2012, Taking a deeper look at the Texas Supreme Court's ruling on water. National Public Radio State Impact. Accessed May 2013 at http://stateimpact.npr.org/texas/2012/03/01/taking-a-deeper-look-at-the-texas-supreme-courts-ruling-on-water/

Edwards Aquifer Authority, 2009, Edwards Aquifer Authority Act. Accessed May 2013 at http://www.edwardsaquifer.org/files/EAAact.pdf.

Hauwert, N.M., 2009, Groundwater flow and recharge within the Barton Springs segment of the Edwards Aquifer, southern Travis County, Texas. Dissertation, The University of Texas at Austin, 328 p

Johnson, S., Schindel, G., Veni, G., Hauwert, N., Hunt, B., Smith, B., Gary, M., 2012, Tracing groundwater lowpaths in the vincinity of San Marcos Springs, Texas. Edwards Aquifer Authority Report No. 12-01.

Kaiser, R.A. and Phillips, L.M., 1998, Dividing the waters: Water marketing as a conflict resolution strategy in the Edwards Aquifer region. Natural Resources Journal, 38, 411-444.

IPCC, 2007, Summary for Policymakers. In: Climate Change 2007: The Physical Science Basis. Contribution of Working Group I to the Fourth Assessment Report of the Intergovernmental Panel on Climate Change [Solomon, S., D. Qin, M. Manning, Z. Chen, M. Marquis, K.B. Averyt, M.Tignor and H.L. Miller (eds.)]. Cambridge University Press, Cambridge, United Kingdom and New York, NY, USA.

Mahler, B.J., Musgrove, M., Sample, T.L., Wong, C.I., 2011, Recent (2008–10) Water quality in the Barton Springs segment of the Edwards aquifer with emphasis on factors affecting nutrients and bacteria. U.S. Geological Survey Scientific Investigation Report 2011-5139.

Martin-Carrasco, F., Garrote, L., Iglesias, A., Mediero, L., 2013, Diagnosing causes of water scarcity in complex water resources systems and identifying risk management actions. Water Resource Management, 27, 1693-1705.

Musgrove, M., L. Stern, and Banner, J., 2010, Springwater geochemistry at Honey Creek State Natural Area, central Texas: Implications for surface water and groundwater interaction in a karst aquifer. Journal of Hydrology, 388, 144–156.

Musgrove, M. and Crow, C.L., 2012, Origin and characteristics of discharge at San Marcos Springs based on hydrologic and geochemical data (2008-10), Bexar,

Comal, and Hays Counties, Texas. USGS Scientific Investigations Report, 2012-5126.

Rose, P.R., 1972, Edwards Group, Surface and Subsurface, Central Texas. Report of Investigations No. 74. Bureau of Economic Geology, The University of Texas at Austin.

Slade, R.M., Jr., Dorsey, M.E., Stewart, S.L., 1986, Hydrology and Water Quality of the Edwards Aquifer Associated with Barton Springs in the Austin Area, Texas. U.S. Geological Survey Water-Resources Investigations Report 86–4036, 117p.

Stricklin, F.L., 1971, Stratigraphy of Lower Cretaceous Trinity Deposits of Central Texas. Report of investigations No. 71. Bureau of Economic Geology, The University of Texas at Austin.

Wierman, D.A., A.S. Broun, and B.B. Hunt. 2010. Hydrogeologic atlas of the Hill Country Trinity Aquifer; Blanco, Hays and Travis Counties, central Texas. Hays-Trinity Groundwater Conservation District. Available at http://repositories.lib.utexas.edu/handle/2152/8977.

Chapter 2 references

Andrews, F.L., 1984, Effects of storm-water runoff on water quality of the Edwards Aquifer near Austin, Texas. Water Research Investigation Report 84-4124.

Abbott, P.L., 1975, On the hydrology of the Edwards Limestone, south-central Texas: Journal of Hydrology, v. 24, p. 251–269.

Bailly-Comte, V., Martin, J.B., Jourde, H., Screaton, E.J., Pistre, S, Langston, A., 2010. Water exchange and pressure transfer between conduits and matrix and their influence on hydrodynamics of two karst aquifers with sinking streams. Journal of Hydrology 386, 55-66.

Banner, J.L., Jackson, C.S., Zong-Liang, Y., Hayhoe, K., Woodhouse, C., Gulden, L., Jacobs, K., North, G., Leung, R., Washington, W., Jiang, X., Casteel, R., 2010, Climate change impacts on Texas water: a white paper assessment of the past, present and future and recommendations for action. Texas Water Journal 1, 1-19.

Banner, J. L., Kaufman, J., 1994, The isotopic record of ocean chemistry and diagenesis preserved in non-luminescent brachiopods from Mississippian carbonate rocks, Illinois and Missouri, Geological Society of America Bulletin, 106, 1074–1082.

Barrett, M.E., Charbeneau, R.J., 1997, A parsimonious model for simulating flow in a karst aquifer. Journal of Hydrology, 196, 47-65.

Barrett, M.H., Hiscock, K.M., Pedley, S., Lerner, D.N., Tellam, J.H., French, M.J., 1999. Marker species for identifying urban groundwater recharge sources: a review and case study in Nottingham, UK: Water Resources, 33, 3083-3097.

Birk, S., Liedl, R., Sauter, M., 2004, Identification of localized recharge and conduit flow by combined analysis of hydraulic and physicochemical spring responses (Urenbrunnen, SW-Germany). Journal of Hydrology 286, 179-193.

Cardenas, M.B., Slottke, D.T., Ketcham, R.A., Sharp, J.M. 2007. Navier-Stokes flow and transport simulations using real fractures shows heavy tailing due to eddies. Geophysical Research Letters 34, L14404.

Christian, L.N., Banner, J.L., Mack, L.E., 2011. Sr isotopes as tracers of anthropogenic influences on stream water in the Austin, Texas, area, Chemical Geology 282, 84-97.

Cooke, M. J., Stern, L. A., Banner, J. L., Mack, L. E., 2007, Evidence for the silicate source of relict soils on the Edwards Plateau, central Texas. Quaternary Research 67, 275–285.

Davis, J.C., 2002, Statistics and data analysis in geology: New York, Wiley, 638 p.

Desmarais, K., Rojstaczer, S., 2002. Inferring source waters from measurements of carbonate spring response to storms. Journal of Hydrology **260,** 118–134.

Fishman, M.J., 1993, Methods of analysis by the U.S. Geological Survey National Water Quality Laboratory—Determination of inorganic and organic constituents in water and fluvial sediments: U.S. Geological Survey Open-File Report 93–125, 217 p.

Florea, L.J., Vacher, H.L., 2006. Springflow hydrographs: Eogenetic vs. telogenetic karst. Ground Water 44, 352-361.

Florea, L.J., Vacher, H.L. 2007. Eogenetic karsty hydrology: Insights from the 2004 hurricanes, peninsular Florida. Ground Water 45, 439-446.

Ford, D.C., Williams, P.W., 1989. Karst Geomorphology and Hydrology. Unwin Hyman, London, 601 p.

Garner, B.D., 2005. Geochemical evolution of ground water in the Barton Springs segment of the Edwards Aquifer. Dissertation, The University of Texas at Austin, 317 p.

Garner, B.D., Mahler, B.J., 2007, Relation of specific conductance in ground water to intersection of flow paths by wells, and associated major ion and nitrate geochemistry, Barton Springs segment of the Edwards aquifer, Austin, Texas, 1978–2003: U.S. Geological Survey Scientific Investigations Report 2007–5002, 39 p.

Griffiths, J.F., Ainsworth, G., 1981. One Hundred Years of Texas Weather 1880-1979. College Station: Texas A&M Univ., Office of the State Climatologist. 205 p.

Gulley, J., Martin, J.B., Screaton, E.J., Moore, P.J. 2011. River reversals into karst springs: A model for cave enlargement in eogenetic karst aquifers. Geological Society of America Bulletin 123, 457-467.

Halihan, T., Wicks, C.M., 1998. Modeling of storm responses in conduit flow aquifers with reservoirs. Journal of Hydrology, 208, 82-91.

Hauwert, N.M., 2009. Groundwater flow and recharge within the Barton Springs segment of the Edwards Aquifer, southern Travis County, Texas. Dissertation, The University of Texas at Austin, 328 p

Hauwert, N.M., Johns, D.A., Aley, T.J., Sansom, J.W., 2004, Groundwater tracing study of the Barton Springs segement of the Edwards aquifer, southern Travis and northern Hays counties, Texas. Report by the Barton Springs/Edwards Aquifer Conservation District and City of Austin Watershed Protection and Development Review Department, 110p.

Heinz, B., Birk, S., Liedl, R., Geyer, T., Straub, K.L., Andresen, J., Bester, K., Kappler, A., 2009. Water quality deterioration at a karst spring (Gallusquelle, Germany) due to combined sewer overflow: evidence of bacterial and mirco-pollutant contamination. Environmental Geology, 57, 797-808.

Herman, E.K., Toran, L., White, W.B., 2009. Quantifying the place of karst aquifers in the groundwater to surface water continuum: A time series analysis study of storm behavior in Pennsylvania water resources. Journal of Hydrology 376, 307-317.

Hess, J.W., White, W.B., 1988. Storm response of the karstic carbonate aquifer of south central Kentucky. Journal of Hydrology 99, 235-252.

Koepnick, R.B., Burke, W.H., Denison, R.E., Hetherington, E.A., Nelson, H.F., Otto, J.B., Waite, L.E., 1985. Construction of the seawater 87Sr/86Sr curve for the Cenozoic and Cretaceous: Supporting data. Chemical Geology 58, 55–81.

Lakey B., Krothe, N.C., 1996. Stable isotopic variation of storm discharge from a perennial karst spring, Indiana. Water Resource Research 32, 721-731.

Larkin, T.J., Bomar, G.W., 1983. Climatic atlas of Texas: Texas Department of Water Resources, Limited Printing Report LP–192, 151 p.

Lower Colorado River Authority, 2011. http://hydromet.lcra.org/full.aspx.

Mahler, B.J., Musgrove, M., Sample, T.L., Wong, C.I., 2011, Recent (2008–10) Water quality in the Barton Springs segment of the Edwards aquifer with emphasis on factors affecting nutrients and bacteria. U.S. Geological Survey Scientific Investigation Report 2011-5139.

Mahler, B.J., Garner, B.D., 2009. Using nitrate to quantity quick flow in a karst aquifer. Ground Water 47, 350-360.

Mahler, B.J., Massei, N., 2007, Anthropogenic contaminants as tracers in an urbanizing karst aquifer. Journal of Contaminant Hydrology 91, 81-106.

Mahler, B.J., Garner, B.D., Musgrove, MaryLynn, Guilfoyle, A.L., Rao, M.V., 2006. Recent (2003–05) water quality of Barton Springs, Austin, Texas, with emphasis on factors affecting variability. U.S. Geological Survey Scientific Investigations Report 2006–5299, 83 p.

Martin, J.B., Dean, R.W., 2001. Exchange of water between conduits and matrix in the Floridan aquifer. Chemical Geology 179, 145-165.

Massei, N., Mahler, B.J., Bakalwicz, M., Fournier, M., Dupont, J.P., 2007. Quantitative interpretation of specific conductance frequency distributions in karst. Ground water, 45, 288-293.

Moore, P.J., Martin, J.B., Screaton, E.J., 2009. Geochemical and statistical evidence of recharge, mixing, and controls on spring discharge in an eogenetic karst aquifer. Journal of Hydrology 376, 443-455.

Musgrove, M., Banner, J. L., 2004, Controls on the spatial and temporal variability of vadose dripwater geochemistry: Edwards Aquifer, central Texas, Geochimica et Cosmochimica Acta 68, 1007-1020.

National Climate Data Center, http://lwf.ncdc.noaa.gov/temp-and-precip/time-series/,accessed 23 May 2012.

National Institute of Standards and Technology, Standard reference materials—SRM987-Strontium Carbonate Isotopic Standard, https://www-s.nist.gov/srmors/view_detail.cfm?srm=987, accessed 23 May 2012.

National Weather Service, http://www.srh.noaa.gov/ewx/?n=austinmabryclidata.htm, accessed 23 May 2012.

Oetting, 1995. Evolution of fresh and saline groundwaters in the Edwards aquifer, central Texas: geochemical and isotopic constraints on processes of fluid-rock interaction and fluid mixing. Dissertation, The University of Texas at Austin, 203 p.

Oetting, G.C., Banner, J.L., Sharp, J.M., 1996. Regional controls on the geochemical evolution of saline groundwaters in the Edwards aquifer, central Texas. Journal of Hydrology 181, 251-283.

Parkhurst, D.L., Appelo, C.A.J., 1999. User's guide to PHREEQC (ver. 2)—A computer program for speciation, reaction-path, one-dimensional transport, and inverse geochemical calculations. U.S. Geological Survey Water-Resources Investigations 99–4259, 312 p.

Palmer WC. 1965. Meteorological Drought. Research Paper No. 45. Washington (DC): U.S. Weather Bureau. 58 p.

Perez, Roberto, 1986, Potential for updip movement of salinewater in the Edwards aquifer, San Antonio, Texas: U.S. Geological Survey Water-Resources Investigations Report 86–4032, 21 p.

Peterson, E.W., Wicks, C.M. 2005. Fluid and solute transport from a conduit to the matrix in a carbonate aquifer system. Mathematical Geology 37, 851-867.

Pronk, M., Goldscheider, N., Zopfi, J. 2007. Particle-size distribution as indicator for fecal bacteria contamination of drinking water from karst springs. Environmental Science and Technology 41, 8400-8405.

Quinlan, J.F., 1989. Ground-water monitoring in karst terranes—Recommended protocols and implicit assumptions. U.S. Environmental Protection Agency EPA 600/X–89/050.

Raeisi, E., Groves, C., Meiman, J. 2007. Effects of partial and full pipe flow on hydrochemographs of Logsdon river, Mammoth Cave Kentucky USA. Journal of Hydrology 337, 1-10.

Ray, J.A., 1997, Overflow conduit systems in Kentucky: A consequence of limited underflow capacity. Engineering Geology and Hydrogeology of Karst Terrains 6th Multidisciplinary Conference on Sinkholes and the Engineering and Environmental Impacts of Karst, Springfield, MO, 69-67.

Rose, P.R., 1972. Edwards Group, surface and subsurface, central Texas. Report of investigations (University of Texas at Austin. Bureau of Economic Geology), no.74. Austin.

Rounds, S.A., 2006, Alkalinity and acid neutralizing capacity (ver. 3.0): U.S. Geological Survey Techniques of Water-Resources Investigations, book 9, chap. A6, section 6.6, available at http://pubs.water.usgs.gov/twri9A6/.

Ryan, M., Meiman, J., 1996. An examination of short-term variations in water quality at a karst spring in Kentucky. Ground Water 34, 23-30.

Seager, R., Ting, M., Held, I., Kushnier, Y., Lu, J., Vecchi, G., Huang, H.P., Harnik, N., Leetmaa, A., Lau, N.C., 2007. Model Projections of an imminent transition to a more arid climate in southwestern North America. Science 316, 1181-1184.

Senger, R.K., Kreitler, C.W. 1984. Hydrogeology of the Edward aquifer, Austin area, central Texas. Report of Investigations, Bureau of Economic Geology, The University of Texas at Austin.

Slade, R.M., Jr., Dorsey, M.E., Stewart, S.L., 1986. Hydrology and water quality of the Edwards aquifer associated with Barton Springs in the Austin area, Texas. U.S. Geological Survey Water-Resources Investigations Report 86–4036, 117 p.

Smart, C.C., 1988. Artificial tracer techniques for the determination of the structure of conduit aquifers. Ground Water 26, 445-453.

U.S. Geological Survey National Water Information System, 2012. http://waterdata.usgs.gov/tx/nwis/.

Vacher, H.L., Mylroie, J.E., 2002. Eogenetic karst from the perspective of an equivalent porous medium. Carbonates and Evaporates 17, 182-196**.**

White, W.B., 1999. Conceptual models for karstic aquifers. In: Palmer, A.N., Palmer, M.V., Sasowsky, I.D. (Eds.), Karst Modeling, vol. 5. Karst Waters Institute Special Publication, pp. 11–16.

Wierman, D.A., Broun, A.S., Hunt, B.B., 2010. Hydrogeologic atlas of the Hill Country Trinity Aquifer, Blanco, Hay, and Travis Counties, Central Texas. Hays-Trinity Groundwater Conservation District.

Wilde, F.D., Radtke, D.B., Gibs, J., Iwatsubo, R.T., 1999. National field manual for the collection of water-quality data—Collection of water samples: U.S. Geological Survey Techniques of Water-Resources Investigations, book 9, chap. A4, 49–52.

Wong, C., Banner, J. L., 2010. Response of cave air CO_2 and drip water to brush clearing in central Texas: Implications for recharge and soil CO_2 dynamics. Journal of Geophysical Research, 115, 1-13.

Wong, C., Banner, J. L., Musgrove, M., 2011. Seasonal dripwater Mg/Ca and Sr/Ca variations driven by cave ventilation: Implications for and modeling of speleothem paleoclimate records. Geochimica et Cosmochimica Acta 75, 3514–3529.

Chapter 3 References

Amrhein, C., J. E. Strong, and P. A. Mosher (1992) Effect of deicing salts on metal and organic matter mobilization in roadside soils, *Environ. Sci. Technol., 26*, 703–707, doi:10.1021/es00028a006.

Arnold, C.L. and C.J. Gibbons (1996) Impervious surface coverage – The emergence of a key environmental indicator, *Journal of the American Planning Association, 62*, 243-258.

Atkinson, T.C. (1977) Diffuse and conduit flow in limestone terrain in the Mendip Hills, Somerset (Great Britain). *Journal of Hydrology, 35*, 93-110.

Austin Water (2012) Wastewater treatment plants, http://austintexas.gov/department/wastewater-treatment-plants.

Barrett, M.H., K.M. Hiscock, S. Pedley, D.N. Lerner, J.H. Tellam, and M.J. French (1999) Marker species for identifying urban groundwater recharge sources: a review and case study in Nottingham, UK., *Water Resource Research, 33*, 3083–3097.

Barton Springs Edwards Aquifer Conservation District (2012) History, http://www.bseacd.org/about-us/history/.

Bastviken, D., P. Sanden, T. Svensson, C. Stahlberg, M. Magounakis, and G. Oberg (2006) Chloride retention and release in a boreal forest soil: effects of soil water residence time and nitrogen and chloride loads. *Environmental Science and Technology, 40*, 2977-2982.

Booth, D.B., J.R. Karr, S. Schauman, C.P. Konrad, S.A. Morley, M.G. Larson, and S.J. Burges (2004) Reviving urban streams: Land use, hydrology, biology, and human behavior. *Journal of the American Water Resources Association, 40*, 1351-1364.

Carey, R.O. and K.W. Migliaccio (2009) Contribution of wastewater treatment plant effluents to nutrient dynamics in aquatic systems: A review. *Environmental Management, 44*, 205-217.

Christian, L.N., Banner, J.L., Mack, L.E. (2011) Sr isotopes as tracers of anthropogenic influences on stream water in the Austin, Texas, area. *Chem. Geol., 282*, 84–97.

City of Austin (2012a) Watershed protection: Salamanders http://austintexas.gov/department/salamanders.

City of Austin (2012b) Water Quality Sampling Data, https://data.austintexas.gov/Environmental/Water-Quality-Sampling-Data/5tye-7ray.

Cottingham, J. (2009) Developers win again. The Austin Chronicle News Brief, Feb 2, 2009, http://www.austinchronicle.com/news/2009-02-20/744359/.

Craig, H. (1961) Isotope variations in meteoric waters. *Science, 133*, 1702-1703.

Dearmont, D., B.A. McCarl, and D.A. Tolman (1998) Costs of water treatment due to diminished water quality: A case study in Texas, *Water Resources Research, 34*, 849-853.

Fishman, M.J. (1993) Methods of Analysis by the U.S. Geological Survey National Water Quality Laboratory—Determination of Inorganic and Organic Constituents in Water and Fluvial Sediments: U.S. Geological Survey Open- File Report 93–125, 217p.

Godsey, S.E., J.W. Kirchner, and D.W. Clow (2009) Concentration-discharge relationships reflect chemostatic characteristics of US catchments, *Hydrologcal Processes, 23*, 1844-1864.

Hatt, B.E., T.D. Fletcher, C.J. Walsh, and S.L. Taylor (2004) The influence of urban density and drainage infrastructure on the concentration and loads of pollutants in small streams, *Environmental Management, 34*, 112-124.

Hauwert, N.M. (2009) Groundwater Flow and Recharge within the Barton Springs Segment of the Edwards Aquifer, Southern Travis County, Texas. Dissertation. The University of Texas at Austin, 328p.

Helsel, D. R., and R.M. Hirsch (2002) Statistical methods in water resources: U.S. Geological Survey Techniques of Water-Resources Investigations, book 4, chap. A3, 524 p. Available online at http://water.usgs.gov/pubs/twri/twri4a3/.

Herrington, C., M. Menchaca, M. Westbrook (2010) Wastewater disposal practices and change in development in the Barton Springs Zone. City of Austin SR 11-01, available at http://assets.austintexas.gov/watershed/publications/files/SR-11-01%20Wastewater%20in%20the%20BSZ.pdf.

Holland, A.F., D.M. Sanger, C.P. Gawle, S.B. Lerberg, M.S. Santiago, G.H. Riekerk, L.E. Zimmerman, G.I. Scott (2004) Linkages between tidal creek ecosystems and the landscape and demographics attributes of their watersheds. *Journal of Experimental Marine Biology and Ecology, 298*, 151-178.

Hong, B., K.E. Limburg, J.D. Erickson, J.M. Gowdy, A.A. Nowosielski, J.M., Pollimeni, and K.M. Stainbrook (2009) Connecting the ecological-economic dots in human-dominated watersheds: Models to link socio-economic activities on the landscape to stream ecosystem health. *Landscape and urban planning, 91*, 78-87.

Katz, B.G., D.W. Griffin, and J.H. Davis (2009) Groundwater quality impacts from the land application of treated municipal wastewater in a large karstic spring basin: Chemical and microbiological indicators. *Science of the Total Environment, 407*, 2872-2886.

Katz, B.G., D.W. Griffin, P.B. McMahon, H.S. Harden, E. Wade, R.W. Hicks, J.P. Chanton (2010) Fate of effluent-borne contaminants beneath septic tank drainfeilds overlying a karst aquifer. *Journal of Environmental Quality, 39*, 1181-1195.

Kelly, V.R., G.M. Lovett, K.C. Weathers, S.E. Findlay, D.L., Strayer, D.J. Burns, and G.E. Likens (2008) Long-term sodium chloride retention in a rural watershed: Legacy effects of road salt on streamwater concentration. *Environmental Science Technology, 42*, 410-415.

Larkin, T.J., Bomar, G.W. (1983) Climatic Atlas of Texas: Texas Department of Water Resources, Limited Printing Report LP–192, 151p.

Lovett, G.M., G.E. Likens, D.C. Buso, C.T. Driscoll, and S.W. Bailey (2005) The biogeochemistry of chlorine at Hubbard Brook, NH, USA. *Biogeochemistry, 72*, 191-232.

McMahon, Gerard, and T.F. Cuffney (2000) Quantifying urban intensity in drainage basins for assessing stream ecological conditions: *Journal of the American Water Resources Association, 36*, 1247-1261.

Mason, C. F., S. A. Norton, I. J. Fernandez, and L. E. Katz (1999), Deconstruction of the chemical effects of road salt on stream water chemistry, *J. Environ. Qual., 28*, 82– 91.

Mahler, B.J., M. Musgrove, C. Herrington, and T.L. Sample (2011a) Recent (2008-10) concentrations and isotopic compositions of nitrate and concentrations of wastewater compounds in the Barton Springs zone, south-central Texas, and their potential relation to urban development in the contributing zone. USGS Scientific Investigations Report, 2011-5018.

Mahler, B.J., M. Musgrove, T.L. Sample, C.I. Wong (2011b) Recent (2008–10) Water Quality in the Barton Springs Segment of the Edwards Aquifer with Emphasis on Factors Affecting Nutrients and Bacteria. U.S. Geological Survey Scientific Investigation, Report 2011–5139.

May, C.W., R.R. Horner, J.R. Kar, B.W. Mar, and E.B. Welch (1997) Effects of urbanization on small streams in the Puget Sound lowland ecoregion. *Water Protection Techniques, 2*, 483-494.

Musolff, A., S. Leschik, M. Moder, G. Strauch, F. Reinstorf, M. Schirmer (2009) Temporal and spatical patterns of micropollutants in urban receiving waters. *Environmental Pollution, 157*, 3069-3077.

National Atmospheric Deposition Program (2012) National Trends Network, http://nadp.sws.uiuc.edu/ntn/ (accessed 23.05.12).

National Climate Data Center (2012) Plot Time Series, http://lwf.ncdc.noaa.gov/temp-and-precip/time-series/ (accessed 23.05.12).

Novotny, E.V., A.R. Sander, O. Mohseni, and H.G. Stefan (2009) Chloride ion transport and mass balance in a metropolitan area using road salt. *Water Resources Research, 45*, W12410.

Palmer, W. C, (1965) Meteorological Drought. Res. Paper No.45, 58pp., Dept. of Commerce, Washington, D.C.

Pape J. R., J.L. Banner, L.E. Mack, M. Musgrove, A. Guilfoyle (2010) Controls on oxygen isotope variability in precipitation and cave drip waters, central Texas, USA, *Journal of Hydrology, 385*, 203–215.

Parkhurst, D.L. and C.A.J. Appelo (1999) User's Guide to PHREEQC (ver. 2)—A Computer Program for Speciation, Reaction-Path, One-Dimensional Transport, and Inverse Geochemical Calculations. U.S. Geological Survey Water-Resources Investigations 99–4259, 312p.

Passarello, M.C., J.M. Sharp, S.A. Pierce (2012) Estimating Urban-Induced Artificial Recharge: A case study for Austin, TX. *Environmental and Engineering Geosciences, 18*, 25-36.

Pfeifer, L.R., and E.M. Bennett (2011) Environmental and social predictors of phosphorous in urban streams on the Island of Montreal, Quebec. *Urban Ecosystems, 14*, 485-499.

Price, A. (2009) Top 10 Users from the Austin Water Utility: Austin American Statesman, August 17, 2009, available at http://www.statesman.com/news/content/news/stories/local/2009/08/17/0817water.html.

Rose, P.R. (1972) Edwards Group, Surface and Subsurface, Central Texas. Report of Investigations. Bureau of Economic Geology, No. 74. University of Texas at Austin.

Runkel, R.L., C.G. Crawford, and T.A Cohn (2004) Load Estimator (LOADEST)—A FORTRAN program for estimating constituent loads in streams and rivers: U.S. Geological Survey Techniques and Methods Book 4, Chapter A5, 69 p.

Schoonover, J.E., B.G. Lockaby, and S. Pan (2005) Changes in chemical and physical properties of stream water across an urban-rural gradient in western Georgia. *Urban Ecosystems, 8*, 107-124.

Slade, R.M., Jr., Dorsey, M.E., Stewart, S.L. (1986) Hydrology and Water Quality of the Edwards Aquifer Associated with Barton Springs in the Austin Area, Texas. U.S. Geological Survey Water-Resources Investigations Report 86–4036, 117p.

Stricklin, FL (1971) Stratigraphy of Lower Cretaceous Trinity Deposits of Central Texas. Report of investigations (University of Texas at Austin. Bureau of Economic Geology), no. 71.

Texas Commission of Environmental Quality, 2012. Title 30 Environmental Quality, Part 1 Texas Commission on Environmental Quality, Chapter 307 Texas Surface Water Quality Standards, Rule 307.10, Appendix A, pg 20. Available at http://info.sos.state.tx.us/fids/201003720-6.pdf

Tong, S.T., and W. Chen (2002) Modeling the relationship between land use and surface water quality. *Journal of Environmental Management, 66*, 377-393.

Tu, J., Z.G. Xia, K.C. Clarke, and A. Frei (2007) Impact of urban sprawl on water quality in eastern Massachusetts, USA. Environmental Management, 40, 183-200.

U.S. Geological Survey (2012) National Water Information System http://waterdata.usgs.gov/tx/nwis (accessed 23.05.12).

Vazquez-Sune, E., X. Sanchez-Vila, J., Carrera (2010) An approach to identify urban groundwater recharge. *Hydrology and Earth System Sciences, 14*, 2085-2097.

Wang, X. and Z. Yin (1997), Using GIS to assess the relationship between land use and water quality at a watershed level. *Environmental International, 23*, 103-114.

Williams, M., C. Hopkinson, E. Rastetter, J. Vallino, and L. Claessens (2005) Relationshps of land use and stream solute concentrations in the Ipswich River Basin, northeastern Massachusetts. *Water, Air, Soil Pollution, 161*, 55-74.

Wong, C., B. J. Mahler, M. Musgrove, and J.L. Banner (2012) Changes in sources and storage in a karst aquifer during a transition from drought to wet conditions. *Journal of Hydrology, 468-469*, 159-172, doi.org/10.1016/j.jhydrol.2012.08.030.

Yang Y., D.N. Lerner, M.H. Barrett, J. Tellam (1999) Quantification of groundwater recharge in the city of Nottingham, UK. *Environmental Geology, 38*, 183–198.

Chapter 4 references

Andrews, A., Hunt, B. B., and Smith, B. A. 2013. Hydrological and Geochemical Characteristics in the Edwards and Trinity Hydrostratigraphic Units Using Multiport Monitor Wells in the Balcones Fault Zone, Hays County, Central Texas. Geological Society of America South Central Meeting, Abstracts with Programs, 45, no. 3: 91.

Ashworth, J. B. 1983. Ground-Water Availability of the Lower Cretaceous Formations in the Hill Country of South-Central Texas. Texas Water Development Report, no. 273.

Banner, J. L. 2004. Radiogenic isotopes: systematics and applications to earth surface processes and chemical stratigraphy. Earth-Science Reviews, no. 65: 141–194.

Banner, J. L., and G.N. Hanson. 1990. Calculation of simultaneous isotopic and trace-element variations during water-rock interaction with applications to carbonate diagenesis. Geochimica et Cosmochimica Acta, 54:3123-3137.

Banner, J. L. and J. Kaufman. 1994. The isotopic record of ocean chemistry and diagenesis preserved in nonluminescent brachiopods from Mississippian carbonate rocks, Illinois and Missouri. Geological Society of America Bulletin, no. 106: 1074-1082.

Banner, J. L., M. Musgrove, R.L. Edwards, Y. Asmerom, and J.A. Hoff. 1996. High-resolution temporal record of Holocene ground-water chemistry: Tracing links between climate and hydrology. Geology, 24: 1049-1052.

Barker, R.A., and A.F. Ardis. 1996. Hydrogeologic framework of the Edwards-Trinity aquifer system, west-central Texas. US Geological Survey Professional Paper, 1421-B, 61p.

Barlow, P.M. and S.A. Leake. 2012. Streamflow depletion by wells--Understanding and managing the effects of groundwater pumping on streamflow. US Geological Survey Circular, 1376, 95p.

Barton Springs Edwards Aquifer Conservation District. 2008. District Management Plan, 66 p. Available at http://www.bseacd.org/uploads/RulesRegs/BSEACD_Management_Plan_TWDB_Approved_9_15_08.pdf.

Bouwer, H., 1989. The Bouwer and Rice slug test--an update, Ground Water, 27, no. 3: 304-309.

Bouwer, H. and R.C. Rice, 1976. A slug test method for determining hydraulic conductivity of unconfined aquifers with completely or partially penetrating wells, Water Resources Research, 12, no. 3: 423-428.

Butler, J.J., Jr., 1998. The Design, Performance, and Analysis of Slug Tests, Lewis Publishers, Boca Raton, 252p.

Christian, L. N., J. L. Banner, and L. E. Mack. 2011. Sr isotopes as tracers of anthropogenic influences on stream water in the Austin, Texas, area. Chemical Geology, no. 282: 84-97.

Collins, E.W., and S.D. Hovorka. 1997. Structure map of the San Antonio segment of the Edwards Aquifer and Balcones fault zone, south-central Texas: Structural framework of a major limestone aquifer: Kinney, Uvalde, Medina, Bexar, Comal, and Hays Counties: The University of Texas at Austin, Bureau of Economic Geology, Miscellaneous Map No. 38, scale 1:250,000, 2 sheets.

Davidson, S.C.. 2008. Hydrological characterization of baseflow to Jacob's Well spring, Hays County, Texas. MS Thesis, The University of Texas at Austin.

Gary, M., Veni, G., Shade, B., and Gary, R. 2011. Spatial and Temporal Recharge Variability Related to Groundwater Interconnection of the Edwards and Trinity Aquifers, Camp Bullis, Bexar and Comal Counties, Texas. In Interconnection of the Trinity (Glen Rose) and Edwards Aquifers along the Balcones Fault Zone and Related Topics, Proceedings from Karst Conservation Initiative Meeting, Feburary 17th, 2011, 6-10. Available at http://www.speleogenesis.info/directory/karstbase/pdf/seka_pdf9869.pdf.

Green, R.T., Bertetti, F.P., and Candelario, M.O. 2011. Edwards Aquifer – Upper Glen Rose Aquifer Hydraulic Interaction. In Interconnection of the Trinity (Glen Rose) and Edwards Aquifers along the Balcones Fault Zone and Related Topics, Proceedings from Karst Conservation Initiative Meeting, Feburary 17th, 2011, 30-35. Available at http://www.speleogenesis.info/directory/karstbase/pdf/seka_pdf9869.pdf.

Hauwert, N.M., 2009. Groundwater flow and recharge within the Barton Springs segment of the Edwards Aquifer, southern Travis County, Texas. Dissertation, The University of Texas at Austin, 328 p.

Hauwert, N. 2011. Could much of Edwards aquifer "matrix storage" actually be Trinity aquifer contributions from the Blanco River? In Interconnection of the Trinity (Glen Rose) and Edwards Aquifers along the Balcones Fault Zone and Related Topics, Proceedings from Karst Conservation Initiative Meeting, February 17th, 2011, 15-24. Available at http://www.speleogenesis.info/directory/karstbase/pdf/seka_pdf9869.pdf.

Hunt, B.B., Smith, B.A., Slade, R., Gary, R.H., and Holland, W. F. 2012. Temporal Trends in Precipitation and Hydrologic Responses Affecting the Barton Springs

Segment of the Edwards Aquifer, Central Texas. Gulf Coast Association of Geological Societies Transactions, 62nd Annual Convention, October 21-24, 2012, Austin, TX. Available at http://www.bseacd.org/uploads/HuntEtAl,2012,Temporal%20Trends.pdf

Hunt, B.B, B.A. Smith, J. Kromann, and D.A. Wierman. 2010. Compilation of pumping tests in Travis and Hays Counties, central Texas. Barton Springs Edwards Aquifer Conservation District Data Series Report 2010-0701. Available at http://repositories.lib.utexas.edu/handle/2152/9005.

Johnson, S., Geary, S., Veni, G. 2010. Tracing groundwater flowpaths in the Edwards aquifer recharge zone, Panther Springs Creek Basin, northern Bexar County, Texas. Edwards Aquifer Authority, Report No. 10-01, 39p. Available at http://www.edwardsaquifer.org/files/Panther%20Springs%20Creek%20Traces%202010.pdf.

Jones, I. 2011. Interaction Between the Hill Country Portion of the Trinity and Edwards Aquifers: Model Results. In Interconnection of the Trinity (Glen Rose) and Edwards Aquifers along the Balcones Fault Zone and Related Topics, Proceedings from Karst Conservation Initiative Meeting, Feburary 17th, 2011, 36-37. Available at http://www.speleogenesis.info/directory/karstbase/pdf/seka_pdf9869.pdf.

Jones, I., Anaya, R., Wade, S. 2011. Groundwater Availability Model: Hill Country Portion of the Trinity Aquifer of Texas. Texas Water Development Board, Report 377, 160p. Available at http://www.twdb.state.tx.us/publications/reports/numbered_reports/doc/R377_HillCountryGAM.pdf.

Koepnick R. B., W. H. Burke, R. E. Denison, E. A. Hetherington, H. F. Nelson, J. B. Otto, and L.E. Wait. 1985. Construction of the seawater 87Sr/86Sr curve for the Cenozoic and Cretaceous: Supporting data. Chemical Geology, no. 58: 55–81.

Kromann, J.S., Wong, C. I., Hunt, B., Smith, B. 2011. An investigation of vertical mixing between two carbonate aquifers using a multiport monitor well, central Texas. American Geophysical Union 2011 Fall Meeting Abstract.

Larkin, T.J., and G.W. Bomar. 1983. Climatic atlas of Texas: Texas Department of Water Resources. Limited Printing Report LP–192, 151 p.

Mace, R.E., A.H. Chowdhury, R. Anaya, and S.C. Way. 2000. Groundwater availability of the Trinity aquifer, Hill Country area, Texas – Numerical simulations through 2050. Texas Water Development Board Report, no. 296, 90 p.

Mazor, E., 1995. Aquifer definition: specific (by water properties) or generalized (by stratigraphic or geographic terms), examples from Israel. Applications of Tracers in Arid Zone Hydrology (Proceedings of the Vienna Symposium, August 1994). IAHS Publication, 232.

Mahler, B.J., Massei, N., 2007, Anthropogenic contaminants as tracers in an urbanizing karst aquifer. Journal of Contaminant Hydrology, 91: 81-106.

Muller, D.A. 1990. Ground-water evaluation in and adjacent to Dripping Springs, Texas. Texas Water Development Board Report 322, 59 p. Available at http://www.twdb.state.tx.us/publications/reports/numbered_reports/doc/R322/r322_DrippingSprings_opt.pdf.

Musgrove, M., and J.L. Banner. 2004. Controls on the spatial and temporal variability of vadose dripwater geochemistry: Edwards Aquifer, central Texas. Geochimica Cosmochimica Acta, 68:1007–1020.

Musgrove, M., L. Stern, and Banner, J. 2010. Springwater geochemistry at Honey Creek State Natural Area, central Texas: Implications for surface water and groundwater interaction in a karst aquifer. Journal of Hydrology, 388: 144–156.

Musgrove, M. and Crow, C.L. 2012. Origin and characteristics of discharge at San Marcos Springs based on hydrologic and geochemical data (2008-10), Bexar, Comal, and Hays Counties, Texas. USGS Scientific Investigations Report, 2012-5126.

National Climate Data Center. 2012. Annual Precipitation and Temperature for Austin, Texas. Web. http://lwf.ncdc.noaa.gov/temp-and-precip/time-series/.

National Oceanic and Atmospheric Administration. Texas Palmer Drought Severity Index (PDSI) August 1895-2011. 2012. Web. http://lwf.ncdc.noaa.gov/temp-and-precip/time-series/index.php?parameter=pdsi&month=8&year=2009&filter=1&state=41&div=0.

Oetting, 1995. Evolution of fresh and saline groundwaters in the Edwards aquifer, central Texas : geochemical and isotopic constraints on processes of fluid-rock interaction and fluid mixing. Dissertation, The University of Texas at Austin, 203 p.

Oetting, G.C., Banner, J.L., Sharp, J.M., 1996. Regional controls on the geochemical evolution of saline groundwaters in the Edwards aquifer, central Texas. Journal of Hydrology, 181:251-283.

Quinlan, James F., Peter L. Smart, Geary M. Schindel, E. Calvin Alexander, Alan J. Edwards, and A. Richard Smith, 1991. Recommended administrative/regulatory definition of karst aquifer, principles for classification of carbonate aquifers, practical evaluation of vulnerability of karst aquifers, and determination of optimum sampling frequency at springs. In Hydrology, Ecology, Monitoring, and Management of Ground Water in Karst Terranes Conference (3rd. Nashville. Tenn. 1991). JF Quinlan and A. Stanley, Editors. National Ground Water Association. Dublin, Ohio, pp. 573-635.

Rose, P.R., 1972. Edwards Group, surface and subsurface, central Texas. Report of investigations (University of Texas at Austin. Bureau of Economic Geology), no.74. Austin.

Schindel, G. and Johnson, S. 2011. Using tracer testing data for resource management planning. In Interconnection of the Trinity (Glen Rose) and Edwards Aquifers along the Balcones Fault Zone and Related Topics, Proceedings from Karst Conservation Initiative Meeting, Feburary 17th, 2011, 38. Available at http://www.speleogenesis.info/directory/karstbase/pdf/seka_pdf9869.pdf.

Senger, R.K., and C.W. Kreitler. 1984. Hydrogeology of the Edward aquifer, Austin area, central Texas. Report of Investigations, Bureau of Economic Geology, The University of Texas at Austin.

Slade, R., Jr., M. Dorsey, and S. Stewart, 1986, Hydrology and water quality of the Edwards Aquifer associated with Barton Springs in the Austin area, Texas: U.S. Geological Survey Water-Resources Investigations, Report 86-4036, 117 p.

Small, T.A., J.A., Hanson, N.M. Hauwert. 1996. Geologic framework and hydrogeologic characteristics of the Edwards aquifer outcrop (Barton Spring segment), Northeastern Hays and southwestern Travis Counties, Texas. US Geological Survey Water Resource Investigations Report, 96-4306, 15p.

Smith, B. A., and Hunt, B. B. 2008. Multilevel Monitoring and Characterization of the Edwards and Trinity Aquifers of Central Texas. Gulf Coast Association of Geological Societies Transactions, 58: 833-840. Available at http://www.bseacd.org/publications/reports#EdwardsTrinity

Smith, B. A., and Hunt, B. B. 2009. Potential Hydraulic Connections Between the Edwards and Trinity Aquifers in the Balcones Fault Zone of Central Texas. Bulletin of the South Texas Geological Society, L, no. 2:15-34. Available at http://www.bseacd.org/publications/reports#EdwardsTrinity

Smith, B. A., and Hunt, B. B. 2010. "Flow Potential Between Stacked Karst Aquifers in Central Texas, USA. In Advances in Research in Karst Media Environmental Earth Sciences, Eds., Andreo, B., Carrasco, F., Duran, J.J., LaMoreaux, J.W., 43-48.

Smith, B. A., and Hunt, B. B. 2011. Potential for Vertical Flow Between the Edwards and Trinity Aquifer, Barton Springs Segment of the Edwards Aquifer. In Interconnection of the Trinity (Glen Rose) and Edwards Aquifers along the Balcones Fault Zone and Related Topics, Proceedings from Karst Conservation Initiative Meeting, Feburary 17th, 2011, 11-14. Available at http://www.speleogenesis.info/directory/karstbase/pdf/seka_pdf9869.pdf.

Stricklin, F.L., C.I. Smith, C.I., and F.E. Lozo. 1971. Stratigraphy of Lower Cretaceous Trinity deposits of central Texas. Bureau of Economic Geology Report of Investigations, The University of Texas at Austin, 63 p.

Suarez D. L. (1996) Beryllium, magnesium, calcium, strontium and barium. In Methods of Soil Analysis, Part 3: Chemical Methods— SSSA Book Series No. 5, Soil Science Society of America and American Society of Agronomy.

Texas Water Development Board. 2012. Groundwater Database. Web. http://www.twdb.state.tx.us/groundwater/data/gwdbrpt.asp

Wierman, D.A., A.S., Broun, L. Llano, and A.H. Backus. 2008. Cypress Creek/Jacob's Well Hydrogeologic Report. Hays Trinity Groundwater Conservation District. Available at http://haysgroundwater.com/files/Documents/Report%28TitlePage-Ch6%29.pdf

Wierman, D.A., A.S. Broun, and B.B. Hunt. 2010. Hydrogeologic atlas of the Hill Country Trinity Aquifer; Blanco, Hays and Travis Counties, central Texas. Hays-Trinity Groundwater Conservation District. Available at http://repositories.lib.utexas.edu/handle/2152/8977.

Winter, T. C., J.W. Harvey, O.L. Franke, W.A. Alley. 1998. Ground water and surface water; a single resource**.** US Geological Survey Circular, 1139, 79p.

Wong, C., J.L. Banner, and M. Musgrove. 2011. Seasonal dripwater Mg/Ca and Sr/Ca variations driven by cave ventilation: Implications for and modeling of speleothem paleoclimate records, Geochimica et Cosmochimica Acta, 75: 3514–3529.

Wong, C., B.J. Mahler, M. Musgrove, and J.L. Banner. 2012. Changes in sources and storage in a karst aquifer during a transition from drought to wet conditions. Journal of Hydrology, 468: 159-172.

Chapter 5 references

Asmerom, Y., Polyak, V., Burns, S., 2010. Variable winter moisture in the southwest United States linked to rapid glacial climate shifts. Nature Geoscience, 3, 114-117.

Banner, J.L., Guilfoyle, A., James, E.W., Stern, L.A., Musgrove, M. 2007. Seasonal variations in modern speleothem calcite growth in central Texas, U.S.A. Journal of Sedimentary Research, 77, 615-622.

Banner, J. L., M. Musgrove, R.L. Edwards, Y. Asmerom, and J.A. Hoff. 1996. High-resolution temporal record of Holocene ground-water chemistry: Tracing links between climate and hydrology. Geology, 24: 1049-1052.

Beach, P., 2012, Drought cost Texas close to $8 billion in agricultural losses in 2011, study finds. Austin American Statesman, March 21, 2012. Accessed at http://www.statesman.com/news/news/state-regional/drought-cost-texas-close-to-8-billion-in-agricultu/nRmNt/.

Blum, M.D., Toomey, R.S., Valastro, S., 2004, Fluvial response to Late Quaternary climatic and environmental change, Edwards Plateau, Texas. Palaeogeography, Paleoclimatology, Paleoecology, 108, 1-21.

Bond, G., Kromer, B., Beer, J., Muscheler, R., Evans, M.N., Showers, W., Hoffmann, S., Lotti- Bond, R., Hajdas, I., Bonani, G., 2001. Persistent solar influence on North Atlantic climate during the Holocene. Science 278, 1257–1266.

Boulter, C., Bateman, M.D., Frederick, C.D., 2010. Understanding geomorphic responses to environmental change: a 19 000-year case study from semi-arid central Texas, USA. Journal of Quaternary Science, 25, 889-902.

Breecker, D.O., Payne, A.E., Quade, J., Banner, J.L., Ball, C.E., Meyer, K.W., Cowan, B.D., 2012. The sources and sinks of CO_2 in caves under mixed woodland and grassland vegetation. Geochimica et Cosmochimica Acta, 96, 230-246.

Chapman, M.R., Shackleton, N.J., 2000. Evidence of 550-year and 1000-year cyclicities in North Atlantic circulation patterns during the Holocene. The Holocene 10, 287–291.

Cheng, H., Edwards, R.L., Hoff, J., Gallup, C.D., Richards, D.A., and Asmeron, Y., 2000, The half-lives of uranium-234 and thorium-230: Chemical Geology, 169, 17–33.

Clark, I., Fritz, P.,1997. Environmental Isotopes in Hydrology. Lewis Publishers, New York.

Cleaveland, M.K., Votteler, T.H., Stahle, D., Casteel, R.C., Banner, J.L. 2011, Extended chronology of drought in south-central and west Texas. Texas Water Journal, 2, 54-76.

Cooke, M.J., Stern, L.A., Banner, J.L., Mack, L.E., Stafford, T.W. Jr., Toomey III, R.S. 2003. Precise timing and rate of massive late Quaternary soil denudation. Geology, 31, 853-856.

Cowan, B., Osborne, M. Banner, J. L., 2013. Temporal variability of cave-air CO_2 in central Texas. Journal of Cave and Karst Studies.

Debret, M., Bout-Roumazeilles, V., Grousset, F., Desmet, M., McManus, J.F., Massei, N., Sebag, D., Petit, J.-R., Copard, Y., Trentesaux, A., 2007. The origin of the 1500-year climate cycles in Holocene North-Atlantic records. Climate of the Past, 3, 569-575.

deMenocal, P.B., Ortiz, J., Guilderson, T., Sarntheim, M., 2000. Coherent high- and low-latitude climate variability during the Holocene warm period. Science 288, 2198–2202.

Denniston, R.F., González, L.A., Asmerom, Y., Polyak, V., Reagan, M.K., and Saltzman, M.R., 2001, A high-resolution speleothem record of climatic variability at the Allerød–Younger Dryas transition in Missouri, central United States:

Palaeogeography, Palaeoclimatology, Palaeoecology, v. 176, p. 147–155, doi: 10.1016/S0031-0182(01)00334-0.

Desmarchelier, J.M., Goede, A., Ayliffe, L.K., McCulloch, M.T., and Moriarty, K., 2000, Stable isotope record and its palaeoenvironmental interpretation for a late Middle Pleistocene speleothem from Victoria Fossil Cave, Naracoorte, South Australia: Quaternary Science Reviews, v. 19, p. 763–774, doi: 10.1016/S0277-3791(99)00037-2.

Dorale, J.A., Edwards, R.L., Ito, E., and González, L.A., 1998, Climate and vegetation history of the midcontinent from 75 to 25 ka: A speleothem record from Crevice Cave, Missouri, USA: Science, v. 282, p. 1871–1874, doi: 10.1126/science.282.5395.1871.

Edwards, R.L., Chen, J.H., Wasserburg, G.J., 1987, 238U-234U-230Th–232Th systematics and the precise measurement of time over the past 500,000 years: Earth and Planetary Science Letters, 81, 175–192.

Edwards, R.L., Beck, J.W., Burr, G.S., Donahue, D.J., Chappell, J.M.A., Bloom, A.L., Druffel, E.R.M., and Taylor, F.W., 1993, A large drop in atmospheric 14C/12C and reduced melting in the Younger Dryas, documented with 230Th ages of corals: Science, 260, 962–968.

Ellwood, B.B, Gose, W.A., 2006. Heinrich H1 and 8200 yr B.P. climate events recorded in Hall's Cave Texas. Geology, 34, 753.

Feng, W., Banner, J.L., Guilfoyle, A., Musgrove, M., James, E. 2012. Oxygen isotopic fractionation between drip water and speleothem calcite: A 10-year monitoring study, central Texas, USA. Chemical Geology, 305-305, 53-67.

Feng, W., Hardt, B.F., Banner, J.L., Meyer, K.J, James, E.W., MaryLynn Musgrove, Edwards, R.L., Cheng, H., Changing moisture sources to the US southwest in response to global climate change. In review with Geology.

Genty, D., Blamart, D., Ouahdi, R., Gilmour, M., Baker, A., Jouzel, J., and van Exter, S., 2003, Precise dating of Dansgaard-Oeschger climate oscillations in western Europe from stalagmite data. Nature, 421, 833-837.

Ghil M., R. M. Allen, M. D. Dettinger, K. Ide, D. Kondrashov, M. E. Mann,A. Robertson, A. Saunders, Y. Tian, F. Varadi, and P. Yiou, 2000, Advanced spectral methods for climatic time series, Reviews of Geophysics,40, 3.1-3.41.

Goede, A., 1994, Continuous early last glacial palaeoenvironmental record from a Tasmanian speleothem based on stable isotope and minor element variations. Quaternary Science Reviews, v. 13, p. 283–291, doi:10.1016/0277-3791(94)90031-0.

Goede, A., Green, D.C., and Harmon, R.S., 1986, Late Pleistocene palaeotemperature record from a Tasmanian speleothem: Australian Journal of Earth Sciences, v. 33, p. 333–342.

Guilfoyle, A. 2006. Temporal and spatial controls on cave water and speleothem calcite isotopic and elemental chemistry, central Texas. Master's Thesis. The University of Texas at Austin, 337 pp.

Gupta, A.K., Das, M., Anderson, D.M., 2005. Solar influence on the Indian summer monsoon during the Holocene. Geophysical Research Letters 32, L17703. doi:10.1029/2005GL022685.

Higgins, R.W., Yao, Y., Yarosh, E.S., Janowiak, J.E., Mo, K.C., 1997. Influence of the Great Plains low-level jet on summertime precipitation and moisture transport over the central United States. Journal of Climate, 10, 481-507.

Humphrey, J.D., Ferring, C.R., 1994. Stable isotopic evidence for latest Pleistocene and Holocene climatic change in north-central Texas: Quaternary Research, 41, 200–213.

Jones, I. C. and Banner, J. L., 2003. Hydrogeologic and climatic influences on spatial and interannual variation of recharge to a tropical karst island aquifer, Water Resources Research 39, 1253-1263.

Jones, I. C., Banner, J. L., and Humphrey, J. D., 2000. Estimating recharge in a tropical karst aquifer. Water Resources Research, 36, 1289-1299.

Kennett, D.J., Breitenbach, S.F., Aquino, V.V., Asmerom, Y., Awe, J., Baldini, J.U., Bartlein, P., Culleton, B.J., Claire Ebert, C., Jazwa, C., Macri, M.J., Marwan, N., Polyak, V., Prufer, K.M., Ridley, H.E., Sodemann, H., Winterhalder, B., Haug, G.H., 2012. Development and disintegration of Maya political systems in response to climate change. Science, 338, 788-791.

Lachniet, M.S., 2009. Climate and environmental controls on speleothem oxygen-isotope values. Quaternary Science Reviews, 28, 412-432.

Larkin, T.J., Bomar, G.W., 1983. Climatic atlas of Texas: Texas Department of Water Resources, Limited Printing Report LP–192, 151 p.

LoDico, J.M., Flower, B.P., Quinn, T.M., 2006. Subcentennial-scale climatic and hydrologic variability in the Gulf of Mexico during the early Holocene. Paleoceanography, 21, PA3015. doi:10.1029/2005PA001243.

Mickler, P. M., Banner, J. L., Stern, L. A., Asmerom, Y., Edwards, R. L., and Ito, E., 2004, Stable isotope variations in modern tropical speleothems: Evaluating equilibrium vs. kinetic isotope effects. Geochimica et Cosmochimica Acta 68, 4381–4393,

Musgrove, M., Banner, J.L., Mack, L.M., Combs, D.M., James, E.W., Cheng, H., Edwards, R.L. 2001. Geochronology of late Pleistocene to Holocene speleothems

from central Texas: Implications for regional paleoclimate. Geological Society of America Bulletin, 113, 1532-1543.

Musgrove, M., Banner, J. L., 2004, Controls on the spatial and temporal variability of vadose dripwater geochemistry: Edwards Aquifer, central Texas, Geochimica et Cosmochimica Acta 68, 1007-1020.

National Hurricane Center, Tropical Cyclone Reports. http://www.nhc.noaa.gov/data/#tcr, accessed June 2013.

National Weather Service, http://www.srh.noaa.gov/ewx/?n=austinmabryclidata.htm, accessed 23 May 2012.

Niggemann, S., Mangini, A., Mudelsee, M., Richter, D.K., Wurth, G., 2003. Sub-Milankovitch climatic cycles in Holocene stalagmites from Sauerland, Germany. Earth and Planetary Science Letters 216, 539–547.

Nordt, L.C., Boutton, T.W., Hallmark, C.T., Waters, M.R. 1994. Late Quaternary vegetation and climate changes in central Texas based on the isotopic composition of organic carbon. Quaternary Research, 41, 109-120.

Nordt, L.C., Boutton, T.W., Jacob, J.S., Mandel, R.D., 2002. C4 plant productivity and climate-CO_2 variations in south-central Texas during the late Quaternary. Quaternary Research, 58, 182-188.

Oglesby, R.J., Maasch, K.A., Saltzman, B., 1989. Glacial metlwater cooling of the Gulf of Mexico: GCM implications for Holocene and present-day climates. Climate Dynamics, 3, 115-133.

Oster, J.L., Montanez, I.P., Guilderson, T.P., Sharp, W.D., Banner, J.L., 2010, Modeling speleothem $\delta^{13}C$ variability in a central Sierra Nevada cave using ^{14}C and $^{87}Sr/^{86}Sr$. Geochimica et Cosmochimica Acta 74, 5228-5242.

Pape J. R., J.L. Banner, L.E. Mack, M. Musgrove, A. Guilfoyle (2010) Controls on oxygen isotope variability in precipitation and cave drip waters, central Texas, USA, Journal of Hydrology, 385, 203–215.

Poore, R.Z., Dowsett, H.J., Verardo, S., 2003. Millennial- to century-scale variability in Gulf of Mexico Holocene climate records. Paleoceanography, 18, PA1048. doi:10.1029/2002PA000868.

Poore, R.Z., Quinn, T.M., Verardo, S., 2004. Century-scale movement of the Atlantic Intertropical Convergence Zone linked to solar variability. Geophysical Research Letters, 31, L12214. doi:10.1029/2004GL019940.

Richey, J. N., R. Z. Poore, B. P. Flower, T. M. Quinn, 2007. 1400 yr multiproxy record of climate variability from the northern Gulf of Mexico, Geology, 35, 423– 426, doi:10.1130/G23507A.1.

Richey, J.N., Poore, R.Z., Flower, B.P., Hollander, D.J., Quinn, T.M., 2009. Regionally coherent Little Ice Age cooling in the Atlantic Warm Pool. Geophysical Research Letters, 36, L21703. doi:10.1029/2009GL040445.

Ropelewski, C.F.; and M.S. Halpert. 1986. North American precipitation and temperature patterns associated with the El Niño–Southern Oscillation (ENSO). Monthly Weather Review, 114, 2352–2362.

Russell, J.M., Johnson, T.C., 2005. Late Holocene climate change in the North Atlantic and equatorial Africa: millennial-scale ITCZ migration. Geophys. Res. Lett. 32, L17705.

Scholtz, D., Hoffman, D.L., 2011. StalAge – An algorithm designed for construction of speleothem age models. Quaternary Geochronology, 6, 369-382.

Toomey, R.S., Blum, M.D., Valastro, S. 1993. Late Quaternary climates and environments of The Edwards Plateau, Texas. Global and Planetary Change, 7, 299-320.

Vachon, RW, Welker, JM, White, JWC, Vaughn, BH, 2010, Monthly precipitation isoscapes ($\delta^{18}O$) of the United States: Connections with surface temperatures, moisture source conditions, and air mass trajectories. Journal of Geophysical Research, 115, D21126.

Viau, A.E., Gajewski, K., Fines, P., Atkinson, D.E., Sawada, M.C., 2002. Widespread evidence of 1500 yr climate variability in North America during the past 14,000 yr. Geology, 30, 455-458.

Wanner, H., Solomina, O., Grosjean, M., Ritz, S.P., Jetel, M., 2008. Structure and origin of Holocene cold events. Quaternary Science Reviews, 30, 3109-3123.

Wanner, H., Solomina, O., Grosjean, M., Ritz, S., Jetel, M., 2011, Structure and origin of Holocene cold events. Quaternary Science Reviews, 30, 3109-3123.

Wong, C., Banner, J. L., 2010. Response of cave air CO_2 and drip water to brush clearing in central Texas: Implications for recharge and soil CO_2 dynamics. Journal of Geophysical Research, 115, 1-13.

Wong, C., Banner, J. L., Musgrove, M., 2011. Seasonal dripwater Mg/Ca and Sr/Ca variations driven by cave ventilation: Implications for and modeling of speleothem paleoclimate records. Geochimica et Cosmochimica Acta 75, 3514–3529.

Willard, D.A., Bernhardt, C.E., Korejwo, D.A., Meyers, S.R., 2005. Impact of millennialscale Holocene climate variability on eastern North American terrestrial ecosystems: pollen-based climatic reconstruction. Global and Planetary Change 47,17–35.

Yu, Z.C., Campbell, I.D., Campbell, C., Vitt, D.H., Bond, G.C., Apps, M.J., 2003. Carbon sequestration in western Canadian peat highly sensitive to Holocene wet-dry climate cycles at millennial timescales. Holocene 13, 801–808.

VITA

Originally from the rainy state of Oregon, Corinne completed her undergraduate degrees (B.S. in Geological Sciences and B.A. in Environmental Studies) at the University of the Pacific (Stockton) in sunny California. For those of you not from California, do not be led astray by its name - The University of the Pacific is not by the Pacific Ocean. After a brief time in the Peace Corps in The Gambia (West Africa), she found herself in the almost desert of central Texas where she completed her Master's degree in Geological Science. Not sufficiently dried out from her soggy upbringing, she remained in the semi-arid (sometimes sub-humid) region to complete this dissertation. Now completely parched, Corinne is looking forward to wetter adventures, perhaps at higher latitudes.

Email: ciwong@utexas.edu

This dissertation was typed by Corinne Wong